Optimisation de la dosimétrie appliquée en thérapie photodynamique pour l'évaluation et la prédiction de l'efficacité du traitement de tumeurs

Julie Garrier

Nancy-Université
Université Henri Poincaré

Ecole Doctorale BioSE (Biologie-Santé-Environnement)

Thèse

Présentée et soutenue publiquement pour l'obtention du titre de :

DOCTEUR DE L'UNIVERSITE HENRI POINCARE

Mention : « Sciences de la Vie et de la Santé »

par **Julie GARRIER**

Optimisation de la dosimétrie appliquée en thérapie photodynamique pour l'évaluation et la prédiction de l'efficacité du traitement de tumeurs

Le 28 Octobre 2011

Membres du Jury

Rapporteurs :	Monsieur Norbert LANGE	Professeur Ass., Université Genève (Genève)
	Monsieur Patrice PROGNON	Professeur, Hôpital Georges Pompidou (Paris)
Examinateurs :	Madame Susanna GRÄFE	Docteur d'Université, Biolitec AG (Iéna)
	Madame Beate RÖDER	Professeur, Humboldt-Université (Berlin)
	Madame Lina BOLOTINE	Docteur, CRAN Nancy-Université CNRS CAV, Directeur de thèse
	Monsieur François GUILLEMIN	Professeur, CRAN Nancy-Université CNRS CAV, Co-Directeur de thèse

Centre de Recherche en Automatique de Nancy (CRAN), Nancy-Université,
CNRS UMR 7039, Centre Alexis Vautrin
6, Avenue de Bourgogne 54511 Vandœuvre-lès-Nancy, France

« La théorie, c'est quand on sait tout et que rien ne fonctionne. La pratique, c'est quand tout fonctionne et que personne ne sait pourquoi ».

Albert Einstein

REMERCIEMENTS

Monsieur le Professeur François Guillemin,

Je tiens à vous exprimer mes sincères remerciements pour m'avoir accueillie au sein de votre établissement et m'avoir offert de travailler dans votre équipe de recherche. Votre expertise scientifique mais également clinique fut précieuse à l'évolution de ma démarche scientifique. Je fus la première étudiante du laboratoire à bénéficier d'un financement CIFRE pour la réalisation de ce travail, merci encore de la confiance que vous m'avez accordée, en espérant en avoir été digne.

Madame le Docteur Lina Bolotine-Bezdetnaya,

De simples remerciements me paraissent insuffisants au vu de l'engagement dont vous avez fait preuve auprès de moi. Je tiens à vous remercier avant tout pour votre soutien indéfectible tant au niveau professionnel que personnel. Vous avez cru en moi quand moi-même j'étais sur le point de ne plus y croire. Merci pour votre enthousiasme contagieux et nos discussions, qu'elles soient scientifiques ou non. Je vous dois beaucoup et j'espère vous faire honneur aujourd'hui à travers ce travail.

Monsieur le Docteur Norbert Lange,

Je vous adresse mes plus vifs remerciements pour avoir accepté d'évaluer mes travaux. Vos compétences accrues dans le domaine de la thérapie photodynamique et votre expertise scientifique, en particulier sur l'utilisation du modèle de la CAM et des formulations liposomales, ont fait de vous un rapporteur incontournable pour ce travail. Je suis très honorée de l'intérêt que vous portez à cette étude.

Monsieur le Professeur Patrice Prognon,

C'est un honneur pour moi que vous ayez accepté d'évaluer mes travaux en tant que rapporteur. Votre double compétence à la fois scientifique et clinique m'offre une formidable opportunité d'approfondir mes connaissances et de parfaire mes réflexions scientifiques.

To Professor Beate Röder,

I am very grateful for your contribution in the evaluation of my work. Your experience and remarks will complete the reflection made during my thesis and promote this work.

To Doctor Susanna Gräfe,

I would like to express my deepest gratitude for having given me the opportunity to collaborate with you for several years. It is a pleasure for me that you accepted to be a member of the thesis jury. I wish that I will benefit from your knowledge, your professionalism and your kindness for still a long time.

Messieurs les Responsables du CRAN,

Je remercie Monsieur le Professeur Alain Richard, Directeur du CRAN, ainsi que Monsieur le Professeur Didier Wolf, Responsable du groupe thématique Ingénierie pour la Santé, pour leur investissement et leur intérêt pour mon travail de thèse.

Mesdames et Messieurs les Collaborateurs,

Ces mots sont destinés à l'ensemble des personnes avec qui j'ai eu le plaisir de collaborer ici et ailleurs au cours de ces 3 années. Je tiens à remercier en particulier **M^{me} Aude Bressenot**, mon médecin anatomopathologiste apoptologue préféré, **Mr Dominique Dumas et Mr Sébastien Hupont**, pour les heures passées avec moi devant les microscopes et macroscopes à faire, défaire et refaire, **M^{me} Anne-Laure Leblanc** pour son amitié et ses conseils avisés en matière d'expérimentation animale et le **personnel** des laboratoires d'anatomopathologie du Centre Alexis Vautrin et du CHRU de Brabois pour leur gentillesse et leur disponibilité.

Les membres du laboratoire CRAN-CAV,

Cette expérience de 3 ans de doctorat complétée de 2 ans de Master, m'a permis de rencontrer des personnes qui m'ont enrichie professionnellement et personnellement. Un remerciement tout particulier à **M^{me} Sophie Marchal** pour vos conseils et votre initiation précoce au phénomène d'apoptose**, Mr Vadim Reshetov**, mon binôme physicien avec qui j'ai été ravie de collaborer**, M^{me} Marie-Ange d'Hallewin** pour vos commentaires spontanés et votre bienveillance. Un grand merci à tous mes autres collègues qu'il serait trop long d'énumérer mais qui se reconnaitront et sans qui cette aventure n'aurait pu aboutir.

Mes proches,

Un immense merci à mes parents, ma famille et mes amis. Vous m'avez soutenue tout au long de mon périple doctoral… en particulier toi, toi qui te reconnaîtras en lisant ces lignes: merci d'avoir cru en moi, en mes capacités et merci de m'avoir aidée à devenir ce que je suis

aujourd'hui. Enfin, mes derniers mots seront pour les absents, ceux qui me manquent cruellement en ce jour : papy, pépère et Hélène vous êtes partis trop tôt…

Nos soutiens financiers,

Je remercie l'ANRT ainsi que le Centre Alexis Vautrin et la Ligue contre le Cancer pour leur soutien financier sans qui nos recherches ne pourraient aboutir.

TABLE DES MATIERES

LISTE DES ABREVIATIONS

ADN	Acide désoxyriboNucléique
AlClPc	Aluminium Chloride Phthalocyanine
ALA	AminoLevulinic Acid
AMM	Autorisation de Mise sur le Marché
ARN	Acide RiboNucléique
AFA	Acide acétique, Formol, Alcool
AIF	Apoptosis Inducing Factor
APAF-1	Apoptosis Activating Factor
ATPase	Adénosine Triphosphate synthase
Bax	Bcl-2–associated X protein
Bcl-2	B-cell leukemia/lymphoma 2
CAD	Caspase-Activated DNase
CAM	ChorioAllantoic Membrane
Caspase	Cysteinyl ASPartate-specific proteASES
CAV	Centre Alexis Vautrin
Ce6	Chlorin e6
Ce6-PVP	Chlorin e6 and PolyVinylPyrrolidone
CI	Conversion Interne
CIS	Conversion InterSystème
CRAN	Centre de Recherche en Automatique de Nancy
dATP	désoxy-Adénosine TriPhosphate
DFF45	DNA Fragmentation Factor 45
DISC	Death Inducing Signaling Complex
DL	Death Ligands
DMLA	Dégénérescence Maculaire Liée à l'Age
DPPC	DiPalmitoylPhosphatidylCholine
DPPG	DiPalmitoylPhosphatidylGlycérol
DSPE-PEG	DiStearoylPhosphatidylEthanolaminem PEG 2000
EDD	Embryonic Developement Day
EPR	Enhanced Permeability Retention
ERO	Espèce Réactive de l'Oxygène

ES	Erreur Standard
FITC	Fluorescein IsoThioCyanate
HAL	Hexyl-5-AminoLevulinate
HDL	High Density Lipoprotein
H&E	Hématoxyline-Eosine
HH	Stade de développement embryonnaire défini par Hamburger & Hamilton
Hp	Hématoporphyrine
HpD	Hematoporphyrin Derivative
HPPH	2-[1-hexyloxyethyl]-2-devinyl pyropheophorbide-a
hν	Irradiation
HY	Hypericine
IAA	Indole-3-acetic acid
ICAD	Inhibitor of Caspase-Activated DNase
IDL	Intervalle drogue-lumière
Ig	Immunoglobuline
INPL	Institut national polytechnique de Lorraine
LDL	Low-Density Lipoprotein
MB	Methylene Blue
m-THPC	Méta-tétrahydroxyphényl-chlorine, Foscan®
Methyl-ALA	Methyl ester of 5-aminolevulinic acid
NO	Monoxyde d'azote
Npe6	mono-L-aspartyl chlorin e6 (MACE)
PARP	Poly (ADP-ribose) polymerase
PBR	Récepteurs aux Benzodiazépines
PBS	Phosphate Buffered Saline
Pc4	Phtalocyanine 4
PDT	Photodynamic therapy
PECAM	Platelet Endothelial Cell Adhesion Molecule
PEG	Polyéthylène glycol
PMN	Polymorphonucléaires
PpIX	Protoporphyrine IX
PS	Photosensibilisateur
RIF-1	Radiation Induced Fibrosarcoma
RPMI	Roswell Park Memorial Institute

S	Substrat
SCID	Severe Combined ImmunoDeficiency
SnET2	Tin ethyl etiopurpurin
TNFR	Tumor Necrosis Factor Receptor
TUNEL	Terminal deoxynucleotidyl transferase-mediated dUTP Nick End Labelling
Tx	Thromboxane
UV	UltraViolet

TABLE DES ILLUSTRATIONS

LISTE DES TABLEAUX

INTRODUCTION

La thérapie photodynamique (PDT) est une modalité de traitement des petites tumeurs superficielles et accessibles à la lumière. Son principe repose sur l'action d'une molécule photoactivable, le photosensibilisateur (PS), qui s'accumule de manière préférentielle dans les tissus néoplasiques. Sous l'effet d'une irradiation lumineuse et en présence d'oxygène, ce PS génère des espèces réactives de l'oxygène cytotoxiques. L'effet tumoricide de ce traitement résulte de la combinaison de dommages cytotoxiques directs sur les cellules tumorales et de dommages indirects caractérisés par l'altération de la vascularisation tumorale combinée à une activation du système immunitaire. La contribution relative de chacun de ces types de dommages dans la photodestruction des tissus tumoraux est à l'heure actuelle peu définie et apparaît spécifique à chaque PS.

Le Foscan® (méta-tetra(hydroxyphenyl)chlorine, m-THPC, Temoporfin) est un photosensibilisateur de seconde génération, reconnu comme étant le plus actif sur le marché. Il est actuellement utilisé pour le traitement palliatif et curatif de carcinomes épidermoïdes de la tête et du cou ayant résisté aux thérapies conventionnelles. Les protocoles cliniques actuels favorisent l'accumulation du Foscan® dans les cellules tumorales et produisent après PDT une forte réponse inflammatoire liée à une importante nécrose des tissus ce qui entraine une efficacité thérapeutique relative. La mort cellulaire par apoptose permet d'éviter cette réaction inflammatoire ainsi que la perte de substance liée à la nécrose.

La mTHPC existe également sous des formes hydrosolubles de type liposomal appelées Foslip® et Fospeg®. Les formulations liposomales des PSs reçoivent à l'heure actuelle un engouement tout particulier de part leurs propriétés à augmenter la vitesse de pénétration et le taux de rétention des photosensibilisateurs dans les tissus tumoraux. Néanmoins, un paramètre majeur reste à évaluer en préambule d'un traitement PDT : la redistribution du PS à partir de ces formulations. Les variations de ce paramètre ont pour finalité d'obtenir une meilleure efficacité du traitement.

Les travaux entrepris dans le cadre de cette thèse ont pour but d'optimiser l'efficacité du traitement photodynamique avec la mTHPC en se basant sur sa distribution intratumorale et en favorisant la mort cellulaire par apoptose. Ce ciblage tumoral passif a été obtenu grâce à la modulation du temps séparant l'administration du PS de son irradiation (intervalle drogue lumière, IDL) et par conséquent du type de dommages photoinduits (directs ou indirects).
De plus, l'évaluation de la redistribution de la mTHPC à partir de nouvelles formulations liposomales (Foslip® et Fospeg®), a également été réalisée afin de démontrer son influence sur l'efficacité du traitement par PDT ainsi que sur les dommages photoinduits.

CHAPITRE I

Synthèse Bibliographique

1. LA THERAPIE PHOTODYNAMIQUE

1.1 Historique

Dès l'Antiquité, les Egyptiens, les Indiens et les Chinois utilisaient la lumière solaire seule ou combinée à des substances naturelles (psoralènes) pour le traitement de lésions cutanées telles que le vitiligo, le psoriasis et les cancers ainsi que pour des pathologies générales telles que les psychoses (1,2). Cependant, le concept de « thérapie photodynamique », définie alors comme l'action combinée d'une molécule photoactivable, de la lumière et de l'oxygène, n'apparut qu'au XIXème siècle avec la publication d'une étude réalisée par Oscar Raab (3). En effet, le phénomène phototoxique fut analysé scientifiquement pour la première fois en 1897 par cet étudiant de l'Université de Munich, qui mit en évidence l'action cytotoxique de colorants tels que l'acridine et ses dérivés sur des paramécies en présence de lumière. Dès 1902, Ledoux-Lebards poursuivit ces travaux et décrivit le rôle majeur de l'oxygène dans cette toxicité photoinduite (4) . Le Professeur Hermann Von Tappeiner, directeur de thèse d'Oscar Raab, fut le premier à employer le terme de "réactions photodynamiques" pour caractériser le phénomène observé (5) et l'expérimenta avec succès en 1903, grâce à l'action combinée de la lumière solaire et de l'éosine, chez des patients souffrant de lésions cutanées syphilitiques ou tuberculeuses (6).

A la recherche de nouvelles substances photoactives, Walter Hausmann étudia en 1911 les effets de l'hématoporphyrine (Hp) qui se révéla très efficace sur de petites lésions cutanées dues au psoriasis en association avec une irradiation aux rayons ultraviolets (UV) (7). L'accumulation préférentielle de l'Hp au sein de tumeurs fut mise en évidence en 1924 par Auler et Banzer chez l'Homme (8), suivis par Figge *et al.* qui proposèrent alors l'Hp comme photosensibilisateur (PS) pour la thérapie photodynamique (PDT) en raison de sa rétention spécifique dans le tissu tumoral (9). L'Hp, constituée d'un mélange complexe de porphyrines et d'impuretés, fut purifiée en 1955 par Samuel Schwartz (10) pour donner naissance à l'hématoporphyrine dérivée (HpD) (11) qui fut appliquée chez l'homme pour l'amélioration des méthodes de diagnostic, en particulier endoscopiques (12,13).

La thérapie photodynamique connut un essor au cours des années 70. L'HpD commença à être utilisée vers 1974 comme agent thérapeutique sous l'impulsion, notamment, de l'équipe de Thomas Dougherty (Roswell Park Cancer Institute, Université de Buffalo). Ces chercheurs

montrèrent l'efficacité anti-cancéreuse à long terme de la thérapie photodynamique sur des modèles animaux tels que les rats et les souris, puis sur l'Homme (14). Dougherty *et al* ont également isolé, par purification de l'HpD par chromatographie d'exclusion, un sous-mélange plus connu aujourd'hui sous l'appellation de Photofrin®. Le Photofrin® a été approuvé pour la première fois au Canada en 1993 pour le traitement du papillome de la vessie puis son utilisation s'est répandue aux Etats-Unis, en Europe et au Japon pour le traitement de tumeurs des voies aérodigestives supérieures (15).

La recherche se concentre actuellement sur l'élaboration de nouveaux photosensibilisateurs, sur la compréhension des propriétés optiques des tissus et sur l'optimisation des protocoles utilisés dans le cadre de traitements par thérapie photodynamique. L'efficacité clinique de la PDT s'appuie sur une dosimétrie très complexe incluant des paramètres tels que la dose de lumière et de PS, le mode d'administration de la lumière (simple, fractionné ou métronomique) et du PS (topique, intraveineux, oral) et le temps séparant l'administration du PS de l'irradiation lumineuse. L'étude et la compréhension de l'influence réciproque de ces paramètres est une composante essentielle de la stratégie visant à développer les applications cliniques de la thérapie photodynamique.

1.2 Principe & réactions photochimiques

La thérapie photodynamique (PDT) est basée sur l'activation par la lumière de molécules photoactivables (photosensibilisateur) préférentiellement retenues par les tissus néoplasiques. Le temps séparant l'administration du PS de l'irradiation lumineuse de la tumeur est appelé l'intervalle drogue-lumière (IDL). Sous l'effet de l'irradiation lumineuse et en présence d'oxygène, ces colorants, non toxiques à l'obscurité, génèrent des espèces réactives de l'oxygène (ERO) de courte durée de vie, capables de provoquer des altérations tissulaires létales en réagissant avec les composants biologiques situés dans l'environnement immédiat du PS.

En photobiologie, le terme "d'action photodynamique" est réservé aux réactions de photosensibilisation consommant de l'oxygène moléculaire (5). Selon le diagramme simplifié de Jablonski (Figure 1), après irradiation et absorption d'un photon, le PS passe de l'état fondamental ($^1PS_0$) à un état triplet excité ($^1PS^*_2$) qui va être stabilisé par conversion interne (CI) au niveau d'excitation singulet de plus faible énergie (PS^*_1) et de courte durée de vie.

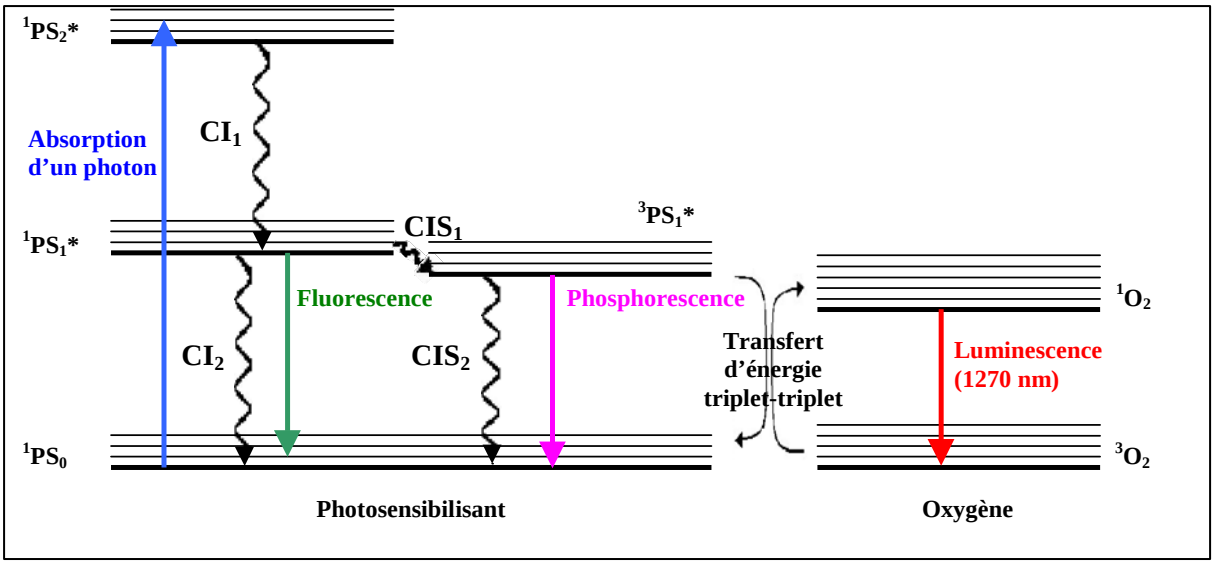

Figure 1. Diagramme simplifié de Jablonski

Peu de réactions peuvent avoir lieu à partir de cet état électronique de la molécule en raison de sa faible durée de vie (10^{-9} s). Le plus souvent, $^1PS^*_1$ rejoint un état triplet de plus faible énergie ($^3PS_1$*) par conversion intersystème (CIS)

Dans son état triplet de durée de vie plus longue (10^{-6} à 1s en fonction de son environnement), le photosensibilisateur est un agent très réactif qui va intervenir dans les réactions photochimiques de type I et II (16) (Figure 2).:

♦ **la réaction de Type I** : le PS sous son état triplet peut prendre part à un processus de transfert d'électrons ou d'hydrogènes avec un substrat biologique pour former des radicaux libres et des ions radicalaires. L'oxygène moléculaire intervient en générant des EROs, telles que le peroxyde d'hydrogène (H_2O_2), les ions superoxyde ($O_2^{\bullet -}$) et le radical hydroxyle ($^{\bullet}OH$)

♦ **la réaction de Type 2** : l'état triplet excité peut subir un processus photochimique en réagissant avec l'oxygène moléculaire et conduire à la formation d'une espèce particulièrement réactive de l'oxygène, l'oxygène singulet ($^1O_2$), de courte durée de vie.

Un rendement quantique en état triplet élevé ainsi qu'un état triplet de longue durée de vie constituent donc des pré requis pour une photosensibilisation efficace (17).

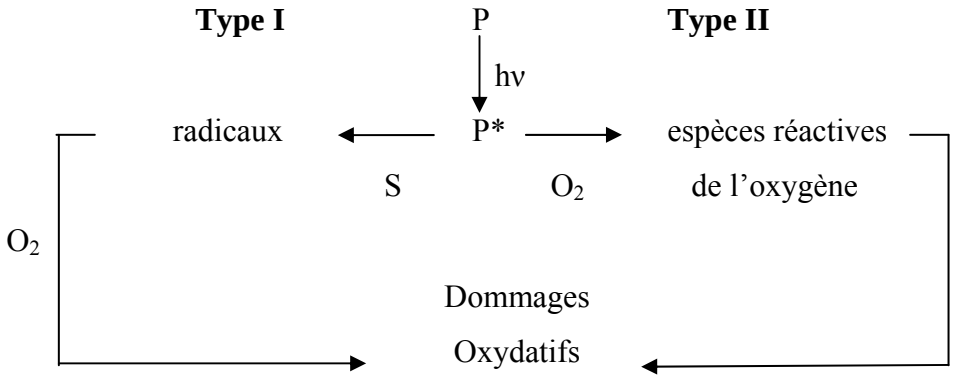

Figure 2. Les réactions photochimiques de type I et II faisant intervenir le photosensibilisateur à l'état triplet suite à son activation par la lumière.

1.2.1 Les réactions photochimiques de type I

Comme décrit précédemment, les réactions photochimiques de type I se traduisent par la production de radicaux libres ou d'ions radicalaires suite au transfert d'électrons ou d'hydrogènes entre le photosensibilisateur à l'état triplet et le substrat biologique S.
Le transfert d'électrons peut s'effectuer du photosensibilisateur vers le substrat (Eq. 1) ou du substrat vers le photosensibilisateur (Eq. 2). Cependant, la plupart des substrats biologiques vont subir une oxydation (Eq. 2).

(Eq. 1) $^3P^* + S \longrightarrow P^{\bullet +} + S^{\bullet -}$

(Eq. 2) $^3P^* + S \longrightarrow P^{\bullet -} + S^{\bullet +}$

De la même manière, le photosensibilisateur à l'état triplet (Eq. 3) et le substrat (Eq. 4) peuvent tous les deux jouer le rôle de donneur d'hydrogène.

(Eq. 3) $^3PH^* + S \longrightarrow P^{\bullet} + SH^{\bullet}$

(Eq. 4) $^3P^* + SH \longrightarrow PH^{\bullet +} S^{\bullet}$

Les espèces radicalaires générées au cours des réactions de type I peuvent intervenir dans d'autres réactions :

♦ les **formes oxydées** du photosensibilisateur (Eq. 5) ou du substrat (Eq. 6) peuvent par exemple rapidement réagir avec l'oxygène moléculaire (O_2) présent pour former des radicaux péroxydes, initiant ainsi une chaîne d'auto-oxydation.

(Eq. 5) $\begin{cases} P^{\bullet} + O_2 \longrightarrow POO^{\bullet} \\ POO^{\bullet} + PH \longrightarrow P^{\bullet} + POOH \end{cases}$

(Eq. 6) $\begin{cases} S^{\bullet} + O_2 \longrightarrow SOO^{\bullet} \\ SOO^{\bullet} + SH \longrightarrow S^{\bullet} + SOOH \end{cases}$

♦ les **formes semi-réduites** du photosensibilisateur ou du substrat peuvent également interagir de manière efficace avec l'oxygène. Dans ce cas, le transfert d'électrons qui a lieu entre les deux réactifs entraîne la formation de l'anion superoxyde, $O_2^{\bullet-}$ (Eq. 7).

(Eq. 7) $P^{\bullet-}$ (ou $S^{\bullet-}$) + $O_2 \longrightarrow$ P (ou S) + $O_2^{\bullet-}$

Une fois formé, l'anion superoxyde $O_2^{\bullet-}$ peut réagir directement avec différents substrats ou comme précurseur d'autres espèces réactives de l'oxygène. Il intervient notamment dans la formation du péroxyde d'hydrogène (H_2O_2) et du radical hydroxyle ($^{\bullet}OH$).

Même si **l'oxygène n'est pas impliqué dans la première étape du mécanisme**, sa présence dans l'environnement influence fortement les réactions photochimiques. Les processus de type I induisent la formation d'espèces réactives de l'oxygène comme le péroxyde d'hydrogène (H_2O_2), l'anion superoxyde ($O_2^{\bullet-}$) et le radical hydroxyle ($^{\bullet}OH$) qui sont reconnues comme de puissants oxydants d'une grande variété de biomolécules telles que le cholestérol ou encore les chaînes latérales de certains acides aminés (tryptophane, histidine et méthionine) (18).

1.2.2 Les réactions photochimiques de type II

Dans les réactions photochimiques de type II, **la présence d'oxygène est requise dès la première étape du processus**. Dans ce cas, un transfert d'énergie s'effectue depuis le photosensibilisateur à l'état triplet vers l'oxygène moléculaire. Le processus (Eq. 8) permet la régénération du photosensibilisateur dans son état fondamental et conduit à la formation d'oxygène singulet ($^1O_2$) qui correspond à l'état singulet de l'oxygène dont l'énergie est la plus faible.

(Eq. 8) $^3P^* + O_2 \longrightarrow P + {}^1O_2$

Le rendement quantique de production d'oxygène singulet du photosensibilisateur est un paramètre d'importance en PDT. Ce paramètre a déjà été reporté pour plus d'une centaine de molécules d'intérêt en biologie (19).

Un mécanisme alternatif d'interaction entre l'état triplet excité du photosensibilisateur et l'oxygène moléculaire implique directement un transfert d'électrons. Cette réaction entraîne la production de l'anion superoxyde et de la forme radicalaire cationique du photosensibilisateur mais reste cependant minoritaire en PDT.

1.3 Les mécanismes de photodestruction des tumeurs

Les effets antitumoraux de la PDT découlent de 2 mécanismes interconnectés (Figure 3) :

- des dommages **directs** se traduisant par un effet cytotoxique sur les cellules tumorales
- des dommages **indirects** sur la vascularisation tumorale qui se manifestent par :
  - une altération de l'oxygénation et de l'apport en nutriments des tumeurs
  - l'induction d'une forte réaction inflammatoire pouvant donner lieu au développement d'une immunité systémique.

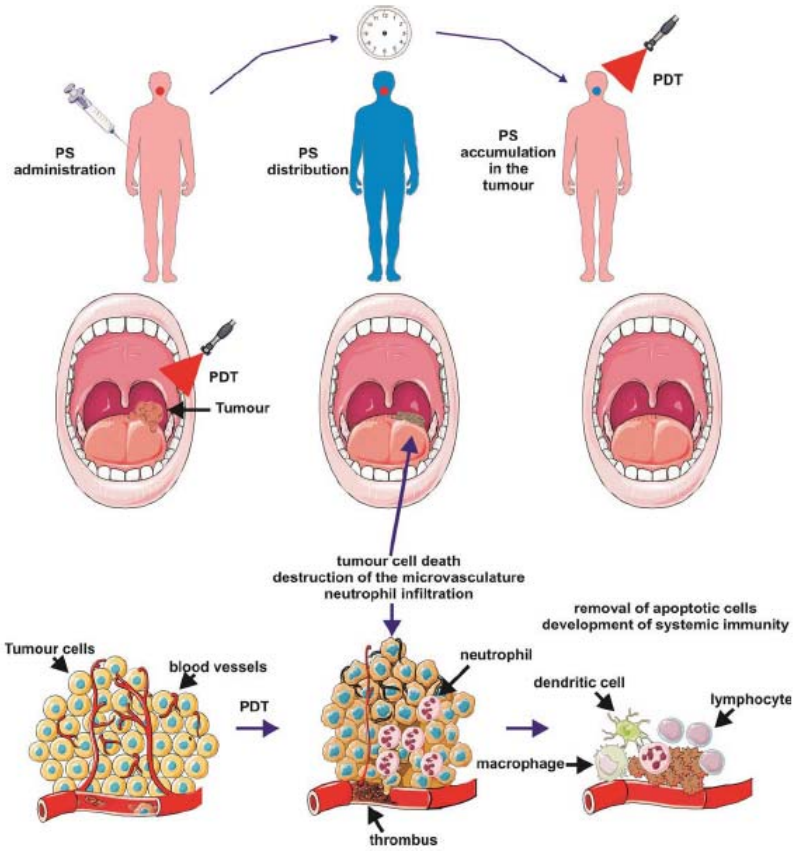

Figure 3. Principes de photodestruction de tumeurs par la Thérapie Photodynamique (d'après Agostinis et al. (20))

La contribution relative de chacun de ces mécanismes dépend principalement du type et de la dose de PS utilisés, de l'intervalle drogue-lumière, de la dose de lumière administrée, de l'oxygénation de la tumeur et fort probablement d'autres variables encore non identifiées (20). Le traitement PDT a la capacité d'induire une mort cellulaire selon diverses voies : la nécrose, l'apoptose ou l'autophagie (20). Le type de mort cellulaire photoinduite est étroitement lié à la localisation subcellulaire du photosensibilisateur. Durant la PDT, la formation d'une espèce particulièrement réactive de l'oxygène a notamment été mise en évidence : **l'oxygène singulet** ($^1O_2$), Cette molécule possède une courte durée de vie (10-320 nanosecondes) et ne diffuse qu'à une faible distance (10-55 nm) (21). Par conséquent, les sites primaires des photodommages sont étroitement liés au site de localisation intracellulaire spécifique du photosensibilisateur (22).

Localisation subcellulaire des PS

La distribution subcellulaire des photosensibilisateurs dépend en grande partie de leur degré d'hydrophobicité. Les photosensibilisateurs **hydrophobes** ont la capacité de traverser les membranes plasmiques via un processus de diffusion passive pour aller se localiser dans les structures membranaires des différents organites intracellulaires. Les organites présents dans la zone périnucléaire tels que l'appareil de Golgi et le réticulum endoplasmique sont les premiers concernés. En revanche, le noyau n'est pas un organe cible des photosensibilisateurs (23) ce qui, dans un contexte clinique, est d'une importance capitale car cela évite la formation de dommages au niveau de l'ADN qui pourraient avoir des effets carcinogènes irréversibles.

L'un des organites ciblés majoritairement et efficacement par la PDT est **la mitochondrie** (24-26). L'accumulation dans la mitochondrie de photosensibilisateurs tels que les composés lipophiliques cationiques, peut être facilitée par le gradient électrochimique de la membrane mitochondriale. De plus, les photosensibilisateurs neutres peuvent également s'accumuler dans la mitochondrie (27) de part leur affinité particulière pour certains types de lipides tels que la cardiolipine (*e.g* Phtalocyanine 4, Pc 4 (28)) ou le phosphatidyl glycol très présents au niveau de la membrane interne de la mitochondrie (29). Les porphyrines endogènes, et parmi elles la Protoporphyrine IX (PpIX), sont également des ligands des récepteurs périphériques des benzodiazépines (PBR) localisés dans la mitochondrie. D'autres porphyrines de structure voisine de la PpIX ont également une forte affinité pour les PBR (30). L'Hypéricine, particulièrement hydrophobe, se localise préférentiellement dans le réticulum endoplasmique après internalisation (31). De plus le rôle essentiel que joue la mitochondrie dans l'initiation

de **l'apoptose** par la PDT est incontestable (32). Cet aspect sera discuté ultérieurement dans le paragraphe intitulé « mort cellulaire photoinduite par PDT ».

Les photosensibilisateurs **hydrophiles** quant à eux, n'ont pas la capacité de diffuser au travers de la membrane plasmique et sont incorporés dans la cellule par endocytose. Ainsi, la mono-L-aspartyl chlorine e6 (NPe6, Talaporfin) est localisée préférentiellement au niveau des lysosomes. De manière générale, la photoactivation de photosensibilisateurs localisés dans les lysosomes et la membrane plasmique induit la mort des cellules par nécrose, alors que celle des photosensibilisateurs localisés dans les mitochondries induit l'apoptose (33).

Dommages vasculaires

Le flux sanguin est le moyen d'apporter aux tissus et aux tumeurs l'oxygène et les nutriments indispensables à leur survie. La PDT peut induire une altération du système vasculaire qui alimente la tumeur, la privant ainsi de l'oxygène et des nutriments nécessaires à sa croissance. Dans ce cas, les dommages vasculaires induisent indirectement la mort des cellules tumorales par ischémie (34). La perturbation de la microcirculation tissulaire induite par PDT fut rapportée pour la première fois en 1963 (35). L'équipe de Star *et al*. utilisa le modèle de la chambre intravitale chez des rats porteurs de tumeurs mammaires traitées par HpD-PDT (36). Ils mirent en évidence une vasoconstriction initiale des vaisseaux tumoraux suivie de réponses hétérogènes telles qu'un arrêt du flux sanguin, des hémorragies ou la formation d'agrégats plaquettaires dans de plus larges vaisseaux.

Les mécanismes des dommages vasculaires photoinduits ont été décrits selon deux événements initiateurs potentiels, conduisant chacun à une destruction tumorale par collapsus vasculaire, arrêt du flux sanguin et hémorragie (37) :

- *les dommages directs aux cellules endothéliales*

Les cellules endothéliales sont exposées à des doses plus importantes de PS et d'oxygène (38). Le traitement par PDT peut induire une rapide dépolymérisation des microtubules du cytosquelette cellulaire (suite à un influx calcique), entrainant un arrondissement et une contraction des cellules endothéliales et par conséquent une interruption des jonctions cellulaires et la perte des communications intercellulaires (34). Tous ces évènements conduisent à une augmentation de la perméabilité vasculaire, une fuite des éléments sanguins et une diminution de la perfusion tumorale (39). L'exposition de la matrice extracellulaire et de la lame basale suite à l'altération de l'endothélium entraine une activation des plaquettes et

des neutrophiles polymorphonucléaires (PMN) qui viennent adhérer à la paroi de l'endothélium et réduisent ainsi le diamètre luminal. Cette activation est concomitante à la production de thromboxane (Tx), une prostaglandine vasoconstrictrice au pouvoir agrégeant de la famille des eïcosanoïdes, qui contribue à amplifier l'agrégation plaquettaire et qui constitue également un puissant vasoconstricteur.

- *la rupture de l'équilibre entre facteurs vasoconstricteurs et vasodilatateurs*

A titre d'exemple, le monoxyde d'azote (NO) est un facteur vasodilatateur et anti-coagulant permettant d'éviter la thrombose des vaisseaux tumoraux. Son oxydation par les EROs rompt l'équilibre préexistant au sein des vaisseaux tumoraux entre facteurs pro- et anti-coagulants. Parallèlement, les produits générés (principalement le péroxyde nitrique, ONO_2) induisent l'apoptose des cellules endothéliales et la formation de caillots sanguins conduisant à l'occlusion vasculaire (40). La privation des cellules tumorales en oxygène et nutriments, associée à une deuxième vague de radicaux a été démontrée comme conduisant à une nécrose puis à une cure tumorale.

Activation du système immunitaire

Les recherches pré-cliniques conduites chez divers modèles animaux ont permis une meilleure compréhension des réponses immunitaires photoinduites (41,42). Diverses études réalisées sur des tumeurs portées par des souris immunocompétentes ou immunodéficientes ont révélé que, malgré une efficacité similaire de la PDT à court terme, seules les souris immunocompétentes présentaient une réponse complète au traitement, témoignant ainsi de l'implication majeure du système immunitaire dans la réussite du traitement par PDT (43,44).

1.4 Mort cellulaire induite par PDT

1.4.1 La nécrose

La nécrose est traditionnellement considérée comme une forme de mort cellulaire passive et non régulée. Elle est la forme principale de mort cellulaire lors d'accidents traumatiques, suite à certaines pathologies ou lors de déficits métaboliques. La nécrose est morphologiquement caractérisée par un gonflement de la cellule et une vacuolisation du cytoplasme. La rupture de la membrane plasmique qui en résulte conduit à la libération dans le milieu extérieur du contenu cytoplasmique. (Figure 4).

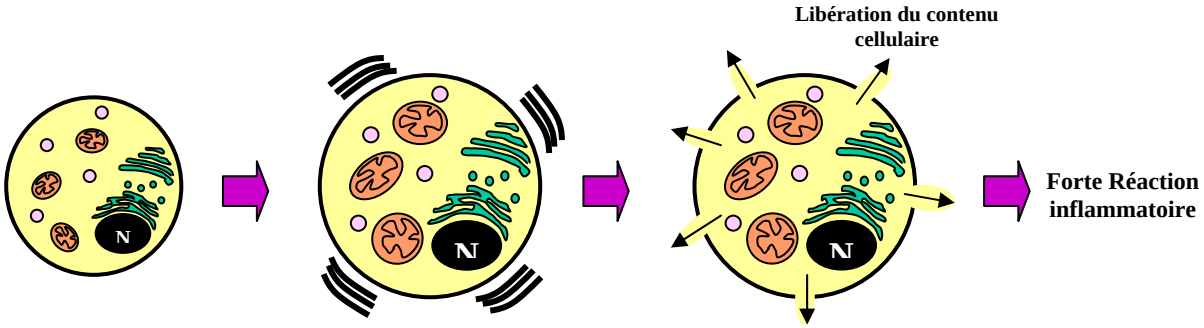

Figure 4. Modifications morphologiques au cours de la mort cellulaire par nécrose

La nécrose est accompagnée habituellement d'une réponse inflammatoire qui consiste en la présence d'exsudats et de cellules spécialisées du système hématopoïétique comme les lymphocytes et les macrophages (45). A la suite d'un stress photooxidatif, les PSs induisent la péroxydation du cholestérol membranaire ainsi que d'autres phospholipides insaturés. Ces dommages sont à l'origine de phénomènes d'enflement et de bourgeonnement, de la libération de vésicules contenant des enzymes membranaires et d'une inhibition de l'activité des ATPases (46). La perte de l'intégrité membranaire et de l'homéostasie ionique conduit rapidement les cellules à la mort par nécrose.

Dans un contexte clinique, la mort par nécrose des tissus s'accompagne d'une perte de substance donnant lieu à d'importantes douleurs pour le patient mais également de possibles complications liées à la dégradation trop brutale des tissus (perforations d'organes…).

1.4.2 L'apoptose

L'apoptose est définie comme une mort cellulaire génétiquement programmée et met en jeu différentes voies de signalisation intracellulaire complexes aboutissant au démantèlement cellulaire**.** L'apoptose fut pour la première fois décrite par Kerr *et al* (47). Elle joue un rôle essentiel durant le développement et l'homéostasie tissulaire et sa dérégulation a des conséquences pathologiques telles que des anomalies du développement, des désordres immunitaires, des maladies neurodégénératives ou des cancers.

Les caractéristiques morphologiques de l'apoptose (Figure 5) sont les suivantes:

- ♦ Bourgeonnement de la membrane plasmique,
- ♦ Rétrécissement cellulaire par condensation du cytoplasme et de la chromatine,
- ♦ Fragmentation de l'ADN internucléosomal,
- ♦ Formation de vésicules : les corps apoptotiques.

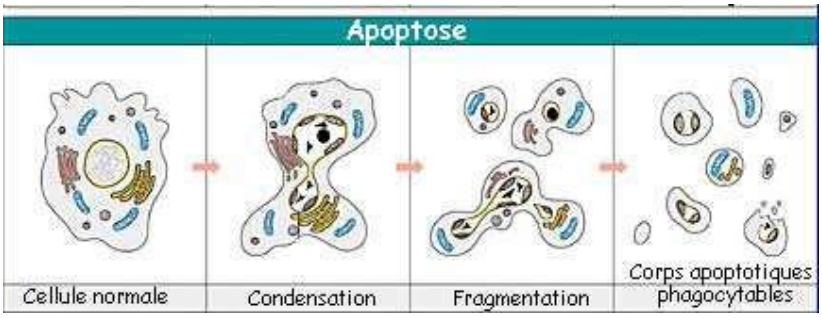

Figure 5. Modifications morphologiques au cours de l'apoptose (d'après lecerveau.mcgill.ca)

Trois voies d'induction d'apoptose par la PDT ont été décrites (Figure 6) (48) . La **voie extrinsèque** faisant intervenir des récepteurs membranaires de la super-famille des TNFR (Tumor Necrosis Factor Receptor) et la **voie indépendante des caspases** ont un impact mineur par rapport à la **voie intrinsèque** faisant intervenir la mitochondrie. En effet, du fait de l'importance du stress oxydatif produit au niveau des organites cellulaires, la voie intrinsèque de l'apoptose est majoritaire en PDT.

La réponse apoptotique intrinsèque induite par la PDT s'explique entre autre par le fait que de nombreux PS ont pour cible la mitochondrie (23,49). De plus, certains PSs se localisant dans d'autres organites tels que les lysosomes, le réticulum endoplasmique ou l'appareil de Golgi (23,24,50,51) peuvent induire une apoptose des cellules par l'intermédiaire de signaux qui convergeront vers la mitochondrie. Celle-ci joue donc un rôle central dans le processus apoptotique (52-54).

La voie intrinsèque de l'apoptose se caractérise par la libération rapide du cytochrome c mitochondrial vers le cytosol (55,56) accompagnée ou non de la perte du potentiel membranaire mitochondrial (53). La formation d'un complexe appelé « apoptosome », entre le cytochrome c, l'APAF-1 (apoptosis activating factor), le dATP et la procaspase 9 (57) va conduire à l'activation de la cascade des caspases, notamment les caspases effectrices 3, 6 et 7 qui sont des éléments centraux dans le processus de mort cellulaire programmée (56,58). L'activation des caspases aboutit alors au clivage de substrats indispensables à la survie cellulaire (Figure 6) tels que la protéine DFF45 (ICAD) dont le clivage par les caspases effectrices induit l'activation de nucléases. L'ADN est digéré au niveau de sites internucléosomaux puis il y a formation de corps apoptotiques qui sont ensuite phagocytés par les macrophages. D'autres protéines sont également altérées : inactivation des protéines topoïsomérases de réparation et de réplication de l'ADN due au clivage de PARP, inactivation des protéines intervenant dans l'épissage de l'ARN messager, destruction des lamines due au

clivage de la caspase 6 entraînant une condensation de la chromatine, clivage des protéines du cytosquelette d'où une perte de structure et d'adhésion cellulaires.

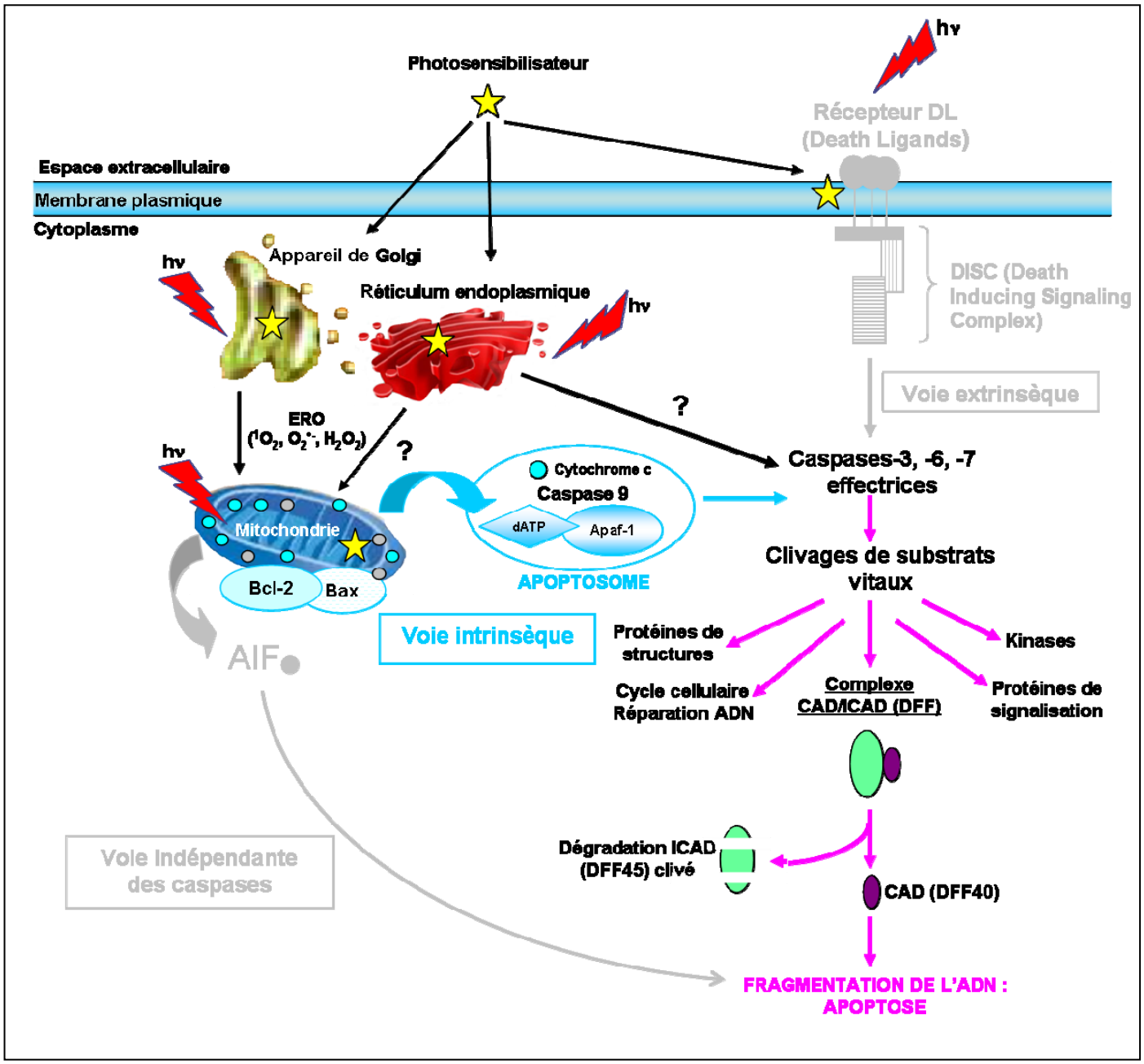

Figure 6. Les différentes voies d'activation de l'apoptose induites par la thérapie photodynamique

1.4.2.1 *In vitro*

In vitro, l'apoptose peut être conditionnée par différents paramètres tels que le type cellulaire employé (cellule compétente pour l'apoptose), la concentration et la localisation intracellulaire du PS (33). Considérant que les mitochondries sont des organites-clés dans l'apoptose photoinduite, il est logique que l'apoptose induite par la PDT soit très rapide (quelques heures) (33). Malgré cela, il a été rapporté que les photosensibilisateurs avec une localisation autre que mitochondriale, émettent des signaux toxiques qui convergent sur les mitochondries (48) (Figure 6)**.**

1.4.2.2 *In vivo*

In vivo, les études sur l'apoptose induite par PDT portent sur différents types de tumeurs pour différents types de photosensibilisateurs. Le tableau 1 issu de la revue d'Oleinick *et al* (33) a été mis à jour et liste ces différentes études. Même si à l'heure actuelle diverses techniques sont disponibles pour la détection de l'apoptose *in vivo* (immunohistochimie, TUNEL (terminal deoxynucleotidyl transferase-mediated dUTP nick end labelling), électrophorèse sur gel d'acrylamide…), la localisation intratumorale ainsi que la quantification des cellules apoptotiques photoinduites par PDT n'ont été que très peu étudiées *in vivo*.

Une seule publication a montré une apoptose initiale des cellules endothéliales 4 heures post PDT suivie d'une extension au parenchyme tumoral suite à un traitement Photofrin®-PDT sur des tumeurs de sarcomes humains xénogreffées sur souris « nude ». Cette localisation intratumorale de l'apoptose a été réalisée via une technique imminohistochimique de co-marquage des cellules endothéliales (anticorps anti-PECAM : Platelet Endothelial Cell Adhesion Molecule) et de l'apoptose par la technique du TUNEL (59).

Il y a également une seule observation d'apoptose induite par la mTHPC-PDT *in vivo* à la suite du traitement de tissus crâniens normaux et tumoraux. L'analyse histologique a montré la mort des cellules majoritairement par nécrose avec un taux d'apoptose assez faible qui apparait inversement proportionnel à la dose de lumière appliquée (60)**.** L'apoptose photoinduite par un traitement mTHPC-PDT *in vivo* reste très peu décrite. Aucune optimisation des conditions de traitement favorisant la mort par apoptose du tissu tumoral n'a encore été mise en évidence.

Photosensibilisateurs	Modèles animaux	Références
Photofrin® ALA/Pp IX, mTHPC AlClPc, SnET2	Cerveau normal, lapins Tumeurs intracrâniennes VX2, souris	(60)
Photofrin®	Sarcome humain A673, souris « nude »	(59)
	Glioblastome intracérébral humain U87, souris « nude »	(61)
	Carcinome épidermoïde murin NR-S1, souris	(62)
	Tumeur humaine biliaire NOZ, souris	(63)
	Mélanome humain HTB-67, souris SCID	(64)
	Adénocarcinome humain pulmonaire ASTC-a-1, souris « nude »	(65)
ALA, PpIX, HAL	Gliosarcome 9L, rat	(66)
	Adénocarcinome colique murin Colo-26, souris	(67)
	Tumeur vésicale orthotopique, rat	(68)
	Carcinome épidermoïde humain Me180, souris « nude »	(69)
Methyl ester of 5-aminolevulinic acid (Methyl-ALA)	Adénocarcinome humain ovarien HTOA, MCAS et TOV21G, souris « nude »	(70)
mTHPC PEG conjugué	Adénocarcinome mammaire, souris	(71)
Verteporfin	Néovascularisation choroïdale, rat	(72)
	Carcinome épidermoïde A431, souris « nude »	(73)
Npe6	Tumeur humaine glandes salivaires HSG, souris « nude »	(74)
Chlorine e6 (Ce6)	Tumeur épithéliale rénale RK3E-ras, rat	(75)
Talaporfin sodium	Tumeur cérébrale, rat	(76)
HPPH (2-[1-hexyloxyethyl]-2-devinylpyropheophorbide)	Adénocarcinome colique murin Colo-26, souris	(77)
Hypéricine	Fibrosarcome humain radio-induit RIF-1, souris	(78)
	Tumeur vésicale, souris « nude »	(79)
	Adénome pituitaire GH4C1, rat	(80)
Phtalocyanine 4 (Pc4)	Fibrosarcome humain radio-induit RIF-1, souris	(81)
	Papillome cutané chimio ou radio-induit, souris	(82)
	Papillome cutané chimio-induit, souris	(83)
	Carcinome humain ovarien OVCAR-3, souris « nude »	(84)
	Adénocarcinome colique humain SW480, souris « nude »	(85)
	Adénocarcinome mammaire murin LM2, souris	(86)
	Carcinome hépatique HepG2, souris « nude » Carcinome colique HT29, souris « nude »	(87)
Indole-3-acetic acid (IAA)	Tumeur hépatique SK-HEP-1, souris « nude »	(88)
Methylène blue (MB)	Mélanome humain B16F1, souris SCID	(89)
	Adénocarcinome mammaire JC, souris	(90)

Tableau 1. L'apoptose photoinduite par PDT évaluée dans des modèles précliniques

1.5 Les photosensibilisateurs

1.5.1 Propriétés idéales d'un photosensibilisateur

L'hématoporphyrine et ses dérivés purifiés comme le Photofrin®, le Photosan® et le Photohem® ont été les premiers PSs utilisés en PDT et sont référencés comme étant des PSs de première génération. Ces PSs présentent cependant des inconvénients majeurs. Leur sélectivité tumorale réduite et leur clairance lente conduisent à une photosensibilisation cutanée de plusieurs semaines à laquelle s'ajoute une faible absorption dans le rouge qui rend le traitement des tumeurs profondes difficiles. De plus, ces composés sont des mélanges de composition complexe et difficile à reproduire qui faussent les études dose-réponse. Ces inconvénients ont conduit à l'élaboration d'une liste de critères auxquels un PS doit répondre:

- composé **pur** et facile à synthétiser
- faible **toxicité** à l'obscurité et photosensibilité cutanée limitée
- bonne **sélectivité** tumorale et clairance rapide
- **rendement quantique** en oxygène singulet élevé
- forte **absorption** entre 620 et 800 nm (fenêtre thérapeutique).

Le paramètre le plus critique reste la profondeur de pénétration de la lumière dans les tissus qui dépend de divers phénomènes tels que la réflexion, la diffusion, la transmission, l'absorption ou une combinaison d'entres eux (Figure 7). La lumière bleue pénètre moins profondément dans les tissus que la lumière rouge et infrarouge. La zone allant de 620 à 800 nm est la seule à présenter une relation étroite entre la profondeur de pénétration de la lumière et la longueur d'onde de la source lumineuse incidente. Ainsi, à l'intérieur de cette « fenêtre thérapeutique », plus la longueur d'onde est élevée et plus la lumière pénètre profondément dans les tissus (3-8 mm de 630 à 800 nm) (91).

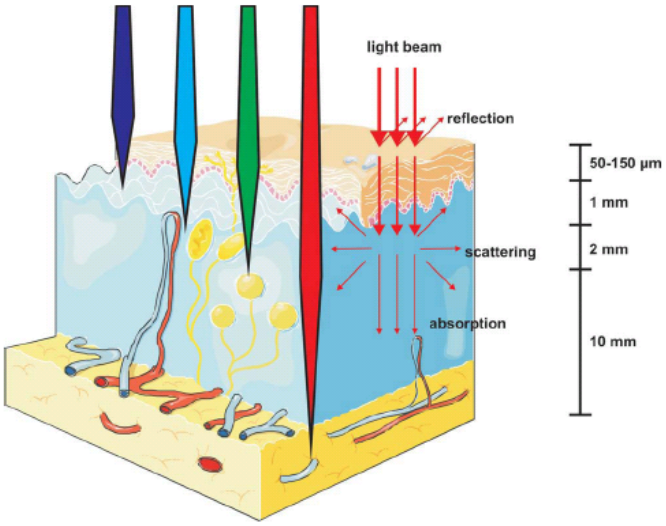

Figure 7. Profondeur de pénétration de la lumière dans les tissus en fonction de la longueur d'onde utilisée (d'après Agostinis et al. (20))

Les principaux PSs utilisés pour la PDT et ayant obtenu une autorisation de mise sur le marché (AMM) sont présentées dans le Tableau 2.

PHOTOSENSIBILISATEUR	STRUCTURE	LONGUEUR D'ONDE (nm)	AMM	ESSAIS	TYPES DE CANCER
Porfimer sodium (Photofrin) (HpD)	Porphyrine	630	Mondial	-	Poumons, oesophage, voie billiaire, vessie, cerveau, ovaire
ALA	Précurseur Porphyrine	635	Mondial	-	Peau, vessie, cerveau, oesophage
Esters d'ALA	Précurseur Porphyrine	635	Europe	-	Peau, vessie
Temoporfin (Foscan®) (mTHPC)	Chlorine	652	Europe	Etats-Unis	Tête et cou, poumon, cerveau, peau, voie billiaire
Verteporfin (Visudine)	Chlorine	690	Mondial (DMLA)	Royaume Uni	Ophthalmique, pancreas, peau
HPPH	Chlorine	665	-	Etats-Unis	Tête et cou, oesophage, poumon
SnEt2 (Purlytin)	Chlorine	660	-	Etats-Unis	Peau,sein
Talaporfin (LS11, NPe6)	Chlorine	660	-	Etats-Unis	Foie, colon, cerveau
Ce6-PVP (Fotolon), dérivés Ce6 (Radachlorin, Photodithazine)	Chlorine	660	-	Biélorussie Russie	Sarcome nasopharyngé, cerveau
Silicon phthalocyanine (Pc4)	Phthalocyanine	675	-	Etats-Unis	Lymphome cutané cellules T
Padoporfin (TOOKAD)	Bacteriochlorine	762	-	Etats-Unis	Prostate
Motexafinlutetium (Lutex)	Texaphyrine	732	-	Etats-Unis	Sein

Tableau 2. Liste des photosensibilisateurs actuellement utilisés en clinique (d'après Agostinis et al (20))

1.5.2 Les photosensibilisateurs de 2ème et 3ème générations

Les PS de deuxième génération ont été mis au point afin de pallier les défauts de ceux de première génération. La majorité d'entre eux testés en clinique sont de nature tétrapyrrolique (porphyrines, chlorines, bactériochlorines) et présentent un fort rendement quantique en oxygène singulet ainsi qu'une forte absorption dans les grandes longueurs d'onde.

Les PS de troisième génération sont en fait des PS de deuxième génération modifiés de façon à cibler activement les cellules tumorales. L'addition de divers groupements chimiques (acides aminés, sucres, protéines, polymères, hydrates de carbone), le couplage à des anticorps spécifiques ou l'inclusion de PS dans des liposomes sont les stratégies les plus fréquemment utilisées (92). En effet, ces groupements sont intéressants de part leur affinité

particulière pour les antigènes ou les récepteurs surexprimés à la surface des cellules tumorales ou bien encore leur propriétés pharmacocinétiques particulières.

1.5.3 La mTHPC : meta-tetra(hydroxyphenyl) chlorine

1.5.3.1 Description & caractéristiques

La mTHPC (Foscan®, Temoporfin) est un photosensibilisateur de seconde génération découvert en 1989 par l'équipe de Bonnet *et al*. (93) (Figure 8) et actuellement commercialisé par Biolitec GmbH (Iéna, Allemagne).

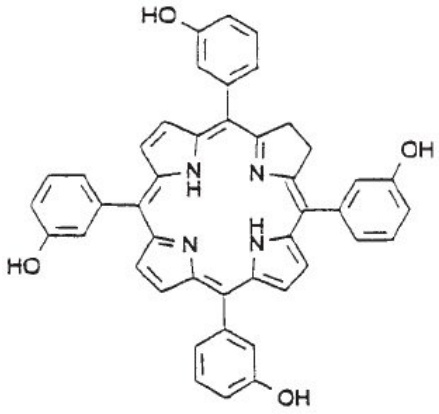

Figure 8. Structure moléculaire de la mTHPC

Cette molécule est issue de la réduction d'une double liaison du noyau tétrapyrrolique de la porphyrine analogue (la méta-tétrahydroxyphényl-porphyrine) et présente de nombreux avantages (Tableau 3).

Propriétés photodynamiques	**Avantages**
Pureté > 99%	Composition stable du médicament
Coefficient d'extinction molaire (29 600 $M^{-1}.cm^{-1}$ à 650 nm)	Absorption optimale ε 20 fois > celui du Photofrin®
Absorption à 652 nm (rouge)	Pénétration plus profonde de la lumière dans les tissus
Longue durée de vie de l'état triplet (250 ns dans méthanol)	Production d'un plus grand nombre d'espèces réactives de l'oxygène
Grande sélectivité pour les cellules cancéreuses	Cellules saines préservées
Faible photosensibilité cutanée (36 semaines)	Diminution des effets secondaires par exposition au soleil
Fort rendement quantique en état triplet (0,89 dans méthanol)	Production d'un plus grand nombre d'espèces réactives de l'oxygène
Faible toxicité à l'obscurité	Diminution des effets secondaires pour le patient

Tableau 3. Avantages conférés par les propriétés photodynamiques du Foscan®

La mTHPC est un produit pur à plus de 99 %, faiblement toxique à l'obscurité et présentant une accumulation préférentielle dans le tissu tumoral. Elle possède un pic d'absorption dans le rouge à une longueur d'onde de 652 nm (Figure 9) et un coefficient d'extinction molaire élevé dans le méthanol de 29600 $M^{-1}.cm^{-1}$. A ces propriétés, s'ajoute un fort rendement quantique en état triplet (0,89 dans le méthanol) et une grande capacité de rétention et d'accumulation dans les tissus néoplasiques (94).

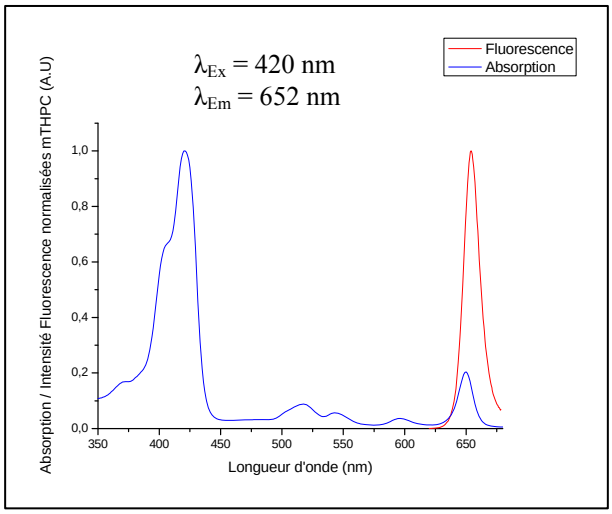

Figure 9. Spectres d'absorption et d'émission de fluorescence de la mTHPC dans l'éthanol

Toutes ces propriétés ont permis au Foscan® de recevoir son autorisation de mise sur le marché en 2001 en Europe comme traitement palliatif de nombreux types de cancers de la tête et du cou ayant préalablement résistés aux autres thérapeutiques et ne relevant ni de la chirurgie, ni de la radiothérapie, ni de la chimiothérapie. A l'heure actuelle, le Foscan® est un des PSs les plus actifs sur le marché. A titre d'exemple, le Foscan® est 100 à 200 fois plus actif que le Photofrin®, son ancêtre de première génération.

Le Foscan® présente un avantage important par rapport aux autres photosensibilisateurs approuvés en clinique qui réside dans son effet cytotoxique élevé qui permet d'utiliser des fluences moins importantes (10-20 J/cm²) que pour le Photofrin® (100-200 J/cm²) ou l'ALA/PpIX (100 J/cm²). La sensibilisation cutanée est également moindre (2-4 semaines) par rapport au Photofrin® (4-12 semaines).

1.5.3.2 Pharmacocinétique & localisation intratumorale

Des études précliniques ont montré l'importance de l'IDL dans la PDT avec le Foscan®. De longs intervalles drogue-lumière semblent limiter les dommages sur les tissus sains et ciblent d'avantage les tissus cancéreux. C'est pourquoi actuellement, un IDL de 96 heures est préconisé pour le traitement par mTHPC-PDT en clinique. Néanmoins, les travaux réalisés dans des modèles précliniques montrent qu'un IDL plus court semble plus efficace. L'étude sur des tumeurs xénogreffées a permis d'établir que l'efficacité de la mTHPC-PDT est optimale à un IDL de 3 heures et étroitement corrélée aux dommages vasculaires observés, eux-mêmes en relation avec la localisation plasmatique du PS (95,96). Ainsi Jones *et al* ont observé que le pic d'activité de la PDT obtenu avec un IDL de 2 heures pour des tumeurs xénogreffées sur des rats BDIX se traduisait par un effet vasculaire du traitement alors que le second pic observé avec un IDL de 24 heures correspondait à un effet beaucoup plus direct de la PDT sur les cellules tumorales (97).

Néanmoins, il persiste des incohérences entre la quantité de PS présente dans le plasma et l'apparition de dommages vasculaires suite au traitement (98). Notre équipe, en collaboration avec l'équipe américaine du Pr. Foster (Université de Rochester, New York), a proposé une autre approche de la biodistribution de la mTHPC dans les tissus tumoraux en utilisant une technique de microspectrofluorimétrie confocale (99). Ce travail a mis en évidence le gradient tumoral de la mTHPC à partir des vaisseaux indiquant le confinement de la mTHPC dans les vaisseaux pour un IDL de 3 heures, sa fuite des vaisseaux à 6 heures et sa localisation dans les cellules néoplasiques 24 heures après injection. Cependant, la corrélation entre ce type de distribution (distribution « cartographique ») de la mTHPC et l'efficacité n'a jamais été établie.

Le profil pharmacocinétique du Foscan® dans le plasma humain se distingue nettement de celui obtenu chez la souris (100) ainsi que de ceux obtenus avec les autres photosensibilisateurs (100,101). Dans le plasma humain, il semble qu'un niveau stable en Foscan® soit maintenu au moins pendant 10 heures alors que chez la souris une chute bi-exponentielle classique de la concentration en Foscan® est observée (100).
Cette spécificité observée chez l'humain a été attribuée à deux processus distincts : soit une agrégation du Foscan®, soit la liaison du Foscan® avec une fraction plasmatique de lipoprotéines de haute densité (HDL) immédiatement après injection, suivie d'une lente

redistribution vers l'ensemble des lipoprotéines du plasma (101). Cependant l'étude de Triesscheijn *et al* (100) ne montre pas de différence de liaisons aux HDL entre l'humain et la souris. De plus, une augmentation du taux de LDL dans le plasma de la souris, de façon à être comparable au plasma humain, ne modifie pas la pharmacocinétique du Foscan® chez la souris. Les auteurs écartent l'hypothèse d'une influence des lipoprotéines du plasma sur la pharmacocinétique plasmatique du Foscan® (100). Toutes espèces confondues, le Foscan® s'accumule majoritairement dans les organes perfusés tels que les reins, les poumons et le foie (102). Le ratio de concentration tumeur/tissu sain varie de 1 à 14 suivant le modèle tumoral et le tissu sain pris en compte (95,97).

2. CIBLAGE PASSIF PHOTOINDUIT DE TUMEURS

Publication n°1 : “Contrasting facets of nanoparticles-based phototherapy : photodamage and photo-regeneration”

Ce second chapitre présente une revue réalisée sur invitation (NOVA Publishers) pour un ouvrage intitulé : « **Photodynamic Therapy : New Research** ». Ce rapport décrit notamment l’intérêt des formulations liposomales de photosensibilisateurs ainsi que les paramètres importants à prendre en compte lors de l’utilisation de ces nanovésicules lipidiques pour un traitement photodynamique efficace.

La seconde partie de cette revue porte sur un aspect très différent de la PDT, à savoir sa capacité à stimuler la cicatrisation et donc la réparation tissulaire suite à une blessure. Cette partie a été réalisée en relation avec un article récemment accepté pour publication et figurant en dans la partie « Production Scientifique » de ce manuscrit :

***Julie Garrier**, Lina Bezdetnaya, Catherine Barlier, Susanna Gräfe, François Guillemin, Marie-Ange D’Hallewin.*

”Foslip® - based Photodynamic Therapy as a means to improve Wound Healing”

PhotoDiagnosis and Photodynamic Therapy. 2011; 8(4):321-327.

In: Photodynamic Therapy: New Research
Editor: Mohamed Lotfy Taha Elsaie, Ph.D, pp. xx
ISBN

Chapter

CONTRASTING FACETS OF NANOPARTICLES-BASED PHOTOTHERAPY: PHOTO-DAMAGE AND PHOTO-REGENERATION

Julie Garrier*, Vadzim Reshetov*∂, Vladimir Zorin∂, François Guillemin*, Lina Bezdetnaya*

j.garrier@nancy.unicancer.fr, vadim.reshetov@gmail.com, vpzorin@mail.ru, f.guillemin@nancy.unicancer.fr, l.bolotine@nancy.unicancer.fr

* Centre de Recherche en Automatique de Nancy (CRAN), Nancy-University, CNRS, Centre Alexis Vautrin, Vandœuvre-lès-Nancy, France

∂ Laboratory of Biophysics and Biotechnology, Physics Faculty, Belarusian State University, Belarus.

Abstract

The present review describes two different applications of the phototherapy. The first one referred as Photodynamic Therapy (PDT) is widely used for pathologically proliferated tissues, including cancer. PDT is based on the combined action of three parameters: photosensitizer, light and oxygen, resulting in the production of toxic reactive oxygen species. To improve the selectivity of phosensitizers for pathological tissues the liposomal photosensitizers formulations have been proposed favoring tumor targeting. The comprehension of the mechanisms that govern the drug release processes of photosensitizers in liposomal nanostructres and as such their pharmacokinetics behavior is essential and is addressed in the present review.

Another facet of nanoparticle-based photoinduced therapy is related to tissue regeneration. Complex mechanisms of photoinduced wound healing and repair will be considered, including the role of different cell types, growth factors and antimicrobial action.

In conclusion, PDT offers two contrasting strategies either to eradicate pathological tissues or to stimulate tissue repair. In fine, consideration of all parameters involved in this kind of phototherapy is required to obtain a desired effect and optimize clinical protocols.

Garrier.J

Introduction

Photodynamic Therapy (PDT) is regarded as an exposure therapy used in clinical settings. This treatment strategy is based on the combined action of a molecule called the photosensitizer (PS), light and molecular oxygen. PDT involves the PS administration followed by local light illumination of targeted tissues at the appropriate wavelength to activate the PS. The molecule can further react with oxygen to produce damaging reactive oxygen species (ROS).

This photoinduced oxidative stress is the basis of damaging effect of PDT resulting in destruction of pathological tissues. PDT is applied for cancer treatment, specifically for small localized tumors accessible to the visible light irradiation (bladder, skin, head and neck, esophageal…). Tumoricidal effect of PDT is triggered by a direct damage of malignant cells producing cell death by necrosis and/or apoptosis. PDT also affects tumor vasculature, causing the shutdown of vessels with subsequent depriving of the tumor with oxygen and nutrients. Finally, PDT can immunostimulate or immunosupress the immune system. A serious limitation of photodynamic therapy (PDT) is the absence of specific cancer targeting, resulting in an excessive tissue destruction, which can provoke life threatening situations. To partially overcome these constraints, incorporation of the active compound into liposomal nanoparticles can be proposed. Embedding of active drugs in liposomes favours passive targeting of tumors through Enhanced Permeability Retention (EPR) effect. Liposomal formulations of second-generation photosensitizers enable a more selective and more rapid accumulation of drugs in the tumors, with a faster clearance, together with a better efficiency. The possible difficulties consist in specific photosensitizer behaviour in bulk lipid milieu. Therefore, a comprehension of redistribution patterns of PSs from liposomes of different motifs to biological structures *in vitro* is essential. Kinetic parameters will directly influence spatial intratumoral distribution of PSs and provide indications to the photosensitizer transport from the vessels towards extravascular structures. The visualization of these processes in real time *in vivo* is a crucial point. The model that is particularly well adapted to study vasculature effects of exposure therapy treatments is the chick chorioallantoic membrane (CAM). Advantages of this model for PDT effects are described in the present review. *In fine*, consideration of all above mentioned parameters that will rend possible an optimization of clinical protocols is the core of present review.

Another facet of nanoparticle-based photoinduced therapy is related to the improvement of tissues regeneration, mostly referred here as wound healing or repair. The grounds of photo-induced tissues repair are complex and not completely elucidated, the main mechanisms to consider are photoinduced immunomodulation, microorganisms' inactivation and growth factors stimulating production. In function of the photosensitizer, light dose and the type of tissue wound healing process can be altered, stimulated or unchanged.

Thus, beneficial and damaging effects of phototherapy will be discussed in the present review.

1. THE PHOTODYNAMIC THERAPY (PDT)

Photodynamic therapy (PDT) is a therapeutic strategy for the treatment of localized tumors accessible to light illumination. It consists of the systemic or local administration of a molecule called "photosensitizer" (PS) which accumulates selectively in malignant tissues

due to physiological alterations in the pathological environment like *e.g* leaky vasculature, abnormal enzymatic activity, pH variations or reduced lymphatic drainage. The local irradiation of the diseased area activates the PS combined with light and molecular oxygen to lead to the generation of cytotoxic reactive oxygen species (ROS) [1].

Photochemical reactions of type 1 and type 2 constitute the origin of the efficacy of the PDT treatment. In the Type 1 reaction, the PS reacts directly with a substrate (cell membrane or a molecule) to form radicals which can further react with molecular oxygen to produce ROS. Alternatively, in the Type 2 reaction, the triplet PS can transfer its energy directly to the molecular oxygen to form excited state singlet oxygen or perform an electron transfer to molecular oxygen and generate superoxide anion radical. Both Type 1 and Type 2 reactions can occur simultaneously and the ratio between them depends on the PS used and the concentration in substrates and oxygen [2]. Due to the high reactivity, short diffusion distance (0.01 µm - 0.02 µm) and short half-life of singlet oxygen (40 ns) and hydroxyl radicals, only molecules and structures that are proximal to the production site (*i.e* PS localization site) are directly affected by PDT [3, 4]. The tumoricidal effect of PDT is triggered by the direct damage of malignant cells and/or indirect vascular damage accompanied by an immune response. The contribution of each type of damage depends on different parameters: the type of the PS and its localization in the tumor, the rate of vascularity and macrophage content in the tumor [5].

Photosensitive agents and light have been used for medical purposes for a long time. The first health agency approval for PDT was obtained in 1993 in Canada for the prophylactic treatment of bladder cancer with Photofrin®[1]. Regulatory approvals for the clinical use of PSs and PDT light applicators now exist in many countries around the world though the total number of approved clinical indications is still limited. Potential clinical applications of PDT are diversified [6]. Dermatological, ophthalmic and cardiovascular diseases are considered but here we shall focuse on oncological diseases. Different types of cancer were tested for the treatment by PDT and some of them were finally approved : head and neck cancers, urological and gynecological cancers [7].

1.1 Dosimetry

The optimization of the applied dosimetry in PDT treatment is still a very important research topic passing through the study of the major parameters of interest: the photosensitizer administration (route, conditions, formulation), the time of the administration and irradiation and the irradiation procedure (delivered light intensity) [8].

1.1.1 Drug light interval (DLI)

PS distribution in the tumor can be modulated by the drug light interval (DLI) which corresponds to the time that separates the PS administration from the illumination [9]. Indeed, compartmental targeting of the tumor microvasculature or parenchyma is closely related to the PS distribution, governed by the pharmacokinetic and cell/tissue binding properties of the PS.

Vascular damage are observed when irradiation is performed with short DLI which corresponds to vascular localization of the PS [10-12]. On the contrary, for long DLI, direct tumor cell destruction is obtained when the PS content is high within the tumor cells [13, 14]. The mechanism responsible of the tumor cell destruction depends on the intracellular localization of the PS. Photosensitizers can be located in the mitochondria, the endoplasmic

reticulum, the plasmic membrane or lysosomes and PDT treatment can trigger the cell death either by apoptosis or necrosis [15-20].

1.1.2 Light delivery

The choice of the light source, irradiation wavelength, light dose and intensity are primordial for a successful PDT treatment. The light source must exhibit suitable spectral characteristics that coincide with the maximum absorption wavelength range of the PS applied in order to generate enough ROS to produce a cytotoxic effect [2]. A critical parameter for consideration in discussing the efficacy of PDT is the depth of light penetration through tissues which is dependent on several processes including reflection, scattering, transmission, absorption or a combination of these. The 620 to 800 nm wavelength range is often called the "therapeutic window" where light penetration is maximal (3-8 mm for 630-800 nm) [21]. Photodynamic dose treatment is described as a fluence (J/m^2) and a fluence rate (W/m^2). It has been nicely demonstrated with biological outcomes, such as skin photosensitivity, clonogenic assays, tumor regrowth assay and tumor cure rates, that PSs have lower efficacy when high optical fluence rates are used [22, 23].

1.1.3 Oxygenation

Oxygen is absolutely necessary for an effective PDT treatment. Numerous studies performed *in vitro* and *in vivo* demonstrated that lack of oxygen diminishes the PDT efficiency [24-26]. Several techniques have been proposed to deal with tissue oxygen depletion during PDT such as fractionating light irradiation or reducing the fluence rate [26-28]. These techniques are to promote tissue oxygen re-perfusion to compensate for the oxygen depletion caused by the photochemical reactions. Particularly, the modulation of the irradiance was shown to be directly related to the preservation of oxygen conditions during the treatment correlated with a better mTHPC-PDT outcome [22, 29, 30]. As an example, Coutier *et al* observed that tumors treated with fluence rates of 5 and 30 mW/cm^2 exhibited significantly longer tumor quadrupling times than those treated at 160 and 90 mW/cm^2 and the tumor regrowth profile correlated with the pO_2 values monitored during irradiation. Improved tumor destruction can be expected by reducing the rate and the extent of oxygen depletion using low fluence rates.

1.1.4 Photosensitizers

The prerequisites for an ideal sensitizer include chemical purity, selectivity for malignant cells, chemical and physical stability, low dark but strong photocytotoxicity, activation at wavelenghts with optimal tissue penetration and rapid clearance from the body without inducing significant skin photosensitivity [31]. Those properties are resumed by optimal Absorption, Distribution, Metabolism and Excretion (ADME). Moreover, photosensitizers must have a high singlet oxygen quantum yield, not induce mutagenic or carcinogenic effects and be inexpensive and commercially available [32]. The first porphyrins used in PDT did not respect these guidelines, were inhomogeneous, poorly defined mixtures of different hematoporphyrins extracted from blood and therefore conducted to higher skin photosensitization and a lack of selectivity [33]. Most of the current photosensitizers have porphyrin-related structures, including hematoporphyrin derivatives, phtalocyanines, chlorins and bacteriochlorins which all exhibit different photochemical and photophysical properties in terms of mechanisms of action and light activation [31]. O'Connor *et al* made an exhaustive article presenting different types of PSs and their characteristics [32]. A PS can be administrated exogenously, or endogenously and produces photosensitive metabolites (*e.g*

protoporphyrin IX from 5-aminolevulinic acid). Majority of photosensitizers are hydrophobic and form aggregates in biological environment making difficult intravenous administration and reducing PDT efficiency. The monomer form of PS is generally most photophysically active compared to aggregates [9]. To overcome this problem of aggregation, PSs are generally either formulated in various colloidal drug delivery systems such as liposomes, micelles and biodegradable nanoparticles or conjugated with hydrophilic polymers [34, 35]. Plenty of newly designed PS have been patented and tested in preclinical studies but only few of them gained marketing authorization, mainly due to the difficulty to reach all the requisites cited above.

1.2 Liposomal formulations of photosensitizers

As stated above, the majority of novel photosensitizer molecules are of hydrophobic nature. Although this feature is required to penetrate cellular walls in order to accumulate in cells [36] and to be able to be transported by lipoproteins, it induces immediate aggregation upon injection into aqueous media, thus diminishing the photosensitizer efficacy [37, 38] generally due to the decrease of singlet oxygen formation yield [39, 40]. Therefore, water-soluble drug delivery systems are needed to overcome the problem of photosensitizer aggregation and to maintain the high efficacy of the photodynamic treatment. Additionally, the delivery systems should be preferably designed to provide targeting capabilities, improving the pharmacokinetic properties of the drug formulation, while remaining biodegradable and non-toxic.

1.2.1 Description & classification

To date, a number of drug delivery systems has been designed, including oil-in-water emulsions, polymer conjugates, micelles, dendrimers, polymer nanoparticles and metal nanoparticle carriers [41, 42], among the most widely studied being the liposomal delivery systems [43]. In this review we will focus on liposomes as delivery agents.

Liposomes are defined as ideally spherical self-closed phospholipid vesicles consisting of one or several bilayers, first discovered by A. Bangham and co-workers almost 50 years ago [44]. Due to characteristic bilayer structure, encircling a certain aqueous volume, liposomes may encapsulate both hydrophobic and hydrophilic drugs [45, 46]. The size of liposomes ranges from about 20 nm to several microns, structurally represented by concentric lipid bilayers of nanometer-scale thickness (e.g., ~ 4 nm for dipalmitoylphosphatidylcholine (DPPC) [47]. Amphiphilic lipids comprising the lipid bilayer consist of hydrophilic polar headgroup and hydrophobic hydrocarbon chains, which structure promotes the spontaneous aggregation of such molecules and the self-formation of bilayer in water [48] under certain circumstances. Depending on the number of lipid bilayers, liposomes are structurally classified into multilamellar and unilamellar vesicles [49]. Unilamellar vesicles have a single lipid bilayer, sub-divided into small unilamellar vesicles (diameter 20-100 nm), large unilamellar vesicles (diameter 100-500 nm) and giant unilamellar vesicles (diameter > 1 micron) [50]. Multilamellar vesicles possess several bilayers, and are of more than 500 nm diameter, reaching up to 10 microns [50]. Liposomes are generally produced by either extrusion through a polycarbonate membrane, sonication, reverse-phase evaporation, or injection method (see [51] for review). The main components of liposomes are generally synthetic (DPPC, dipalmitoylphosphatidylglycerol, dimiristoylphosphatidylcholine, distearoylphosphatidylcholine) or natural (soy bean, egg lecithin) phospholipids, which provides a basis for biocompatibility.

1.2.2 Liposomal inclusion of photosensitizers

1.2.2.1 Photochemical and photophysical properties

As summarized by Lang *et al* [38], there are 3 main effects of liposomes on photosensitizers: monomerization of aggregated hydrophobic drugs as a result of localization in the lipid bilayer, a significant increase in the local photosensitizer concentration and the viscosity effect, thus structuring the microenvironment of the drug. Monomerization of hydrophobic sensitizers represents a well-studied effect, shown for a variety of drugs such as hematoporphyrin [36], benzoporphyrin derivative monoacid ring A [52], phthalocyanines [52], and chlorins [53]. The increase in the local concentration may actually lead to altered photophysical properties of photosensitizer. For instance, in Foslip® commercial liposomal formulation, the local concentration of mTHPC reaches 0.1 mM (at only 1 μM in solution) resulting in a phenomenon of Photoinduced Quenching [54]. Another consequence could be the effect inverse to monomerization, that is, aggregation, as was shown for porphyrins [55].

Incorporation of photosensitizers into liposomes changes the photophysical properties of the drugs, such as fluorescence and absorbance characteristics (usually red-shift of the maxima) [56, 57], changed fluorescence quantum yield [38, 53, 58], excited states lifetimes and the yield of singlet oxygen generation, which are sensitive to the microenvironment. An excellent review is available on the photophysical properties of porphyrin sensitizers in liposomal delivery systems [38]. It should be noted that the effect of significant local concentration may also influence the singlet oxygen quantum yield (decrease in case of aggregation), thus directly affecting the treatment efficiency of the formulation [59]. The changes in fluorescent properties of the photosensitizers provide a tool for the quantifying the interactions of the drug with liposomes and serum proteins, as was explored, e.g., in [60, 61], for the interaction of deuteroporphyrin and aluminium phtalocyanine with membrane models and lipoproteins. Polarization of photosensitizer fluorescence in liposomes due to the increased microviscosity in liposomes provides another tool for studying the drug localization in vesicles as well as serving as a phase transition-sensitive probe [38].

However, not only liposomes change the characteristics of photosensitizers upon incorporation, but also the drug itself may change the physico-chemical properties of the formulation. It was recently shown on a clinically approved Foscan® sensitizer (active substance – mTHPC) that the inclusion of high loads of mTHPC into DPPC-based liposomes significantly shifts phase transition temperature of the liposomes [62]. In case of Foslip® formulation described there, a decrease of more than 5 °C was registered. At the same time, no increase of the liposome size was noted. While the phase transition characterizes the active content release property, this effect implies the complex interdependence of drug and liposomal carrier properties, which need to be verified while studying the newly-developed lipid-based drug formulation. In a different study of mTHPC-loaded liposomes it was shown that at the maximal drug loads the localization of the drug in liposomes may actually change [53]. Indeed, instead of being localized fully in the lipid bilayer, a part of mTHPC was residing in the polymer shell of Fospeg® liposomes, thus also changing the release of the drug from the formulation.

1.2.2.2 Photosensitizer release

The liposomes being designed as drug delivery systems, the knowledge of the characteristics of the drug release is of utter importance for the successful application of the formulation, and the controlled drug release remains the holy grail of the liposome

biotechnology. The extents of drug entrapment and retention as well as the factors influencing them are important considerations in the design of liposome-mediated drug delivery systems. While hydrophilic drugs are retained in the aqueous core of the liposomes, and are subject to diffusion through the lipid bilayer [63, 64], hydrophobic ones retained in the lipid bilayer have minimal entrapment and retention problems due to high lipid-water partition coefficients. The incorporation of cholesterol into the lipid bilayer membrane is a common method to enhance the stability of liposomes, reduce the permeability of the membranes to water-soluble molecules and increase the fluidity or microviscosity of the bilayer [65, 66]. A comprehensive review of the drug release mechanisms from liposomes is available elsewhere [63]. These mechanisms include, among others, diffusion-controlled release, dissolution/degradation release, release by ion exchange, osmosis, external influence (heating or irradiation). It should be noted that the permeability of the lipid bilayer, directly related to drug release properties, is affected by liposome size, pH of the environment and drug properties [63].

1.2.2.2.1 Methods of investigation

Apart from conventional methods of drug release estimation, such as radiolabeled molecules (e.g., [67]), ultracentrifugation or size-exclusion chromatography, liposome-entrapped photosensitizers offer a distinct method to control the release of the entrapped drug from liposomes. A novel approach to analyze drug transfer to large oil-in-water emulsion droplets by flow cytometry was suggested by Petersen *et al* [68]. Although inapplicable to drug release to nanosized blood components, it estimated the characteristic release times of mTHPC to cell-sized acceptors using flow cytometry technique and registering mTHPC fluorescence. In another example, energy transfer between lipid bilayer-incorporated fluorescent marker and entrapped chlorin (mTHPC) and mTHPC fluorescence anisotropy were applied to estimate the drug release from DPPC/DPPG liposomes [69]. As a peculiar to mTHPC characteristic, the phenomenon of drug photoinduced fluorescence quenching was discovered in mTHPC liposomal formulations with high drug loads [54]. This effect consisted in the formation of small percentage of photoproducts after low-intensity laser irradiation, which, in conditions of efficient homogenous energy transfer between mTHPC molecules in lipid bilayer, quenched the fluorescence of the whole population of mTHPC in a liposome. It was recently used to study the mTHPC release from Foslip® and Fospeg® liposomal formulations to blood serum proteins, investigating the effect of the temperature and acceptors on the characteristics of drug release [53].

1.2.2.2.2 Processes implicating in the PS redistribution

It is generally considered that the photosensitizer redistribution from liposomes may proceed through the aqueous phase or due to collision of drug-loaded liposomes with plasma proteins [70]. In the former case, the rate of the sensitizer transfer is determined by the rate constant of the dye desorption from the lipid bilayer and is independent of the concentration of acceptor structures. In the latter case, the photosensitizer molecules migrate due to collisions between liposomes and plasma proteins. Its rate constant is determined by the frequency of collisions and, as a consequence, by serum concentration. Sometimes the combined mechanism is discussed, as it is applicable to mTHPC [67].

At the same time, the drug release from the liposomes is not the only source of photosensitizer loss from the vesicles. It was reported that direct transfer of phospolipid material to serum lipoproteins may take place [71], mainly as a loss of phospholipids to HDL [72], which is mediated by phospholipids transfer protein [73, 74]. This results in the

destruction of liposomes and consequent release of the content. In this case it shall be noted that the lipoprotein association pattern of the drug being released gradually from the disintegrating liposomes may vary from that of the injected liposome-free drug undergoing the stages of desaggregation [75]. Noteworthy, association of the photosensitizer released from the liposomes with LDL particles may increase the uptake of the drug by tumor cells by LDL-mediated endocytosis. Also, the uptake of intact photosensitizer-loaded liposomes by cells in a process of clathrin-mediated endocytosis [76] may change the subcellular localization of the drug, thus changing subcellular cytotoxic events in the course of PDT treatment.

Apart from liposome disintegration, liposomes injected into the bloodstream associate quickly with plasma proteins in a process called opsonization [77] and endocytosed by the cells of mononuclear phagocyte system (MPS) [78], rapidly decreasing the concentration of liposomes in blood circulation. These two effects are responsible for the extremely short half-life of the conventional liposomal formulations in blood, in the range of minutes [79]. Although the rapid uptake is preferred for the treatment of MPS-localized infections [80], the removal of liposomes from circulation is the major disadvantage for other drug delivery purposes including PDT treatment. This may be considered as a drawback compared with the use of liposome-free drugs.

1.2.2.2.3 Improvement of pharmacokinetic properties

One of the main methods of prolonging the liposome circulation is the coating the liposome surface with biocompartible PEG polymer (typically 4-6 mol%), forming a layer that prevents rapid opsonization and protein adsorption of the liposome surface [81, 82], increasing the circulation time from minutes to hours. It should be noted that the attachment of PEG to the surface of a liposome does not fully prevent liposome uptake by the reticuloendothelial system but only reduces the uptake rate [83]. One of the most significant advantages of such sterically stabilized liposomes is the nonsaturable, log-linear pharmacokinetics [43]. Sterically stabilized liposomes likely resist uptake by the high-affinity, low-capacity reticuloendothelial system macrophages, resulting in increased circulation lifetimes [84]. Additionally, it prevents liposomes aggregation during the storage and administration [85]. The drawback of such approach is the reduced ability of PEGylated liposomes to interact with target membranes [51]. This is critical since the singlet oxygen generated by the irradiated photosensitizer shows an extremely short migration radius. For instance, Gijsens *et al* demonstrated that sterically stabilized liposomes containing hydrophilic photosensitiser aluminium phthalocyanine tetrasulphonate did not display any *in vitro* photocytotoxic activity on malignant cells, while the free compound did [86]. Ichikawa *et al* noted that tumor accumulation of benzoporphyrin derivative monoacid ring A at 3 h after its injection with PEG-liposomes in Meth A-sarcoma bearing mice was significantly higher than the one observed after injection with nonmodified liposomes. However, significant tumor growth suppression after PDT was only observed for conventional but not for PEGylated formulation [87].

Due to the fact that they exploit the natural distribution pattern (passive diffusion and phagocytosis processes), liposomes, oil dispersions, biodegradable polymeric particles and hydrophilic polymer-PS conjugates are considered as passive targeting systems [34]. Several studies have shown that the selective accumulation in target tissues such as tumors or neovasculature of these targeting carriers is due to the phenomenon known as “Enhanced Permeability and Retention effect” (EPR). Indeed, the tumoral microenvironment presents a vascular defective architecture which increases the tumoral permeability for various vascular

factors [88]. The description of the EPR effect and influencing factors are described in the following part of these review.

2. PHOTOINDUCED PASSIVE TARGETING

Similar to normal tissue, tumor growth depends on a functional vascular network for the delivery of oxygen and nutrients and removal of metabolic wastes. Tumor targeting with PDT can be divided into two different approaches: a passive targeting and an active targeting. Passive photodynamic targeting refers to an approach based on the accumulation of the PS in the targeted compartment as a result of physicochemical factors of drug carriers, such as material composition, size and surface properties (e.g electric charge), and by pathophysiological and pharmacological factors such as tumor microenvironment as well as EPR effect [5, 89, 90]. On the opposite, active photodynamic targeting relies on photosensitizer structural modification or a targeted drug delivery system so that the compound can be selectively bound to and retained in the targeted compartment (cellular/vascular) based on molecular recognition.

In the present review, we will focuse on the different ways of passive targeting of the vascular (neovasculature) or of the cellular (parenchyma) compartment of the tumor.

2.1 Specific light delivery

Selectivity of PDT mainly results from the fact that illumination itself limits the area that is being damaged and includes tumor cells, tumor stroma (including vasculature and fibroblasts) and tumor infiltrating cells of the immune system. Selective tumor targeting can be achieved with PDT by using specific light delivery provided by recent developments in various laser light sources and fiber optic delivery devices [91]. Indeed, the local irradiation of the malignant tissues permit to prevent photoinduced damages to surrounding healthy tissues and target selectively the tumor.

2.2 DLI modulation: compartmental targeting

As cited previously, modulation of DLIs directly influences the local distribution of the PS in the tumor. Short DLIs are used to obtain a vascular localization of the PS in the tumor whereas long DLI permit to have PS in neoplastic cells. Zhou *et al* noticed the importance of the choice of the DLI to obtain a good treatment efficacy together with a maximal protection of normal tissues [92]. Several teams had applied this concept of compartmental targeting to enhance photodynamic efficacy [93-98]. Many subsequent investigations commented on the impact of DLI on the photodynamic effect, with significant improvement of efficiency with shorter DLIs, corresponding to high plasma levels of the drug [99-101]. The single targeting of the cellular compartment or the vascular compartment never concluded in a complete tumor cure. As a consequence, the use of two PS administrations was proposed, each one at different time before irradiation, in order to obtain high drug levels in both cellular and vascular compartments of the tumor. In general, this protocol did not significantly improve the results. Veenhuizen *et al* investigated the impact of a double injection of mTHPC 1-3h and 48h before irradiation but the response of the tumor was better at short DLI even if mTHPC level in the tumor was maximal at long DLI [12]. Identical observations were made by the same team when both injections were separated by 72 hours, despite the fact that the total drug dose was doubled [10]. Using a so-called vascular photosensitizer, Dolmans *et al* [11] demonstrated that a double injection of a pyropheophorbide derivative at 15 minutes and

4 hours before irradiation induced a significant tumor growth delay compared to a single drug dose at any of those times. For them, this improvement was related to a more homogeneous staining of both endothelial and perivascular structures following a double injection. A more recent article presented a very important improvement of PDT efficacy by using the same protocol of fractionation of the injection keeping the same total administrated dose of photosensitizer. Based on previously established intratumoral distribution of mTHPC [102], Garrier *et al* treated mice bearing tumors with a mTHPC fractionated injection at 24 hours and 3 hours before illumination (30 mW/cm², 10 J/cm²) in order to target both tumoral compartments [103]. The fractionated injection protocol, based of the use of two DLIs, yielded a 100% tumor cure correlated to a massive apoptosis of neoplastic cells and destruction of the neovasculature. This study demonstrated the importance of the compartmental targeting which critically influences PDT efficiency.

2.3 Pharmacokinetics: stability and bioavailability of liposomes

2.3.1 Enhanced Permeability Retention effect (EPR)

Investigations of Matsumura and Maeda firstly described that the majority of solid tumors presented a defective architecture of blood vessels which increases the permeability for various factors [104-113] called the "Enhanced Permeability Retention" (EPR) [113]. The EPR effect is based on this unique anatomical-pathophysiological nature of tumor blood vessels which facilitates transport of macromolecules into tumor tissues. EPR effect was not only observed for proteins but also with drug-polymer conjugates, micelles and liposomes and has thus now become the "gold standard" in anticancer strategies using macromolecular agents [88].

Any liposomal formulation needs to balance the liposomal stability in the circulation with drug availability/release once it arrives at the target tissue. Actually, liposomal technology is still unable to selectively release drugs in the target tissue and different factors, described below, can all affect the liposomal stability and the release of therapeutic agents [35, 83].

2.3.2 Factors influencing EPR effect

2.3.2.1 Size, composition & charge

The size of liposomes used in a drug delivery system should be large enough to prevent their rapid leakage into blood capillaries but small enough to escape capture by fixed macrophages that are lodged in high quantity in the reticuloendothelial system (RES) [114]. The size of the sinusoid in the spleen and fenestra of the Kuffer cells in the liver varies from 150 to 200 nm [115] and the size of gap junction between endothelial cells of the leaky tumor vasculature may vary from 100 to 600 nm [116]. Consequently, liposomes need to have a size up to 100 nm to reach tumor tissues by passing through these two particular vascular structures [114]. It was observed that an increase of the size of liposomes triggered a more rapid uptake by the reticuloendothelial system (RES) [83, 117, 118]. The dependency of size on liposomal clearance rates is relatively less for stabilized formulations than for conventional liposomes [119, 120]. For neutral conventional liposomes, the window for optimal behavior is narrow, meaning that for effective application, liposomes should be small enough (preferably, <100 nm) but still maintain reasonable drug encapsulation efficiencies [83].

The EPR effect is a molecular weight-dependent phenomenon which does not exist in normal tissues [88]. Macromolecules larger than 40 kDa, which is the threshold of renal

clearance, selectively leak out from tumoral vasculature and gradually accumulate in tumor tissues. Moreover, these accumulated macromolecules remained in tumor for a relatively long time.

Besides the size of liposomes, the clearance of liposomes is affected by their composition. Indeed, liposomal structure can significantly influence the stability and the drug release from liposomes [35]. The presence of cholesterol probably has one of the most important roles in the maintenance of membrane bilayer stability and long circulation times *in vivo*. Indeed, it was demonstrated that the presence of cholesterol and saturated phospholipids increased the rigidity of the lipidic bilayer and reduced the drug release. On the contrary, an excess of fluid lipid components gave to the liposomes the ability to easily break up and release the drug during circulation [35, 83]. An absence of cholesterol destabilized conventional liposomes by interactions with High Density Lipoprotein (HDL) [74] and triggered the elimination of their components from the circulation. Pegaz *et al* evidenced an important difference of extravasation between Visudyne® and mTHPC loaded liposomes [121] in the model of the chick chorioallantoic membrane. Visudyne® extravasates from CAM blood vessels very rapidly whereas mTHPC loaded in liposomes is confined into the vessels, at least during the first minute of observation. Those results indicated that the lipid composition of the liposomes governs their membrane fluidity and plays an important role in its behavior in the bloodstream. Indeed, mTHPC loaded liposomes composition is based on DPPC and DPPG whereas Visudyne® is based on more fluid lipids namely dimyristoylphosphatidylcholine and egg yolk phosphatidylglycerol (DMPC-EPG). This difference in composition explains the rapid extravasation of the Visudyne® compared to mTHPC loaded liposomes [122]. Thus, the lipid composition of the drug carrier, governing its membrane fluidity, has a very important incidence on the photosensitizer distribution in biological environment. The same principles were observed recently by Ytzhak *et al*, with hematoporphyrin embedded in liposomes with different lipid compositions, who found a correlation between the structure and unsaturation of lipids and the leakage of the plasmic membrane following photosensitization [123]. When liposomes were composed of a lipid mixture similar to that of natural plasmic membranes and photosensitization is being carried out under usual photodynamic therapy (PDT) conditions, photodamage to the lipids is not likely to cause enhanced permeability of ions through the membrane, which would have been a mechanism that leads to cell death.

The effect of liposome surface charge on liposome clearance kinetics is an increasingly misused predictive factor of circulation lifetimes [83]. Early studies have shown that the presence of negatively charged lipids in liposomes, including phosphatidic acid, phosphatidylserine and phosphatidylglycerol, results in a rapid uptake by the reticuloendothelial system [118, 124]. However, this relationship between the presence of charged lipids and circulation lifetimes is extremely complex and cannot be readily explained with simple models in which the presence of an anionic lipid necessitates increased clearance from the circulation [83]. Gabizon and Papahadjopoulos characterized the effect of surface charge on liposome clearance in mice using liposomes with different anionic phospholipids [125]. They noted that the inclusion of supplementary anionic lipids resulted in longer circulation lifetimes. Moreover, the vascular endothelial luminal surface is known to carry a negative charge which attracts positive charged basic proteins or cationic polymers in the proximity of vascular endothelial cells. This binding reaction leads to a reduced tumor drug accumulation by means of the EPR effect [126, 127].

2.3.2.2 Redistribution in plasma

Liposomes present a short plasma half-life which is in a range of minutes [77]. Two different phenomena impair the circulation time of conventional liposomes. On the one hand, a lipid exchange between the liposomes and lipoproteins (especially High Density Lipoprotein, HDL) leads to an irreversible disintegration of the liposome with the subsequent release of the PS in the bloostream and its association with lipoproteins and others plasma proteins. On the other hand, conventional liposomes become easily opsonized by plasma proteins and taken up by cells of the mononuclear phagocyte system leading to a high liposomal concentration in organs and tissues with a rich mononuclear phagocyte system (liver, spleen, bone marrow) [75, 128]. As most tumor cells are reported to express an elevated number of LDL (Low Density Lipoproteins)-receptors due to their rapid proliferation that increases the cholesterol demand for membrane synthesis [79], the final association with LDL might enhance the tumoral uptake of liposome-released photosensitizers by LDL-receptor-mediated endocytosis. In this context, the final lipoprotein association pattern of the PS, gradually released from disintegrating liposomes over a longer period of time, might vary signicantly from the pattern seen after a single bolus injection of the free PS [8, 75]. Indeed, different possibilities were evidenced dependently of physicochemical properties of the PS and plasma protein-binding behavior. As described above, free hydrophobic photosensitizers, associated with plasma proteins (LDL) to be transported in the circulation, can accumulate preferentially into both compartments via LDL-receptors-mediated endocytosis [129-131] or they can released from the PS-lipoprotein complex in the interstitial space and diffuse passively into tumor cells [132]. For hydrophilic photosensitizers, they can bind to albumin and HDL and be taken up by tumor cells via the nonspecific endocytosis pathway [133].

2.3.2.3 Reticuloendothelial system (RES)

The reticuloendothelial system (RES) can be described as a surveillance system for macromolecules. It is found in high quantity in organs like liver and spleen and can be a major obstacle to tumor delivery of macromolecular drugs. Many approaches based on surface modifications were explored to prevent phagocytic clearance by the RES. The most commonly used strategy is to conjugate PEG onto the surface of liposomes [88]. The PEGylation of liposome results in a hydrated barrier that provides good steric hindrance to the attachment of phagocytes. Moreover, PEGylation increases the circulation half-life of liposomes thus benefits EPR-based targeting of drugs to tumors [134].These liposomes wearing modifications with glycolipids or PEGylated lipids are referred to as “sterically stabilized” liposomes. Alternatively, the term Stealth® liposomes has been proposed [75, 135].

2.3.2.4 Tumoral microenvironment

2.3.2.4.1 Tumoral lymphatic system

A lack of effective lymphatic drainage is usually evidenced in solid tumors [108, 113, 136-138]. In normal tissues, the lymphatic system has the ability to recognize macromolecules and lipid particles from the interstitial space. Impairment of the tumoral lymphatic system leads to a prolonged retention of liposomes in the tumor interstitial area [35]. Tumor interstitium is also characterized by a high interstitial pressure, leading to an outward convective interstitial fluid flow, as well as the absence of an anatomically well-defined functioning lymphatic network. Hence, the transport of an anticancer drug in the

interstitium will be governed by the physiological and physicochemical properties of the interstitium and by the physicochemical properties of the molecule itself. In tumor tissues, not only there is an impaired lymphatic clearance but also the lymphatic system is the major route for metastasis of tumor cells in normal tissues [88, 104, 111].

2.3.2.4.2 Vascular mediators

Different vascular factors are implicated in the EPR effect such as bradykinin, nitric oxide, VEGF, prostaglandins, collagenase, peroxynitrite, cytokines… [111]. A recent review from Fang *et al* described with precision each of these factors [88] and their mode of action, particularly the process of extravasation of the macromolecules. EPR effect appears to be the result of multifactorial events *in vivo* which need to be deeply studied for the development of potential new strategies to modulate the EPR effect.

2.3.2.4.3 Heterogeneity of tumors

Some parts of tumors, particularly the central area, do not exhibit the EPR effect and show less accumulation of macromolecules than other parts [88, 139]. Mice bearing tumors, which is the most frequently used experimental model, present necrotic and hypovascular areas proportionally extended to the size of the tumor. Consequently, the EPR effect, which is dependent on the neovascularization, does not present an homogenous pattern in the totality of the tumoral tissue.

2.3.2.4.4 Tumor blood vasculature

Contrary to normal tissues, solid tumors present a higher vascular density (hypervasculature) especially when tumors are small [88]. Tumor angiogenesis is described as one of the most important features that sustains rapid tumor growth via an angiogenesis stimulating factor: the Vascular Endothelial Growth Factor (VEGF) [140-142]. Indeed, fast-growing cancer cells demand the recruitment of new vessels or rerouting of existing vessels near the tumor mass to supply them with oxygen and nutrients [114]. The newly formed vessels have abnormal morphology characterized by defective endothelial cells with wide fenestrations of 100 to 600 nm [143], irregular vascular alignment, lack of a smooth muscle layer or innervation and a wide lumen [104, 109, 110, 136]. This disorganized morphology results from the imbalance of angiogenic regulators (VEGF) and matrix metalloproteinases [144]. Macromolecular transport pathways across tumor vessels occur via open gaps (interendothelial junctions and transendothelial channels), vesicular vacuolar organelles and fenestrations. Modifications of the blood flow behavior were also noted in the tumor vasculature. Indeed, blood flow was described as irregular and inconsistent in these vessels with frequent inversion of the flow direction [145]. These architectural and anatomical features of a tumor vascular system constitute the foundation of the EPR effect which leads to extravasation of macromolecular and lipid drugs. For the passively targeted liposomes, EPR is probably the only mechanism leading to selective tumor distribution [35].

2.4 Photoinduced damage by passive targeting with liposomes

2.4.1 Specific models for vasculature visualization

Disruption of the neovasculature is known to play a crucial role in the eradication of tumors by PDT. Nevertheless, *in vitro* models can not give any information regarding vascular photothrombosis [146]. Vessel damage was first observed during the course of phototherapy in studies of Star *et al [147]*, Selman *et al [148]* and others [149]. The study of

Star used a rat mammary tumor model grown in transparent sandwich chambers and allowed direct visualization of morphological changes in vessel physiology during and after PDT.

2.4.1.1 Window-chamber model (WCM)

It consist in a transparent window (1 cm in diameter) which is surgically placed into the dorsal skin of rodents (mice or rats) under general anesthesia. This allows direct visualization of the skin vasculature at high resolution under confocal microscopy [150-153]. As an example, De Visscher *et al* presented the window-chamber model installed in rats with mammary carcinoma transplanted in the subcutaneous tissue [154]. After intravenous injection, mTHPC fluorescence was detected with CCD camera in tumor tissue, vasculature and surrounding connective tissue. Just after injection, the vascular mTHPC fluorescence was high for Foscan® and Fospeg® but not for Foslip®. Each photosensitizer presented a different fluorescence intensity curve in time. Indeed, the maximum tumor fluorescence is reached at 48 hours for Foslip® and 24 hours for Foscan® and Fospeg®. Khurana *et al* used the same model but for a PDT treatment of AMD with Visudyne® in mice in order to demonstrate relationships between the PS quantification and light dose for a localized irradiation [150]. Even if this WCM model appears helpful, another model, offering a large variety of advantages, is actually in real development: the chick chorioallantoic membrane model.

2.4.1.2 Chick chorioallantoic membrane (CAM)

2.4.1.2.1 Description

The chick chorioallantoic membrane assay is a commonly used method for studying angiogenic activities or drug delivery *in vivo* [155, 156]. It is a vascular membrane found in eggs of birds and reptiles. CAM corresponds to a transparent and highly vascularized membrane formed during the embryo development and results in a highly vascularized mesoderm composed of arteries, veins and an intricate capillary plexus [157]. First tumor transplantations to the CAM were described more than 100 years ago [158] but CAM tumor models remain sparse and poorly characterized as compared to murine models [158, 159]. The CAM assay is characterized by several major advantages such as the ease of access, the extensive vascularization and the relatively simple experimental approach and the natural immunodeficient environment of the developing embryo. This opens up the possibility to screen many samples in an inexpensive way [155]. Moreover, experiments in CAM do not need anesthesia contrary to the window-chamber model or standard rodents models. Until embryo development day 10, the chick embryo immune system remains incomplete with a lack of both B and T cell-mediated immune functions. Consequently, the young embryos are not fully immunocompetent and appear very appropriate to avoid the reject of xenografted cells or tissues.

The presence of T and B cells can be respectively first detected at EDD 11 and 12 [160]. After EDD 15, the B cell repertory begins to diversify and by EDD 18 chicken embryos become immunocompetent. It is essential to note that there are only 3 forms of immunoglobulins: IgM, IgG and IgA [161] in chicken compared to humans who possess 2 supplementary forms IgD and IgE.

Concerning the chick embryo culture, two approaches have been developed. An "*in ovo*" method where the embryos are left inside the eggshell during their development contrary to the "*ex ovo*" method where the embryos are cultivated in recipients simulating the eggshell (shell-less culture). The choice of the method depends of the age of the embryo and the nature

of the intervention [156]. Administrations routes used with chick embryos are similar to those used on humans: topical or intravenous (IV) [121, 122, 162] or intraperitoneal (IP) [163, 164]. Other routes as injection into the yolk sac [59] or in the amnion [165] can be used but without equivalence in humans.

2.4.1.2.2 Photodynamic evaluation

The CAM model has been used to evaluate photosensitizers ability to induce vasculature damage. The photodynamic angioocclusion with Visudyne® was particularly well monitored by the team of Debefve *et al [166, 167]* in the model of the CAM. They detailed this process in real-time by using a CCD camera after an intravenous injection of the PS into the CAM. The effect of light activation was probed by the monitoring of an intravenous injection of a fluorescent dye (FITC-Dextran) 24 hours after PDT treatment. They observed a platelets accumulation at intravascular junctions within seconds after Visudyne® light activation and capillaries were closed 15 minutes later. An occlusion of the treated area was observed after 5 minutes with doses of Visudyne® and light similar to those used clinically. Other teams used the CAM model to test Visudyne® efficacy on vascular occlusion and demonstrated an improved therapy outcome [168, 169].

The team of Chin and colleagues worked with a topical application of Hypericin (HY) and Hypocrellin B (perylenequinones family) on human bladder cell line inoculated on the CAM [170]. Authors demonstrated a selective accumulation of both photosensitizers in the xenografted tumor and in the vasculature of the CAM together with very similar degrees of photoinduced damage to the CAM. More recently, the same team published a more detailed report on photoinduced cellular and vascular damage indicating that the tumor therapy based on targeting the vasculature of the tumor induced a higher relative regression percentage of treated tumor compared to cellular targeted PDT [98]. Saw *et al* published several articles on the transport of Hypericin formulations (NMP, N-methyl pyrrolidone 4.8 (High Dose group, HD) or 0.6 % (Low Dose group, LD) in CAM vasculature after topical administration [171-173]. The HD treated CAM demonstrated a vessel regression that was 2.37 times higher compared to LD treated CAM. One more time, the formulation considerably impacts on vasculature targeting PDT [172]. Hypericin–PDT effects showed to be HY and NMP concentrations-dependent and NMP appeared to be a promising solvent and penetration enhancer for HY-PDT [171]. Moreover, in the last study, NMP formulations produced significantly higher contrast for tumor tissues and permitted a more precise fluorescence diagnosis of human bladder cancer cells implanted in CAM [173].

Pegaz *et al* studied the photothrombic activity of mTHPC-loaded liposomal formulations in CAM [121]. They tested two different formulations: conventional liposomes (Foslip®) or the corresponding long circulating poly(ethylene glycol) (PEG)ylated liposomes (Fospeg®). The light dose necessary to induce the desired vascular damage with Foslip® was twice higher (100 J/cm²) than with Fospeg® (50 J/cm²) and offers PEG liposomes as a suitable delivery system for the treatment of choroidal neovascularization associated with AMD. Moreover, authors observed that mTHPC loaded in liposomes is confined into the vessels independently of the type of liposomal formulation. So, the PEG formulation did not significantly influence the extravasation of the PS.

Ismail *et al* examined the effect of PDT using topical methylene blue free and combined with liposomes as a PS for treating human ovarian malignant tumors cultivated on CAM [174]. Both formulations photoinduced a complete tumor remission from the surface of the

CAM even if the liposomal formulation induced higher fluorescence intensities in the tumor (accumulation in cell cytoplasm) and penetrated more deeply than the free PS. Free methylene blue had a vascular effect contrary to liposomal formulations which targeted the tumor with minimal effects on the surrounding and vascular tissues. Consequently, the authors proposed a combined treatment with free methylene blue as a debulking agent completed with another formulation (methylene blue-liposome) for the fine destruction of tumor remnants. Another comparative test of aqueous and liposomal formulations of Povidone-Iodine administrated onto the CAM revealed significantly less photoinduced angioirritative reactions of the CAM (coagulation, hemorrhages) with the liposomal formulation than with the aqueous formulation [175].

The large number of tumor models and PS loaded liposomes rend difficult the prediction of the PDT efficacy. Even if liposomal formulations were demonstrated to improve pharmacokinetics of PS, they not always improve their tumoral efficacy.

2.4.2 Liposomal photosensitizers for PDT efficacy

The majority of exogenous photosensitizers present a peak plasma concentration 5 minutes after intravenous administration followed by a fast exponentional decay in plasma drug level. The time period when the PS is confined into the tumoral vasculature (short DLI) provides a temporal therapeutic window for vascular targeting. PDT during this time period offers a great opportunity to potent vascular damage including blood cells, endothelial cells and vessel-supporting structures [9].

The primary pathway for the vascular effects of PDT most likely begins with initial damage to the vascular endothelial cells, leading to exposure of the vascular basement membrane and, thereby, to the creation of thrombogenic sites within the vessel lumen. This initiates a cascade of responses, including platelet aggregation, release of vasoactive molecules, leukocyte adhesion, and increases in vascular permeability and vessels constriction [129, 150, 176]. Based on the EPR effect, the therapeutic agents have also the capacity to accumulate in malignant tissues [107]. PSs used to passively target tumor cells should be macromolecules (above 40 kDa) and have a long circulation time. Indeed, it was demonstrated that tumor drug uptake is proportional to the drug circulation time [9]. After the extravasation of the PS into the interstitial space, the drug needs to be associated with tumor cell membranes or internalized into tumor cells to generate photocytotoxicity [9].

Different categories of liposomal photosensitizing agents are existing actually. Liposomal porphyrin, phtalocyanine, chlorin, bacteriochlorin and others “home-made” photosensitizers are described in the litterature [35]. The passive photodynamic vascular-targeting approach is considered actually as the most successful PDT application and is used in current clinical context for the treatment of Age-Related Macular Degeneration (AMD) with Visudyne® (lipid formulation of benzoporphyrin derivative monoacid ring A (BPD-MA), Verteporfin). Visudyne® is the only photosensitizer which had received approval worldwide for AMD [177]. It corresponds to a unilamellar liposomal formulation improving its solubility [9]. The objective of the PDT treatment of AMD with Visudyne® is to shut down the abnormal choroidal neovasculature without damaging the normal retinal blood vessels. Richter *et al* compared liposomal formulation of BPD-MA to the free BPD-MA [8]. Authors demonstrated that both formulations had the same tumor and normal tissues distribution but the liposomal drug appeared to enter in the tissues more rapidly and to be cleared also more rapidly. However, liposomal BPD-MA presented a better efficacy in tumor damage after PDT treatment with an intravenous injection and a DLI of 3 hours. The difference in PDT efficacy

probably results from liposomal formulation allowing more BPD-MA to be associated with lipoproteins so that tumor cells can effectively take up the drug. Liposomal BPD-MA is also able to deliver BPD-MA to proliferating endothelial cells overexpressing LDL receptors [178]. Ishikawa *et al* [87] wanted to study the avoidance of reticuloendothelial system (RES)-trapping by using liposomal formulation of BPD-MA modified with polyethylene glycol (PEG-LipBPD-MA). The tumoral accumulation of BPD-MA in mice was significantly higher 3 hours after PEG-LipBPD-MA administration compared to non modified liposomal BPD-MA. On the contrary, tumor growth suppression was only observed following a PDT treatment with liposomal BPD-MA and not with PEG-LipBPD-MA. Thus, PEGylation enhances the passive targeting of liposomal BPD-MA in tumor but decreases the susceptibility of the drug in PDT. The explanation could be that liposomal carriers release very slowly BPD-MA at the tumor site. Furthermore, PEG in liposomes may protect direct interaction of liposomes with tumor cells whereas non-coated liposomes may contact more easily with tumor cells and deliver BPD-MA. PEG can also protect liposomes from interactions with macrophages in the interstitial space of tumors. In conclusion, although PEGylation of liposomes enhances its accumulation in tumor tissues, it does not always beneficial for therapy.

Actually, one of the most potent second generation photosensitizers is the meso-tetra(hydroxyphenyl)chlorin (mTHPC, Foscan®). It was approved for the palliative treatment of head and neck cancers. Generalized skin sensitization after systemic administration has been shown to be shorter as compared to porphyrin based photosensitizers [179]. Incorporation of mTHPC in lipid carriers has been proposed in order to improve pharmacokinetics, reduce systemic side effects as well as enhance specific drug delivery [180, 181]. Two formulations are actually used: conventional liposomes (Foslip®) or the corresponding long circulating poly(ethylene glycol) (PEG)ylated liposomes (Fospeg®). There are actually only few studies of the photodynamic treatment with Foslip® and/or Fospeg® realized *in vivo*. As an example, Buchholz *et al* compared the pharmacokinetics of Foscan® and Foslip® in a model of spontaneous feline squamous cell carcinoma in terms of tumor, skin and plasma pharmacokinetics [180]. They observed that the liposomal formulation of mTHPC had fluorescence intensities, fluorescence ratios (tumor /skin) and bioavailability in the tumor 2 to 4 times higher compared to free mTHPC. Moreover, maximal fluorescence intensity in the tumor was shown to occur 5.5 times earlier with liposomal mTHPC. Following this study, Buchholz and colleagues showed in the same model that this favorable pharmacokinetics of the liposomal drug resulted in a complete response rate of 100% [182]. The overall 1-year control rate was 75%. The tumor recurrence rate was 20% with a median time to recurrence of approximately 172 days. Once again, those results confirmed that lipidic formulations improve the pharmacokinetics properties of photosensitizers and consequently the PDT outcome. The same year, Svensson *et al* published a report which addressed Foslip® pharmacokinetics from 2 hours to 8 hours following intravenous administration in a murine model [183]. A rapid clearance from the plasma was noted and a noticeable average tumor/muscle ratio of 6.6 was evidenced. More recently, a Foslip®-PDT treatment of mice bearing subcutaneous tumors demonstrated 80% of tumor cures with a DLI of 6 hours which corresponded to an intratumoral vascular and parenchymal localization of the PS [181]. The highest tumor to muscle ratios were obtained at 6 hours and 15 hours after the intravenous injection of Foslip®. In the study of Westermann *et al*, the photodynamic treatment of human colon carcinoma xenografted in nude mice with Foscan® or Fospeg® 72 hours post-injection lead to the same potential to induce tumor regression although a longer blood circulating half-life and a better tumor to normal tissue ratio of mTHPC for the PEGylated formulation [184]. Another difference between Foscan® and Fospeg® was evidenced by fluorescence microscopy. Indeed, Fospeg® was localized near the tumor vessels whereas Foscan® more distributed inside the tumor tissue. Once again, this study confirms the possible improvement of pharmacokinetics of PS by their introduction in liposomes and

PEGylation but the PDT outcome persists to be unpredictable in relation to the intratumoral distribution and dosimetry used during the treatment.

2.5 Impact of the immune system

Pre-clinical research in various animal models has contributed immensely to our understanding of PDT-induced host immune responses as well as direct local cellular and vascular effects [185, 186]. Comparison of the antitumor effects of PDT in normal and immunodeficient mice revealed that despite comparable short-term outcomes complete antitumor responses were observed only in immunocompetent animals indicating that the engagement of the immune system is what makes PDT so effective [187, 188]. PDT has a significant effect on the immune system which can be either immunostimulatory or immunosuppressive [189, 190]. Most of the commonly used cancer therapies are immunosuppressive. Chemotherapy and ionizing radiations are delivered at important dose to destroy the tumor but are also known to be toxic for the bone marrow which produces all immune cells. Consequently, neutropaenia and other forms of myelosuppression are often the dose-limiting toxicity of these therapies [189]. Surgery can also have an immunosuppressive effect which triggers an important diminution of lymphocytes and natural killer cell function [191]. The ideal cancer therapy would destroy the tumor but also activate the immune system to recognize, track down and destroy any remaining tumor cells [189]. Different studies, both *in vitro* and *in vivo*, evaluated the relationship between the mode of tumor cell death and the efficiency of induction of the immune response. The majority of papers showed that cancer therapies which predominantly induced necrosis are actually better at activating the immune system than methods that predominantly induced apoptosis [192-194]. In fact, the necrosis corresponds to a liberation of cytosolic constituents into the extracellular space through the damaged plasma membrane which triggers a robust inflammatory response [189]. In the case of a tumor cell death by apoptosis, organelles are maintained isolated in apoptotic bodies which are phagocytosed by macrophages [195]. The acute inflammation induced by necrosis potentiates immunity by attracting host leukocytes into the tumor and increasing antigen presentation. PDT increases the immunogenicity of dead tumor cells by exposing or creating new antigens and by inducing heat-shock proteins (HSP) that increase the efficiency of antigen cross-presentation to form more effective tumor-specific cytotoxic T cells [189]. Particularly, the extracellular heat-shock protein 70 (HSP 70) was evidenced to be induced by PDT and released from necrotic tumor cells [187, 196, 197].

PDT can produce tumor cures and long-lasting tumor-specific immunity (memory) as has been shown by the rejection of tumors on re-challenge in certain mouse and rats models. One of the first studies highlighting PDT-induced antitumor immunity in mice models was performed by Canti *et al* [198]. Authors worked with immunosuppressed and normal surviving mice that were previously treated with aluminium disulfonated phtalocyanines (AlS2Pc)-PDT. The re-challenge with MS2 fibrosarcoma tumor cells led to death of the immunosuppressed surviving mice while normal surviving mice tend to resist the re-challenge. The team of Korbelik *et al* is a particularly well known group for its work on the activation of the adaptative immunity necessary for a most effective tumor control [188, 199, 200]. Indeed, they demonstrated that an adoptive transfer of bone marrow cells [188] or lymphocytes [199] from immunocompetent to immunodeficient animals allowed a complete restoration of the curative antitumor effects of PDT. It was also shown that PDT has the ability to instigate antitumor T-cell specific immunity which also leads to generation of immune memory cells that are recoverable from distant sites [186]. Those experiments illustrated perfectly the importance of the immune system for the success of the photodynamic treatment.

Photodynamic therapy was presented here as many studies described it: a treatment which has the ability to induce irreversible damages to pathological tissues, via vascular shutdown and induction of cell death pathways, specifically described for different types of cancers. Another facet of the PDT treatment is its potential to improve the regeneration of tissues. Immune system always plays a very important role and we are going to present the interest of the PDT to promote the wound healing process, particularly in the skin.

3. PHOTOINDUCED TISSUE REGENERATION BY PDT

3.1 Wound healing definition & description

Wound healing is a highly orchestrated process which requires interactions between soluble mediators, extracellular matrix components, resident and hematopoetic cells, as keratinocytes, fibroblasts, endothelial cells, nerve cells and infiltrating leukocyte subtypes as neutrophils, macrophages, mast cells and lymphocytes. Each of these components interferes differentially in the classically defined three phases of the wound healing that overlap in time and space: inflammation, tissue formation and tissue remodeling [201, 202].

Phase 1: Inflammation. Inflammation occurs immediately after tissue damage. Components of the coagulation cascade, inflammatory pathways and immune system are enrolled to prevent ongoing blood and fluid losses and to remove dead and devitalized tissues to prevent infection. Haemostasis is achieved progessively by the initial formation of a platelet plug followed by a fibrin matrix which will be employed as a scaffold for infiltrating cells [203]. Activation of the complement, degranulation of platelets and products coming from bacterial degradaton permit to recuit neutrophils. Two to three days later, monocytes emigrate from blood into the wound and differenciate into macrophages [203].

Phase 2: Tissue formation. This step occurs 2-10 days after injury and is characterized by cellular proliferation and migration of different cell types [203]. In tissue formation, epithelialization and newly formed granulation tissue, consisting of endothelial cells, macrophages and fibroblasts, begin to cover and fill the wound area to restore tissue integrity [204]. Fibrin, fibronectin, vitronectin and tenascin are components of the provisional extracellular wound matrix which facilitates cell adhesion, migration and proliferation [205].At the onset of Phase 2, keratinocytes migrate over the injured dermis (re-epithelialization) and new blood vessels are formed by angiogenesis process. The association of neovessels, fibroblasts and macrophages replace the fibrin matrix with granulation tissue. The latter can be used as a substrate for the migration of keratinocytes which will proliferate and mature to restore the barrier function of the epithelium at later stages of the repair process. Once the denuded wound surface has been covered by a monolayer of keratinocytes, epidermal migration ceases and a new stratified epidermis with underlying basal lamina is re-established from the margins of the wound inward [205].

Phase 3: Tissue remodelling. This phase starts 2-3 weeks after injury and can lasts one year or more. Most of the processes engaged precedently cease and different cell types as endothelial cells, macrophages and myofibroblasts die by apoptosis or exit from the wound. Only a mass composed by few cells, collagen fibers and extracellular matrix proteins persist at the previous wound site [203]. During this last phase, a balance is reached between synthesis of new components of scar matrix and their degradation by proteases. The mechanisms determining granulation tissue regression and its transformation into scar tissue

is not well understood. Even if typical features of these events are evidenced (regression of vascular structures, maturation of fibroblasts into myofibroblasts, resolution of the inflammatory response…), the balance between the stimulation of anti-inflammatory mediators and the downregulation of proinflammatory factors has not been clearly identified [205].

3.2 Factors involved in wound healing

The major steps constituting wound repair remain actually poorly characterized at the molecular level. Nevertheless, important roles of some cells and factors have been highlighted.

3.2.1 Cell lineages

Polymorphonuclear leukocytes (PMN). The early inflammatory phase or repair is characterized by local activation of the innate immune system, resulting in an early influx of polymorphonuclear leukocytes (neutrophils, PMN) followed by invasion of blood monocytes which differenciate into tissue macrophages [205]. Immediately after injury, extravasated blood constituents form a hemostatic plug. Platelets and PMN, entrapped and aggregated in the blood clot, release a wide variety of factors which are responsible of the amplification of the aggregation response, a coagulation cascade and can act as chemoattractants for cells involved in the inflammatory phase [206]. Few hours post-injury, neutrophils transmigrate across the endothelial cell wall of blood capillaries previously activated by proinflammatory cytokines IL-1β, tumor necrosis factor (TNF-α) and interferon (IFN-γ). These factors lead to the expression of different adhesion molecules: P- and E-selectin, ICAM-1 and -2, essential for leukocyte adhesion and diapedesis. Different studies demonstrated, in mice deficient for P and/or E selectins or ICAM-1, a dramatic delay in wound closure in relation with a decrease of macrophages infiltration [207, 208]. Indeed, adhesins interact with integrins present at the cell surface of neutrophils (CD11a/CD18, CD11b/CD18, CD11c/CD18, CD11d/CD18) [209]. Chemokines and their receptors play a crucial role for neutrophil recruitment during wound repair [201]. Engelhardt *et al* particulary evidenced IL-8, the growth-related oncogene α and the monocyte chemoattractant protein-1 (MCP-1). Moreover, bacterial products in the wound area can accelerate the neutrophil locomotion. Finally, recruited neutrophils realize the debridement of devitalized tissue and phagocytosis of infectious agents by releasing highly active antimicrobial substances (reactive oxygen species, cationic peptides, eicosanoids) and proteases (elastase, proteinase-3, cathepsin G…) [204, 205].

Monocytes/Macrophages. Beside their functions as antigen presenting cells and phagocytes, macrophages play a central role in wound repair due to their capacity to synthesize inflammatory cytokines and growth factors, such as Transforming Growth Factors α-β (TGF α-β), basic Fibroblast Growth Factor (bFGF), Platelet Derived Growth Factor (PDGF) and Vascular Endothelial Growth Factor (VEGF) [205, 210]. Monocytes emigrate from blood into the wound by following gradients of chemoattractic factors like growth factors, proinflammatory cytokines, chemokines macrophage inflammatory proteins (MIP-1α, MCP-1, RANTES) [211, 212]. After a skin injury, the neutrophil infiltration halts after few days and neutrophils are phagocytosed by macrophages recruited from the blood 2 days after injury.

Mast cells. Mast cells are members of leukocytes cells represented in most tissues. They are able to synthetize an important quantity of proinflammatory mediators and cytokines which promote inflammation and vascular changes [204, 205, 213, 214] Contradiction results

on the role of mast cells have been obtained up to now [213-215]. Indeed, some teams reported an absence or a poor impact of mast cell-deficiency on skin repair, particularly on re-epithelialization, collagen synthesis and angiogenesis [216, 217] On the contrary, a more recent study evidenced a significant impact of mast cell-deficiency on vascular permeability and PMN influx [218]. Noli *et al* reported the potential detrimental effect of an excessive and uncontrolled mediator release (hyperdegranulation). The repair response appears to be highly dependent of the model system used to clarify the role of mast cells. Particularly, mutant mice present abnormalities which might influence the wound healing process and genetic aspects need to be identify.

T cells. T cells are another leukocyte subset observed in human skin wounds during the phase of tissue remodelling when wound closure is completed and local infections overcome. Lymphocyte chemotaxis is highly dependent on chemokines, in particular interferon-γ-inducible protein-10 (IP-10) and the monokine induced by interferon -γ (MIG), both provided by macrophages. T cells can also influence the healing response by direct cell-cell interactions with resident (keratinocytes, fibroblasts) and non resident (platelets, macrophages) cells at the wound site [204, 205].

3.2.2 Growth factors

Some different factors interfere in the wound repair process, particulary during the second phase of tissue formation [203, 211]. Indeed, the re-epithelialization phase needs the intervention of the hepatocyte growth factor (HGF) by linking with the receptor tyrosine kinase MET. *Chmielowiec et al* demonstrated that cells which were deficient in the protein MET can not contribute to the formation of a neo-epidermis [219]. Other growth factors like members of the FGF (fibroblast growth factor) or EGF (endothelial growth factor) family are involved in re-epithelialization but have not the capacity to compensate a lack of HGF mediated signalling. On the other side, certain growth factors can negatively regulate wound re-epithelialization. For example, it was shown that mice expressing a gene encoding a dominant negative TGF-β receptor in the epidermis presented a strong acceleration of the re-epithelialization [220]. Concerning angiogenesis, the most important promoting factors are vascular endothelial growth factor A (VEGF-A) and fibroblast growth factor 2 (FGF-2 or bFGF). For example, the administration of VEGF-A on wounds observed in a diabetic animal model permitted to restore a normalized healing [221, 222].

3.2.3 Extracellular matrix components

Re-epithelialization process needs the intervention of an important quantity of proteins among which various extracellular-matrix proteins and their receptors, proteases (matrix metalloproteinases), cytoskeletal proteins and enzymes which regulate the cellular redox balance [223]. Numerous studies have demonstrated that the composition of the underlying extracellular matrix can modify the rate of keratinocyte migration [224, 225]. The most important constituent of the extracellular matrix is the collagen. During the initial phase of wound healing, type III collagen and fibronectin are deposited and later type III collagen will be replaced by type I collagen which promotes keratinocytes migration. It is likely that type IV collagen contributes to this effect but the action mechanism is not well known [226]. Fibronectin, laminin and vitronectin are others components identified as factors for promoting keratinocytes migration [226-229]. Matrix metalloproteinases are essential for the re-epithelialization because they degrade extracellular matrix thus removing both damaged tissue and provisional matrices and allowing cell migration [226].

In conclusion, understanding the network of wound healing involves a profound analysis of all soluble mediators and adhesion factors essential in the recruitment and trafficking of leukocytes during the inflammatory reaction. Cellular responses to injury involve direct cell-cell and cell-matrix interactions as well as the indirect crosstalk between different cell populations by soluble mediators. Cutaneous wound healing implicates complex and essential interactions between the epidermal and dermal compartments. An important quantity of factors have been identified by their action between epidermal and dermal cells to facilitate wound repair [211]. There is a crucial and sensitive balance between stimulating and inhibiting mediators during wound healing process in order to achieve tissue homeostasis following injury [211].

3.3 Clinical context

In humans, wound healing problems can be translated by two opposite observations: either a delayed wound healing, which occurs with diabetes or radiation exposure, or an excessive wound healing observed with hypertrophic and keloid scars [230]. Excessive healing is constated by a large deposition of extracellular matrix and alterations in local vascularization and cell proliferation [203]. Intralesional steroids are the most effective and widely used treatment for keloids. Surgical excision of keloïds generally results in recurrence rate of keloïds related to a stimulation of an additional collagen synthesis resulting in rapid regrowth and often a larger keloïd [230]. Administration of single agents therapies like growth factors [231, 232] was tested but not led to substantial advances in patient care probably related to the rapid degradation of this components at the wound site. Radiation therapy has been shown to effectively reduce the recurrence rate of keloïds by directly damaging fibroblasts which alter collagen structure and organization [230]. The more recent propositon to both overhealing and underhealing is the administration of cells with the ability to produce all components necessary to regulate the microenvironnement of the wound area [203].

Other parameters need to be taken in account for the study of wound healing process. Indeed, the age of the subject, the nutrition [233, 234], the imune state, the local vascularisation and hypoxia of the wound area [223], the stress [235] are parameters which can influence dramatically wound healing. For example, anoxia is a contributor to non healing wounds and increasing delivery of oxygen to tissue is one clinical approach to enhancing wound repair. The changes in oxygen tension could initiate, as yet unclear signaling cascades that culminate in proliferation and increased collagen production [236]. Over the past decade, it has become clear that stress can significantly slow down wound healing. It can have different origins as glucocorticoids or proinflammatory cytokines and it can induce substantial tissue hypoxia responsible of a lack of wound healing.

3.4 PDT and wound healing: the pros and cons

Whereas PDT is mainly applied in oncologic settings, it has also widely been used to target vasculature in age related macular degeneration, and is now under investigation for its microbial activity, especially in wounds or peridontitis [237]. In the following paragraphs, PDT effects on wound healing are presented by their opposite actions: inhibition versus promotion of healing response.

3.4.1 Nefast effects on wound repair

Only few studies exposing negative effects of PDT on wound healing have been published. Different studies in animal models have demonstrated that PDT has significant impact on wound healing, including delay of early granulation tissue formation, delay in re-epithelialization, necrosis of muscle and mucosal tissues [238]. One laboratory had particularly insisted on those negative aspects [239-241]. They used PDT as an adjuvant intraoperative treatment to improve locoregional control specifically on revascularization of a rat fasciocutaneous flap. Indeed, initial free vascular flaps are dependent on their vascular pedicle and long-term survival is facilitated by revascularization of the surrounding tissue bed. By using 5 mg/kg of Photofrin® and fluences at 25, 50 and 75 J/cm², Kubler *et al* showed delayed wound healing, causing effusions, discoloration of the flaps, necrosis, scab formation, lower tensile strength and a prolonged and more widespread inflammatory reaction in pedicled flaps when the operative bed was treated by PDT [240, 241]. Authors insisted on the fact that their rat model is extremely sensitive, both systemically and locally, to the effects of PDT. That's why it appears essentially to choose with precautions the animal model and compare different models between them before to experiment. In their last study, authors realized a fasciocutaneous flap on rats and treated them by Photofrin®-PDT with two different primary ischemic times: 2 or 4 hours. With 2 hours of ischemia, a decrease of the revascularization was observed in the PDT treated group on postoperative days (POD) 6 and 7. With 4 hours of ischemia, the decrease appeared already at POD 5, 6 and 7 only in the PDT treated group. PDT has been shown both to delay wound healing and to have a deleterious effect on flap survival after a primary ischemic insult. This delay may make the flap dependent on its pedicled blood supply for a prolonged period [239]. Another article, published later, sought to evaluate Photochlor (HPPH) photodynamic therapy (HPPH-PDT) as an adjuvant therapy to prevent recurrence of tumor after surgical removal in a model of canine hemangiopericytomas. Photochlor was injected intravenously at a dose of 0.3 mg/kg. Forty-eight hours later the treatment consisted of surgical removal of the tumor followed by HPPH-PDT. Photochlor photodynamic therapy applied after surgery appears to have no advantage over other forms of therapy in regards to preventing recurrence. Delayed wound healing and infections are problematic and make HPPH-PDT an undesirable addition to surgery for the treatment of this tumor type [242].

Some teams revealed also an absence of PDT effect on wound healing [243-245]. As an example, Parekh *et al* observed that PDT after systemic administration of either benzoporphyrin derivative (BPD-MA) or chloraluminium sulphophtalocyanin (CASP) had no influence on rate or final appearance of wound healing as observed after pathological analysis two weeks later [244]. They also precise that even if the rat offers a good model for detecting inhibition of wound healing, any acceleration or improvement in wound healing would be difficult to detect. So, the absence of effect could be an undetected effect. Once again, the type of animal model seems critical. Furthermore, previous studies have suggested that laser light alone benefits wound healing at low powers [246-248] and delays the healing process at high powers [249]. The use of low-level light therapy (LLLT) has been advocated, however it is highly contradictory in humans as well as in rodent models . *In vitro* and *in vivo* studies as well as human clinical trials show antagonistic results [250].

3.4.2 Improvements of wound repair

Majority of papers concerning PDT and wound healing let appeared a promoting effect of the treatment during various phases of the healing process.

3.4.2.1 Re-epithelialization & re-endothelialization

Different studies have suggested a promotive influence of PDT on wound healing in rats in terms of reepithelialization and remodeling [251-255]. Skin illumination to perform PDT after systemic administration of a photosensitizer is known to induce skin necrosis, however low doses light appeared to fasten the process of wound healing [253]. Jayasree *et al* administered aminolevulinic acid (ALA) intraperitoneally or hematoporphyrin derivative orally in rats, followed by HeNe and or NdYAG illumination [253]. They noted a clearly improved macros and microscopic healing after ALA based PDT, without however any effect on tensile strength at 3 weeks post injury. Particularly, they constated a re-epithelialization by day 15 in treated groups versus not in controls, mature collagen and reduced wound width at day 21 post-PDT versus immature collagen in controls. Other recent studies also reported that topical application of a photosensitizer and repeated illumination improved wound healing [252, 255]. Indeed, rat punch biopsy wounds treated with local administration of phtalocyanines followed by daily illumination at low light dose for 1 week presented a faster healing: an enhanced collagen content and matrix remodelling and greater epithelial regeneration [255]. Topical application of toluidine blue after punch biopsy in rats third-degree burns, followed by light only or PDT also improved healing as compared to controls. An increased collagen and intense angiogenesis were observed on day 3 conducting to an intense and parallel and organized collagen and epithelialization on day 7. The difference observed at day 14 between the 2 groups (PDT versus control) mainly consisted in a 100 % epidermal regeneration for PDT as opposed to 50 % in the control group [252]. The beneficial effects of PDT were attributed to both the low level illumination, and the bactericidal effect of PDT. For Adili *et al*, rat carotid injuries treated by Verteporfin®-PDT presented an increased endothelial cell lining 5 and 14 days after PDT, a higher proliferation on PDT-matrix and an increased bFGF-mRNA quantified by PCR [251]. More recently, Reddy *et al* [254] used methyl aminolevulinic acid photodynamic therapy (MAL-PDT) on patients with superficial and nodular basal cell carcinomas (BCCs). Two separated treatments at 7 days interval were administered as adjunctive treatment for Mohs micrographic surgery. A more rapid re-epithelialization of wounds and decreased scarring response was observed after PDT. In the majority of the papers, re-epithelialization is the first process which appeared to be promoted by PDT without however clear explanations about molecular processes engaged in the reaction.

3.4.2.2 Fibroblasts & Myofibroblasts

Even if the re-epithelialization is the principal studied aspect in wound healing, the migration of fibroblasts and myofibroblasts during the remodelling phase can be modulated by PDT treatment. Stasi *et al* presented a model of a rabbit glaucoma treated with sclerectomy and Verteporfin®-PDT [256]. The treatment triggered a decrease of the fibroproliferative response compare to control group, confirmed by histology. An increase of granulation tissue with abundant endothelial channels that allowed aqueous humour filtering to the bleb was also noted. This result indicated that the aggressive wound healing in this rabbit model of glaucoma surgery, chosen specifically for this particularity, can be significantly delayed by the use of PDT with intravenous photosensitizer administered postoperatively. The team of Adili *et al*, already cited in the previous paragraph, promoted a decreased myofibroblast migration and consequently a favourable healing with a model of rat carotid injuries treated by methylene blue-PDT [257]. The potential of PDT to limit (myo)fibroblasts migration during the wound healing process avoid the formation of fibrosis. Mechanisms of interaction between PDT and fibroblasts are not yet identified.

3.4.2.3 Antimicrobial action

Infections are widely known to perturb the wound healing process by delaying the re-epithelialization due to bacterial proliferation. At the beginning, PDT of wound infections has not been explored probably due to inefficient photosensitizer, a lack of selectivity for prokaryotic cells and the difficulties inherent in monitoring the response of localized infections in small rodents [258]. In recent years, antimicrobial effects of PDT recovered interest and was proposed as a therapy for a large variety of localized infections. PDT has been successfully used to kill pathogens and even to save life in several animal models of localized infections such as surface wounds, burns, oral sites, abscesses and the middle ear [237]. PDT presents several advantages compared to other standard therapies. Indeed, no pathogens resistance was demonstrated after PDT, the treatment can be used for non-perfused tissue (burns) and is less toxic compared to others [259].

Hamblin *et al* were the first team to report the use of mouse wound infection models to investigate the effect of PDT on treating excisional wounds infected with *Escherichia coli* and *Pseudomonas aeruginosa [258, 260]*. The experiments consisted in single wounds (100 mm^2) realized on the backs of healthy mice and infected with a suspension of bioluminescent bacteria transduced with a plasmid containing a bacterial lux gene operon which permitted to monitor the infection in real time by a sensitive charge-coupled camera. Wounds were treated one hour later by a topical polycationic photosensitizer conjugate at 160 J/cm^2 in four 40 J/cm^2 aliquots with imaging taking place after each aliquot [258]. The PDT treated group led to a 99% reduction in luminescence. Moreover, authors observed that PDT of infected wounds did not lead to any inhibition of wound healing which can be explained by the combination of the topical delivery method together with the large conjugate size and the relatively short incubation time [258]. In their following study, authors used the same model and observed that with a *P.aeruginosa* infection all non-treated mice died within 5 days contrary to PDT-treated group where 90% of mice survived [260]. PDT treated wounds healed significantly faster compared to other groups and authors believe that the explanation lies in the ability of topical PDT to inactivate extracellular virulence factors (proteases, lipases, toxins and siderophores) which are abundantly expressed by *P. aeruginosa* and have been proposed to aid in bacterial invasion and tissue damage [260, 261]. Using similar mouse models, Wong *et al* and Zolfaghari *et al* studied the effect of methylene blue and toluidine blue O mediated PDT on *Vibrio vulnificus* and methicillin-resistant *S. aureus* wound infections. A significant reduction of bacterial numbers was observed in both studies and PDT can cure mice with otherwise fatal *V. vulnificus* wound infections [262, 263].

3.4.2.4 Immunomodulation

The role of PDT in the stimulation of the host immune system is an important topic which has not so far been much investigated for infectious disease [237]. It was already demonstrated that PDT has the capacity to increase the host immune response against the cancer [187, 189, 264]. Indeed, the photo-induced direct damage of neoplastic cells, creating and releasing a mixture of tumor antigens and cellular danger signals, triggers an acute inflammatory response which activates and matures dendritic cells and other cellular components of both the innate and adaptive immune systems [189].

In principle, we could apply the same process for the improvement of wound healing but actually, according to our knowledge, the relation with wound healing was not described. The impact of PDT on immune response in wounds infections stays an undiscovered field of research for the future and dramatically needs deeper investigations.

Conclusion

As described in this review, the Photodynamic Therapy efficacy is based on the combined action of three essential parameters: the photosensitizer, the light and oxygen. On the first hand, it is possible to exploit the PDT ability to inhibit proliferative evolution of pathological cells, particularly in the treatment of cancerous diseases. On the other hand, PDT can also have an opposite effect, promoting the tissue repair by the stimulation of growth factors synthesis. Even if these two opposite aspects of PDT implicate the same parameters, underlined mechanisms are completely different. The predominance of each effect (photoinduced damaging or repair) will depend on the complex relationship between different parameters (fluence, fluence rate, drug delivery…) implicated in phototherapy and as such their comprehension is essential.

References

[1] T. J. Dougherty, C. J. Gomer, B. W. Henderson, G. Jori, D. Kessel, M. Korbelik, J. Moan and Q. Peng, *J Natl Cancer Inst.* **90**, 12 (1998).
[2] K. Plaetzer, B. Krammer, J. Berlanda, F. Berr and T. Kiesslich, *Lasers Med Sci.* **24**, 2 (2009).
[3] J. Moan and K. Berg, *Photochem Photobiol.* **53**, 4 (1991).
[4] A. P. Castano, T. N. Demidova and M. R. Hamblin, *Photodiagnosis Photodyn Ther.* **1**, (2004).
[5] N. Solban, I. Rizvi and T. Hasan, *Lasers Surg Med.* **38**, 5 (2006).
[6] Z. Huang, *Technol Cancer Res Treat.* **4**, 3 (2005).
[7] M. Triesscheijn, P. Baas, J. H. Schellens and F. A. Stewart, *Oncologist.* **11**, 9 (2006).
[8] A. M. Richter, E. Waterfield, A. K. Jain, A. J. Canaan, B. A. Allison and J. G. Levy, *Photochem Photobiol.* **57**, 6 (1993).
[9] B. Chen, B. W. Pogue, P. J. Hoopes and T. Hasan, *Crit Rev Eukaryot Gene Expr.* **16**, 4 (2006).
[10] P. Cramers, M. Ruevekamp, H. Oppelaar, O. Dalesio, P. Baas and F. A. Stewart, *Br J Cancer.* **88**, 2 (2003).
[11] D. E. Dolmans, A. Kadambi, J. S. Hill, K. R. Flores, J. N. Gerber, J. P. Walker, I. H. Borel Rinkes, R. K. Jain and D. Fukumura, *Cancer Res.* **62**, 15 (2002).
[12] R. Veenhuizen, H. Oppelaar, M. Ruevekamp, J. Schellens, O. Dalesio and F. Stewart, *Int J Cancer.* **73**, 2 (1997).
[13] H. J. Jones, D. I. Vernon and S. B. Brown, *Br J Cancer.* **89**, 2 (2003).
[14] M. Triesscheijn, M. Ruevekamp, M. Aalders, P. Baas and F. A. Stewart, *Photochem Photobiol.* **81**, 5 (2005).
[15] J. Dahle, H. B. Steen and J. Moan, *Photochem Photobiol.* **70**, 3 (1999).
[16] D. Kessel and Y. Luo, *Cell Death Differ.* **6**, 1 (1999).
[17] D. Kessel, Y. Luo, Y. Deng and C. K. Chang, *Photochem Photobiol.* **65**, 3 (1997).
[18] M. H. Teiten, L. Bezdetnaya, P. Morliere, R. Santus and F. Guillemin, *Br J Cancer.* **88**, 1 (2003).
[19] M. H. Teiten, S. Marchal, M. A. D'Hallewin, F. Guillemin and L. Bezdetnaya, *Photochem Photobiol.* **78**, 1 (2003).
[20] S. R. Wood, J. A. Holroyd and S. B. Brown, *Photochem Photobiol.* **65**, 3 (1997).
[21] D. Nowis, M. Makowski, T. Stoklosa, M. Legat, T. Issat and J. Golab, *Acta Biochim Pol.* **52**, 2 (2005).

[22] B. W. Henderson, T. M. Busch and J. W. Snyder, *Lasers Surg Med.* **38**, 5 (2006).
[23] J. P. Celli, B. Q. Spring, I. Rizvi, C. L. Evans, K. S. Samkoe, S. Verma, B. W. Pogue and T. Hasan, *Chem Rev.* **110**, 5.
[24] T. H. Foster, D. F. Hartley, M. G. Nichols and R. Hilf, *Cancer Res.* **53**, 6 (1993).
[25] T. H. Foster, R. S. Murant, R. G. Bryant, R. S. Knox, S. L. Gibson and R. Hilf, *Radiat Res.* **126**, 3 (1991).
[26] B. W. Henderson, T. M. Busch, L. A. Vaughan, N. P. Frawley, D. Babich, T. A. Sosa, J. D. Zollo, A. S. Dee, M. T. Cooper, D. A. Bellnier, W. R. Greco and A. R. Oseroff, *Cancer Res.* **60**, 3 (2000).
[27] A. Curnow, J. C. Haller and S. G. Bown, *J Photochem Photobiol B.* **58**, 2-3 (2000).
[28] T. M. Sitnik, J. A. Hampton and B. W. Henderson, *Br J Cancer.* **77**, 9 (1998).
[29] B. W. Henderson, S. O. Gollnick, J. W. Snyder, T. M. Busch, P. C. Kousis, R. T. Cheney and J. Morgan, *Cancer Res.* **64**, 6 (2004).
[30] S. Coutier, L. N. Bezdetnaya, T. H. Foster, R. M. Parache and F. Guillemin, *Radiat Res.* **158**, 3 (2002).
[31] C. A. Robertson, D. H. Evans and H. Abrahamse, *J Photochem Photobiol B.* **96**, 1 (2009).
[32] A. E. O'Connor, W. M. Gallagher and A. T. Byrne, *Photochem Photobiol.* **85**, 5 (2009).
[33] J. Moan and Q. Peng, *Anticancer Res.* **23**, 5A (2003).
[34] Y. N. Konan, R. Gurny and E. Allemann, *J Photochem Photobiol B.* **66**, 2 (2002).
[35] B. Chen, B. W. Pogue and T. Hasan, *Expert Opin Drug Deliv.* **2**, 3 (2005).
[36] G. Oenbrink, P. Jurgenlimke and D. Gabel, *Photochem Photobiol.* **48**, 4 (1988).
[37] N. Brasseur, H. Ali, R. Langlois and J. E. van Lier, *Photochem Photobiol.* **47**, 5 (1988).
[38] K. Lang, J. Mosinger and D. M. Wagnerova, *Coord Chem Rev.* **248**, 3-4 (2004).
[39] F. Ricchelli, S. Gobbo, G. Moreno, C. Salet, L. Brancaleon and A. Mazzini, *Eur J Biochem.* **253**, 3 (1998).
[40] R. W. Boyle and D. Dolphin, *Photochem Photobiol.* **64**, 3 (1996).
[41] R. Singh and J. W. Lillard, Jr., *Exp Mol Pathol.* **86**, 3 (2009).
[42] A. Puri, K. Loomis, B. Smith, J. H. Lee, A. Yavlovich, E. Heldman and R. Blumenthal, *Crit Rev Ther Drug Carrier Syst.* **26**, 6 (2009).
[43] V. P. Torchilin, *Nat Rev Drug Discov.* **4**, 2 (2005).
[44] A. D. Bangham and R. W. Horne, *J Mol Biol.* **8**, (1964).
[45] R. M. Fielding, *Clin Pharmacokinet.* **21**, 3 (1991).
[46] D. M. Lidgate, P. L. Felgner, J. S. Fleitman, J. Whatley and R. C. Fu, *Pharm Res.* **5**, 12 (1988).
[47] Z. V. Leonenko, E. Finot, H. Ma, T. E. Dahms and D. T. Cramb, *Biophys J.* **86**, 6 (2004).
[48] C. Tanford, *Krieger Publishing Co.* (1991).
[49] R. Perez-Soler, *Cancer Treat Rev.* **16**, 2 (1989).
[50] Y. Barenholz, C. and D.J., *Encyclopedia of pharmaceutical technology, J.S.a.J.C. Boylan, Ed. Marcel Dekker Inc.: New York, Basel and Hong Kong.* (1994).
[51] A. S. Ulrich, *Biosci Rep.* **22**, 2 (2002).
[52] A. Segalla, C. Milanesi, G. Jori, H. G. Capraro, U. Isele and K. Schieweck, *Br J Cancer.* **69**, 5 (1994).
[53] V. Reshetov, D. Kachatkou, T. Shmigol, V. Zorin, M. A. D'Hallewin, F. Guillemin and L. Bezdetnaya, *Photochem Photobiol Sci.* **10**, 6 (2011).
[54] D. Kachatkou, S. Sasnouski, V. Zorin, T. Zorina, M. A. D'Hallewin, F. Guillemin and L. Bezdetnaya, *Photochem Photobiol.* **85**, 3 (2009).
[55] V. V. Borovkov, M. Anikin, K. Wasa and Y. Sakata, *Photochemistry and Photobiology.* **63**, 4 (1996).
[56] D. Brault, C. Vever-Bizet and T. Le Doan, *Biochim Biophys Acta.* **857**, 2 (1986).

[57] B. Ehrenberg, Z. Malik and Y. Nitzan, *Photochem Photobiol.* **41**, 4 (1985).
[58] F. Ricchelli and S. Gobbo, *Journal of Photochemistry and Photobiology B: Biology.* **29**, 1 (1995).
[59] V. Gottfried, D. Peled, J. W. Winkelman and S. Kimel, *Photochem Photobiol.* **48**, 2 (1988).
[60] S. Bonneau, P. Morliere and D. Brault, *Biochem Pharmacol.* **68**, 7 (2004).
[61] S. Bonneau, C. Vever-Bizet, P. Morliere, J. C. Maziere and D. Brault, *Biophys J.* **83**, 6 (2002).
[62] J. Kuntsche, I. Freisleben, F. Steiniger and A. Fahr, *Eur J Pharm Sci.* **40**, 4 (2010).
[63] B. Maherani, E. Arab-Tehrani and M. Linder, *Curr Drug Targets.* **12**, 4 (2011).
[64] M. U. Uhumwangho, R.S and O., *J. Med. Biomed. Res.* **4**, 1 (2005).
[65] J. Senior and G. Gregoriadis, *Life Sci.* **30**, 24 (1982).
[66] K. Egbaria and N. Weiner, *Advanced Drug Delivery Reviews.* **5**, 3 (1990).
[67] H. Hefesha, S. Loew, X. Liu, S. May and A. Fahr, *J Control Release.* **150**, 3 (2011).
[68] S. Petersen, A. Fahr and H. Bunjes, *Mol Pharm.* **7**, 2 (2010).
[69] V. Reshetov, T. Zorina, M. A. D'Hallewin, L. Bolotine and V. Zorin, *Journal of Applied Spectroscopy.* **78**, 1 (2011).
[70] K. E. Boyle, M. C. Phillips and S. Lund-Katz, *Biochim Biophys Acta.* **1430**, 2 (1999).
[71] A. R. Tall and P. H. Green, *J Biol Chem.* **256**, 4 (1981).
[72] A. R. Tall and D. M. Small, *Adv Lipid Res.* **17**, (1980).
[73] A. R. Tall, *J Lipid Res.* **27**, 4 (1986).
[74] J. Damen, J. Dijkstra, J. Regts and G. Scherphof, *Biochim Biophys Acta.* **620**, 1 (1980).
[75] A. S. Derycke and P. A. de Witte, *Adv Drug Deliv Rev.* **56**, 1 (2004).
[76] S. A. Mousavi, L. Malerod, T. Berg and R. Kjeken, *Biochem J.* **377**, Pt 1 (2004).
[77] D. D. Lasic, F. J. Martin, A. Gabizon, S. K. Huang and D. Papahadjopoulos, *Biochim Biophys Acta.* **1070**, 1 (1991).
[78] D. V. Devine and J. M. Marjan, *Crit Rev Ther Drug Carrier Syst.* **14**, 2 (1997).
[79] R. Z. Renno and J. W. Miller, *Adv Drug Deliv Rev.* **52**, 1 (2001).
[80] M. K. Basu and S. Lala, *Curr Mol Med.* **4**, 6 (2004).
[81] A. L. Klibanov, K. Maruyama, V. P. Torchilin and L. Huang, *FEBS Lett.* **268**, 1 (1990).
[82] G. Blume and G. Cevc, *Biochim Biophys Acta.* **1146**, 2 (1993).
[83] D. C. Drummond, O. Meyer, K. Hong, D. B. Kirpotin and D. Papahadjopoulos, *Pharmacol Rev.* **51**, 4 (1999).
[84] T. M. Allen, C. B. Hansen and D. E. L. De Menezes, *Adv Drug Deliv Rev.* **16**, 2-3 (1995).
[85] C. Allen, N. Dos Santos, R. Gallagher, G. N. Chiu, Y. Shu, W. M. Li, S. A. Johnstone, A. S. Janoff, L. D. Mayer, M. S. Webb and M. B. Bally, *Biosci Rep.* **22**, 2 (2002).
[86] A. Gijsens, A. Derycke, L. Missiaen, D. De Vos, J. Huwyler, A. Eberle and P. de Witte, *Int J Cancer.* **101**, 1 (2002).
[87] K. Ichikawa, T. Hikita, N. Maeda, Y. Takeuchi, Y. Namba and N. Oku, *Biol Pharm Bull.* **27**, 3 (2004).
[88] J. Fang, H. Nakamura and H. Maeda, *Adv Drug Deliv Rev.* **63**, 3.
[89] D. K. Chatterjee, L. S. Fong and Y. Zhang, *Adv Drug Deliv Rev.* **60**, 15 (2008).
[90] A. M. Bugaj, *Photochem Photobiol Sci.* .
[91] M. H. Gold, *Facial Plast Surg Clin North Am.* **15**, 2 (2007).
[92] C. N. Zhou, W. Z. Yang, Z. X. Ding, Y. X. Wang, H. Shen, X. J. Fan and X. W. Ha, *Adv Exp Med Biol.* **193**, (1985).
[93] M. C. Aalders, M. Triesscheijn, M. Ruevekamp, M. de Bruin, P. Baas, D. J. Faber and F. A. Stewart, *J Biomed Opt.* **11**, 4 (2006).

[94] B. Chen, B. W. Pogue, I. A. Goodwin, J. A. O'Hara, C. M. Wilmot, J. E. Hutchins, P. J. Hoopes and T. Hasan, *Radiat Res.* **160**, 4 (2003).
[95] B. Chen, T. Roskams and P. A. de Witte, *Photochem Photobiol.* **76**, 5 (2002).
[96] T. Karmakova, A. Feofanov, A. Pankratov, N. Kazachkina, A. Nazarova, R. Yakubovskaya, V. Lebedeva, R. Ruziyev, A. Mironov, J. C. Maurizot and P. Vigny, *J Photochem Photobiol B.* **82**, 1 (2006).
[97] L. B. Li and R. C. Luo, *Lasers Med Sci.* **24**, 4 (2009).
[98] M. Olivo and W. Chin, *J Environ Pathol Toxicol Oncol.* **25**, 1-2 (2006).
[99] A. Ferrario, D. Kessel and C. J. Gomer, *Cancer Res.* **52**, 10 (1992).
[100] C. J. Gomer and A. Ferrario, *Cancer Res.* **50**, 13 (1990).
[101] M. Harada, J. Woodhams, A. J. MacRobert, M. R. Feneley, H. Kato and S. G. Bown, *J Photochem Photobiol B.* **79**, 3 (2005).
[102] S. Mitra, E. Maugain, L. Bolotine, F. Guillemin and T. H. Foster, *Photochem Photobiol.* **81**, 5 (2005).
[103] J. Garrier, A. Bressenot, S. Grafe, S. Marchal, S. Mitra, T. H. Foster, F. Guillemin and L. Bezdetnaya, *Int J Radiat Oncol Biol Phys.* **78**, 2.
[104] J. Fang, T. Sawa and H. Maeda, *Adv Exp Med Biol.* **519**, (2003).
[105] K. Greish, *J Drug Target.* **15**, 7-8 (2007).
[106] A. K. Iyer, G. Khaled, J. Fang and H. Maeda, *Drug Discov Today.* **11**, 17-18 (2006).
[107] H. Maeda, *Adv Enzyme Regul.* **41**, (2001).
[108] H. Maeda, *Adv Drug Deliv Rev.* **46**, 1-3 (2001).
[109] H. Maeda, G. Y. Bharate and J. Daruwalla, *Eur J Pharm Biopharm.* **71**, 3 (2009).
[110] H. Maeda, J. Fang, T. Inutsuka and Y. Kitamoto, *Int Immunopharmacol.* **3**, 3 (2003).
[111] H. Maeda, T. Sawa and T. Konno, *J Control Release.* **74**, 1-3 (2001).
[112] H. Maeda, J. Wu, T. Sawa, Y. Matsumura and K. Hori, *J Control Release.* **65**, 1-2 (2000).
[113] Y. Matsumura and H. Maeda, *Cancer Res.* **46**, 12 Pt 1 (1986).
[114] K. Cho, X. Wang, S. Nie, Z. G. Chen and D. M. Shin, *Clin Cancer Res.* **14**, 5 (2008).
[115] E. Wisse, F. Braet, D. Luo, R. De Zanger, D. Jans, E. Crabbe and A. Vermoesen, *Toxicol Pathol.* **24**, 1 (1996).
[116] F. Yuan, M. Dellian, D. Fukumura, M. Leunig, D. A. Berk, V. P. Torchilin and R. K. Jain, *Cancer Res.* **55**, 17 (1995).
[117] R. M. Abra and C. A. Hunt, *Biochim Biophys Acta.* **666**, 3 (1981).
[118] J. H. Senior, *Crit Rev Ther Drug Carrier Syst.* **3**, 2 (1987).
[119] P. L. Ahl, S. K. Bhatia, P. Meers, P. Roberts, R. Stevens, R. Dause, W. R. Perkins and A. S. Janoff, *Biochim Biophys Acta.* **1329**, 2 (1997).
[120] M. C. Woodle, K. K. Matthay, M. S. Newman, J. E. Hidayat, L. R. Collins, C. Redemann, F. J. Martin and D. Papahadjopoulos, *Biochim Biophys Acta.* **1105**, 2 (1992).
[121] B. Pegaz, E. Debefve, J. P. Ballini, G. Wagnieres, S. Spaniol, V. Albrecht, D. V. Scheglmann, N. E. Nifantiev, H. van den Bergh and Y. N. Konan-Kouakou, *Eur J Pharm Sci.* **28**, 1-2 (2006).
[122] N. Lange, J. P. Ballini, G. Wagnieres and H. van den Bergh, *Invest Ophthalmol Vis Sci.* **42**, 1 (2001).
[123] S. Ytzhak, J. P. Wuskell, L. M. Loew and B. Ehrenberg, *J Phys Chem B.* **114**, 31.
[124] J. Senior, J. C. Crawley and G. Gregoriadis, *Biochim Biophys Acta.* **839**, 1 (1985).
[125] A. Gabizon and D. Papahadjopoulos, *Biochim Biophys Acta.* **1103**, 1 (1992).
[126] R. B. Campbell, D. Fukumura, E. B. Brown, L. M. Mazzola, Y. Izumi, R. K. Jain, V. P. Torchilin and L. L. Munn, *Cancer Res.* **62**, 23 (2002).

[127] M. Nakamura, P. Davila-Zavala, H. Tokuda, Y. Takakura and M. Hashida, *Biochem Biophys Res Commun.* **245**, 1 (1998).
[128] A. J. Schroit, J. Madsen and R. Nayar, *Chem Phys Lipids.* **40**, 2-4 (1986).
[129] V. H. Fingar, *J Clin Laser Med Surg.* **14**, 5 (1996).
[130] C. M. Allen, R. Langlois, W. M. Sharman, C. La Madeleine and J. E. Van Lier, *Photochem Photobiol.* **76**, 2 (2002).
[131] W. M. Sharman, J. E. van Lier and C. M. Allen, *Adv Drug Deliv Rev.* **56**, 1 (2004).
[132] M. Van de Putte, T. Roskams, J. R. Vandenheede, P. Agostinis and P. A. de Witte, *Br J Cancer.* **92**, 8 (2005).
[133] D. Kessel, K. L. Whitcomb and V. Schulz, *Photochem Photobiol.* **56**, 1 (1992).
[134] M. L. Immordino, F. Dosio and L. Cattel, *Int J Nanomedicine.* **1**, 3 (2006).
[135] G. E. Francis, C. Delgado, D. Fisher, F. Malik and A. K. Agrawal, *J Drug Target.* **3**, 5 (1996).
[136] K. Greish, J. Fang, T. Inutsuka, A. Nagamitsu and H. Maeda, *Clin Pharmacokinet.* **42**, 13 (2003).
[137] H. Maeda and Y. Matsumura, *Crit Rev Ther Drug Carrier Syst.* **6**, 3 (1989).
[138] R. K. Jain, *J Control Release.* **74**, 1-3 (2001).
[139] A. Nagamitsu, K. Greish and H. Maeda, *Jpn J Clin Oncol.* **39**, 11 (2009).
[140] J. Folkman, *N Engl J Med.* **285**, 21 (1971).
[141] J. Folkman, *Nat Med.* **1**, 1 (1995).
[142] J. Folkman, *J Natl Cancer Inst.* **82**, 1 (1990).
[143] J. N. Moreira, R. Gaspar and T. M. Allen, *Biochim Biophys Acta.* **1515**, 2 (2001).
[144] P. Carmeliet and R. K. Jain, *Nature.* **407**, 6801 (2000).
[145] K. Hori, M. Suzuki, S. Tanda, S. Saito, M. Shinozaki and Q. H. Zhang, *Jpn J Cancer Res.* **82**, 11 (1991).
[146] W. T. Li, *Curr Drug Metab.* **10**, 8 (2009).
[147] W. M. Star, H. P. Marijnissen, A. E. van den Berg-Blok, J. A. Versteeg, K. A. Franken and H. S. Reinhold, *Cancer Res.* **46**, 5 (1986).
[148] S. H. Selman, M. Kreimer-Birnbaum, J. E. Klaunig, P. J. Goldblatt, R. W. Keck and S. L. Britton, *Cancer Res.* **44**, 5 (1984).
[149] V. H. Fingar, S. W. Taber, P. S. Haydon, L. T. Harrison, S. J. Kempf and T. J. Wieman, *In Vivo.* **14**, 1 (2000).
[150] M. Khurana, E. H. Moriyama, A. Mariampillai, K. Samkoe, D. Cramb and B. C. Wilson, *J Biomed Opt.* **14**, 6 (2009).
[151] M. Khurana, E. H. Moriyama, A. Mariampillai and B. C. Wilson, *J Biomed Opt.* **13**, 4 (2008).
[152] S. J. Stern, S. Flock, S. Small, S. Thomsen and S. Jacques, *Otolaryngol Head Neck Surg.* **105**, 4 (1991).
[153] S. J. Stern, S. T. Flock, S. Small, S. Thomsen and S. Jacques, *Am J Surg.* **160**, 4 (1990).
[154] S. De Visscher, D. J. Robinson, S. Kascakova, R. De Bruin, A. van der Poeg, H. J. Sterenborg, J. L. Roodenburg and M. J. Witjes, *Head and Neck Oncology.* (2009).
[155] M. Hagedorn, M. Balke, A. Schmidt, W. Bloch, H. Kurz, S. Javerzat, B. Rousseau, J. Wilting and A. Bikfalvi, *Dev Dyn.* **230**, 1 (2004).
[156] A. Vargas, M. Zeisser-Labouebe, N. Lange, R. Gurny and F. Delie, *Adv Drug Deliv Rev.* **59**, 11 (2007).
[157] D. O. DeFouw, V. J. Rizzo, R. Steinfeld and R. N. Feinberg, *Microvasc Res.* **38**, 2 (1989).
[158] J. B. Murphy and P. Rous, *J Exp Med.* **15**, 2 (1912).
[159] E. I. Deryugina and J. P. Quigley, *Histochem Cell Biol.* **130**, 6 (2008).
[160] E. M. Janse and S. H. Jeurissen, *Immunobiology.* **182**, 5 (1991).

[161] T. F. Davison, *Br Poult Sci.* **44**, 1 (2003).
[162] A. Vargas, B. Pegaz, E. Debefve, Y. Konan-Kouakou, N. Lange, J. P. Ballini, H. van den Bergh, R. Gurny and F. Delie, *Int J Pharm.* **286**, 1-2 (2004).
[163] M. J. Hammer-Wilson, D. Cao, S. Kimel and M. W. Berns, *Photochem Photobiol Sci.* **1**, 9 (2002).
[164] R. Hornung, M. J. Hammer-Wilson, S. Kimel, L. H. Liaw, Y. Tadir and M. W. Berns, *J Photochem Photobiol B.* **49**, 1 (1999).
[165] M. Peterka and I. Klepacek, *Reprod Toxicol.* **15**, 2 (2001).
[166] E. Debefve, B. Pegaz, H. van den Bergh, G. Wagnieres, N. Lange and J. P. Ballini, *Angiogenesis.* **11**, 3 (2008).
[167] E. Debefve, B. Pegaz, J. P. Ballini and H. van den Bergh, *Photochem Photobiol.* **85**, 6 (2009).
[168] K. S. Samkoe and D. T. Cramb, *J Biomed Opt.* **8**, 3 (2003).
[169] M. F. Zuluaga, C. Mailhos, G. Robinson, D. T. Shima, R. Gurny and N. Lange, *Invest Ophthalmol Vis Sci.* **48**, 4 (2007).
[170] W. Chin, W. Lau, S. L. Lay, K. K. Wei and M. Olivo, *Int J Oncol.* **25**, 4 (2004).
[171] C. L. Saw, P. W. Heng, W. W. Chin, K. C. Soo and M. Olivo, *Cancer Lett.* **238**, 1 (2006).
[172] C. L. Saw, M. Olivo, W. W. Chin, K. C. Soo and P. W. Heng, *Biol Pharm Bull.* **28**, 6 (2005).
[173] C. L. Saw, M. Olivo, W. W. Chin, K. C. Soo and P. W. Heng, *J Photochem Photobiol B.* **86**, 3 (2007).
[174] M. S. Ismail, U. Torsten, C. Dressler, J. E. Diederichs, S. Hüske, H. Weitzel and H.-P. Berlien, *Lasers Med Sci.* **14**, (1999).
[175] P. Wutzler, A. Sauerbrei, A. Hartl and K. Reimer, *Dermatology.* **207**, 1 (2003).
[176] B. Krammer, *Anticancer Res.* **21**, 6B (2001).
[177] K. W. Woodburn, C. J. Engelman and M. S. Blumenkranz, *Retina.* **22**, 4 (2002).
[178] U. Schmidt-Erfurth, T. Hasan, K. Schomacker, T. Flotte and R. Birngruber, *Lasers Surg Med.* **17**, 2 (1995).
[179] C. Hopper, *Lancet Oncol.* **1**, (2000).
[180] J. Buchholz, B. Kaser-Hotz, T. Khan, C. Rohrer Bley, K. Melzer, R. A. Schwendener, M. Roos and H. Walt, *Clin Cancer Res.* **11**, 20 (2005).
[181] H. P. Lassalle, D. Dumas, S. Grafe, M. A. D'Hallewin, F. Guillemin and L. Bezdetnaya, *J Control Release.* **134**, 2 (2009).
[182] J. Buchholz, M. Wergin, H. Walt, S. Grafe, C. R. Bley and B. Kaser-Hotz, *J Vet Intern Med.* **21**, 4 (2007).
[183] J. Svensson, A. Johansson, S. Grafe, B. Gitter, T. Trebst, N. Bendsoe, S. Andersson-Engels and K. Svanberg, *Photochem Photobiol.* **83**, 5 (2007).
[184] P. Westerman, T. Glanzmann, S. Andrejevic, D. R. Braichotte, M. Forrer, G. A. Wagnieres, P. Monnier, H. van den Bergh, J. P. Mach and S. Folli, *Int J Cancer.* **76**, 6 (1998).
[185] Y. G. Qiang, C. M. Yow and Z. Huang, *Med Res Rev.* **28**, 4 (2008).
[186] M. Korbelik, *Lasers Surg Med.* **38**, 5 (2006).
[187] A. D. Garg, D. Nowis, J. Golab and P. Agostinis, *Apoptosis.* **15**, 9.
[188] M. Korbelik, G. Krosl, J. Krosl and G. J. Dougherty, *Cancer Res.* **56**, 24 (1996).
[189] A. P. Castano, P. Mroz and M. R. Hamblin, *Nat Rev Cancer.* **6**, 7 (2006).
[190] G. Canti, A. De Simone and M. Korbelik, *Photochem Photobiol Sci.* **1**, 1 (2002).
[191] C. S. Ng, T. W. Lee, S. Wan, I. Y. Wan, A. D. Sihoe, A. A. Arifi and A. P. Yim, *J Invest Surg.* **18**, 2 (2005).
[192] O. Kepp, A. Tesniere, L. Zitvogel and G. Kroemer, *Curr Opin Oncol.* **21**, 1 (2009).

[193] L. Zitvogel, N. Casares, M. O. Pequignot, N. Chaput, M. L. Albert and G. Kroemer, *Adv Immunol.* **84**, (2004).
[194] L. Zitvogel and G. Kroemer, *Cell Death Differ.* **15**, 1 (2008).
[195] D. Kessel and J. J. Reiners, Jr., *Photochem Photobiol.* **83**, 5 (2007).
[196] M. Korbelik, J. Sun and I. Cecic, *Cancer Res.* **65**, 3 (2005).
[197] S. Mitra, E. M. Goren, J. G. Frelinger and T. H. Foster, *Photochem Photobiol.* **78**, 6 (2003).
[198] G. Canti, D. Lattuada, A. Nicolin, P. Taroni, G. Valentini and R. Cubeddu, *Anticancer Drugs.* **5**, 4 (1994).
[199] M. Korbelik and G. J. Dougherty, *Cancer Res.* **59**, 8 (1999).
[200] M. Korbelik, S. Merchant and N. Huang, *Photochem Photobiol.* **85**, 6 (2009).
[201] R. Gillitzer and M. Goebeler, *J Leukoc Biol.* **69**, 4 (2001).
[202] A. J. Singer and R. A. Clark, *N Engl J Med.* **341**, 10 (1999).
[203] G. C. Gurtner, S. Werner, Y. Barrandon and M. T. Longaker, *Nature.* **453**, 7193 (2008).
[204] S. A. Eming, T. Krieg and J. M. Davidson, *J Invest Dermatol.* **127**, 3 (2007).
[205] S. A. Eming, M. Hammerschmidt, T. Krieg and A. Roers, *Semin Cell Dev Biol.* **20**, 5 (2009).
[206] A. M. Szpaderska, E. I. Egozi, R. L. Gamelli and L. A. DiPietro, *J Invest Dermatol.* **120**, 6 (2003).
[207] T. Nagaoka, Y. Kaburagi, Y. Hamaguchi, M. Hasegawa, K. Takehara, D. A. Steeber, T. F. Tedder and S. Sato, *Am J Pathol.* **157**, 1 (2000).
[208] M. Subramaniam, S. Saffaripour, L. Van De Water, P. S. Frenette, T. N. Mayadas, R. O. Hynes and D. D. Wagner, *Am J Pathol.* **150**, 5 (1997).
[209] A. A. Kulidjian, R. Inman and T. B. Issekutz, *Semin Immunol.* **11**, 2 (1999).
[210] C. Sunderkotter, K. Steinbrink, M. Goebeler, R. Bhardwaj and C. Sorg, *J Leukoc Biol.* **55**, 3 (1994).
[211] S. Werner and R. Grose, *Physiol Rev.* **83**, 3 (2003).
[212] C. Wetzler, H. Kampfer, B. Stallmeyer, J. Pfeilschifter and S. Frank, *J Invest Dermatol.* **115**, 2 (2000).
[213] C. Noli and A. Miolo, *Int Wound J.* **7**, 6.
[214] M. F. Ng, *Int Wound J.* **7**, 1.
[215] C. Noli and A. Miolo, *Vet Dermatol.* **12**, 6 (2001).
[216] E. I. Egozi, A. M. Ferreira, A. L. Burns, R. L. Gamelli and L. A. Dipietro, *Wound Repair Regen.* **11**, 1 (2003).
[217] Y. Iba, A. Shibata, M. Kato and T. Masukawa, *Int Immunopharmacol.* **4**, 14 (2004).
[218] K. Weller, K. Foitzik, R. Paus, W. Syska and M. Maurer, *Faseb J.* **20**, 13 (2006).
[219] J. Chmielowiec, M. Borowiak, M. Morkel, T. Stradal, B. Munz, S. Werner, J. Wehland, C. Birchmeier and W. Birchmeier, *J Cell Biol.* **177**, 1 (2007).
[220] C. Amendt, A. Mann, P. Schirmacher and M. Blessing, *J Cell Sci.* **115**, Pt 10 (2002).
[221] R. D. Galiano, O. M. Tepper, C. R. Pelo, K. A. Bhatt, M. Callaghan, N. Bastidas, S. Bunting, H. G. Steinmetz and G. C. Gurtner, *Am J Pathol.* **164**, 6 (2004).
[222] O. Z. Lerman, R. D. Galiano, M. Armour, J. P. Levine and G. C. Gurtner, *Am J Pathol.* **162**, 1 (2003).
[223] Raja, K. Sivamani, M. S. Garcia and R. R. Isseroff, *Front Biosci.* **12**, (2007).
[224] A. el-Ghalbzouri, S. Gibbs, E. Lamme, C. A. Van Blitterswijk and M. Ponec, *Br J Dermatol.* **147**, 2 (2002).
[225] J. Sutherland, M. Denyer and S. Britland, *J Anat.* **207**, 1 (2005).
[226] E. A. O'Toole, *Clin Exp Dermatol.* **26**, 6 (2001).
[227] K. Zhang and R. H. Kramer, *Exp Cell Res.* **227**, 2 (1996).

[228] T. Wen, Z. Zhang, Y. Yu, H. Qu, M. Koch and M. Aumailley, *Wound Repair Regen.* **18**, 3.
[229] B. Hollier, D. G. Harkin, D. Leavesley and Z. Upton, *Exp Cell Res.* **305**, 1 (2005).
[230] S. Davidson, N. Aziz, R. M. Rashid and A. Khachemoune, *Medscape J Med.* **11**, 1 (2009).
[231] G. H. Rudkin and T. A. Miller, *Plast Reconstr Surg.* **97**, 2 (1996).
[232] V. K. Rumalla and G. L. Borah, *Plast Reconstr Surg.* **108**, 3 (2001).
[233] M. Arnold and A. Barbul, *Plast Reconstr Surg.* **117**, 7 Suppl (2006).
[234] S. L. Kavalukas and A. Barbul, *Plast Reconstr Surg.* **127 Suppl 1**, .
[235] L. M. Christian, J. E. Graham, D. A. Padgett, R. Glaser and J. K. Kiecolt-Glaser, *Neuroimmunomodulation.* **13**, 5-6 (2006).
[236] J. D. Davidson and T. A. Mustoe, *Wound Repair Regen.* **9**, 3 (2001).
[237] T. Dai, Y. Y. Huang and M. R. Hamblin, *Photodiagnosis Photodyn Ther.* **6**, 3-4 (2009).
[238] A. F. Jefferis, E. B. Chevretton and M. C. Berenbaum, *Acta Otolaryngol.* **111**, 1 (1991).
[239] M. J. Belmont, N. Marabelle, T. S. Mang, R. Hall and M. K. Wax, *Laryngoscope.* **110**, 6 (2000).
[240] A. Kubler, R. K. Finley, 3rd, I. A. Born and T. S. Mang, *Lasers Surg Med.* **18**, 4 (1996).
[241] J. V. Moore, C. M. West and C. Whitehurst, *Phys Med Biol.* **42**, 5 (1997).
[242] D. L. McCaw, J. T. Payne, E. R. Pope, M. K. West, R. V. Tompson and D. Tate, *Lasers Surg Med.* **29**, 1 (2001).
[243] A. K. Haylett, K. Higley, M. Chiu, D. C. Shackley and J. V. Moore, *Photochem Photobiol Sci.* **1**, 9 (2002).
[244] S. G. Parekh, K. B. Trauner, B. Zarins, T. E. Foster and R. R. Anderson, *Lasers Surg Med.* **24**, 5 (1999).
[245] F. F. Sperandio, A. Simoes, A. C. Aranha, L. Correa and S. C. Orsini Machado de Sousa, *Photomed Laser Surg.* **28**, 5.
[246] F. A. Al-Watban, X. Y. Zhang and B. L. Andres, *Photomed Laser Surg.* **25**, 2 (2007).
[247] F. A. Al-Watban and X. Y. Zhang, *J Clin Laser Med Surg.* **15**, 5 (1997).
[248] F. A. Al-Watban and X. Y. Zhang, *J Clin Laser Med Surg.* **22**, 1 (2004).
[249] G. E. Romanos, S. Pelekanos and J. R. Strub, *Lasers Surg Med.* **16**, 4 (1995).
[250] W. Posten, D. A. Wrone, J. S. Dover, K. A. Arndt, S. Silapunt and M. Alam, *Dermatol Surg.* **31**, 3 (2005).
[251] F. Adili, T. Scholz, M. Hille, J. Heckenkamp, S. Barth, A. Engert and T. Schmitz-Rixen, *Eur J Vasc Endovasc Surg.* **24**, 2 (2002).
[252] V. G. Garcia, M. A. de Lima, T. Okamoto, L. A. Milanezi, E. C. Junior, L. A. Fernandes, J. M. de Almeida and L. H. Theodoro, *Lasers Med Sci.* **25**, 2 (2010).
[253] R. S. Jayasree, A. K. Gupta, K. Rathinam, P. V. Mohanan and M. Mohanty, *J Biomater Appl.* **15**, 3 (2001).
[254] K. K. Reddy, C. W. Hanke and E. P. Tierney, *J Drugs Dermatol.* **9**, 2.
[255] J. C. Silva, Z. G. Lacava, S. Kuckelhaus, L. P. Silva, L. F. Neto, E. E. Sauro and A. C. Tedesco, *Lasers Surg Med.* **34**, 5 (2004).
[256] K. Stasi, J. Paccione, G. Bianchi, A. Friedman and J. Danias, *Acta Ophthalmol Scand.* **84**, 5 (2006).
[257] J. Heckenkamp, F. Adili, J. Kishimoto, M. Koch and G. M. Lamuraglia, *J Vasc Surg.* **31**, 6 (2000).
[258] M. R. Hamblin, D. A. O'Donnell, N. Murthy, C. H. Contag and T. Hasan, *Photochem Photobiol.* **75**, 1 (2002).
[259] T. N. Demidova and M. R. Hamblin, *Int J Immunopathol Pharmacol.* **17**, 3 (2004).
[260] M. R. Hamblin, T. Zahra, C. H. Contag, A. T. McManus and T. Hasan, *J Infect Dis.* **187**, 11 (2003).

[261] B. Wretlind and O. R. Pavlovskis, *Rev Infect Dis.* **5 Suppl 5**, (1983).
[262] T. W. Wong, Y. Y. Wang, H. M. Sheu and Y. C. Chuang, *Antimicrob Agents Chemother.* **49**, 3 (2005).
[263] P. S. Zolfaghari, S. Packer, M. Singer, S. P. Nair, J. Bennett, C. Street and M. Wilson, *BMC Microbiol.* **9**, (2009).
[264] A. P. Castano, P. Mroz, M. X. Wu and M. R. Hamblin, *Proc Natl Acad Sci U S A.* **105**, 14 (2008).

In: Exposure Therapy: New Developments ISBN
Editor: Jennifer E. Murray, Ph.D, pp. xx

List of abbreviations

ADME: Absorption, Distribution, Metabolism and Excretion
ALA: AminoLevulinic Acid
AMD: Age related Macular Degeneration
BCC: Basal Cell Carcinoma
bFGF : basic Fibroblast Growth Factor
BPD-MA : BenzoPorphyrin Derivative Monoacid ring A
CAM: ChorioAllantoic Membrane
CASP: ChlorAluminium SulphophtaloCyanin
CD : Cluster of Differentiation
DLI: Drug Light Interval
DMPC-EPG: DiMyristoylPhosphatidylCholine and Egg yolk PhosphatidylGlycerol
DPPC: DiPalmitoylPhosphatidylCholine
DPPG: DiPalmitoylPhosphatidylGlycerol
EPR: Enhanced Permeability Retention
FGF: Fibroblast Growth Factor
FITC: Fluorescein IsoThioCyanate
HD: High Dose
HDL: High Density Lipoprotein
HeNe: Helium Neon
HGF: Hepatocyte Growth Factor
HPPH: 2-[1-hexyloxyethyl]-2 Devinyl PyroPHeohorbide-a
HY: HYpericin
IFN : Interferon
ICAM : InterCellular Adhesion Molecule
Ig: Immunoglobulin
IL : Interleukin
IP: IntraPeritoneally
IP10: Interferon-γ- inducible Protein-10
IV: IntraVenously
LD: Low Dose
LDL: Low Density Lipoprotein
LLLT: Low-Level Light Therapy
MAL-PDT: Methyl AminoLevulinic acid PhotoDynamic Therapy
MCP : Monocyte Chimoattractant Protein
MET: MNNG HOS Transforming gene receptor
MIG: Monokine induced by Interferon -γ
MIP : Macrophage Inflammatory Protein
mTHPC: Meso-Tetra(HydroxyPhenyl) Chlorine
MPS: Mononuclear Phagocyte System
NdYAG: Neodymium-doped Yttrium Aluminium Garnet
NMP: N-methyl pyrrolidone
PDGF : Platelet-Derived Growth Factor

PDT: PhotoDynamic Therapy
PEG: PolyEthylene Glycol
PEG-LipBPD-MA : PEGylated Liposomal BenzoPorphyrin Derivative Monoacid ring A
PMN : PolyMorphoNuclear leukocytes
PS: PhotoSensitizer
RANTES: Regulated upon Activation, Normal T-cell Expressed, and Secreted
RES: ReticuloEndothelial System
ROS: Reactive Oxygen Species
TGF : Transforming Growth Factor
TNF : Tumor Necrosis Factor
VEGF: Vascular Endothelial Growth Factor

OBJECTIFS

L‘ effet tumoricide de la PDT résulte de la combinaison de dommages cytotoxiques directs sur les cellules tumorales et de dommages indirects caractérisés par l'altération de la vascularisation tumorale combinée à une activation du système immunitaire. Ce ciblage passif tumoral est à l'heure actuelle peu décrit mais peut notamment être obtenu grâce à la modulation de l'IDL mais également grâce à l'utilisation de formulations liposomales qui constituent les deux axes de recherche de cette étude.

En ce qui concerne l'IDL, les protocoles cliniques actuels de traitement par PDT sont établis sur l'idée selon laquelle l'illumination doit être effectuée au moment où la quantité de photosensibilisateur est maximale dans la tumeur afin d'obtenir une efficacité optimale. Néanmoins, plusieurs études de biodistribution ont mis en évidence, et cela pour divers PSs, que la meilleure efficacité était obtenue pour des IDLs différents de celui correspondant à la quantité maximale de PS dans la tumeur. Ainsi, les études de biodistribution standard ne permettent pas d'identifier les conditions optimales de traitement. En revanche, notre laboratoire a mis en évidence le rôle majeur de la distribution intratumorale spatio-temporelle de la mTHPC directement liée à l'IDL utilisé (99,103).

Les formulations liposomales des PSs constituent un axe de recherche en plein essor. Elles ont été reconnues pour leurs propriétés spécifiques permettant d'augmenter la vitesse de pénétration des PSs dans les tumeurs ainsi que leur taux de rétention (effet EPR). Néanmoins, une récente publication de notre laboratoire a fait état d'une différence de redistribution de la mTHPC en fonction du type de formulation liposomale utilisée (conventionnelle Foslip® ou PEGylée Fospeg®) (104). Ainsi, l'évaluation de la redistribution du PS à partir des formulations liposomales est une étape cruciale avant l'évaluation de l'efficacité thérapeutique.

Le premier objectif de cette étude fut d'utiliser un ciblage compartimenté de tumeurs (vaisseaux versus cellules tumorales) afin de potentialiser l'efficacité du traitement par mTHPC-PDT et de favoriser la mort par apoptose des tissus pathologiques. La stratégie employée a consisté en l'utilisation d'un co-ciblage des vaisseaux et des cellules tumorales *via* un fractionnement de l'administration de la mTHPC à un temps long et un temps court avant l'illumination.

Le second objectif fut d'évaluer la différence de redistribution de la mTHPC à partir de Foslip® et de Fospeg® via la technique du « *photoinduced quenching* » et d'étudier l'influence de cette redistribution sur l'efficacité de la PDT, en particulier sur les dommages vasculaires. Le modèle choisi a été la membrane chorioallantoïdienne de poulet (CAM) seule ou xénogreffée, particulièrement bien adaptée à l'étude des dommages vasculaires.

CHAPITRE II

Résultats

1. DOMMAGES PHOTOINDUITS PAR mTHPC

1.1 Dommages tumoraux photoinduits par le traitement mTHPC-PDT

La première partie des résultats consiste en un article publié en 2010 et portant sur l'étude des dommages tumoraux photoinduits par un traitement mTHPC-PDT et l'induction de la mort des cellules tumorales *via* un processus apoptotique :

Publication n° 2: "Compartmental Targeting for mTHPC-based Photodynamic Treatment *In Vivo*: Correlation of Efficiency, Pharmacokinetics, and Regional Distribution of Apoptosis"

Garrier J, *Bressenot A, Grafe S, Marchal S, Mitra S, Foster TH, Guillemin F, Bezdetnaya L.*
Int J Radiat Oncol Biol Phys; 2010. 78(2):563-571

Le choix de la dose de 0,3 mg/kg de Foscan® utilisée dans cette publication est issu d'études préliminaires de notre laboratoire réalisées en collaboration avec Biolitec GmbH. Ces travaux avaient démontré une efficacité importante d'un traitement Foscan®-PDT avec une dose de 0,3 mg/kg et un IDL de 3 heures sans aucune toxicité induite chez l'animal. En revanche, des doses de mTHPC plus importantes telles que 0,5 mg/kg s'étaient quant à elles révélées certes très efficaces pour l'éradication de la tumeur mais malheureusement très toxiques pour l'animal en induisant une nécrose profonde de la zone irradiée s'étendant aux tissus sains environnants et pouvant même parfois conduire à la perte d'un membre pour l'animal.
La dose de 0,3 mg/kg fut donc retenue et validée également de part le fait qu'elle est communément utilisée dans la littérature pour les travaux portant sur la thérapie photodynamique avec le Foscan® chez des modèles murins (96, 97, 100).

Int. J. Radiation Oncology Biol. Phys., Vol. 78, No. 2, pp. 563–571, 2010

0360-3016/$–see front matter

ELSEVIER

doi:10.1016/j.ijrobp.2010.04.009

BIOLOGY CONTRIBUTION

COMPARTMENTAL TARGETING FOR mTHPC-BASED PHOTODYNAMIC TREATMENT *IN VIVO*: CORRELATION OF EFFICIENCY, PHARMACOKINETICS, AND REGIONAL DISTRIBUTION OF APOPTOSIS

Julie Garrier, M.Sc.,* Aude Bressenot, M.D., M.Sc.,† Susanna Gräfe, Ph.D.,‡ Sophie Marchal, Ph.D.,* Soumya Mitra, Ph.D.,¶ Thomas H. Foster, Ph.D.,¶ François Guillemin, M.D., Ph.D.,* and Lina Bezdetnaya, M.D., Ph.D.*

*Centre de Recherche en Automatique de Nancy (CRAN-UMR 7039), Nancy-University, CNRS, Centre Alexis Vautrin, Vandœuvre-lès-Nancy, France; †Service d'Anatomie et de Cytologie Pathologiques, CHU de Brabois, Vandœuvre-lès-Nancy, France; ‡Research and Development, Biolitec AG, Jena, Germany; ¶Department of Imaging Sciences, University of Rochester, Rochester, New York

Purpose: The present study investigates the efficacy of compartmental targeting in grafted tumors treated by meta-tetra(hydroxyphenyl)chlorin (mTHPC)-mediated photodynamic therapy (PDT). The therapeutic efficacy was, furthermore, related to a regional photoinduced distribution of apoptosis and an mTHPC biodistribution profile.

Methods and Materials: Mice bearing EMT6 tumors were subjected to a single irradiation (10 J/cm^2) of red laser light (652 nm) at different intervals after a single- (0.3 mg/kg or 0.15 mg/kg) or double-intravenous (2 × 0.15 mg/kg) injection(s) of mTHPC. Efficiency of the treatment was evaluated by monitoring tumor regrowth. mTHPC pharmacokinetics were assessed by high-performance liquid chromatography analysis of excised organs. The regional distribution of apoptosis in tumor sections was investigated with a newly developed colabelling immunohistochemistry technique.

Results: A fractionated double-injection protocol of mTHPC with 24 h and 3 h drug-light intervals (DLI) yielded 100% tumor cure, with tumors presenting a massive apoptosis of neoplastic cells along with a distortion of vessels. The best efficiency for a single injection (0.3 mg/kg) was about 54% tumor cure and corresponded to a DLI of 3 h. At this DLI, tumors showed apoptosis of endothelial cells in residual vessels. Concentrations of mTHPC observed in plasma and tumor for the fractionated injection were not statistically different and were less than the total drug dose in each compartment.

Conclusions: The present work suggests that clinical PDT protocols with mTHPC could be greatly improved by fractionation of the drug administration. Time points should be chosen based on the intratumoral spatiotemporal drug distribution. © 2010 Elsevier Inc.

Apoptosis, Compartmental targeting, mTHPC, Photodynamic therapy.

INTRODUCTION

Photodynamic therapy (PDT) is a therapeutic strategy for the treatment of localized tumors that are accessible to light irradiation. It is based on the combined action of a photosensitizer (PS), light, and molecular oxygen, which leads to the generation of toxic reactive oxygen species. The tumoricidal effect of PDT is triggered by the direct damage of malignant cells and/or indirect vascular damage accompanied by an inflammatory response (1). Meta-tetra(hydroxyphenyl)chlorin (mTHPC) is a second-generation photosensitizer, approved in the EU in 2001 for the palliative treatment of head and neck cancers. It is the most potent photosensitizer, which is characterized by a low required light dose and reduced skin photosensitivity than other PS (2).

Compartmental targeting of the tumor microvasculature or parenchyma is closely related to the PS distribution, governed by the pharmacokinetic and cell/tissue-binding properties of the PS. PS distribution can be modulated by the drug-light interval (DLI), which is defined as the time that separates PS

Reprint requests to: Lina Bezdetnaya, M.D., Ph.D., CRAN-UMR 7039, Nancy-University, CNRS, Centre Alexis Vautrin, Avenue de Bourgogne, F-54511 Vandœuvre-lès-Nancy, France. Tel: 33 (0)3 83 59 83 06; Fax: 33 (0)3 83 59 83 78; E-mail: l.bolotine@nancy.fnclcc.fr

This research was supported by the Alexis Vautrin Cancer Center and the French Ligue Nationale contre le Cancer and by U.S. National Institutes of Health grant CA68409 (to S.M. and T.H.F.).

This work was presented at the 13th Congress of the European Society of Photobiology, Wroclaw, Poland, Sept 5-10, 2009.

Conflict of interest: none.

Acknowledgment—We thank Dr. Marie-Ange D'Hallewin for critical reading of the manuscript and helpful remarks.

Received Oct 12, 2009, and in revised form April 12, 2010. Accepted for publication April 14, 2010.

administration from light irradiation (3). PDT with short DLIs damages mainly endothelial cells (4–6), whereas longer DLIs favor direct neoplastic cell photodamage (3, 4, 7, 8).

Most pharmacokinetic studies are based on the assessment of drug content in various organs, including the tumor, but very little is known about drug transfer from the vessels to the tumor cells. Recently, Mitra *et al.* (9) first described the dynamics of intratumoral spatial distribution of mTHPC in EMT6 mammary carcinoma tumors with confocal fluorescence microscopy. mTHPC was confined to the vicinity of the vasculature for the first 3 to 6 h, followed by progressive migration to tissue at increasing distances from the vessels. At 24 h postinjection, mTHPC fluorescence could be detected only in tumor cells remote from the perfused vessels.

Some efforts have been undertaken to target both compartments (vessels and tumor cells) simultaneously. Fractionated photosensitizer and/or light administration has been studied with different photosensitizers, with heterogeneous results (4–6). The possible advantage of fractionation of light and/or drug lies in reduced administered doses, since the moderate photooxidative insult has been shown to favor apoptotic cell death (10).

Apoptosis is highly recommended in clinical situations with regard to the absence of a strong inflammatory reaction (11, 12). Photoinduced programmed cell death is characterized by signaling convergent to mitochondria, which induces a cascade of caspase activation. The final cleavage of vital substrates is realized by caspase effectors, particularly caspase-3. Evidence for the occurrence of apoptosis in PDT-exposed tumors is reviewed in Oleinick *et al.* (13), but the discrimination between apoptosis of endothelial and that of parenchymal cells has not been adequately addressed. At early time points post-porfirmer (Photofrin) PDT, apoptosis occurred in tumor endothelial cells lining occluded blood vessels, whereas at longer time points, apoptosis became more widespread (14).

In the present study, we attempted to evaluate the effect of compartmental targeting according to spatial intratumoral mTHPC distribution. The primary objective was to evaluate the therapeutic efficacy of a dual-PS injection in order to target both compartments during a single illumination. The secondary objective was to establish the spatial distribution of PDT-induced apoptosis as a function of illumination and drug administration regimen. For this purpose, we developed a new approach based on the colabelling of apoptotic cells and vessels by cleaved caspase-3 and murine collagen IV antibodies, respectively.

METHODS AND MATERIALS

Chemicals and reagents preparation

Cell culture was performed in phenol-red-free RPMI 1640 medium (Invitrogen, Cergy-Pontoise, France) supplemented with 9% fetal calf serum (PAN Biotech GmbH, Aidenbach, Germany), 1% 200 mM glutamine, and 1% penicillin (10,000 IU/ml)-streptomycin (10,000 μg/ml) (Invitrogen, Cergy-Pontoise, France). mTHPC was provided by Biolitec AG (Jena, Germany). Antibodies to mouse collagen IV (rabbit polyclonal) were purchased from Novotec (Varilhes, France), and goat anti-rabbit immunoglobulin G (IgG) coupled to fluorescein isothiocyanate (FITC) from Beckman Coulter (Roissy, France). Sheep anti-FITC antibody coupled to an alkaline phosphatase was purchased from Roche (Meylan, France) and rabbit antibody anti-cleaved caspase-3 from Cell Signaling (Danvers, MA). Biotinylated goat anti-rabbit IgG and streptavidin alkaline phosphatase were purchased from DakoCytomation (Trappes, France). All solutions were prepared according to standard procedures provided by Sigma-Aldrich (Saint Quentin Fallavier, France). AFA (Alcool Formol Acetic, Labonord, Templemars, France) fixing agent was composed of 75% (vol/vol) absolute ethanol, 20% (vol/vol) 30% (formalin), and 5% (vol/vol) 100% acetic acid. The 0.1 mg/ml collagenase (Eurobio, Les Ulis, France) solution was prepared in $CaCl_2$ solution at 4 g/1,000. Buffer A, containing 0.1 M phosphate-buffered saline, 0.3% (wt/vol) nuclease-free bovine serum albumin, 0.1% (wt/vol) sodium azide, 0.06% (wt/vol) *N*-ethyl-maleimide, and 20% (vol/vol) glycerol, was used to dilute primary antibodies. Fast Blue and Fast Red were composed of 96% (vol/vol) 0.1 M Tris (pH 8.2), 2% (vol/vol) Naphthol (Sigma-Aldrich, Saint Quentin Fallavier, France) ASMX, 2% (vol/vol) MRX50PA (Brij 35, Saponine, Tween 20, MgCl2 1M, Calbiochem, France), 0.05% (vol/vol) 1 M levamisole, and, respectively, 0.3% (wt/vol) Fast Blue or 0.1% (wt/vol) Fast Red. Equilibration buffer (pH 9.4) consisted of 12% (vol/vol) 1 M Tris HCl (pH 7.4), 2.4% (vol/vol) 5 M NaCl, and 6% (vol/vol) 1 M $MgCl_2$ in sterile water. Polyvinyl alcohol (PVA) medium was prepared with 80% (vol/vol) 50 mM Tris HCl buffer (pH 8.5), 20% (vol/vol) glycerol, and 13% (wt/vol) PVA.

Animal model and tumor system

Female BALB/c mice (Harlan, Gannat, France) (18–20g, 8–10 weeks old) were used in compliance with the French Animal Scientific Procedures Act (April 1988). Animals were kept under standard conditions and provided with food and water *ad libitum*. Animals were inoculated subcutaneously in the right flank with exponentially growing EMT6 cells (0.1 ml of 5×10^5 cells/ml in 0.9% NaCl). Experiments were initiated 10 to 12 days later when tumors reached 4 to 5 mm diameter.

Photosensitizer administration and photodynamic treatment

mTHPC was dissolved in a solution of ethanol/polyethylene glycol 400/water (2/3/5, vol/vol/vol). The treatment was carried out with the mice under anesthesia, with an intraperitoneal injection of a ketamine (Ketalar, 50 mg/mL)/xylazine (Rompun, 2%) mixture (90/10 mg/kg body weight). Irradiation was performed at 652 nm by an argon-ion-laser-pumped dye laser (Spectra-Physics, Les Ulis, France) to a total light dose of 10 J/cm^2 at a fluence rate of 30 mW/cm^2. Irradiation was performed through the skin overlaying the tumor, with a spot size of 1 cm. Different treatment regimens are shown in Fig. 1. Irradiation was performed at 3 h or 24 h after a single injection of 0.15 or 0.3 mg/kg. A 6 h DLI was applied after a single injection of 0.3 mg/kg. A separate set of experiments consisted of an injection of 0.15 mg/kg followed 21 h later by a second injection of 0.15 mg/kg and a single irradiation 3 h after the second injection. Mice received 100 μl of mTHPC solution via the tail vein. Controls animals received an intravenous (IV) injection of 0.3 mg/kg body weight mTHPC without irradiation ("no light" group).

Assessment of tumor response

Following treatment, orthogonal diameters of tumors were measured three times weekly. The tumor volume (V) was calculated

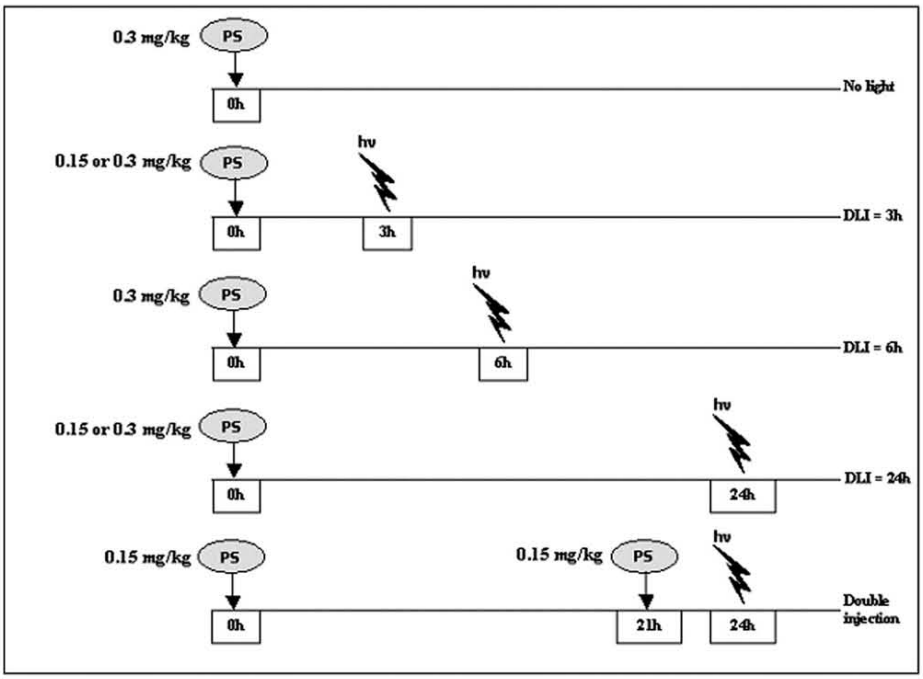

Fig. 1. Time line illustrating treatment protocols for mTHPC PDT in control (drug only) and PDT-treated mice. In the control group, mice received an IV injection of mTHPC (0.3 mg/kg). In PDT-treated groups, mTHPC was administered at 3, 6, and/or 24 h before irradiation with different concentrations. hv = irradiation; PS = photosensitizer.

using $V = Dd^2/2$, where D is the longest diameter, and d is the diameter perpendicular to D. Tumors were monitored until they reached the ethically mandated maximum volume of 1 cm^3. Animals were considered to be cured when they remained tumor free more than 180 days after PDT. Each experimental group included between 5 (control and 0.15 mg/kg groups) and 11 animals.

Histological studies

Three to four animals were used for each treatment condition. Animals were sacrificed 24 h after PDT by anesthetic overdose and cervical dislocation. Tumors were harvested and placed for 24 h in AFA fixing agent. Samples were routinely processed and embedded in paraffin. Necrosis was assessed by hematoxylin-eosin-safran (HES) coloration. Apoptosis distribution was addressed by a colabelling of vessels by collagen IV and apoptotic cells by cleaved caspase-3.

HES staining of necrosis. Three deparaffinized sections of 5-μm thickness obtained serially at 0.2-mm intervals were stained with HES for light microscopy examination and calculation of tumor size. Each section was imaged with a model DMD 108 microscope (Leica Microsystems, Wetzlar GmbH, Germany) at magnifications of $\times$40 to $\times$100. The ratio of necrotic area/tumor area was measured by tracing the demarcation of the tumor and the necrosis on the computer screen using ImageJ software and expressed as a percentage.

Colabelling of blood vessels and apoptosis. Deparaffinized sections were washed and subjected to heat-induced epitope retrieval by incubation in 10 mM EDTA (pH 8.0) for 10 min (120°C), followed by a 2 h cool-down. After being washed, the samples were hydrated for 30 min in Tris buffered saline Tween (TBST) (pH 7.6). Before slides were stained, they were treated at 37°C for 20 min with a 0.1 mg/ml collagenase solution. Primary antibodies were diluted in buffer A. Mouse collagen IV was detected with a polyclonal rabbit anti-mouse antibody at 4°C overnight, followed by goat anti-rabbit IgG coupled to FITC for 1 h. Sheep anti-FITC antibody coupled to an alkaline phosphatase was then applied for 1h and revealed by Fast Blue exposure 40 min later. Staining was fixed for 5 min in an equilibration buffer (pH 9.4). After sections were washed with osmosed water and TBST, they were hydrolyzed with 0.1 N HCL for 20 min and incubated with rabbit anti-cleaved caspase-3 at 4°C overnight.

Biotinylated goat anti-rabbit IgG was used for 1 h followed by 1-h incubation with streptavidin alkaline phosphatase and followed by Fast Red incubation for 40 min. Finally, slides were fixed with PVA. Negative controls were realized by using antibody solvent without primary antibody. After drying, slides were examined with an Axioscop II microscope (Zeiss, Jena, Germany), and images were registered with Axiovision 4.4 software. Apoptotic cells in each tumor were counted in ten consecutive fields away from the necrotic areas at $\times$1,000 magnification and were presented as the mean of the total calculated number of apoptotic cells.

Pharmacokinetic study

After they were anesthetized, animals were subjected to a single- or double-injection of mTHPC with subsequent removal of blood samples by intracardiac puncture at different times after injection. Plasma was collected after centrifugation at 3,000 rpm for 5 min at 4°C and kept at −80°C. For biodistribution studies, selected organs (skin, muscle, tumor) were removed, washed in 0.9% NaCl, and frozen at –80°C. mTHPC tissue concentrations were determined by high-performance liquid chromatography (HPLC) as previously described (15). Briefly, all tissue samples were minced, weighed, and freeze dried. Ten to twenty milligrams of each powdered sample was diluted in 1.5 ml of methanol/DMSO (3/5, vol/vol), mixed for 3 to 5 sec at 451.58 $\times$ g, and finally incubated (60°C) under continuous shaking for 12 h. Solutions were spun at 16,000 $\times$ g in a centrifuge for 5 min, and 1 ml of the supernatant was analyzed by HPLC. Each group consisted of at least 4 animals.

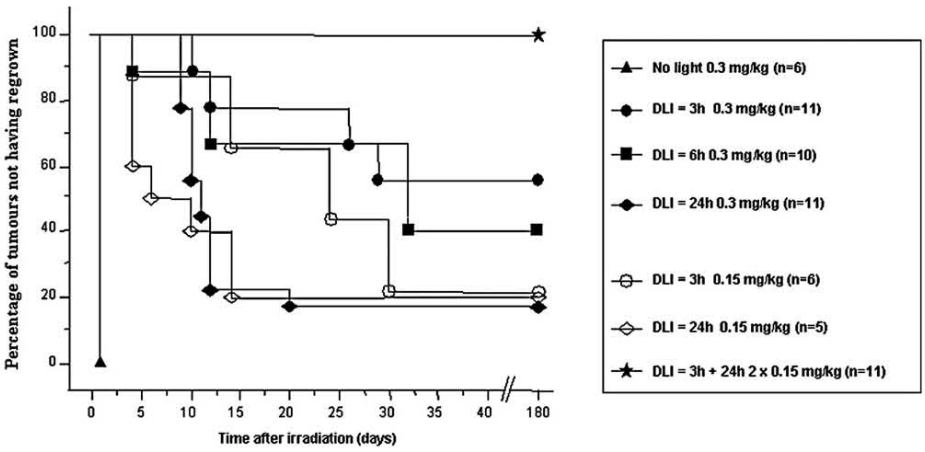

Fig. 2. Regrowth of EMT6 tumors after mTHPC-based PDT. Results are expressed as Kaplan-Meier plots, where the percentage of tumors not exhibiting regrowth is plotted as a function of time after PDT.

Statistics

Statistical analysis of tumor response between groups was carried out using Kaplan-Meier analysis and nonparametric Fischer's test with StatView 5.0 software (SAS institute Inc., SAS Campus Drive, NC) for Windows (Microsoft, Portland, OR). Nonparametric Mann-Whitney's U test was used for pharmacokinetic, apoptosis, and necrosis measurements, with a significance level of $p < 0.05$. Results are presented as mean ± standard error.

RESULTS

Tumor response to mTHPC-PDT treatment as a function of DLIs and mTHPC dose

The Kaplan-Meier plot shown in Fig. 2 demonstrates that 100% of tumor-bearing mice were cured with two administrations of 0.15 mg/kg body weight mTHPC at 24 h and 3 h before a single irradiation. This regimen appeared to be the most effective compared to a single injection, irrespective of the administered dose or DLI. Indeed, with a single injection of 0.15 mg/kg body weight at 3 h or 24 h before illumination, only 20% of mice were cured. A better efficacy was observed with a single injection of mTHPC at 0.3 mg/kg body weight for DLI 3 h and 6 h with 54% and 40% cure rates, respectively. A DLI of 24 h induced a cure rate of less than 20%, irrespective of the drug dose. There were no significant differences ($p > 0.05$) in growth delays between the different DLIs for all single injection treatments.

We noted that PDT damage to normal skin after a single (0.3 mg/kg, DLI 24 h) or a double injection of 0.15 mg/kg mTHPC consisted of a minimal redness during 48 h without subsequent scar formation (Fig. 3). This development

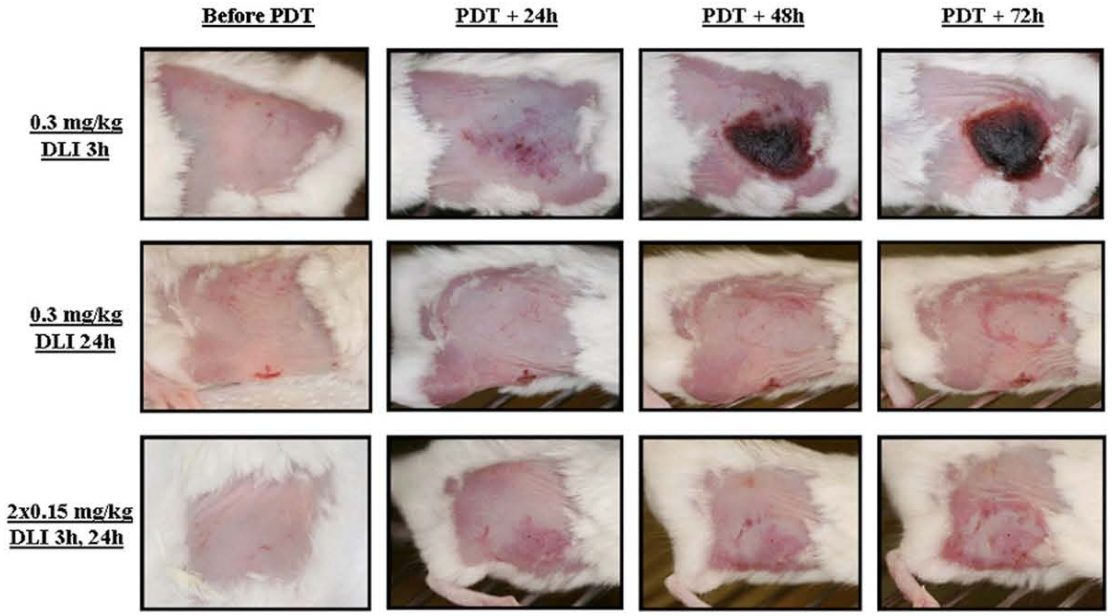

Fig. 3. Representative photographs of skin damage in mice induced by photodynamic treatment with a single (0.3 mg/kg) or a fractionated IV injection (0.15 mg/kg) of mTHPC.

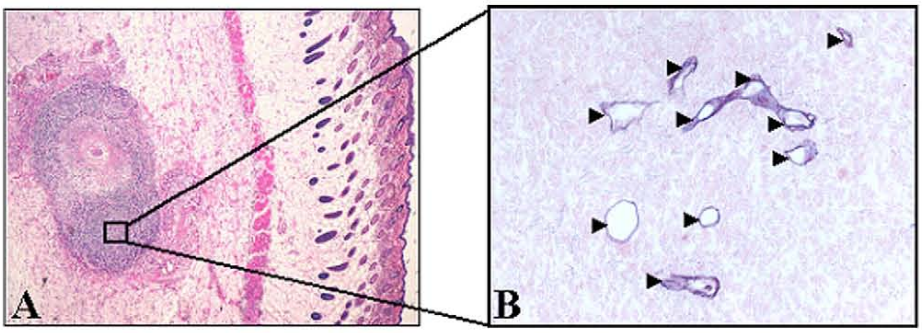

Fig. 4. Immunohistochemical analysis of excised EMT6 controls 24 h after an IV injection of mTHPC (0.3 mg/kg) in tumor-bearing mice. (A) HES coloration (magnification ×40). (B) Higher-power view shows immunohistochemical assessment of apoptosis with anti-cleaved caspase-3 (red) and microvasculature with anti-murine collagen IV (blue) antibodies (magnification ×400). Arrow heads indicate blood vessels.

contrasted deeply with the injection of 0.3 mg/kg and a 3 h DLI, where irradiated skin demonstrated pronounced scab formation (Fig. 3).

Apoptosis and necrosis with compartmental targeting

Control tumors stained by HES (Fig. 4A) presented a central necrotic area (30.8% ± 2.6 %) (Fig. 5) surrounded by proliferating neoplastic cells with numerous mitotic figures. Consequently, for further observations, only nonnecrotic areas were assessed. Anticollagen IV staining (blue) of control tumors (Fig. 4B) revealed the presence of viable vessels in the tissue without apoptotic cell staining (anticleaved caspase-3 staining, red). HES staining of PDT-treated tumors demonstrated in all experimental conditions a significant increase in central necrotic volume (Fig. 5), 1.5 to 2.2 times larger than that of controls. Necrosis was maximal for a DLI of 6 h (66.5% ± 8.7%), without, however, being significant (Fig. 5).

Colocalization of collagen IV (blue) and cleaved caspase-3 revealed two different profiles at a 3 h DLI. Either important apoptosis in the vessels (82 ± 8.7) but not in the parenchyma (11 ± 1.0) (Fig. 6B) or a complete absence of vessels as well as apoptotic cells (Fig. 6D) was observed. At a 6 h DLI, vessel staining was absent, and there was significantly less ($p < 0.05$) parenchymal apoptosis (31 ± 6) (Fig. 6F). For a DLI of 24 h, apoptosis was significantly increased in the parenchyma (63 ± 3.2). Fractionated administration of mTHPC induced massive tumor destruction (Fig. 7C) with exhaustive parenchymal apoptosis (583 ± 43) and distorted vessel structures (Fig. 7D).

mTHPC biodistribution assessed by HPLC

HPLC analysis of mTHPC in plasma, skin, tumor, and muscle is presented in Fig. 8. The highest plasma concentration was found at 3 h following 0.3 mg/kg mTHPC (0.13 ± 0.007 ng /mg tissue), whereas the highest tumor content was observed at 24h postadministration of 0.3 mg/kg mTHPC (0.077 ± 0.014 ng/mg tissue; $p < 0.05$). Fractionated mTHPC injection with a combination of 24 h and 3 h DLIs before HPLC analysis demonstrated comparable concentrations in

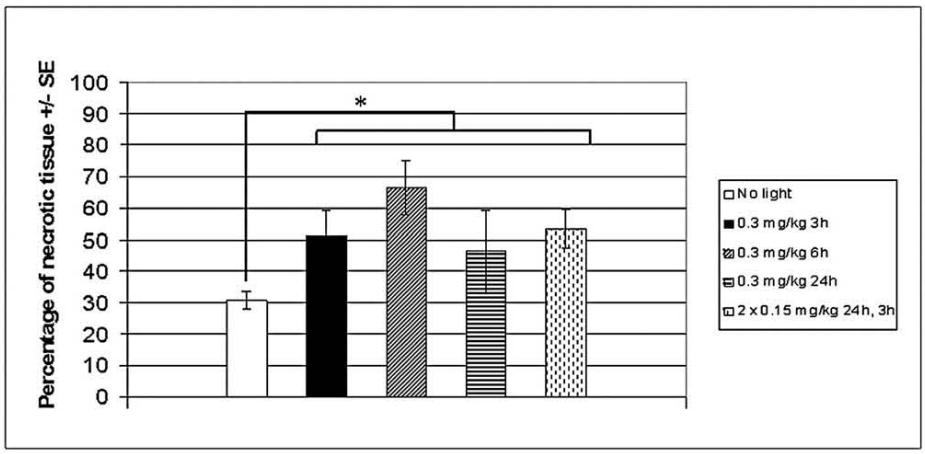

Fig. 5. Necrosis observed in EMT6 tumors excised 24 h after PDT with a single (0.3 mg/kg) or fractionated (2 x 0.15 mg/kg) mTHPC injections. Tumors were processed by HES staining. The ratio of necrotic area/tumor area was measured by tracing the demarcation of the tumor and the necrotic regions using ImageJ software. Mean percentage of necrosis from 3 mice for each group ± standard error is shown. Control mice received the solvent only. $*p < 0.05$ for all PDT-treated groups versus control group.

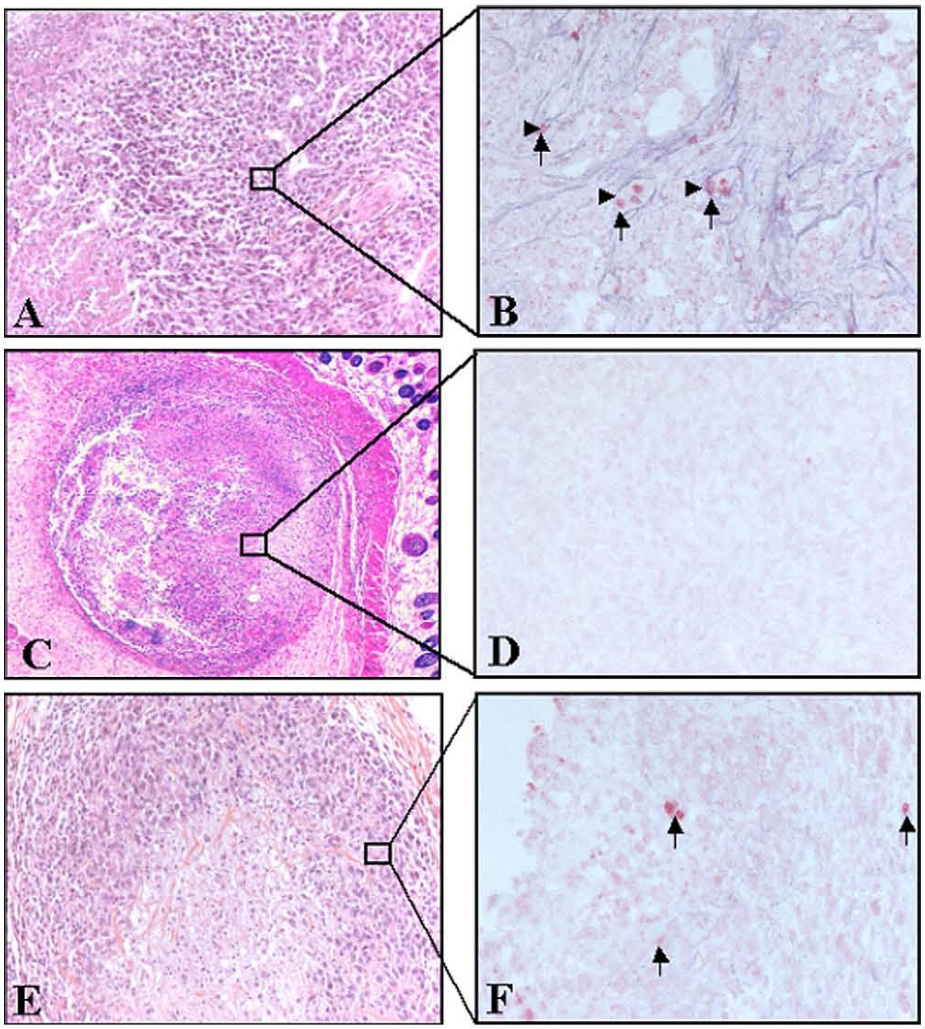

Fig. 6. Immunohistochemical analysis of EMT6 tumors excised 24 h after PDT with a single mTHPC injection (0.3 mg/kg) at DLIs of 3 h (A–D) or 6 h (E–F). (A, C, and E) HES staining (magnification in A and E, ×200, and ×40 for C). (B, D, and F) Immunohistochemical assessment of apoptosis with anti-cleaved caspase-3 (red) and microvasculature with anti-murine collagen IV (blue) antibodies (magnification, ×400). Arrow heads indicate blood vessels, and arrows indicate apoptotic cells.

all compartments (respectively, 0.059 ± 0.003 for plasma, 0.045 ± 0.013 for skin, and 0.056 ± 0.01 ng/mg for tumor tissue; $p > 0.05$). The highest tumor-to-muscle ratio of 4 was observed at 24 h after 0.3 mg/kg mTHPC.

DISCUSSION

Several teams have applied the concept of compartmental targeting to enhance photodynamic efficacy (16–21). Zhou *et al.* (22) noticed the importance of the choice of DLI to obtain a good treatment efficacy together with a maximal protection of normal tissues. Many subsequent investigations commented on the impact of DLI on the photodynamic effect, with significant improvement of efficacy with shorter time intervals, corresponding to high plasma levels of the drug (23–25). Veenhuizen *et al.* (6) investigated the impact of a double injection of 0.3 mg/kg mTHPC at 1 to 3 h and 48 h before illumination. Although mTHPC levels in the tumor were the highest at the longer DLIs, response was better at shorter time intervals and high plasma levels. The combination of two injections with the aim of obtaining high drug levels in both tumor and vascular compartments did not significantly improve results. Identical observations were made by the same group when both injections were separated by a time interval of 72 h, despite the fact that the total drug dose was doubled (4). Using a so-called vascular photosensitizer, Dolmans *et al.* (5) demonstrated that a double injection of this drug at 15 minutes and 4 h before illumination was significantly better than the single drug dose at any of those time points. They attributed this positive effect to the fact that fluorescence studies indicated a more homogeneous staining of both endothelial and perivascular structures following a double injection.

In a previous study, we used high-resolution confocal fluorescence imaging to simultaneously map microscopic intratumoral mTHPC localization with respect to perfused

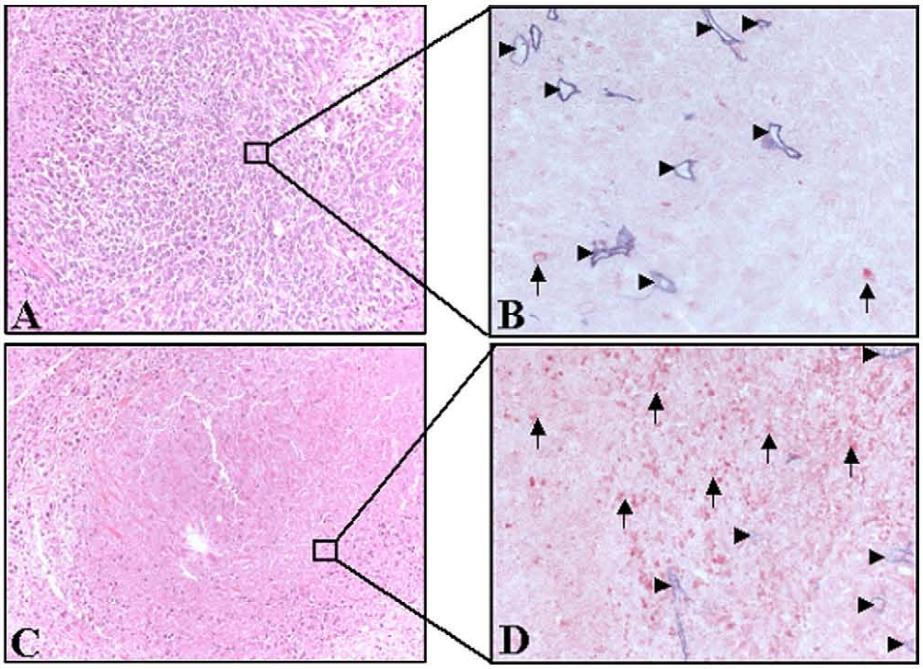

Fig. 7. Immunohistochemical analysis of EMT6 tumors excised 24 h after PDT with a single injection of mTHPC (A and B, 0.3 mg/kg) and a DLI of 24 h or fractionated mTHPC injections (C and D, 2 x 0.15 mg/kg). (A–C) HES staining (×200). (B–D) Immunohistochemical assessment of apoptosis with anti-cleaved caspase-3 (red) and microvasculature with anti-murine collagen IV (blue) antibodies (×400). Arrowheads indicate blood vessels, and arrows indicate apoptotic cells.

vasculature as a function of the time after injection (9). A progressive gradient of PS fluorescence was observed from the lumen to endothelial cells, to parenchyma adjacent to the vessels, and finally to tumor cells remote from the vascular structures. Three hours after injection, maximal mTHPC fluorescence was detected in the periluminal structures (within 15 μm). After 24 h, fluorescence was about three times higher at 140 μm from the vessel, corresponding to parenchyma localization. We therefore chose those two time points to evaluate the impact of fractionated mTHPC delivery on PDT-induced regional distribution of apoptosis and overall tumor regrowth.

With regard to the tumor regrowth curves (Fig. 2), it appears that irrespective of the single drug dose used, longer time intervals (24 h) are less effective, producing a tumor cure rate of <20%. These results are in agreement with those of previous mTHPC studies (4–6). A 100% cure rate was observed when two separate injections of 0.15 mg/kg were administered at 3

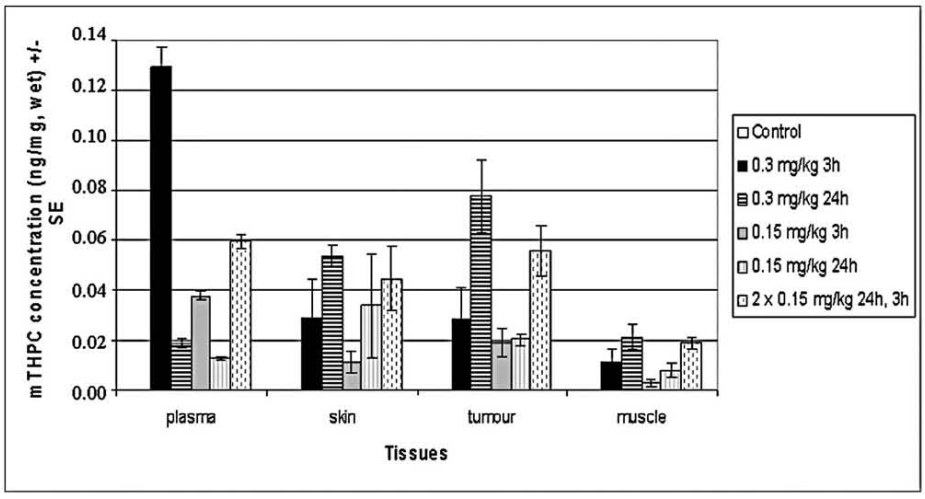

Fig. 8. mTHPC content in different tissues of EMT6 tumor-bearing mice. Mice were subjected to a single (0.15 or 0.3 mg/kg) or a fractionated (2 × 0.15 mg/kg) mTHPC injection. Three or 24 h later, plasma, skin, tumor, and muscle samples were excised and processed for HPLC analysis. Control mice received solvent only. Date are presented as the mean concentration of mTHPC (ng/mg, wet) ± standard error based on 3 mice for control group and 5 mice for other groups.

and 24 h before illumination (Fig. 2). A positive impact of drug fractionation has never been mentioned previously for mTHPC PDT. This should probably be attributed to the time points that were chosen in the earlier studies, 48 and 72 h (4, 6). Indeed, from our intratumor drug distribution studies, it appears that at those longer time points, maximal mTHPC fluorescence within the tumor is extremely remote from the vessels, thus indicating drug accumulation in regions that are potentially hypoxic and result in reduced PDT efficacy (9).

Irrespective of DLI, necrosis strongly contributes to cell death, as observed by HES staining (Fig. 5). This result is anticipated considering that mTHPC is a strong mediator of photoinduced necrosis (26). Regional distribution of apoptotic features induced by PDT has been poorly documented. An immunohistochemistry study by Engbrecht *et al.* (14) demonstrated that Photofrin mediated PDT induced apoptosis first in the endothelial cells bordering occluded blood vessels and then became more widespread at later time points. This observation relied on a double-fluorescent staining of endothelial cells (anti-platelet endothelial cell adhesion molecule [PECAM]) and apoptosis via the terminal deoxynucleotidyl transferase-mediated dUTP nick-end labeling (TUNEL) technique. A more recent study by Henderson *et al.* (10) investigated tumor grafts treated by 2-[1-hexyloxyethyl]-2-devinyl pyropheophorbide-a (HPPH) PDT with high and low fluences and fluence rates (48 and 128 J/cm^2, and 14 and 112 mW/cm^2). They demonstrated that extent and regional distribution of tumor and vascular damage, particularly apoptosis, correlated with fluence and fluence rate used during treatment.

To enable a new approach for simultaneous colabelling of vessels and apoptosis in the same section, cleaved caspase-3 is targeted for apoptosis, and murine collagen IV is used to mark basal membranes of vessels. The advantage of this new method is that on the same sample, apoptosis and vascular structures can be observed along with classical morphopathological features. When the PDT effect is extremely poor (24 h), vessels are intact, and only parenchyma cells show apoptotic features (Fig. 7A and B). Intermediate cure rates obtained with DLIs of 3 and 6 h mostly indicate vascular destruction, since collagen IV staining is absent along with a very limited staining of cleaved caspase-3 (Fig. 6C–F). A fractionated injection results in vascular effects with a poor collagen IV staining, together with massive apoptosis within the bulk tumor (Fig. 7C and D).

CONCLUSIONS

Historically, PDT protocols were established on the assumption that illumination should be performed at the highest tumor-to-normal drug ratios in order to protect healthy surrounding tissue and achieve a good tumoricidal effect (27). These ratios are observed only at long DLIs. Recent preclinical work, however, suggests that better cure rates could be obtained at shorter time intervals, corresponding to high plasma levels of the drug (8). From our work, it appears that the highest efficacy can be obtained when combining both propositions, aiming at the simultaneous destruction of tumor vasculature and neoplastic cells. The time point chosen for drug administration and illumination appears to be critical, since our study is the first to observe a benefit from mTHPC fractionation. It may be hypothesized that this is a consequence of the double injection resulting in a more homogeneous distribution of the drug in vascular structures as well as in tumor cells close to and more distant from vessels. These time points should not be determined solely on the basis of the plasma and bulk tumor drug levels obtained by extraction but rather by the temporal-spatial distribution of the photosensitizer within the tumor.

Although the excellent PDT efficacy obtained from dose fractionation at 24 h and 3 h may be unique to mTHPC due to its tight cell/tissue-binding properties, the tumor response results clearly demonstrate the importance of DLI informed by detailed drug distribution studies like those performed for mTHPC (9, 28).

REFERENCES

1. Dougherty TJ, Gomer CJ, Henderson BW, *et al.* Photodynamic therapy. *J Natl Cancer Inst* 1998;90:889–905.
2. Triesscheijn M, Baas P, Schellens JH, *et al.* Photodynamic therapy in oncology. *Oncologist* 2006;11:1034–1044.
3. Chen B, Pogue BW, Hoopes PJ, *et al.* Vascular and cellular targeting for photodynamic therapy. *Crit Rev Eukaryot Gene Expr* 2006;16:279–305.
4. Cramers P, Ruevekamp M, Oppelaar H, *et al.* Foscan uptake and tissue distribution in relation to photodynamic efficacy. *Br J Cancer* 2003;88:283–290.
5. Dolmans DE, Kadambi A, Hill JS, *et al.* Targeting tumor vasculature and cancer cells in orthotopic breast tumor by fractionated photosensitizer dosing photodynamic therapy. *Cancer Res* 2002;62:4289–4294.
6. Veenhuizen R, Oppelaar H, Ruevekamp M, *et al.* Does tumor uptake of Foscan determine PDT efficacy? *Int J Cancer* 1997; 73:236–239.
7. Jones HJ, Vernon DI, Brown SB. Photodynamic therapy effect of m-THPC (Foscan) in vivo: correlation with pharmacokinetics. *Br J Cancer* 2003;89:398–404.
8. Triesscheijn M, Ruevekamp M, Aalders M, *et al.* Outcome of mTHPC mediated photodynamic therapy is primarily determined by the vascular response. *Photochem Photobiol* 2005; 81:1161–1167.
9. Mitra S, Maugain E, Bolotine L, *et al.* Temporally and spatially heterogeneous distribution of mTHPC in a murine tumor observed by two-color confocal fluorescence imaging and spectroscopy in a whole-mount model. *Photochem Photobiol* 2005;81:1123–1130.
10. Henderson BW, Gollnick SO, Snyder JW, *et al.* Choice of oxygen-conserving treatment regimen determines the inflammatory response and outcome of photodynamic therapy of tumors. *Cancer Res* 2004;64:2120–2126.
11. LaMuraglia GM, Schiereck J, Heckenkamp J, *et al.* Photodynamic therapy induces apoptosis in intimal hyperplastic arteries. *Am J Pathol* 2000;157:867–875.
12. Wyllie AH. Apoptosis: an overview. *Br Med Bull* 1997;53:451–465.
13. Oleinick NL, Morris RL, Belichenko I. The role of apoptosis in response to photodynamic therapy: What, where, why, and how. *Photochem Photobiol Sci* 2002;1:1–21.

14. Engbrecht BW, Menon C, Kachur AV, *et al.* Photofrin-mediated photodynamic therapy induces vascular occlusion and apoptosis in a human sarcoma xenograft model. *Cancer Res* 1999;59:4334–4342.
15. Lassalle HP, Dumas D, Grafe S, *et al.* Correlation between in vivo pharmacokinetics, intratumoral distribution and photodynamic efficiency of liposomal mTHPC. *J Control Release* 2009;134:118–124.
16. Aalders MC, Triesscheijn M, Ruevekamp M, *et al.* Doppler optical coherence tomography to monitor the effect of photodynamic therapy on tissue morphology and perfusion. *J Biomed Opt* 2006;11:044011.
17. Chen B, Pogue BW, Goodwin IA, *et al.* Blood flow dynamics after photodynamic therapy with verteporfin in the RIF-1 tumor. *Radiat Res* 2003;160:452–459.
18. Chen B, Roskams T, de Witte PA. Antivascular tumor eradication by hypericin-mediated photodynamic therapy. *Photochem Photobiol* 2002;76:509–513.
19. Karmakova T, Feofanov A, Pankratov A, *et al.* Tissue distribution and in vivo photosensitizing activity of 13,15-[*N*-(3-hydroxypropyl)]cycloimide chlorin p6 and 13,15-(*N*-methoxy)cycloimide chlorin p6 methyl ester. *J Photochem Photobiol B* 2006;82: 28–36.
20. Li LB, Luo RC. Effect of drug-light interval on the mode of action of Photofrin photodynamic therapy in a mouse tumor model. *Lasers Med Sci* 2009;24(4):597–603.
21. Olivo M, Chin W. Perylenequinones in photodynamic therapy: Cellular versus vascular response. *J Environ Pathol Toxicol Oncol* 2006;25:223–237.
22. Zhou CN, Yang WZ, Ding ZX, *et al.* The biological effects of photodynamic therapy on normal skin in mice. I. A light microscopic study. *Adv Exp Med Biol* 1985;193:105–109.
23. Ferrario A, Kessel D, Gomer CJ. Metabolic properties and photosensitizing responsiveness of mono-l-aspartyl chlorin e6 in a mouse tumor model. *Cancer Res* 1992;52:2890–2893.
24. Gomer CJ, Ferrario A. Tissue distribution and photosensitizing properties of mono-l-aspartyl chlorin e6 in a mouse tumor model. *Cancer Res* 1990;50:3985–3990.
25. Harada M, Woodhams J, MacRobert AJ, *et al.* The vascular response to photodynamic therapy with ATX-S10Na(II) in the normal rat colon. *J Photochem Photobiol B* 2005;79: 223–230.
26. Marchal S, Fadloun A, Maugain E, *et al.* Necrotic and apoptotic features of cell death in response to Foscan photosensitization of HT29 monolayer and multicell spheroids. *Biochem Pharmacol* 2005;69:1167–1176.
27. Pervaiz S, Olivo M. Art and science of photodynamic therapy. *Clin Exp Pharmacol Physiol* 2006;33:551–556.
28. Ball DJ, Vernon DI, Brown SB. The high photoactivity of m-THPC in photodynamic therapy. Unusually strong retention of m-THPC by RIF-1 cells in culture. *Photochem Photobiol* 1999;69:360–363.

1.2 Dommages cutanés photoinduits par le traitement mTHPC-PDT

Cette seconde partie de l'étude des dommages photoinduits par mTHPC s'inscrit dans la continuité de l'article présenté précédemment. Les dommages secondaires cutanés photoinduits par un traitement photodynamique avec le Foscan® ont été évalués dans les mêmes conditions de traitement que celles présentées dans l'article mais sur souris saines.

1.2.1 Introduction

1.2.1.1 Dommages cutanés & PDT

Le traitement des cancers et d'autres maladies non malignes par thérapie photodynamique implique divers effets secondaires dont les plus importants sont la photosensibilisation de la peau et l'impossibilité pour le patient de s'exposer à la lumière durant plusieurs semaines après le traitement. La photosensibilité cutanée a été mise en évidence pour différents photosensibilisateurs tels que l'ALA (105), l'HPPH (106), le Tookad® (107) et la mTHPC (108).

1.2.1.2 Histologie et fonctionnalités de la peau

La peau est un organe composé de plusieurs couches, elles-mêmes constituées de plusieurs types cellulaires et composants extracellulaires, qui produit différentes structures spécialisées appelées des annexes. Une analyse histologique de la peau permet d'identifier 3 couches distinctes: l'épiderme, le derme et l'hypoderme (Figure 10).

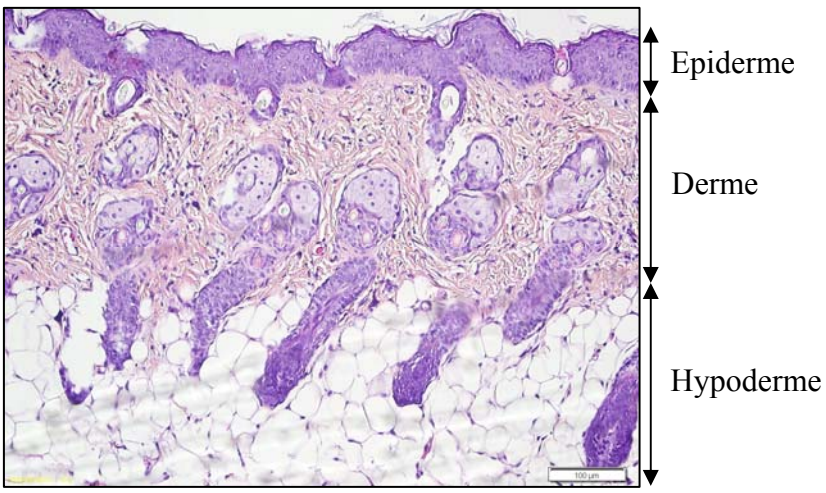

Figure 10. Coupe histologique de la peau de souris saines BALB/c femelles adultes. Coloration Hématoxyline-Eosine (H&E)

L'**épiderme** est un épithélium de revêtement, pavimenteux et pluristratifié (malpighien) kératinisé constitué de diverses cellules jointives et divisé en différentes couches cellulaires (Figure 11). La **couche basale** aussi appelée assise germinative ou « *stratum germinativum* », correspond à la couche la plus profonde. Elle repose sur une lame basale et est constituée de cellules en prolifération qui assurent une régénération continue du tissu. Au cours de leur vie, ces cellules sont progressivement repoussées vers les couches cellulaires périphériques successives suivantes: la **couche à épines (spineuse)**, la **couche granuleuse** puis la **couche cornée**.

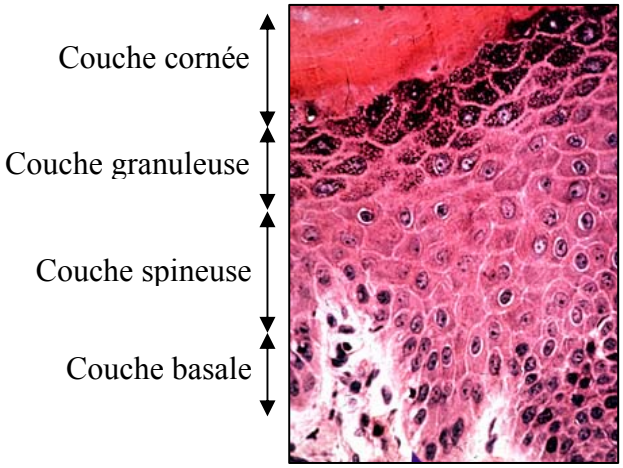

Figure 11. Coupe histologique de peau humaine, coloration H&E (http://www.chups.jussieu.fr)

Le **derme** est un tissu conjonctif dense constitué de fibroblastes sécrétant la matrice extracellulaire (collagène, d'élastine, de fibronectine et de glycoaminoglycanes) et contenant une quantité importante de capillaires sanguins et lymphatiques. Outre son rôle nutritif, le derme joue également un rôle primordial dans la thermorégulation et dans la cicatrisation ainsi que dans l'élimination de produits toxiques.

L'**hypoderme** est un tissu conjonctif lâche servant d'interface (amortissement) entre le derme et les tissus sous-jacents tels que les muscles et les tendons.

L'épaisseur de l'épiderme, du derme et de l'hypoderme varie d'un organisme à l'autre mais également d'un site à l'autre sur un même organisme. De plus, l'âge, le sexe et l'état physiologique de l'individu ont également un impact sur la structure interne de la peau.

Cette étude est un approfondissement des résultats publiés dans l'article publié dans *l'International Journal of Radiation in Oncology Biology Physics*. Les dommages cutanés photoinduits par le traitement Foscan®-PDT y étaient apparus très différents en fonction de l'IDL et de la dose de mTHPC administrée. Ce travail a pour **objectif** une identification et une analyse histologique fine de ces dommages cutanés secondaires.

1.2.2 Matériel & Méthodes

1.2.2.1 Modèle animal et traitement photodynamique

Les expériences ont été réalisées sur des souris saines BALB/c femelles âgées de 8 à 10 semaines et pesant entre 18 et 20 g (Harlan, Gannat, France). Elles ont été élevées avec un cycle jour/nuit de 12 heures et ont eu accès à la nourriture et à l'eau *ad libitum*. Cette étude a été réalisée en accord avec la législation en vigueur définie par la Directive 86/609/Communauté Européenne du 24 novembre 1986 et le Décret 87/848 de 1987 modifié par les Décrets 2001-464 et 2005-264. Les animaux ont reçu un traitement PDT suite à une injection intraveineuse de Foscan® selon le protocole de traitement décrit dans l'article précédent. Huit animaux ont été utilisés pour chaque condition de traitement dont quatre ont été sacrifiés 24 heures après PDT et quatre autres 48 heures après PDT.

1.2.2.2 Histologie et immunohistochimie

Les animaux ont été sacrifiés 24 heures ou 48 heures post-PDT à l'aide d'une anesthésie réalisée par injection intrapéritonéale d'un mélange kétamine (Ketalar®, 90 mg/kg) /xylazine (Rompun®, 10 mg/kg) suivie d'une dislocation cervicale. La peau correspondant à la zone de traitement a été photographiée puis prélevée et fixée dans de l'AFA (acide acétique, formol, alcool) pendant 24 heures. Suite à la fixation, les prélèvements ont été inclus dans de la paraffine et sectionnés en coupes fines de 5 µm selon le même protocole que celui présenté précédemment dans l'article.

Coloration Hématoxyline/Eosine (H&E). La procédure de préparation des échantillons utilisée a été la même que celle présentée dans l'article précédent.

Immunohistochimie de l'apoptose. Le marquage des cellules apoptotiques a été réalisé avec le même anticorps anti-caspase 3 clivée mais avec un protocole de révélation automatisé décrit ci-dessous. Le choix de cet anticorps anti-caspase 3 clivée est issu d'une publication

faite en 2009 et portant sur la fiabilité et la sensibilité de diverses techniques de détection de l'apoptose. L'immunohistochimie réalisée avec l'anticorps anti-caspase 3 clivée s'était révélée comme la technique la plus fiable et la plus sensible pour la mise en évidence de l'apoptose photoinduite des cellules *via* la voie intrinsèque. Cet article figure dans la partie « Production scientifique » de ce manuscrit:

Bressenot A, Marchal S, Bezdetnaya L, ***Garrier J****, Guillemin F, Plenat F.*
"Assessment of apoptosis by immunohistochemistry to active caspase-3, active caspase-7, or cleaved PARP in monolayer cells and spheroid and subcutaneous xenografts of human carcinoma". J Histochem Cytochem 2009; 57(4):289-300.

La mise en évidence des cellules apoptotiques a été effectuée sur les coupes fines avec une méthode de révélation streptavidine-biotine-peroxydase automatisée (Dakocytomation, Danemark). Les coupes ont été déparaffinées par passages successifs dans un bain de toluène puis d'alcool absolu et enfin d'alcool à 95° de 5 minutes chacun. Les lames sont ensuite rincées et réhydratées dans de l'eau osmosée. Le démasquage antigénique est réalisé par incubation des coupes dans un tampon Tris-citrate pH 6,0 durant 20 minutes à 97 °C (PT Link, Dakocytomation, Danemark). L'activité des peroxydases endogènes a ensuite été inhibée via une incubation de 10 minutes dans du peroxyde d'hydrogène à 3%. L'anticorps polyclonal de lapin anti-caspase 3 clivée (Cell Signaling, Danvers, Etats-Unis) a été utilisé pour mettre en évidence les cellules apoptotiques. Cet anticorps, dilué au 1/400ème, a été incubé sur les échantillons pendant 30 minutes à température ambiante suivi de l'anticorps secondaire polyclonal de cochon anti-lapin (Dakocytomation) dilué au 1/1000ème incubé avec les coupes pendant 30 minutes. Les lames ont ensuite été plongées dans une solution de 3,3′-diaminobenzidine (Dako Laboratories, Trappes, France) pendant 1 minute avant que la réaction se soit stoppée dans de l'eau distillée. Les coupes ont été contre-colorées avec de l'hématoxyline. Les contrôles négatifs ont consisté en un remplacement de l'anticorps primaire par de l'eau distillée.

1.2.2.3 Analyse visuelle et histologique des dommages photoinduits

L'analyse visuelle des dommages cutanés a été réalisée à l'aide d'un système d'attribution de scores (Tableau 4) (109). La zone cutanée irradiée a été photographiée 24 heures et 48 heures après le traitement PDT afin de déterminer le degré des dommages cutanés photoinduits. Des scores moyens de dommages ont été calculés en tenant compte du degré de dommages (grade)

pour chaque animal et ont été utilisés pour calculer un score moyen pour chaque condition de traitement.

Grade	Dommages cutanés observés
0	Pas de dommages
1	Rougeur minimale
2	Rougeur
3	Rougeur sévère
4	Formation d'une croûte fine
5	Formation d'une croûte épaisse

Tableau 4. Système d'évaluation visuelle des dommages cutanés photoinduits

L 'analyse histologique des dommages cutanés photoinduits a été réalisée sur 8 coupes histologiques de la peau irradiée de chaque animal. Quatre coupes ont été marquées avec une coloration H&E et les 4 autres coupes ont été utilisées pour la révélation des cellules apoptotiques. Les lames ont été observées à l'aide d'un microscope optique à transmission et du logiciel Cellsens® (Olympus, France) permettant de mesurer l'épaisseur de la peau. Cette épaisseur a été mesurée à trois localisations distinctes sur chaque coupe colorée avec H&E. Les données obtenues ont été utilisées pour calculer une épaisseur moyenne de la peau pour chaque animal et ensuite pour chaque condition de traitement.

1.2.2.4 Statistiques

La significativité des scores moyens de dommages cutanés observés ainsi que des épaisseurs moyennes de la peau mesurées a été analysée à l'aide d'un test non paramétrique Mann & Whitney ($p < 0.05$) et du logiciel Statview® 5.0. Les résultats sont présentés en moyenne ± erreur standard (ES).

1.2.3 Résultats

1.2.3.1 Observation visuelle des dommages cutanés

L'analyse visuelle de la peau des souris traitées par Foscan®-PDT a été réalisée à partir des photographies réalisées 24 heures et 48 heures après le traitement par PDT (Figure 12).

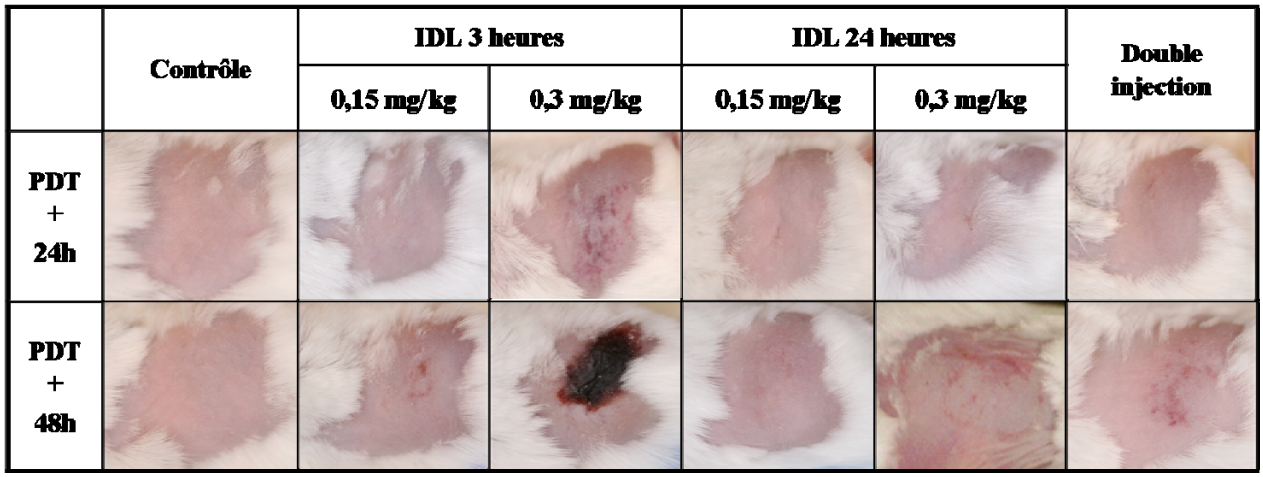

Figure 12. Photographies de la peau de souris saines BALB/c 24 heures ou 48 heures après un traitement PDT avec du Foscan® administré en intraveineuse. Chaque image est représentative des observations faites pour chaque condition de traitement (n = 4 souris pour chaque condition de traitement)

L'établissement des scores de dommages cutanés à permis de mettre en évidence que les dommages les plus sévères étaient obtenus à la suite d'un traitement avec 0,3 mg/kg de mTHPC et un IDL de 3 heures (Figure 13) en particulier 48 heures après PDT (score de dommages cutanés de 4,8 ± 0,3). En revanche, lorsque pour le même IDL, la dose est diminuée de moitié (0,15 mg/kg), les dommages restent superficiels (score de dommages cutanés maximal de 1,8 ± 0,3) malgré une différence significative avec le groupe contrôle. Les animaux traités par double injection présentent des dommages cutanés limités qui ne deviennent significativement différent du groupe contrôle que 48 heures après PDT avec un score de dommages de 1,0 ±0,1.

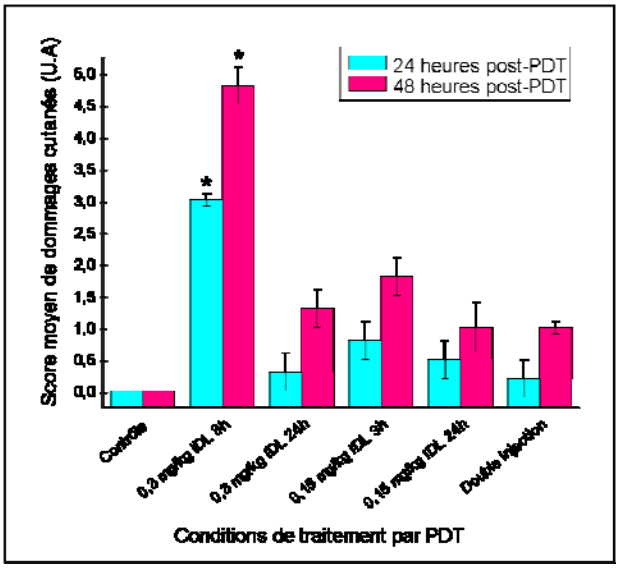

Figure 13. Scores moyens des dommages cutanés induits par un traitement PDT avec le Foscan®.
**** signifie significativement différent du groupe « contrôle » et des autres groupes traités (n = 4 souris pour chaque condition de traitement)***

1.2.3.2 Evaluation histologique des dommages

1.2.3.2.1 24 heures après PDT

Les animaux traités avec un IDL de 3 heures ou de 24 heures et une administration unique de mTHPC de 0,15 mg/kg présentaient une peau ayant un aspect similaire à celle des souris « contrôles » hormis un léger œdème avec l'IDL de 3 heures (Tableau 5). La peau des souris traitées avec une dose de mTHPC de 0,3 mg/kg indépendamment de l'IDL utilisé, présentait des cellules apoptotiques localisées dans la couche germinative de l'épiderme ainsi que dans le derme. Cela s'accompagnait d'une nécrose principalement dermique ainsi que d'un œdème et de nombreuses micro-hémorragies largement distribuées et d'un influx inflammatoire de polynucléaires (Tableau 5). Cependant, la peau des souris traitées avec l'IDL de 3 heures présentait une quantité beaucoup plus importante de ces dommages comparée à la peau des souris traitées avec un IDL de 24 heures (Tableau 5). La mesure de l'épaisseur de la peau (épiderme, derme et hypoderme) dans les différentes conditions de traitement a mis en évidence une variation de l'épaisseur uniquement suite à un traitement PDT avec 0,3 mg/kg de mTHPC et un IDL de 3 heures (Tableau 5). En effet, une augmentation significative de 20% de l'épaisseur de la peau (649,1 ± 57,3 µm) liée à un fort œdème a été observée.

Dose de mTHPC administrée (mg/kg)	IDL	Œdème	Apoptose & Localisation	Nécrose & Localisation	Micro-hémorragies & Localisation	Influx inflammatoire	Epaisseur de la peau (µm)
0,3	Contrôle	-	-	-	-	-	529,8 ± 19,7
	3h	+++	+++ Couche germinative de l'épiderme, derme	+++ Epiderme, derme, hypoderme et muscles	+++ Derme, hypoderme et muscles	+++	649,1 ± 57,3*
	24h	+	+ Couche germinative de l'épiderme, derme	+ Derme	+ Muscles	+	585,3 ± 36,7
0,15	3h	+	-	-	-	-	545,9 ± 16,4
	24h	-	-	-	-	-	508,4 ± 48,0
2 x 0,15 (double injection)	3h, 24h	-	-	-	+ Muscles	-	538,8 ± 54,0

Tableau 5. Critères d'analyse histologique de la peau de souris 24 heures après un traitement par Foscan® soit avec des IDLs de 3 heures ou de 24 heures et des doses de mTHPC de 0,15 mg/kg ou 0,3 mg/kg, soit par double injection de mTHPC.* signifie que l'épaisseur de la peau est significativement différente de celle des souris contrôles.

La figure 14 illustre les dommages cutanés observés 24 heures post-PDT dans la peau de souris traitées avec 0,3 mg/kg de mTHPC avec des IDLs de 3 heures ou de 24 heures. Le marquage immunohistochimique des cellules apoptotiques (marron) visible sur la figure 14 D,E, F au niveau des follicules pileux correspond à un marquage aspécifique lié au système de révélation avidine/biotine. Ce marquage aspécifique a été confirmé sur la peau des souris « contrôles » (Figure 14 D) ainsi que par la réalisation d'un témoin négatif ayant subi le même protocole de révélation mais en l'absence de l'anticorps primaire (anticorps anti-caspase 3 clivée) et sur lequel ce marquage aspécifique était également présent (données non présentées). La peau des souris traitées avec 0,3 mg/kg et un IDL de 3 heures présente d'importants dommages illustrés par une forte mortalité cellulaire à la fois par nécrose (Figure 14 B) et par apoptose (Figure 14 E).

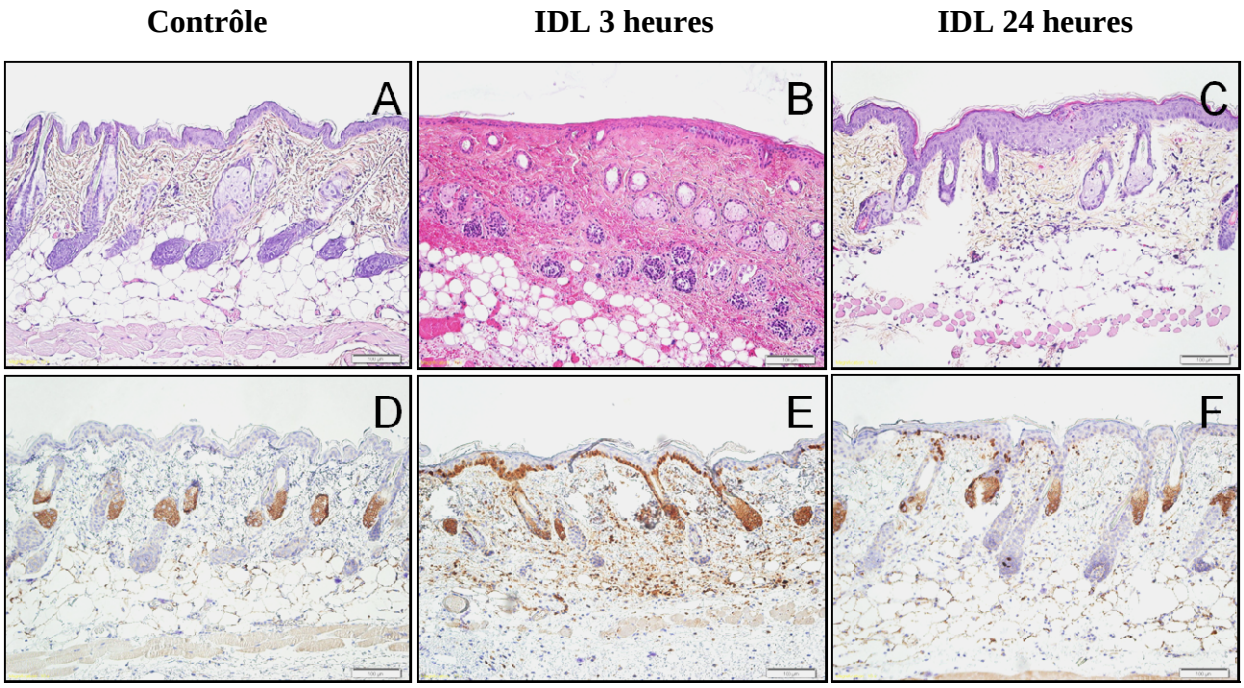

Figure 14. Coupes histologiques de la peau de souris contrôles et de souris traitées par Foscan®-PDT avec 0,3 mg/kg de mTHPC, IDL 3 ou 24 heures. Observation réalisée 24 heures post-PDT. Coloration H&E (A-C) et marquage immunohistochimique des cellules apoptotiques (marron) (D-F)

La peau des souris traitées par double injection de mTHPC présente un aspect histologique similaire à la peau des souris contrôles 24 heures après PDT. Seule la couche musculaire située sous l'hypoderme présente quelques micro-hémorragies (Tableau 5, Figure 15 B). Pour ces animaux, aucune mortalité cellulaire (nécrose, apoptose) n'a été mise en évidence ni au niveau musculaire ni dans le derme (Figure 15 D).

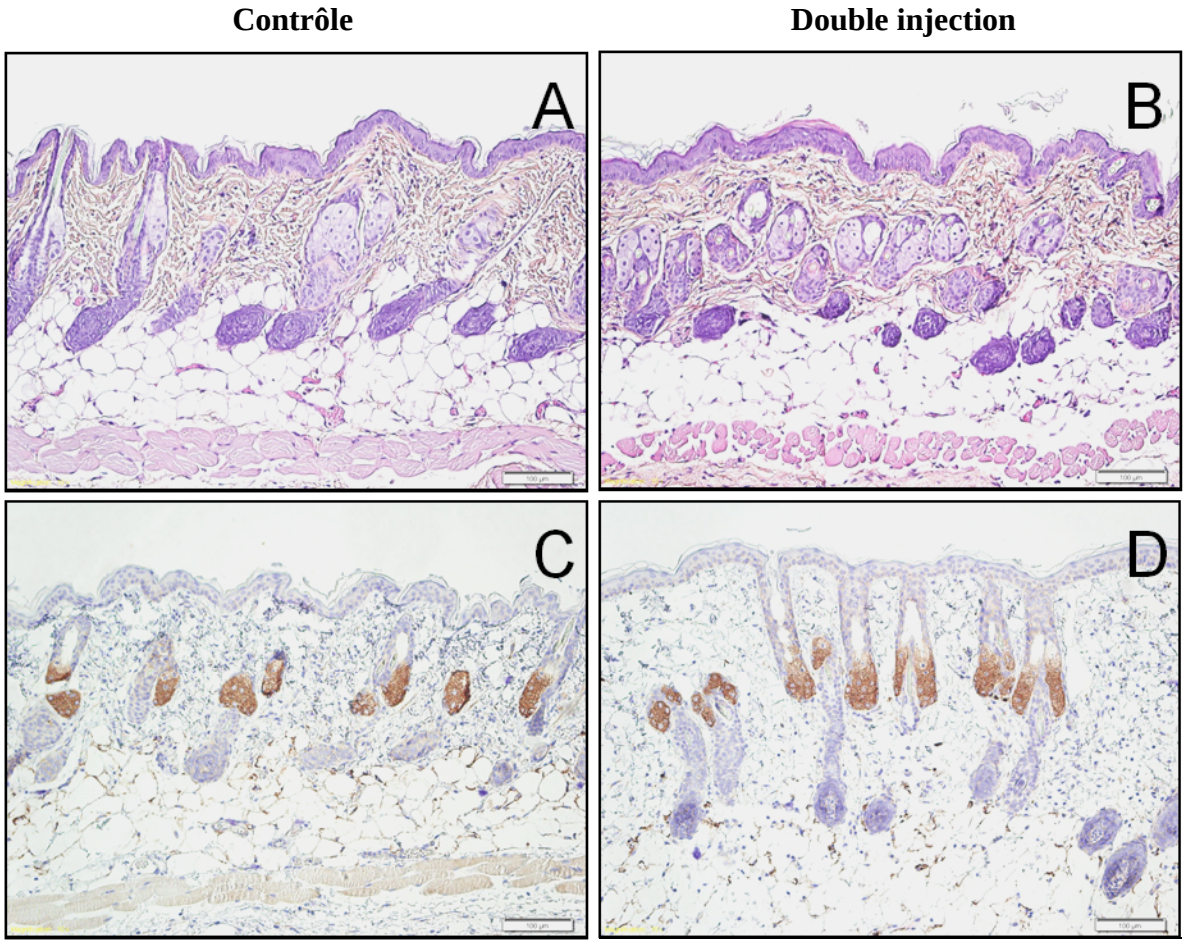

Figure 15. Coupes histologiques de la peau de souris contrôles et de souris traitées par Foscan®-PDT avec une double injection de mTHPC (0,15 mg/kg x 2). Observation réalisée 24 heures post-PDT. Coloration H&E (A, B) et marquage immunohistochimique des cellules apoptotiques (marron) (C, D).

1.2.3.2.2 48 heures après PDT

Les animaux traités avec un IDL de 3 heures ou de 24 heures et une administration unique de mTHPC de 0,15 mg/kg ne présentaient pas de dommages histologiques cutanés 48 heures après le traitement PDT (Tableau 6). En revanche, l'observation des animaux traités avec 0,3 mg/kg de mTHPC a révélé une désépithélialisation totale de la peau avec un IDL de 3 heures (Tableau 6, Figure 16 B) alors que seules des micro-hémorragies hypodermiques et musculaires sont apparues avec un IDL de 24 heures (Tableau 6, Figure 16 C). La mesure de l'épaisseur de la peau dans les différentes conditions de traitement a mis en évidence une diminution significative de 50 % de l'épaisseur de la peau (334,2 ± 24,5 µm) liée à la desquamation pour le groupe d'animaux ayant reçu 0,3 mg/kg avec un IDL de 3 heures (Tableau 6).

La peau des animaux traités par double injection de mTHPC a quant à elle révélé la présence d'un nombre plus important de micro-hémorragies au niveau musculaire et dermique mais la structure cutanée est conservée (Figure 16 D).

Dose de mTHPC administrée (mg/kg)	IDL	Nécrose	Micro-hémorragies & Localisation	Epaisseur de la peau (µm)
0,3	Contrôle	-	-	550,0 ± 30,3
	3h	+++	-	334,2 ± 24,5*
	24h	-	++ Derme, Hypoderme, Muscles	604,0 ± 70,0
0,15	3h	-	-	553,7 ± 55,3
	24h	-	-	516,4 ± 19,6
2 x 0,15 (double injection)	3h, 24h	-	++ Muscles, derme	603,1 ± 43,8

Tableau 6. Critères d'analyse histologique de la peau de souris 48 heures après un traitement par Foscan® soit avec des IDLs de 3 heures ou de 24 heures et des doses de mTHPC de 0,15 mg/kg ou 0,3 mg/kg, soit par double injection de mTHPC.* signifie que l'épaisseur de la peau est significativement différente de celle des souris contrôles.

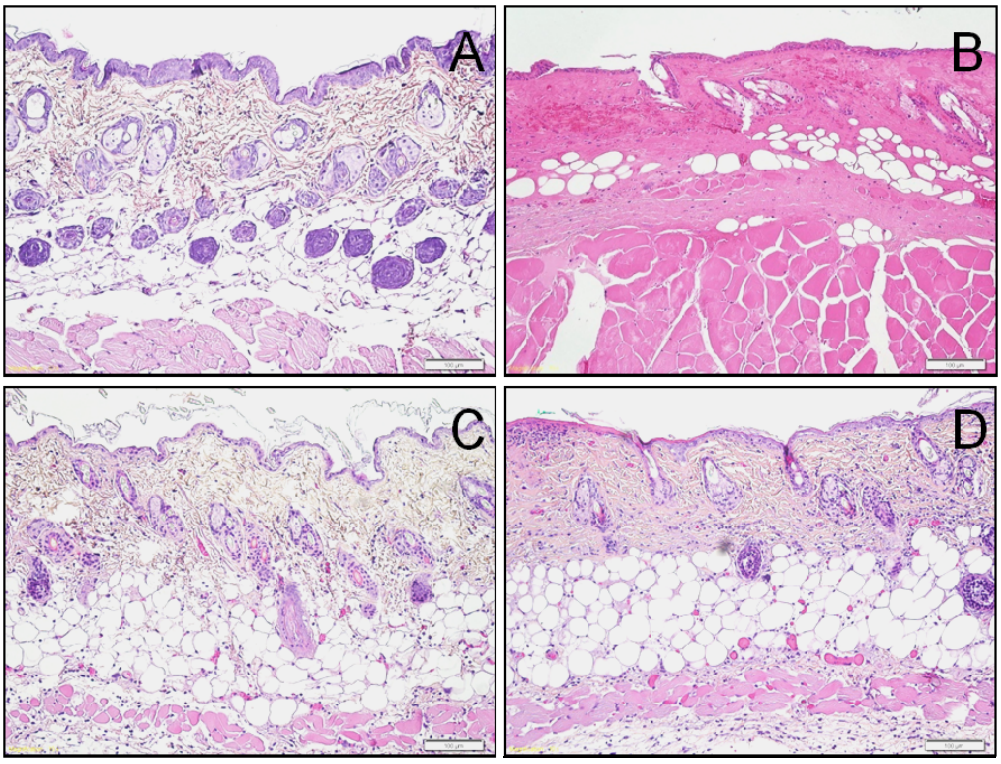

Figure 16. Coupes histologiques de la peau de souris contrôles (A) et de souris traitées par Foscan®-PDT soit avec 0,3 mg/kg de mTHPC et un IDL de 3 heures (B) ou de 24 heures (C), soit par double injection (D). Observation réalisée 48 heures post-PDT. Coloration H&E.

1.2.4 Discussion & Conclusion

Les résultats de biodistribution publiés dans l'*International Journal of Radiation in Oncoly Biology Physics* avaient démontré que les quantités de mTHPC mesurées dans la peau des souris étaient similaires pour toutes les conditions de traitement excepté avec 0,3 mg/kg et un IDL de 24 heures ou la quantité de mTHPC était réduite. Cependant, les dommages cutanés secondaires analysés dans cette étude sont significativement plus importants pour un traitement avec 0,3 mg/kg et un IDL de 3 heures (score de dommages de 4,8 observé 48 heures post PDT) comparé aux autres conditions de traitement. Ainsi, cela confirme une fois encore que les études de biodistribution standard ne permettent pas de prédire l'efficacité du traitement par PDT ni les dommages secondaires photoinduits.

Dans cette étude, les dommages secondaires les plus sévères observés suite à un traitement PDT par Foscan® à une dose de 0,3 mg/kg et un IDL de 3 heures se traduisaient par une nécrose et une apoptose massives accompagnées d'un fort œdème. La couche germinative de l'épiderme présentait de nombreuses cellules apoptotiques ce qui engendre une absence de renouvellement épithélial pour la zone traitée. Les autres conditions de traitement s'accompagnaient de dommages cutanés limités se traduisant par un score maximal de dommages observés de 1,8 ± 0,3 pour une PDT avec 0,15 mg/kg et un IDL de 3 heures.

Un traitement par PDT avec 0,3 mg/kg de mTHPC et un IDL de 3 heures avait résulté en un taux de guérison tumorale de 54 % chez les souris porteuses de tumeurs sous-cutanées mais les dommages cutanés secondaires apparaissent trop importants pour une validation de ce protocole. L'IDL de 24 heures quant à lui engendre des dommages secondaires cutanés moins importants mais correspond à un taux de guérison de seulement 20%. Par conséquent, l'IDL de 24 heures ne constitue pas non plus une bonne condition de traitement par Foscan®-PDT.

Tous les traitements réalisés avec une dose de 0,15 mg/kg et cela indépendamment de l'IDL ont présentés une histologie cutanée similaire à celle de la peau des souris contrôles. Cet aspect positif, lié à la faible dose de mTHPC administrée, est à contrebalancer avec le faible taux de guérisons (20%) associé à cette dose de PS. Un traitement avec une dose de 0,15 mg/kg de Foscan® n'est donc pas à retenir en vue d'une efficacité thérapeutique maximale.

Le traitement avec une double injection de mTHPC s'est avéré le plus efficace en induisant 100 % de guérisons de souris porteuses de tumeur EMT6 et des dommages secondaires restreints au niveau de la peau (rougeur). Ce résultat est issu du fractionnement de la dose de mTHPC permettant ainsi de diminuer la quantité de mTHPC circulante au moment de l'irradiation. La double injection apparaît donc être la stratégie de traitement optimale.

2. EVALUATION DE LA REDISTRIBUTION DE LA mTHPC LIPOSOMALE

La seconde partie de ce chapitre porte sur l'utilisation des formulations liposomales de la mTHPC pour un traitement par thérapie photodynamique. Les formulations liposomales ont été développées afin de palier au problème d'hydrophobicité et d'agrégation des photosensibilisateurs diminuant leur efficacité. Les liposomes maintiennent les PSs dans leur état monomérique et améliorent significativement leurs propriétés pharmacocinétiques. Une récente étude de notre laboratoire a démontré via la technique du « *photoinduced quenching* » la redistribution plasmatique de la mTHPC à partir des liposomes (104). Ainsi, le modèle choisi pour l'évaluation du comportement vasculaire des liposomes chargés en mTHPC a été la membrane chorioallantoïdienne de poulet (CAM).

2.1 Introduction

2.1.1 Le modèle de la membrane chorioallantoïdienne (CAM)

La membrane chorioallantoïdenne (CAM) de poulet est un modèle animal couramment utilisé pour l'étude de la distribution et des effets pro et anti-angiogéniques de divers composés *in vivo* (110,111). C'est un organe transitoire vascularisé présent dans les œufs de reptiles et d'oiseaux (Figure 17). La première transplantation tumorale réalisée sur la CAM fut décrite pour la première fois il y a un siècle (112) mais les modèles tumoraux xénogreffés sur la CAM restent très peu caractérisés comparés à ceux développés avec des modèles murins (113).

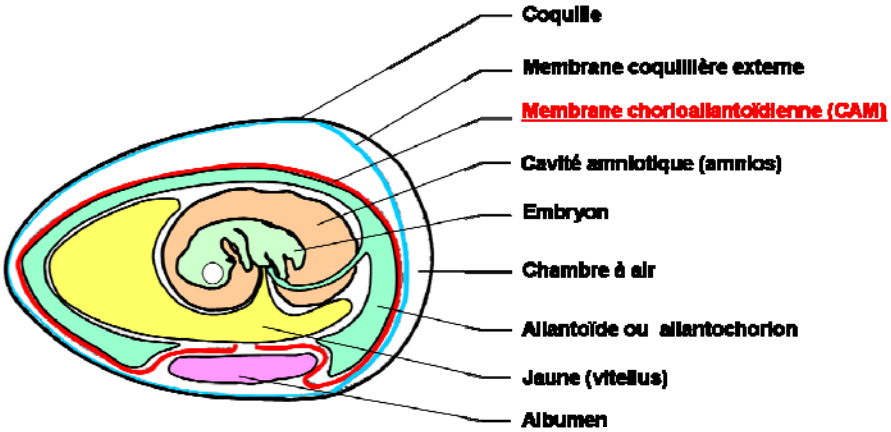

Figure 17. Schéma descriptif des différentes structures anatomiques de l'œuf de poule embryonné D'après Valdes et al. (114) et Eugenín and Eyzaguirre (115)

Le modèle de la membrane chorioallantoïdienne de poulet (CAM) a notamment été décrit dans la revue suivante qui a été réalisée sur invitation et qui figure dans la partie « Production scientifique » de ce manuscrit:

*Marie-Ange D'Hallewin, **Julie Garrier**, Marion Helle, Lina Bezdetnaya, François Guillemin « Animal models for photodiagnosis and photodynamic therapy. Photothéranostique, Israël Journal of Chemistry.*

Hamburger et Hamilton ont établi une classification des stades embryonnaires du poulet (stade HH pour Hamburger et Hamilton) basée sur les caractéristiques morphologiques externes de l'embryon mais distribuée de façon discontinue sur toute la durée du développement (116). Cependant, la classification actuellement la plus couramment utilisée considère le 1er jour d'incubation de l'œuf comme le premier jour de développement embryonnaire (EDD : Embryo Development Day) (111).

La CAM est une membrane transparente formée aux stades EDD4–EDD5 par la fusion des mésodermes de l'allantoïde et du chorion. Elle est composée de 2 épithelia unistratifiés séparés par un tissu conjonctif (Figure 18) riche en artères, veines et vaisseaux lymphatiques qui atteignent leur structure finale à EDD 18 et assurent la connexion avec la circulation sanguine de l'embryon (117,118). La CAM est un organe principalement dédié à la respiration de l'embryon mais elle joue également un rôle majeur dans le stockage des déchets métaboliques et le transport des électrolytes (sodium et chlorures) ainsi que dans la mobilisation du calcium à partir de la coquille nécessaire à la minéralisation des os de l'embryon (119).

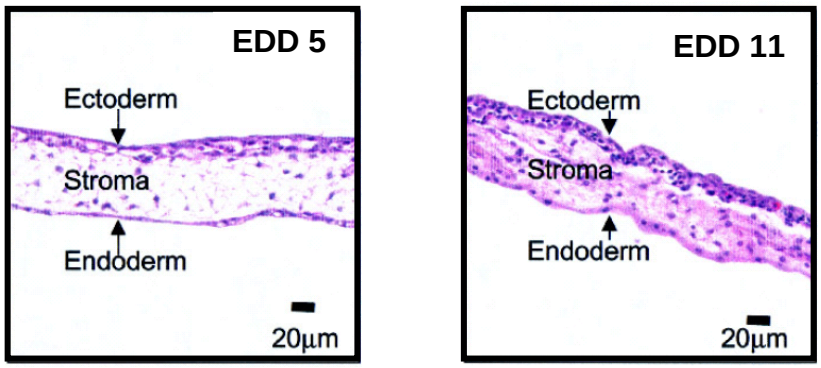

Figure 18. Coupes histologiques de la membrane chorioallantoïdienne à EDD 5 et EDD 11. Coloration hématoxyline/Eosine. D'après Valdes et al.(114)

Le modèle de la CAM présente divers avantages :

- la simplicité d'utilisation
- une structure hautement vascularisée
- une visualisation directe et en temps réel ne nécessitant aucune chirurgie ni anesthésie
- un faible coût : possibilité de réaliser des tests sur de nombreux échantillons (120)
- la transparence et la faible épaisseur (< 200 µm) adaptées aux approches photoniques
- l'immunodéficience : jusqu'à EDD 10, le système immunitaire aviaire reste incomplet lié à un manque de lymphocytes T et B. Par conséquent, cet environnement naturellement immunodéficient permet d'éviter la majorité des rejets observés lors de la xénogreffe de cellules ou de tissus. La présence de cellules T et B peut être respectivement détectée à EDD 11 et EDD 12 (121). Après le stade EDD 15, le répertoire de cellules B se diversifie et les embryons deviennent immunocompétents à EDD 18. Il est important de noter qu'il n'existe que 3 formes d'immunoglobulines (IgM, IgG, IgA) chez le poulet comparé à l'être humain qui possède 2 formes supplémentaires (IgD, IgE) (122).

Cependant, l'utilisation de la CAM implique également quelques inconvénients :

- une durée d'expérimentation limitée à 21 jours (éclosion)
- une existence de très peu de techniques d'analyse basées sur l'utilisation d'anticorps pouvant être utilisées sur la CAM
- des expérimentations devant être réalisées au même EDD car la CAM subit de nombreuses modifications durant le développement embryonnaire. En effet, divers paramètres vont varier tels que la composition de la matrice extracellulaire, le degré de différenciation des cellules endothéliales, les caractéristiques des jonctions inter-endothéliales ainsi que la localisation des vaisseaux (118).

La membrane chorioallantoïdienne apparaît donc comme un modèle parfaitement adapté à notre étude dont l'**objectif** est d'évaluer *in vivo* la redistribution de la mTHPC à partir de formulations liposomales (conventionnelle ou PEGylée) et son influence sur les dommages vasculaires induits par thérapie photodynamique.

2.1.2 Formulations liposomales de la mTHPC

Le **Foslip®** est une formulation liposomale de la mTHPC (Biolitec GmbH, Allemagne) composée d'un mélange de dipalmitoylphosphatidylcholine (DPPC) et de dipalmitoylphosphatidylglycérol (DPPG) avec un ratio de 9 : 1. Le ratio mTHPC : lipides est quant à lui de 1:12.

Le **Fospeg®** correspond à la même formulation que celle du Foslip® sur laquelle des groupements distearoylphosphatidylethanolaminem PEG 2000 (DSPE-PEG) ont été ajoutés (Figure 19) afin d'augmenter la durée de vie des liposomes dans la circulation sanguine. En effet, la couche de PEG a pour but de protéger les liposomes et retarder leur opsonisation par le système réticuloendothélial. Le ratio mTHPC : lipides est ici de 1 : 13.

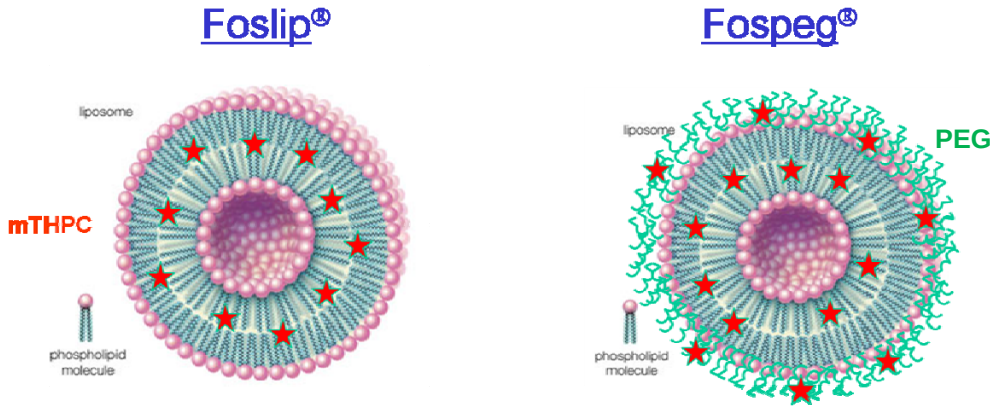

Figure 19. Schéma de la structure du Foslip® et du Fospeg®

2.1.3 Le « *Photoinduced Quenching* »

Les formulations liposomales de la mTHPC (Foslip®, Fospeg®) sont caractérisées par une forte concentration locale en mTHPC. Il a été démontré qu'une irradiation de ces formulations avec une faible dose de lumière induit une diminution significative de la fluorescence émise par la mTHPC qui peut être restaurée après l'ajout d'un détergent détruisant les liposomes (123). Cette observation a été attribuée au phénomène de « *photoinduced quenching* ». L'effet induit par le *photoinduced quenching* provient d'un transfert d'énergie entre les molécules de mTHPC situées à proximité les unes des autres à l'intérieur des liposomes vers les photoproduits non fluorescents issus de l'irradiation.

Suite à une administration intraveineuse, la concentration locale en mTHPC dans les liposomes diminue au cours du temps *via* l'intervention de deux mécanismes concomitants :

- une fuite de la mTHPC des liposomes vers les cellules du système vasculaire et les protéines plasmatiques
- une destruction des liposomes liée à un échange de lipides avec les protéines plasmatiques.

Dans le cadre de notre étude, ces 2 mécanismes sont regroupés sous le terme de « redistribution » de la mTHPC.

2.2 Matériel et Méthodes

2.2.1 Culture cellulaire

La lignée cellulaire utilisée correspond à des cellules EMT6 de carcinome mammaire murin cultivées en monocouche dans du milieu Roswell Park Memorial Institute (RPMI) 1640 (Gibco BRL) sans rouge de phénol supplémenté avec 9% de sérum de veau fœtal inactivé à la chaleur (SVF) (PAN Biotech), 1% de pénicilline-streptomycine (10 000 µg/ml) (Gibco BRL) et 1% de L-glutamine à 200 mM (Gibco BRL). Les cellules sont maintenues dans une étuve à 37°C, 5 % de CO2 et 95% d'humidité et réensemencées dans du milieu neuf tous les 7 jours afin de leur assurer une croissance exponentielle. Pour le développement de tumeurs, les cellules sont cultivées dans des flasques T175 (1 flasque de 175 cm² pour 3 œufs xénogreffés) pendant 1 semaine à une concentration de $0{,}5.10^4$ cellules/ml.

2.2.2 Préparation de la CAM seule et xénogreffée

Les œufs embryonnés (Couvoir de Cerveloup, Vourey, France) sont nettoyés à l'aide d'une compresse imbibée d'eau stérile et placés à température ambiante durant 4 heures. Les œufs sont ensuite transférés dans un incubateur (EHRET type compact S84, Allemagne) à 37,4°C et 80% d'humidité sous rotation. Au stade EDD 3, 6-7 ml d'albumine sont retirés de l'œuf via un trou réalisé dans la partie arrondie de l'œuf et à l'aide d'une seringue stérile connectée à une aiguille de 20G. Cette étape, réalisée en conditions stériles sous une hotte à flux laminaire, permet le décollement de la CAM de la coquille. Une large ouverture est ensuite réalisée à la surface de l'œuf à l'aide de microciseaux afin de contrôler le développement correct de l'embryon. Les embryons morts ou présentant des malformations sont exclus. L'ouverture est ensuite couverte avec du sparadrap (Durapore, Cergy Pontoise, France) et les

œufs sont réincubés sans rotation. Le développement de la CAM est contrôlé tous les 2 jours jusqu'au stade EDD10 (Figure 20).

Au stade EDD 10, un anneau de Téflon de 1 cm de diamètre (Weber, Paris, France) est déposé sur la CAM sous observation à la loupe binoculaire. La surface de la CAM est ensuite éraflée au centre de l'anneau à l'aide d'un scalpel stérile et 7.10^6 cellules EMT6 y sont déposées dans un volume de RPMI de 40 µL. Une tumeur vascularisée est obtenue au bout de 3 à 4 jours (EDD3 –EDD 4).

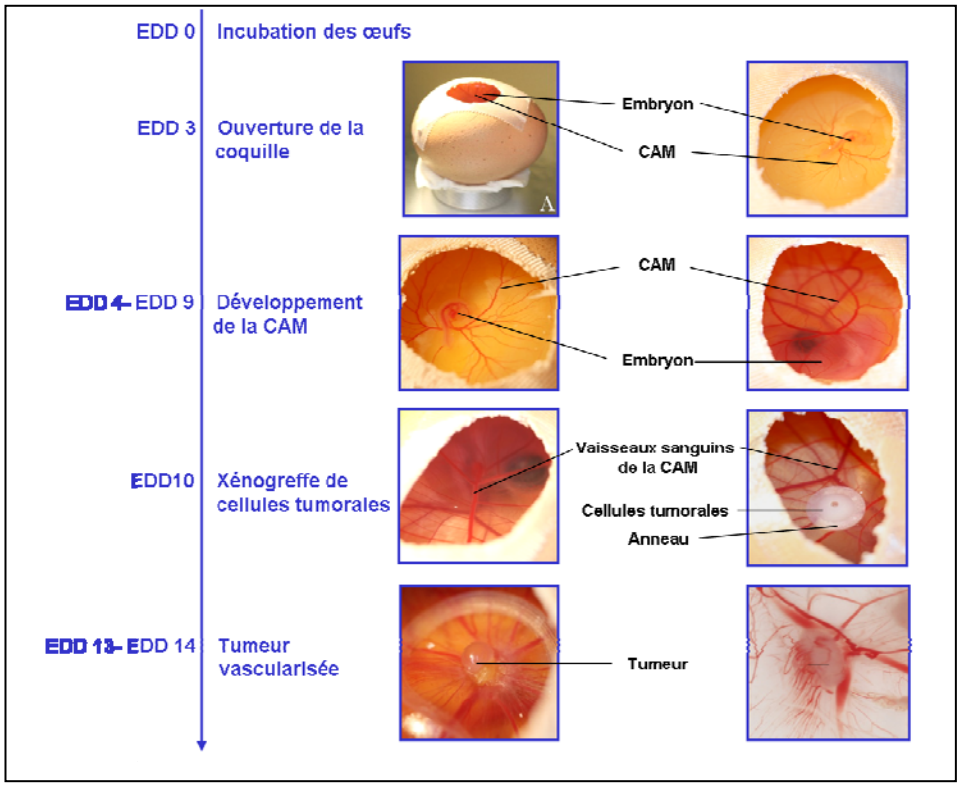

Figure 20. Schéma descriptif de la procédure d'utilisation de la membrane chorioallantoïdienne (CAM) d'œuf de poule embryonné

2.2.3 Préparation et administration de la mTHPC liposomale

Le **Foslip**® a été reconstitué selon le protocole préconisé par Biolitec GmbH qui consiste en l'addition de 3 ml d'eau pour préparation injectable dans le flacon de référence fourni (formulation lyophilisée) de façon à obtenir une concentration finale de 1,5 mg/ml.

Le **Fospeg**® quant à lui a été préparé via une technique d'extrusion publiée précédemment (104). Brièvement, les différents constituants sont pesés et dissous dans 1 ml

de méthanol : DPPC (18 mg/ml), DPPG (2 mg/ml), PEG (2 mg/ml) (Avanti, Alabaster, USA). La mTHPC est ensuite ajoutée à une concentration finale de 1,5 mg/ml et une évaporation du méthanol est réalisée à 70 °C pendant 1 heure. Le film liposomal est ensuite resuspendu dans 1 ml de PBS (pH 7,4 ; Invitrogen, Etats-Unis) à 70 °C sous rotation. L'échantillon subit ensuite 3 cycles thermiques successifs de 15 minutes à -80°C et 10 minutes à 70°C et est placé dans un mini-extrudeur (Avanti, Alabaster, USA) sur une plaque chauffante à 55°C afin d'homogénéiser la taille des liposomes préparés. La suspension est passée 21 fois à travers la membrane de filtration (100 nm polycarbonate Nuclepore®, Avanti Alabaster, USA). La préparation liposomales est ensuite conservée à 4°C et analysée par spectrophotométrie (Lambda 35, Perkin Elmer, Waltham, Etats-Unis) afin d'en déterminer la concentration en mTHPC en utilisant un coefficient d'extinction molaire de 30000 $M^{-1}.cm^{-1}$ à 650 nm dans de l'éthanol.

Le Foslip® et le Fospeg® sont administrés par injection intraveineuse dans la CAM au stade EDD 13 à l'aide d'une seringue stérile à usage unique et d'une aiguille de gauge 34 (Hamilton, Etats-Unis). Le volume d'injection est de 100 µL pour une dose de 1 mg mTHPC/kg pour chaque œuf. Un embryon de poule à EDD 13 pèse selon la littérature environ 10 g (124,125), la quantité de mTHPC administrée dans chaque œuf est donc de 10 µg.

2.2.4 Prélèvement des échantillons et analyse par la mesure du « *photoinduced quenching* »

Le sang des œufs est prélevé à l'aide d'une seringue à insuline stérile héparinée 5 minutes, 15 minutes, 30 minutes, 45 minutes, 1 heure, 2 heures, 3 heures, 6 heures et 24 heures après l'injection. Quatre à cinq œufs ont été utilisés pour chaque temps. Les prélèvements sont ensuite centrifugés à 3000 rpm et 4°C afin de collecter le plasma sanguin dépourvu de cellules. Ce plasma est ensuite analysé selon la technique du « *photoinduced quenching* » décrite dans un récent article de notre laboratoire (104). Brièvement, l'intensité de fluorescence de la mTHPC présente dans l'échantillon préalablement dilué dans du PBS est mesurée à 652 nm à l'aide d'un spectrofluorimètre (LS55, Perkin Elmer, Waltham, Etats-Unis) dans 3 conditions différentes successives :

- avant une irradiation
- après une irradiation de 30 secondes, avec une puissance de 17 mW à l'aide d'un laser à 652 nm et d'un diffuseur frontal

- après l'ajout d'un surfactant, le Triton X-100 (Sigma-Aldrich, Lyon, France) dilué 10 fois (masse/masse) dans du PBS qui va détruire les liposomes.

Le ratio établi entre la mesure de l'intensité de fluorescence après irradiation et celle obtenue après l'ajout de Triton reflète la concentration locale en mTHPC et est un indicateur du phénomène de *photoinduced quenching*. Toutes les mesures ont été réalisées en triplicat.

2.2.5 Traitement PDT et dommages vasculaires photoinduits

Suite à l'administration intraveineuse de Foslip® ou de Fospeg® à EDD 13, la CAM est irradiée à l'aide d'une diode laser à 652 nm (Biolitec GmbH, Iéna, Allemagne) avec une irradiance de 100 mW/cm² et une fluence de 3 J/cm². Ces paramètres d'irradiation ont été choisis à l'issue d'une optimisation montrant un taux de survie de 100 % des embryons pour ces conditions de traitement (données non présentées). Différents IDLs ont été testés : 15 minutes, 1 heure et 3 heures. L'imagerie des dommages vasculaires a été réalisée en partenariat avec la plateforme d'imagerie cellulaire PTIBC-IBISA imagerie et biophysique cellulaire et tissulaire UMR CNRS INPL UHP 7661 et FR CNRS 3209 Bioingénierie Moléculaire, Cellulaire et Thérapeutique (D.Dumas). La CAM a été imagée par réflexion en lumière blanche avant le traitement PDT ainsi que 24 heures après le traitement PDT à l'aide d'un macroscope Leica Z16PO A et du logiciel Leica Application Suite® version 3.6 (Leica, Allemagne). Sur la base des images recueillies, le diamètre des vaisseaux a ensuite été déterminé à l'aide du logiciel Image J® avant et après le traitement PDT afin d'évaluer le degré des dommages vasculaires photoinduits selon l'échelle de dommages présentée dans le tableau 7 d'après Pegaz *et al*. (126).

Taux de dommages vasculaires photoinduits	Observations
0	Pas de dommages
1	Occlusion des capillaires (∅ < 10 µm)
2	Occlusion des capillaires (∅ < 10 µm), occlusion partielle des vaisseaux sanguins (∅ < 30 µm) et diminution du diamètre des gros vaisseaux
3	Occlusion des vaisseaux sanguins (∅ < 30 µm) et occlusion partielle des gros vaisseaux
4	Occlusion totale des vaisseaux (∅ < 70 µm) et occlusion partielle des gros vaisseaux
5	Occlusion de toute la zone traitée

Tableau 7. Echelle d'évaluation des dommages vasculaires induits par un traitement PDT sur la CAM avec le Foslip® et le Fospeg®

La perfusion vasculaire a été visualisée par injection intraveineuse de 100 µL de nanobilles fluorescentes (fluosphere® carboxylate modified microsphere, Invitrogen, Etats-Unis) observées à l'aide d'une lampe à mercure et d'un cube filtre Texas Red dont l'excitation est réalisée entre 540 nm et 580 nm et l'émission entre 610 nm et 680 nm.

2.2.6 Analyses mathématique et statistique

Les intensités de fluorescence de la mTHPC mesurées dans l'étude de redistribution de la mTHPC à partir du Foslip® et du Fospeg® ont été analysées selon la procédure présentée dans l'article de Reshetov *et al* (104) afin de déterminer les pourcentages de redistribution de la mTHPC. Brièvement, un ratio appelé « fluorescence normalisée » est tout d'abord calculé :

$$\text{ratio} = \frac{\text{Intensité de fluorescence à 652 nm de l'échantillon après ajout de Triton}}{\text{Intensité de fluorescence à 652 nm de l'échantillon après l'irradiation}}$$

Cette fluorescence normalisée est ensuite recalculée en tenant compte que cette fluorescence correspond en réalité à la somme des fluorescences normalisées des liposomes donneurs et des structures acceptrices d'énergie (104). Les pourcentages de redistribution de la mTHPC quant à eux sont calculés en tenant compte que le ratio (0.10) observé à t = 0 minutes correspond à un pourcentage de 100 % de mTHPC présente dans les liposomes (aucune redistribution).

La mesure des diamètres des vaisseaux de la CAM traitée par PDT a été réalisée sur 3 œufs pour chaque condition et à trois emplacements distincts sur chaque CAM à l'aide du logiciel ImageJ®. Les données sont présentées sous forme de moyennes et les statistiques ont été réalisées à l'aide d'un test non paramétrique Mann & Whitney ($p < 0,05$) et du logiciel Statview® 5.0.

2.3 Résultats

2.3.1 La redistribution de la mTHPC à partir du Foslip® et du Fospeg®

La figure 21 présente le pourcentage de redistribution de la mTHPC à partir de liposomes suite à une administration intraveineuse de 1 mg/kg de Foslip® ou de Fospeg® dans la CAM. Ce graphique montre une redistribution initialement plus rapide et plus importante de la mTHPC à partir du Foslip® que du Fospeg®.

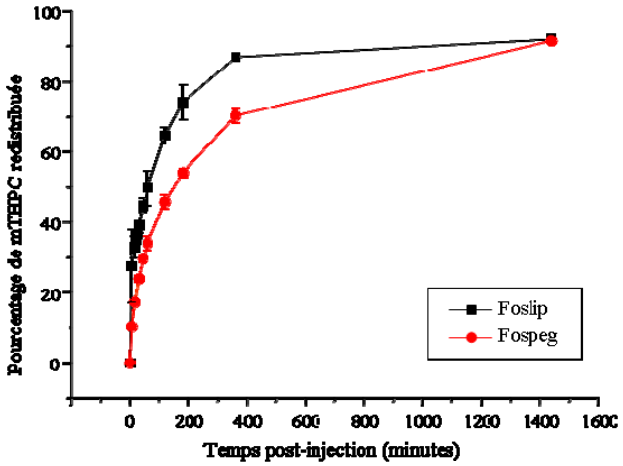

Figure 21. Pourcentage moyen de redistribution (± ES) de la mTHPC liposomale plasmatique suite à une administration intraveineuse de Foslip® ou de Fospeg® (1 mg/kg) dans la CAM à EDD 13 analysée par « photoinduced quenching (n=4 œufs pour chaque temps post-injection).

Les données de ce graphique sont également représentées sous forme de tableau où les pourcentages de redistribution de la mTHPC à partir du Foslip® apparaissent significativement supérieurs à ceux observés avec le Fospeg® excepté 24 heures après l'injection où les pourcentages sont similaires (Tableau 8). A titre d'exemple, dès 15 minutes après injection, le pourcentage de redistribution de la mTHPC à partir du Foslip® (33,0 ± 3,1) correspond à celui observé pour le Fospeg® seulement 1 heure après l'injection (34,0 ± 2,1). Ces observations se perpétuent au cours de l'expérimentation puisque le pourcentage de redistribution à partir du Foslip® observé 1 heure après injection (49,7 ± 4,9) correspond à celui observé pour le Fospeg® 3 heures après l'injection (54,1± 1,2).

Temps post-injection (min)	**Pourcentage moyen de mTHPC redistribuée**	
	Foslip®	**Fospeg®**
0	0	0
5	27,5 ± 10,4*	10,3 ± 0,4*
15	33,0 ± 3,1	17,2 ± 0,5
30	39,2 ± 2,2	24,0 ± 0,9
45	44,8 ± 2,1	29,7 ± 1,1
60	49,7 ± 4,9	34,0 ± 2,1
120	64,7 ± 2,3	45,8 ± 2,1
180	74,2 ± 5,0	54,1 ± 1,2
360	87,0 ± 0,6	70,4 ± 2,0
1440	92,0 ± 0,1*	91,6 ± 0,7*

Tableau 8. Redistribution de la mTHPC liposomale plasmatique suite à une administration intraveineuse de Foslip® ou de Fospeg® (1 mg/kg) dans la CAM analysée par « photoinduced quenching ». * signifie « non significativement différent » (Test non paramétrique Mann & Whitney, p < 0,05 ; moyennes ± erreur standard).

De plus, il est intéressant de noter que dès 15 minutes post-injection, la redistribution de la mTHPC à partir du Foslip® est 2 fois plus importante (33,0 ± 3,1%) que celle observée pour le Fospeg® (17,2 ± 0,5%). Cela signifie que la redistribution de la mTHPC à partir du Foslip® est deux fois plus rapide qu'à partir du Fospeg®. Cependant ce ratio n'est pas conservé pour les autres temps après injection. A 60 minutes post-injection, le ratio n'est plus que de 1,5 déclinant jusque 1,2 à 3 heures post injection. La vitesse de redistribution n'est donc pas constante au cours du temps. Ainsi, ces temps de 15 minutes, 1 heure et 3 heures seront utilisés comme IDLs dans la suite de notre étude afin de comparer les dommages induits par Foslip®/Fospeg®–PDT.

Ces expériences ont également été réalisées sur la CAM xénogreffée avec des cellules EMT6. La présence d'une tumeur n'a pas altéré la redistribution de la mTHPC à partir des liposomes et cela quel que soit le temps d'incubation dans la CAM et la formulation liposomale utilisée (données non présentées).

2.3.2 Les dommages vasculaires photoinduits par les formulations liposomales de la mTHPC

La Figure 22 présente les dommages vasculaires observés 24 heures après un traitement PDT de la CAM avec le Foslip® et pour des IDLs de 15 minutes, 1 heure et 3 heures. L'IDL de 15 minutes n'induit aucun dommage vasculaire (Figure 22 B) et la perfusion vasculaire est parfaitement conservée (Figure 22 C). L'IDL de 1 heure entraine quant à lui de nombreuses micro-hémorragies par rupture de la paroi des vaisseaux sanguins de diamètre moyen (Figure 22 E). Toutefois la perfusion vasculaire semble préservée dans les autres vaisseaux sanguins (Figure 22 F). Le traitement PDT réalisé avec l'IDL de 3 heures induit une destruction du réseau vasculaire de la CAM (Figure 22 H) et une totale occlusion de la zone irradiée (Figure 22 I).

Les dommages vasculaires observés suite à un traitement PDT de la CAM avec le Fospeg® sont illustrés dans la Figure 23. L'IDL de 15 minutes n'induit aucun dommage vasculaire (Figure 23 B) et la perfusion vasculaire est parfaitement conservée (Figure 23 C). L'IDL de 1 heure n'entraine que quelques micro-hémorragies des capillaires sanguins de petit diamètre (Figure 23 E) et la perfusion vasculaire semble parfaitement conservée dans le reste du réseau vasculaire (Figure 23 F). Le traitement PDT réalisé avec l'IDL de 3 heures induit une destruction du réseau vasculaire de la CAM (Figure 23 H) mais la perfusion vasculaire semble préservée dans les vaisseaux sanguins de diamètre important (Figure 23 I).

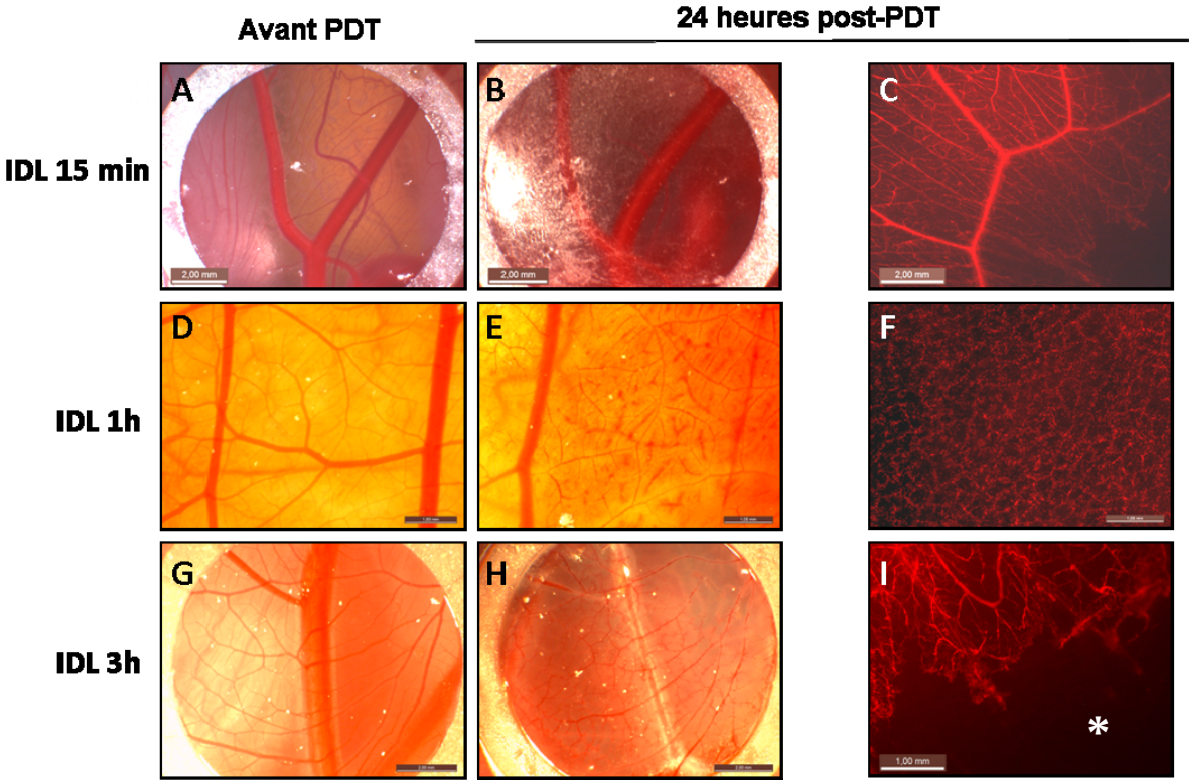

Figure 22. Morphologie de la CAM avant et après un traitement PDT suite à une administration intraveineuse de Foslip® (1mg/kg) avec un IDL de 15 minutes (A,B), 1 heure (D, E) ou 3 heures (G, H). La perfusion vasculaire a été observée par injection I.V de nanobilles fluorescentes (rouge) (C, F, I). indique la zone traitée par PDT.*

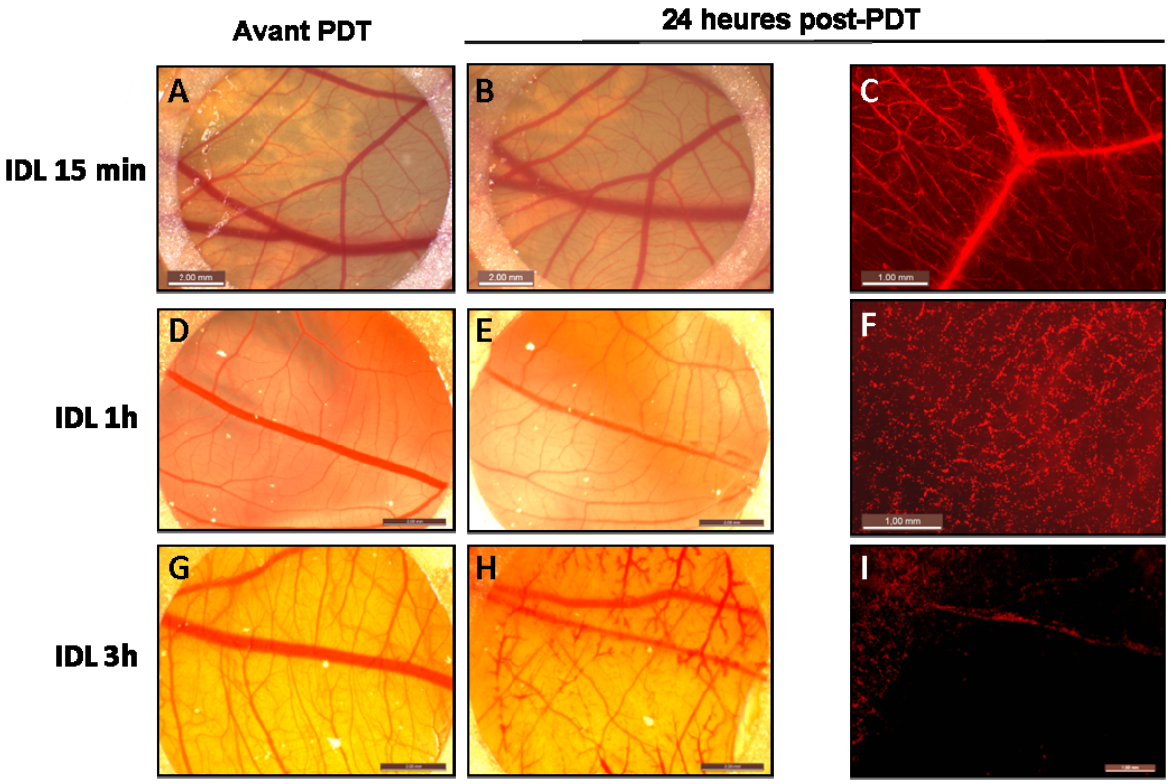

Figure 23. Morphologie de la CAM avant et après un traitement PDT suite à une administration intraveineuse de Fospeg® (1mg/kg) avec un IDL de 15 minutes (A,B), 1 heure (D, E) ou 3 heures (G, H). La perfusion vasculaire a été observée par injection I.V de nanobilles fluorescentes (rouge) (C, F, I).

La quantification de l'occlusion vasculaire induite par le traitement PDT est apparue significativement plus importante avec le Foslip® qu'avec le Fospeg® pour les IDLs de 1 heure et 3 heures (Figure 24). De plus, l'intensité de l'occlusion vasculaire semble corrélée à la durée de l'IDL. En effet, plus l'IDL est important et plus l'occlusion vasculaire photoinduite est étendue.

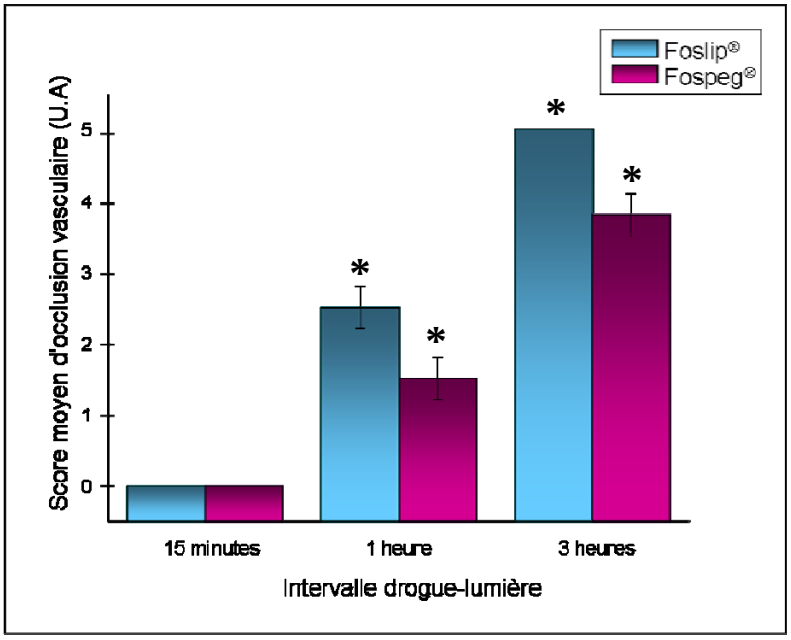

Figure 24. Occlusion vasculaire photoinduite par un traitement PDT de la CAM avec du Foslip® ou du Fospeg® administrés en intraveineuse (1 mg/kg). Score moyen représenté ± erreur standard.
**** signgifie que les données sont significativment différentes entre elles et de celles obtenues pour l'IDL 15 minutes.***

2.4 Discussion & Conclusion

La redistribution de la mTHPC à partir du Foslip® injecté en intraveineuse dans la CAM (1 mg/kg) est apparue plus rapide et plus importante que celle de la mTHPC à partir du Fospeg® administré dans les mêmes conditions. Cette différence de redistribution est liée à l'influence du PEG présent dans la formulation Fospeg® mais pas dans la formulation Foslip®. En effet, il a été montré que la fixation de groupements PEGylés à la surface de liposomes réduisait significativement le taux d'opsonisation et de rétention des liposomes par le système réticuloendothélial (127) et ainsi augmentait le temps de demi-vie plasmatique du photosensibilisateur (128). De plus, la PEGylation empêche l'agrégation des liposomes durant leur stockage mais également au moment de leur administration (129).

Une étude récente de notre laboratoire réalisée par Reshetov *et al* a montré une différence de redistribution de la mTHPC à partir de Foslip® et de Fospeg® incubés *in vitro* dans du plasma humain (104). En effet, la mTHPC était redistribuée beaucoup plus rapidement à partir du Foslip® qu'à partir du Fospeg®. Nos résultats obtenus *in vivo* dans la CAM ont donc confirmé cette observation.

Ces données ont été mises en relation avec une étude des dommages vasculaires photoinduits par Foslip®-PDT et Fospeg®-PDT sur la CAM en fonction de la redistribution de la mTHPC. Les IDLs ont été choisis afin de correspondre à une faible redistribution (15 minutes), une redistribution intermédiaire (1 heure) ou à une redistribution importante de la mTHPC (3 heures). Ainsi les dommages photoinduits ont été évalués de façon à déterminer s'il existe une corrélation entre la redistribution de la mTHPC et les dommages vasculaires induits par le traitement PDT. Une comparaison des dommages photoinduits par le Foslip® et le Fospeg® a également été effectuée. En effet, aucun dommage vasculaire n'a été observé avec un IDL de 15 minutes quelle que soit la dose de lumière administrée (données non présentées). En revanche, les IDLs de 1 heure et 3 heures ont eu un impact important sur la vascularisation de la CAM. Le taux de redistribution de la mTHPC augmente en fonction du temps et semble donc corrélé à l'intensité des dommages vasculaires photoinduits. Ainsi, un taux de redistribution à partir du Foslip® de 74,2 ± 5,0 % avait été mesuré pour un IDL de 3 heures et conduit à une occlusion totale de la zone traitée (score d'occlusion vasculaire de 5) alors qu'un IDL de 1 heure correspond à un score d'occlusion de 2,5 ± 0,3 et un taux de redistribution de la mTHPC de 49,7 ± 4,9 %. Le Fospeg®, quant à lui, induit des dommages moins sévères que le Foslip® pour tous les IDLs (score d'occlusion de 3,8 ± 0,3 pour l'IDL 3 heures) excepté à 15 minutes. A l'heure actuelle, une seule étude compare les dommages vasculaires photoinduits par le Foslip® et le Fospeg® dans la CAM (126). Le traitement photodynamique ayant été réalisé avec un IDL unique et des conditions d'irradiation très différentes des nôtres (une longueur d'onde de 420 nm pour une irradiance de 330 mW/cm² et une fluence de 12,5-100 J/cm²), il est impossible d'effectuer une comparaison des dommages vasculaires photoinduits.

La redistribution de la mTHPC à partir de formulations liposomales de type Foslip® ou Fospeg® influence l'intensité des dommages photoinduits par un traitement photodynamique. L'étude de ce paramètre est donc un prémice à toute expérience visant à l'optimisation des conditions de traitement par PDT avec le Foslip® ou le Fospeg®.

SYNTHESE GENERALE DES RESULTATS

L'effet tumoricide de la thérapie photodynamique repose sur une action combinée d'un photosensibilisateur, de la lumière et de l'oxygène conduisant à l'induction de dommages cellulaires, vasculaires ainsi qu'à une activation des effecteurs immunologiques. La mTHPC est un photosensibilisateur de seconde génération approuvé en 2001 en Europe pour le traitement palliatif de tumeurs superficielles de la tête et du cou. Les protocoles cliniques de traitement actuels s'appuient sur les données issues de pharmacocinétique et de biodistribution standard pour établir les paramètres de traitement à utiliser. Ainsi, l'intervalle drogue lumière appliqué correspond au moment où la quantité de photosensibilisateur est maximale dans le tissu tumoral. Cependant, de nombreuses études, réalisées avec divers photosensibilisateurs, ont révélé que l'efficacité optimale du traitement par PDT n'était pas obtenue lorsque la quantité de PS dans la tumeur était maximale. Par conséquent, les études de biodistribution ne semblent pas permettre d'établir de bonnes conditions de traitement.

Notre laboratoire, en collaboration avec une équipe américaine, a mis en évidence le rôle prépondérant de la distribution intratumorale spatio-temporelle du PS, en particulier de la mTHPC (99). Cette étude a démontré une localisation vasculaire de la mTHPC avec un IDL de 3 heures, puis une fuite des vaisseaux vers le tissu néoplasique à proximité des vaisseaux à 6 heures et une localisation dans le parenchyme tumoral éloigné des vaisseaux avec un IDL de 24 heures. Basé sur cette distribution intratumorale, notre étude a révélé l'efficacité optimale d'un traitement par mTHPC-PDT via un ciblage des vaisseaux et des cellules tumorales. En effet, le traitement avec une injection de 0,3 mg/kg de mTHPC et un IDL de 3 heures s'est conclu par un taux de guérisons de 54% alors qu'un IDL de 24 heures ne donnait que 20% de guérisons. Notre stratégie a donc consisté en un fractionnement de l'administration de la mTHPC (2 x 0,15 mg/kg) respectivement 24 heures et 3 heures avant l'irradiation afin de cibler non seulement le parenchyme tumoral mais également la néovascularisation. Cette double injection a permis d'obtenir un taux de guérisons de 100%, se révélant ainsi comme une stratégie de traitement très prometteuse.

De plus, à l'aide d'une technique de co-marquage immunohistochimique, il a été mis en évidence que le traitement PDT avec une administration fractionnée de Foscan® permettait d'obtenir une éradication des tumeurs *via* une induction massive de la mort cellulaire par apoptose et une destruction de la néovascularisation. Cette observation est cohérente avec celle effectuée pour les IDLs de 3 heures et 24 heures qui correspondaient respectivement à

une apoptose des cellules endothéliales et une apoptose du parenchyme tumoral, liée à la distribution intratumorale de la mTHPC. La favorisation de la mort cellulaire par apoptose est un challenge important dans le contexte clinique. En effet, un traitement anti-cancéreux induit majoritairement une destruction des tissus néoplasiques par nécrose. Cela implique une forte réaction inflammatoire pouvant être douloureuse pour le patient mais surtout une perte de substance pouvant conduire à la perforation de l'organe traité. En revanche, la mort par apoptose de tumeurs est plus douce et n'engendre qu'une faible inflammation sans aucune perte de substance massive. L'évaluation histologique de la nécrose photoinduite par le traitement n'a fait apparaitre aucune différence entre les différents groupes traités quels que soient l'IDL ou la dose de PS administrée. Ainsi, dans le cas présent, la nécrose ne peut expliquer à elle seule la photodestruction des tumeurs et l'apoptose serait donc privilégiée.

Une étude de biodistribution de la quantité de mTHPC présente dans divers organes en fonction de l'IDL appliqué avait également été réalisée. Les quantités de mTHPC observées dans les tumeurs n'ont révélé aucune corrélation avec le taux de guérison observé dans chaque condition de traitement. Cela confirme la complète discordance entre la quantité de PS présente dans les tissus et l'efficacité thérapeutique obtenue et par conséquent le manque de pertinence des études de biodistribution dans l'optimisation des conditions de traitement par PDT.

L'évaluation des dommages secondaires photoinduits au niveau de la peau de souris saines a également mis en évidence une faible phototoxicité du traitement PDT avec une injection fractionnée de mTHPC (score de dommages cutanés de 1, rougeur). En revanche, l'utilisation d'un IDL de 3 heures avait engendré des photodommages cutanés irréversibles (score de dommages de $4,8 \pm 0,3$) au niveau de la peau se traduisant par un important œdème et de nombreuses micro-hémorragies nécrotiques. Cela s'accompagnait d'une destruction de la couche germinative de l'épiderme par apoptose conduisant à une desépithélialisation de la peau irradiée. Ainsi, malgré un taux de guérison de 54 %, l'IDL de 3 heures ne peut pas être considéré comme une condition de traitement valable à cause des dommages secondaires qui ont été induits. Il est important de noter que les scores de dommages cutanés photoinduits dans la peau des souris pour chaque condition de traitement ne présentaient aucune corrélation avec les quantités de mTHPC mesurées dans l'étude de biodistribution décrite précédemment. Les données issues du suivi de la biodistribution des PSs ne permettent donc de prédire ni l'efficacité du traitement ni les dommages secondaires que celui-ci peut engendrer.

En conséquence, le ciblage des vaisseaux et du parenchyme tumoral via une administration fractionnée du PS est une stratégie de traitement très prometteuse dans un contexte clinique, de part son efficacité remarquable mais également de part la favorisation de la mort par apoptose des tissus pathologiques et les dommages secondaires cutanés photoinduits très restreints. Ainsi, les protocoles cliniques de traitement par PDT devraient se baser sur la distribution intratumorale du PS et non pas sur une étude de biodistribution pour la détermination des conditions de traitement à appliquer.

La seconde partie de ce travail a porté sur l'utilisation de formulations liposomales de la mTHPC. L'utilisation de nanovésicules lipidiques améliorant les propriétés pharmacocinétiques des PSs constitue un axe de recherche en plein essor. En effet, les liposomes permettent d'accélérer la vitesse de pénétration des PSs dans les tissus néoplasiques mais également d'augmenter leur taux de rétention. Ils apparaissent donc comme un outil intéressant pour la potentialisation de l'efficacité du traitement photodynamique. Cet aspect a été présenté dans la revue constituant la seconde partie de la synthèse bibliographique de ce manuscrit.
La mTHPC existe sous 2 formes liposomales différentes : le Foslip® et le Fospeg®. Le Fospeg® correspond à la structure du Foslip® sur laquelle des groupements de polyéthylène glycol (PEG) ont été ajoutés. Ces groupements PEG permettent aux liposomes de circuler plus longtemps dans la circulation générale en les protégeant de leur opsonisation par le système réticuloendothélial. Une étude de notre laboratoire portant sur l'efficacité du traitement photodynamique avec le Foslip® a révélé que malgré des profils pharmacocinétiques et une distribution intratumorale de la mTHPC différents, les taux de guérisons obtenus avec un IDL de 6 heures ou un IDL de 15 heures étaient proches (103).

Notre hypothèse est que l'efficacité thérapeutique ne serait non pas liée à la biodistribution mais à un autre paramètre spécifique aux formulations liposomales : la redistribution du PS à partir des liposomes. En effet, des publications récentes de notre laboratoire ont fait état du rôle majeur de la redistribution de la mTHPC à partir de formulations liposomales (104,123) grâce au suivi du « *photoinduced quenching* ». Ce phénomène correspond à une diminution de l'intensité de fluorescence émise par la mTHPC dans les liposomes suite à une irradiation lumineuse avec une faible dose de lumière en relation avec une forte concentration locale. L'énergie émise est transmise aux photoproduits issus de l'irradiation. En revanche, l'ajout d'un détergent de type Triton permet de restaurer le

signal de fluorescence en détruisant les liposomes. En utilisant ce phénomène de « *photoinduced quenching* » Reshetov *et al*. (104) ont notamment montré une redistribution beaucoup plus rapide de la mTHPC à partir du Foslip® comparé au Fospeg® dans du plasma humain *in vitro.* En effet, le PEG semble retarder significativement la redistribution de la mTHPC en stabilisant les liposomes.

Le but de notre étude a donc été de vérifier si ce comportement plasmatique de la mTHPC liposomale observé *in vitro* avait lieu *in vivo* dans la circulation sanguine ainsi que son influence sur les dommages photoinduits par le traitement photodynamique. Pour répondre à cette question, notre étude a été réalisée à l'aide du modèle de la membrane chorioallantoïdienne (CAM). Ce modèle, développé à l'origine pour l'étude des traitements pro et anti-angiogéniques sur la vascularisation, est particulièrement bien adapté à l'étude des dommages vasculaires et décrit dans la publication intitulée « *Animal models for photodiagnosis and photodynamic therapy* » présente dans la partie « Production scientifique » de ce manuscrit.

La redistribution de la mTHPC observée *in vivo* dans le plasma de la CAM selon la technique du *photoinduced quenching* (104) s'est traduite, tout comme dans les expérimentations réalisées *in vitro* dans le plasma humain, par une redistribution initialement plus importante et plus rapide de la mTHPC à partir du Foslip® par rapport à celle observée pour le Fospeg®. Ces résultats confirment la capacité des groupements PEG à stabiliser et protéger les liposomes et par conséquent à retarder la redistribution de la mTHPC. L'évaluation des dommages vasculaires photoinduits par un traitement PDT avec le Foslip® et le Fospeg® sur la CAM a mis en évidence l'importance de la redistribution de la mTHPC à partir des liposomes. En effet, pour un IDL de 15 minutes correspondant à une faible redistribution de la mTHPC, aucun dommage vasculaire n'a été observé pour chacune des deux formulations et cela quelle que soit la dose de lumière administrée. En revanche, pour les IDLs de 1 heure et de 3 heures, les analyses ont révélé la présence de dommages vasculaires photoinduits dont la sévérité était proportionnelle à la durée de l'IDL. En effet, le traitement PDT avec un IDL de 1 heure a conduit à l'occlusion des vaisseaux sanguins de petit diamètre aussi bien pour le Foslip® que le Fospeg®. L'utilisation d'un IDL de 3 heures s'est traduit quant à lui par une occlusion complète de la zone irradiée avec le Foslip® alors que les vaisseaux sanguins de diamètre important (>70 µm) étaient toujours perfusés avec le Fospeg®. Ainsi, la redistribution semble influencer l'intensité des dommages photoinduits. De

plus, les dommages issus de la PDT avec le Fospeg® semblent moins sévères que ceux observés avec le Foslip® dans les mêmes conditions de traitement en relation avec une redistribution plus importante de la mTHPC à partir du Foslip®.

L'ensemble de cette étude présente une stratégie visant à potentialiser les protocoles de traitement cliniques actuels via un ciblage passif de la néovascularisation et du parenchyme tumoral. Ce protocole est basé sur la distribution intratumorale de la mTHPC et non pas sur des études de biodistribution. Cette potentialisation est accentuée par l'induction de la destruction des cellules par apoptose ainsi que par la réduction des dommages secondaires cutanés photoinduits. L'évaluation de la redistribution de la mTHPC à partir de formulations liposomales a confirmé l'impact de cette redistribution sur l'efficacité de la PDT. La prise en compte de ce paramètre apparaît donc indispensable à l'optimisation des protocoles de traitement par Foslip® et Fospeg®. Cette étude nécessite une analyse complémentaire fine des dommages vasculaires induits ainsi que l'évaluation du traitement sur une tumeur xénogreffée sur la CAM et dans un modèle de souris porteuses de tumeur.

CONCLUSION & PERSPECTIVES

Nos travaux ont été conduits dans le but d'améliorer l'efficacité du traitement de tumeurs par mTHPC-PDT et de potentialiser la mort des cellules par apoptose tout en limitant au maximum les dommages secondaires. De plus, l'utilisation de formulations liposomales de la mTHPC a révélé de nouveaux paramètres à prendre en compte dans l'optimisation du traitement.

La première conclusion importante à retenir concerne l'utilisation des études de biodistribution. Nos résultats ont mis en évidence, une fois de plus, la totale discordance existant entre la quantité de PS présente dans la tumeur et le taux de guérison observé. Par conséquent, l'optimisation des protocoles de traitement devrait être basée sur la distribution intratumorale du PS qui s'est avérée représentative des dommages photoinduits observés.

La seconde remarque est relative à la stratégie de traitement par PDT. Le co-ciblage de la néovascularisation et du parenchyme tumoral induit une efficacité nettement supérieure à celle observée lors du ciblage unique de l'un ou l'autre des compartiments. Il semble donc que la potentialisation de l'efficacité du traitement nécessite une atteinte vasculaire mais également parenchymateuse de la tumeur.

De plus, l'utilisation du fractionnement de l'administration du PS a entrainé la favorisation de la mort des cellules par apoptose, au détriment de la nécrose et a contribué à l'efficacité du traitement. La faible réaction inflammatoire obtenue et combinée aux dommages secondaires cutanés minimes pourrait limiter la perte de substance généralement observée après le traitement et apporter un confort non négligeable au patient dans le contexte clinique. A cela s'ajoute la simplicité du protocole établi qui ne fait intervenir qu'une seule irradiation et par conséquent une seule anesthésie du patient.

La dernière conclusion concerne les formulations liposomales des photosensibilisateurs. Malgré leurs propriétés pharmacocinétiques établies, l'évaluation de l'efficacité d'un traitement PDT ne peut se faire qu'à l'aide d'une étude préalable de la redistribution du PS à partir de ces formulations. Les dommages photoinduits par le traitement PDT semblent d'autant plus sévères que la redistribution plasmatique de la mTHPC est importante. La composition de la nanovésicule lipidique (conventionnelle ou stabilisée) doit également être prise en compte ainsi que le modèle d'étude (dans le cas présent humain ou poulet).

Perspectives

Les protocoles cliniques devraient se baser sur la distribution intratumorale du PS mais à l'heure actuelle il serait intéressant de développer une technique non ou peu invasive permettant d'établir cette distribution pour chaque PS et chaque type de tumeur. Le suivi du photoblanchiment du photosensibilisateur pourrait ainsi être un indicateur prédictif de l'efficacité du traitement.

La continuité de ces travaux devrait en premier lieu passer par une évaluation des dommages photoinduits par Foslip® et Fospeg® administrés dans la CAM xénogreffée avec des cellules cancéreuses. Les IDLs appliqués devraient correspondre, tout comme dans notre étude, à des pourcentages de redistribution de la mTHPC différents afin d'être mis en relation avec l'efficacité observée. Une évaluation de la quantité et de la localisation *in ovo* de la mTHPC serait également utile à l'analyse et à la compréhension des dommages photoinduits par PDT.

Enfin, l'aspect le plus méconnu de la PDT reste à étudier : l'activation du système immunitaire. L'utilisation de modèles immunocompétents ou immunodéficients a un impact considérable sur la finalité du traitement. En revanche, à l'heure actuelle le rôle de la PDT dans l'immunomodulation reste très peu décrit. Une évaluation moléculaire et une identification des cytokines pro et anti-inflammatoires impliquées dans la réussite du traitement pourrait contribuer à la prédiction de l'efficacité du traitement de tumeurs.

REFERENCES

1. Moan J, Peng Q. An outline of the hundred-year history of PDT. Anticancer Res 2003; 23(5A):3591-3600.
2. Pervaiz S, Olivo M. Art and science of photodynamic therapy. Clin Exp Pharmacol Physiol 2006; 33(5-6):551-556.
3. Raab O. Uber die wirkung fluoroscierender stoffe auf infusoria. Z Biol 1900; 39:524-530.
4. Ledoux-Lebards. C Annales de l'Institut Pasteur 1902; 16:593-604.
5. von Tappeiner H. Zur Kenntnis der lichtwirkenden (fluoreszierenden) stoffe. Dtsch Med Wochenschr 1904; 8:265-269.
6. von Tappeiner H. Therapeutische versuche mit fluoreszierenden stoffe auf infusoiennach versuchen von Raab. Munch Med Wochenschr 1903; 50:2042-2044.
7. Silver H. Psoriasis vulgaris treated with hematporphyrin. Arch Dermatol Syph 1937; 36:1118-1119.
8. Policard A. Etude sur les aspects offerts par des tumeurs experimentales examinées à la lumière de Wood. C R Soc Biol 1924; 91:1423-1424.
9. Figge FH, Weiland GS, Manganiello LO. Cancer detection and therapy; affinity of neoplastic, embryonic, and traumatized tissues for porphyrins and metalloporphyrins. Proc Soc Exp Biol Med 1948; 68(3):640.
10. Schwartz S, Absolon K, Vermund H. Some relationships of porphyrins, x-rays and tumors. Med Bul 1955; 68:7-13.
11. Lipson RL, Baldes EJ. The photodynamic properties of a particular hematoporphyrin derivative. Arch Dermatol 1960; 82:508-516.
12. Lipson RL, Baldes EJ, Olsen AM. Further Evaluation of the Use of Hematoporphyrin Derivative as a New Aid for the Endoscopic Detection of Malignant Disease. Dis Chest 1964; 46:676-679.
13. Lipson RL, Pratt JH, Baldes EJ, Dockerty MB. Hematoporphyrine Derivative for Detection of Cervical Cancer. Obstet Gynecol 1964; 24:78-84.
14. Dougherty TJ, Kaufman JE, Goldfarb A, Weishaupt KR, Boyle D, Mittleman A. Photoradiation therapy for the treatment of malignant tumors. Cancer Res 1978; 38(8):2628-2635.
15. Dougherty TJ. An update on photodynamic therapy applications. J Clin Laser Med Surg 2002; 20(1):3-7.
16. Foote CS. Definition of type I and type II photosensitized oxidation. Photochem Photobiol 1991; 54(5):659.
17. Takemura T, Ohta N, Nakajima S, Sakata I. Critical importance of the triplet lifetime of photosensitizer in photodynamic therapy of tumor. Photochem Photobiol 1989; 50(3):339-344.
18. Halliwell B. Antioxidant defence mechanisms: from the beginning to the end (of the beginning). Free Radic Res 1999; 31(4):261-272.
19. Redmond RW, Gamlin JN. A compilation of singlet oxygen yields from biologically relevant molecules. Photochem Photobiol 1999; 70(4):391-475.
20. Agostinis P, Berg K, Cengel KA, Foster TH, Girotti AW, Gollnick SO, Hahn SM, Hamblin MR, Juzeniene A, Kessel D, Korbelik M, Moan J, Mroz P, Nowis D, Piette J, Wilson BC, Golab J. Photodynamic therapy of cancer: An update. CA Cancer J Clin 2011.
21. Dysart JS, Patterson MS. Characterization of Photofrin photobleaching for singlet oxygen dose estimation during photodynamic therapy of MLL cells in vitro. Phys Med Biol 2005; 50(11):2597-2616.

22. Moan J, Berg K, Kvam E, Western A, Malik Z, Ruck A, Schneckenburger H. Intracellular localization of photosensitizers. Ciba Found Symp 1989; 146:95-107; discussion 107-111.
23. Peng Q, Moan J, Nesland JM. Correlation of subcellular and intratumoral photosensitizer localization with ultrastructural features after photodynamic therapy. Ultrastruct Pathol 1996; 20(2):109-129.
24. Kessel D, Luguya R, Vicente MG. Localization and photodynamic efficacy of two cationic porphyrins varying in charge distributions. Photochem Photobiol 2003; 78(5):431-435.
25. Kessel D, Luo Y, Deng Y, Chang CK. The role of subcellular localization in initiation of apoptosis by photodynamic therapy. Photochem Photobiol 1997; 65(3):422-426.
26. Allison RR, Sibata CH. Oncologic photodynamic therapy photosensitizers: a clinical review. Photodiagnosis Photodyn Ther 2011; 7(2):61-75.
27. Trivedi NS, Wang HW, Nieminen AL, Oleinick NL, Izatt JA. Quantitative analysis of Pc 4 localization in mouse lymphoma (LY-R) cells via double-label confocal fluorescence microscopy. Photochem Photobiol 2000; 71(5):634-639.
28. Morris RL, Azizuddin K, Lam M, Berlin J, Nieminen AL, Kenney ME, Samia AC, Burda C, Oleinick NL. Fluorescence resonance energy transfer reveals a binding site of a photosensitizer for photodynamic therapy. Cancer Res 2003; 63(17):5194-5197.
29. Chen LB. Mitochondrial membrane potential in living cells. Annu Rev Cell Biol 1988; 4:155-181.
30. Verma A, Facchina SL, Hirsch DJ, Song SY, Dillahey LF, Williams JR, Snyder SH. Photodynamic tumor therapy: mitochondrial benzodiazepine receptors as a therapeutic target. Mol Med 1998; 4(1):40-45.
31. Siboni G, Weitman H, Freeman D, Mazur Y, Malik Z, Ehrenberg B. The correlation between hydrophilicity of hypericins and helianthrone: internalization mechanisms, subcellular distribution and photodynamic action in colon carcinoma cells. Photochem Photobiol Sci 2002; 1(7):483-491.
32. Kessel D, Luo Y. Photodynamic therapy: a mitochondrial inducer of apoptosis. Cell Death Differ 1999; 6(1):28-35.
33. Oleinick NL, Morris RL, Belichenko I. The role of apoptosis in response to photodynamic therapy: what, where, why, and how. Photochem Photobiol Sci 2002; 1(1):1-21.
34. Fingar VH, Taber SW, Haydon PS, Harrison LT, Kempf SJ, Wieman TJ. Vascular damage after photodynamic therapy of solid tumors: a view and comparison of effect in pre-clinical and clinical models at the University of Louisville. In Vivo 2000; 14(1):93-100.
35. Castellani A, Pace GP, Concioli M. Photodynamic effect of haematoporphyrin on blood microcirculation. J Pathol Bacteriol 1963; 86:99-102.
36. Star WM, Marijnissen HP, van den Berg-Blok AE, Versteeg JA, Franken KA, Reinhold HS. Destruction of rat mammary tumor and normal tissue microcirculation by hematoporphyrin derivative photoradiation observed in vivo in sandwich observation chambers. Cancer Res 1986; 46(5):2532-2540.
37. Krammer B. Vascular effects of photodynamic therapy. Anticancer Res 2001; 21(6B):4271-4277.
38. Triesscheijn M, Ruevekamp M, Aalders M, Baas P, Stewart FA. Comparative sensitivity of microvascular endothelial cells, fibroblasts and tumor cells after in

vitro photodynamic therapy with meso-tetra-hydroxyphenyl-chlorin. Photochem Photobiol 2004; 80(2):236-241.
39. Chen B, Pogue BW, Luna JM, Hardman RL, Hoopes PJ, Hasan T. Tumor vascular permeabilization by vascular-targeting photosensitization: effects, mechanism, and therapeutic implications. Clin Cancer Res 2006; 12(3 Pt 1):917-923.
40. Scherz A, Salomon Y. Vascular-targeted photodynamic therapy (VTP) with Tookad: from laboratory bench to clinical trials. . 6th International Symposium on Photodynamic Diagnosis and Therapy in Clinical Practice Brixen, Italy 2006.
41. Korbelik M. PDT-associated host response and its role in the therapy outcome. Lasers Surg Med 2006; 38(5):500-508.
42. Qiang YG, Yow CM, Huang Z. Combination of photodynamic therapy and immunomodulation: current status and future trends. Med Res Rev 2008; 28(4):632-644.
43. Korbelik M, Krosl G, Krosl J, Dougherty GJ. The role of host lymphoid populations in the response of mouse EMT6 tumor to photodynamic therapy. Cancer Res 1996; 56(24):5647-5652.
44. Garg AD, Nowis D, Golab J, Agostinis P. Photodynamic therapy: illuminating the road from cell death towards anti-tumour immunity. Apoptosis 2011; 15(9):1050-1071.
45. Assuncao Guimaraes C, Linden R. Programmed cell deaths. Apoptosis and alternative deathstyles. Eur J Biochem 2004; 271(9):1638-1650.
46. Gibson SL, Murant RS, Hilf R. Photosensitizing effects of hematoporphyrin derivative and photofrin II on the plasma membrane enzymes 5'-nucleotidase, Na+K+-ATPase, and Mg2+-ATPase in R3230AC mammary adenocarcinomas. Cancer Res 1988; 48(12):3360-3366.
47. Kerr JF, Wyllie AH, Currie AR. Apoptosis: a basic biological phenomenon with wide-ranging implications in tissue kinetics. Br J Cancer 1972; 26(4):239-257.
48. Almeida RD, Manadas BJ, Carvalho AP, Duarte CB. Intracellular signaling mechanisms in photodynamic therapy. Biochim Biophys Acta 2004; 1704(2):59-86.
49. Usuda J, Chiu SM, Murphy ES, Lam M, Nieminen AL, Oleinick NL. Domain-dependent photodamage to Bcl-2. A membrane anchorage region is needed to form the target of phthalocyanine photosensitization. J Biol Chem 2003; 278(3):2021-2029.
50. Breckenridge DG, Germain M, Mathai JP, Nguyen M, Shore GC. Regulation of apoptosis by endoplasmic reticulum pathways. Oncogene 2003; 22(53):8608-8618.
51. Noodt BB, Berg K, Stokke T, Peng Q, Nesland JM. Different apoptotic pathways are induced from various intracellular sites by tetraphenylporphyrins and light. Br J Cancer 1999; 79(1):72-81.
52. Kessel D. Transport and localisation of m-THPC in vitro. Int J Clin Pract 1999; 53(4):263-267.
53. Chiu S, Evans HH, Lam M, Nieminen A, Oleinick NL. Phthalocyanine 4 photodynamic therapy-induced apoptosis of mouse L5178Y-R cells results from a delayed but extensive release of cytochrome c from mitochondria. Cancer Lett 2001; 165(1):51-58.
54. Dougherty TJ, Gomer CJ, Henderson BW, Jori G, Kessel D, Korbelik M, Moan J, Peng Q. Photodynamic therapy. J Natl Cancer Inst 1998; 90(12):889-905.
55. Marchal S, Bezdetnaya L, Guillemin F. Modality of cell death induced by Foscan-based photodynamic treatment in human colon adenocarcinoma cell line HT29. Biochemistry (Mosc) 2004; 69(1):45-49.

56. Marchal S, Fadloun A, Maugain E, D'Hallewin MA, Guillemin F, Bezdetnaya L. Necrotic and apoptotic features of cell death in response to Foscan photosensitization of HT29 monolayer and multicell spheroids. Biochem Pharmacol 2005; 69(8):1167-1176.
57. Agostinis P, Buytaert E, Breyssens H, Hendrickx N. Regulatory pathways in photodynamic therapy induced apoptosis. Photochem Photobiol Sci 2004; 3(8):721-729.
58. Moor AC. Signaling pathways in cell death and survival after photodynamic therapy. J Photochem Photobiol B 2000; 57(1):1-13.
59. Engbrecht BW, Menon C, Kachur AV, Hahn SM, Fraker DL. Photofrin-mediated photodynamic therapy induces vascular occlusion and apoptosis in a human sarcoma xenograft model. Cancer Res 1999; 59(17):4334-4342.
60. Lilge L, Portnoy M, Wilson BC. Apoptosis induced in vivo by photodynamic therapy in normal brain and intracranial tumour tissue. Br J Cancer 2000; 83(8):1110-1117.
61. Jiang F, Zhang X, Kalkanis SN, Zhang Z, Yang H, Katakowski M, Hong X, Zheng X, Zhu Z, Chopp M. Combination therapy with antiangiogenic treatment and photodynamic therapy for the nude mouse bearing U87 glioblastoma. Photochem Photobiol 2008; 84(1):128-137.
62. Yokota T, Ikeda H, Inokuchi T, Sano K, Koji T. Enhanced cell death in NR-S1 tumor by photodynamic therapy: possible involvement of Fas and Fas ligand system. Lasers Surg Med 2000; 26(5):449-460.
63. Nonaka T, Nanashima A, Nonaka M, Uehara M, Isomoto H, Asahina I, Nagayasu T. Analysis of apoptotic effects induced by photodynamic therapy in a human biliary cancer cell line. Anticancer Res 2011; 30(6):2113-2118.
64. Banihashemi B, Vlad R, Debeljevic B, Giles A, Kolios MC, Czarnota GJ. Ultrasound imaging of apoptosis in tumor response: novel preclinical monitoring of photodynamic therapy effects. Cancer Res 2008; 68(20):8590-8596.
65. Zhou F, Xing D, Wu S, Chen WR. Intravital imaging of tumor apoptosis with FRET probes during tumor therapy. Mol Imaging Biol 2011; 12(1):63-70.
66. Yamamoto J, Yamamoto S, Hirano T, Li S, Koide M, Kohno E, Okada M, Inenaga C, Tokuyama T, Yokota N, Terakawa S, Namba H. Monitoring of singlet oxygen is useful for predicting the photodynamic effects in the treatment for experimental glioma. Clin Cancer Res 2006; 12(23):7132-7139.
67. Webber J, Luo Y, Crilly R, Fromm D, Kessel D. An apoptotic response to photodynamic therapy with endogenous protoporphyrin in vivo. J Photochem Photobiol B 1996; 35(3):209-211.
68. Arum CJ, Gederaas OA, Larsen EL, Randeberg LL, Hjelde A, Krokan HE, Svaasand LO, Chen D, Zhao CM. Tissue responses to hexyl 5-aminolevulinate-induced photodynamic treatment in syngeneic orthotopic rat bladder cancer model: possible pathways of action. J Biomed Opt 2011; 16(2):028001.
69. He GF, Bian ML, Zhao YW, Xiang Q, Li HY, Xiao C. A study on the mechanism of 5-aminolevulinic acid photodynamic therapy in vitro and in vivo in cervical cancer. Oncol Rep 2009; 21(4):861-868.
70. Wakui M, Yokoyama Y, Wang H, Shigeto T, Futagami M, Mizunuma H. Efficacy of a methyl ester of 5-aminolevulinic acid in photodynamic therapy for ovarian cancers. J Cancer Res Clin Oncol 2011; 136(8):1143-1150.
71. Walt H, Nap M, Dorward AM, Leers MPG, Tennent BJ, Varga Z, Stallmach T, Björklund V, Beamer WG. Early apoptotic responses in transgenic mouse

mammary carcinoma for photodynamic therapy. Photodiagnosis and Photodynamic Therapy 2006; 3:227-233.
72. Matsubara A, Nakazawa T, Noda K, She H, Connolly E, Young TA, Ogura Y, Gragoudas ES, Miller JW. Photodynamic therapy induces caspase-dependent apoptosis in rat CNV model. Invest Ophthalmol Vis Sci 2007; 48(10):4741-4747.
73. Barnes LD, Giuliano EA, Ota J. Cellular localization of Visudyne as a function of time after local injection in an in vivo model of squamous cell carcinoma: an investigation into tumor cell death. Vet Ophthalmol 2011; 13(3):158-165.
74. Kaneko T, Chiba H, Yasuda T, Kusama K. Detection of photodynamic therapy-induced early apoptosis in human salivary gland tumor cells in vitro and in a mouse tumor model. Oral Oncol 2004; 40(8):787-792.
75. Moon YH, Kwon SM, Kim HJ, Jung KY, Park JH, Kim SA, Kim YC, Ahn SG, Yoon JH. Efficient preparation of highly pure chlorin e6 and its photodynamic anti-cancer activity in a rat tumor model. Oncol Rep 2009; 22(5):1085-1091.
76. Namatame H, Akimoto J, Matsumura H, Haraoka J, Aizawa K. Photodynamic therapy of C6-implanted glioma cells in the rat brain employing second-generation photosensitizer talaporfin sodium. Photodiagnosis Photodyn Ther 2008; 5(3):198-209.
77. Henderson BW, Gollnick SO, Snyder JW, Busch TM, Kousis PC, Cheney RT, Morgan J. Choice of oxygen-conserving treatment regimen determines the inflammatory response and outcome of photodynamic therapy of tumors. Cancer Res 2004; 64(6):2120-2126.
78. Chen B, Roskams T, Xu Y, Agostinis P, de Witte PA. Photodynamic therapy with hypericin induces vascular damage and apoptosis in the RIF-1 mouse tumor model. Int J Cancer 2002; 98(2):284-290.
79. Bhuvaneswari R, Gan YY, Soo KC, Olivo M. Targeting EGFR with photodynamic therapy in combination with Erbitux enhances in vivo bladder tumor response. Mol Cancer 2009; 8:94.
80. Cole CD, Liu JK, Sheng X, Chin SS, Schmidt MH, Weiss MH, Couldwell WT. Hypericin-mediated photodynamic therapy of pituitary tumors: preclinical study in a GH4C1 rat tumor model. J Neurooncol 2008; 87(3):255-261.
81. Zaidi SI, Oleinick NL, Zaim MT, Mukhtar H. Apoptosis during photodynamic therapy-induced ablation of RIF-1 tumors in C3H mice: electron microscopic, histopathologic and biochemical evidence. Photochem Photobiol 1993; 58(6):771-776.
82. Kalka K, Ahmad N, Criswell T, Boothman D, Mukhtar H. Up-regulation of clusterin during phthalocyanine 4 photodynamic therapy-mediated apoptosis of tumor cells and ablation of mouse skin tumors. Cancer Res 2000; 60(21):5984-5987.
83. Agarwal R, Korman NJ, Mohan RR, Feyes DK, Jawed S, Zaim MT, Mukhtar H. Apoptosis is an early event during phthalocyanine photodynamic therapy-induced ablation of chemically induced squamous papillomas in mouse skin. Photochem Photobiol 1996; 63(4):547-552.
84. Colussi VC, Feyes DK, Mulvihill JW, Li YS, Kenney ME, Elmets CA, Oleinick NL, Mukhtar H. Phthalocyanine 4 (Pc 4) photodynamic therapy of human OVCAR-3 tumor xenografts. Photochem Photobiol 1999; 69(2):236-241.
85. Whitacre CM, Feyes DK, Satoh T, Grossmann J, Mulvihill JW, Mukhtar H, Oleinick NL. Photodynamic therapy with the phthalocyanine photosensitizer Pc 4 of SW480 human colon cancer xenografts in athymic mice. Clin Cancer Res 2000; 6(5):2021-2027.

86. Yslas EI, Prucca C, Romanini S, Durantini EN, Bertuzzi M, Rivarola V. Biodistribution and phototherapeutic properties of Zinc (II) 2,9,16,23-tetrakis (methoxy) phthalocyanine in vivo. Photodiagnosis Photodyn Ther 2009; 6(1):62-70.
87. Leung SC, Lo PC, Ng DK, Liu WK, Fung KP, Fong WP. Photodynamic activity of BAM-SiPc, an unsymmetrical bisamino silicon(IV) phthalocyanine, in tumour-bearing nude mice. Br J Pharmacol 2008; 154(1):4-12.
88. Park KC, Kim SY, Kim DS. Experimental photodynamic therapy for liver cancer cell-implanted nude mice by an indole-3-acetic acid and intense pulsed light combination. Biol Pharm Bull 2009; 32(9):1609-1613.
89. Chen Y, Zheng W, Li Y, Zhong J, Ji J, Shen P. Apoptosis induced by methylene-blue-mediated photodynamic therapy in melanomas and the involvement of mitochondrial dysfunction revealed by proteomics. Cancer Sci 2008; 99(10):2019-2027.
90. Khdair A, Chen D, Patil Y, Ma L, Dou QP, Shekhar MP, Panyam J. Nanoparticle-mediated combination chemotherapy and photodynamic therapy overcomes tumor drug resistance. J Control Release 2011; 141(2):137-144.
91. Nowis D, Makowski M, Stoklosa T, Legat M, Issat T, Golab J. Direct tumor damage mechanisms of photodynamic therapy. Acta Biochim Pol 2005; 52(2):339-352.
92. Konan YN, Gurny R, Allemann E. State of the art in the delivery of photosensitizers for photodynamic therapy. J Photochem Photobiol B 2002; 66(2):89-106.
93. Bonnett R, White RD, Winfield UJ, Berenbaum MC. Hydroporphyrins of the meso-tetra(hydroxyphenyl)porphyrin series as tumour photosensitizers. Biochem J 1989; 261(1):277-280.
94. Mitra S, Foster TH. Photophysical parameters, photosensitizer retention and tissue optical properties completely account for the higher photodynamic efficacy of meso-tetra-hydroxyphenyl-chlorin vs Photofrin. Photochem Photobiol 2005; 81(4):849-859.
95. Cramers P, Ruevekamp M, Oppelaar H, Dalesio O, Baas P, Stewart FA. Foscan uptake and tissue distribution in relation to photodynamic efficacy. Br J Cancer 2003; 88(2):283-290.
96. Triesscheijn M, Ruevekamp M, Aalders M, Baas P, Stewart FA. Outcome of mTHPC mediated photodynamic therapy is primarily determined by the vascular response. Photochem Photobiol 2005; 81(5):1161-1167.
97. Jones HJ, Vernon DI, Brown SB. Photodynamic therapy effect of m-THPC (Foscan) in vivo: correlation with pharmacokinetics. Br J Cancer 2003; 89(2):398-404.
98. Veenhuizen R, Oppelaar H, Ruevekamp M, Schellens J, Dalesio O, Stewart F. Does tumour uptake of Foscan determine PDT efficacy? Int J Cancer 1997; 73(2):236-239.
99. Mitra S, Maugain E, Bolotine L, Guillemin F, Foster TH. Temporally and spatially heterogeneous distribution of mTHPC in a murine tumor observed by two-color confocal fluorescence imaging and spectroscopy in a whole-mount model. Photochem Photobiol 2005; 81(5):1123-1130.
100. Triesscheijn M, Ruevekamp M, Out R, Van Berkel TJ, Schellens J, Baas P, Stewart FA. The pharmacokinetic behavior of the photosensitizer meso-tetra-hydroxyphenyl-chlorin in mice and men. Cancer Chemother Pharmacol 2007; 60(1):113-122.

101. Hopkinson HJ, Vernon DI, Brown SB. Identification and partial characterization of an unusual distribution of the photosensitizer meta-tetrahydroxyphenyl chlorin (temoporfin) in human plasma. Photochem Photobiol 1999; 69(4):482-488.
102. Ronn AM, Batti J, Lee CJ, Yoo D, Siegel ME, Nouri M, Lofgren LA, Steinberg BM. Comparative biodistribution of meta-Tetra(Hydroxyphenyl) chlorin in multiple species: clinical implications for photodynamic therapy. Lasers Surg Med 1997; 20(4):437-442.
103. Lassalle HP, Dumas D, Grafe S, D'Hallewin MA, Guillemin F, Bezdetnaya L. Correlation between in vivo pharmacokinetics, intratumoral distribution and photodynamic efficiency of liposomal mTHPC. J Control Release 2009; 134(2):118-124.
104. Reshetov V, Kachatkou D, Shmigol T, Zorin V, D'Hallewin MA, Guillemin F, Bezdetnaya L. Redistribution of meta-tetra(hydroxyphenyl)chlorin (m-THPC) from conventional and PEGylated liposomes to biological substrates. Photochem Photobiol Sci 2011; 10(6):911-919.
105. Juzenas P, Juzeniene A. Reduction of cutaneous photosensitivity by application of ointment containing ferrous or cobaltous ions concomitant with the use of topical protoporphyrin IX precursors. Photodiagnosis Photodyn Ther 2010; 7(3):152-157.
106. Bellnier DA, Greco WR, Nava H, Loewen GM, Oseroff AR, Dougherty TJ. Mild skin photosensitivity in cancer patients following injection of Photochlor (2-[1-hexyloxyethyl]-2-devinyl pyropheophorbide-a; HPPH) for photodynamic therapy. Cancer Chemother Pharmacol 2006; 57(1):40-45.
107. Weersink RA, Forbes J, Bisland S, Trachtenberg J, Elhilali M, Brun PH, Wilson BC. Assessment of cutaneous photosensitivity of TOOKAD (WST09) in preclinical animal models and in patients. Photochem Photobiol 2005; 81(1):106-113.
108. Shieh MJ, Peng CL, Chiang WL, Wang CH, Hsu CY, Wang SJ, Lai PS. Reduced skin photosensitivity with meta-tetra(hydroxyphenyl)chlorin-loaded micelles based on a poly(2-ethyl-2-oxazoline)-b-poly(d,l-lactide) diblock copolymer in vivo. Mol Pharm; 7(4):1244-1253.
109. Robinson DJ, de Bruijn HS, van der Veen N, Stringer MR, Brown SB, Star WM. Protoporphyrin IX fluorescence photobleaching during ALA-mediated photodynamic therapy of UVB-induced tumors in hairless mouse skin. Photochem Photobiol 1999; 69(1):61-70.
110. Hagedorn M, Balke M, Schmidt A, Bloch W, Kurz H, Javerzat S, Rousseau B, Wilting J, Bikfalvi A. VEGF coordinates interaction of pericytes and endothelial cells during vasculogenesis and experimental angiogenesis. Dev Dyn 2004; 230(1):23-33.
111. Vargas A, Zeisser-Labouebe M, Lange N, Gurny R, Delie F. The chick embryo and its chorioallantoic membrane (CAM) for the in vivo evaluation of drug delivery systems. Adv Drug Deliv Rev 2007; 59(11):1162-1176.
112. Murphy JB, Rous P. The Behavior of Chicken Sarcoma Implanted in the Developing Embryo. J Exp Med 1912; 15(2):119-132.
113. Deryugina EI, Quigley JP. Chick embryo chorioallantoic membrane model systems to study and visualize human tumor cell metastasis. Histochem Cell Biol 2008; 130(6):1119-1130.
114. Valdes TI, Kreutzer D, Moussy F. The chick chorioallantoic membrane as a novel in vivo model for the testing of biomaterials. J Biomed Mater Res 2002; 62(2):273-282.

115. Eugenin J, Eyzaguirre C. Electrophysiological properties of rat nodose ganglion neurons co-transplanted with carotid bodies into the chick chorioallantoic membrane. Biol Res 2005; 38(4):329-334.
116. Hamburger V, Hamilton HL. A series of normal stages in the development of the chick embryo. 1951. Dev Dyn 1992; 195(4):231-272.
117. DeFouw DO, Rizzo VJ, Steinfeld R, Feinberg RN. Mapping of the microcirculation in the chick chorioallantoic membrane during normal angiogenesis. Microvasc Res 1989; 38(2):136-147.
118. Ribatti D, Nico B, Vacca A, Roncali L, Burri PH, Djonov V. Chorioallantoic membrane capillary bed: a useful target for studying angiogenesis and anti-angiogenesis in vivo. Anat Rec 2001; 264(4):317-324.
119. Kunzi-Rapp K, Kaskel P, Steiner R, Peter RU, Krahn G. Increased blood levels of human S100 in melanoma chick embryo xenografts' circulation. Pigment Cell Res 2001; 14(1):9-13.
120. Balke M, Neumann A, Kersting C, Agelopoulos K, Gebert C, Gosheger G, Burger H, Hagedorn M. Morphologic characterization of osteosarcoma growth on the chick chorioallantoic membrane. BMC Res Notes 2011; 3(1):58.
121. Janse EM, Jeurissen SH. Ontogeny and function of two non-lymphoid cell populations in the chicken embryo. Immunobiology 1991; 182(5):472-481.
122. Davison TF. The immunologists' debt to the chicken. Br Poult Sci 2003; 44(1):6-21.
123. Kachatkou D, Sasnouski S, Zorin V, Zorina T, D'Hallewin MA, Guillemin F, Bezdetnaya L. Unusual photoinduced response of mTHPC liposomal formulation (Foslip). Photochem Photobiol 2009; 85(3):719-724.
124. Debefve E, Pegaz B, Ballini JP, Konan YN, van den Bergh H. Combination therapy using aspirin-enhanced photodynamic selective drug delivery. Vascul Pharmacol 2007; 46(3):171-180.
125. Romanoff AL. Biochemistry of the Avian Embryo: a Quantitative Analysis of Prenetal Development. JohnWiley and Sons, New York 1967:398.
126. Pegaz B, Debefve E, Ballini JP, Wagnieres G, Spaniol S, Albrecht V, Scheglmann DV, Nifantiev NE, van den Bergh H, Konan-Kouakou YN. Photothrombic activity of m-THPC-loaded liposomal formulations: pre-clinical assessment on chick chorioallantoic membrane model. Eur J Pharm Sci 2006; 28(1-2):134-140.
127. Drummond DC, Meyer O, Hong K, Kirpotin DB, Papahadjopoulos D. Optimizing liposomes for delivery of chemotherapeutic agents to solid tumors. Pharmacol Rev 1999; 51(4):691-743.
128. Allen TM, Hansen CB, De Menezes DEL. Pharmacokinetics of long-circulating liposomes. Adv Drug Deliv Rev 1995; 16(2-3):267-284.
129. Allen C, Dos Santos N, Gallagher R, Chiu GN, Shu Y, Li WM, Johnstone SA, Janoff AS, Mayer LD, Webb MS, Bally MB. Controlling the physical behavior and biological performance of liposome formulations through use of surface grafted poly(ethylene glycol). Biosci Rep 2002; 22(2):225-250.

PRODUCTION SCIENTIFIQUE

1. PUBLICATIONS

1.1 Foslip® - based Photodynamic Therapy as a means to improve Wound Healing

Julie Garrier, Lina Bezdetnaya, Catherine Barlier, Susanna Gräfe, François Guillemin et Marie-Ange D'Hallewin.

PhotoDiagnosis and Photodynamic Therapy. 2011; 8(4):321-327

Foslip® - based Photodynamic Therapy as a means to improve Wound Healing

Julie Garrier [a,b], Lina Bezdetnaya [a,b], Catherine Barlier [b], Susanna Gräfe [c], François Guillemin [a,b], Marie-Ange D'Hallewin [a,b]

[a] Centre de Recherche en Automatique de Nancy (CRAN-UMR 7039), Nancy-University, CNRS, Centre Alexis Vautrin, 6 avenue de Bourgogne 54511 Vandœuvre-lès-Nancy, France.

[b] Centre Alexis Vautrin, Service d'Anatomie et de Cytologie Pathologiques, 6 avenue de Bourgogne 54511 Vandœuvre-lès-Nancy, France.

[c] Biolitec AG, Research & Development, Otto-Schott-Straße 15, D-07745 Jena, Germany

E-mail addresses: j.garrier@nancy.fnclcc.fr; l.bolotine@nancy.fnclcc.fr; c.barlier@nancy.fnclcc.fr; susanna.graefe@biolitec.com; f.guillemin@nancy.fnclcc.fr; m.dhallewin@nancy.fnclcc.fr

Corresponding author: **Dr. Marie-Ange D'HALLEWIN**
Centre Alexis Vautrin
Laboratoire CRAN
6, avenue de Bourgogne
54511 VANDOEUVRE-LES-NANCY
Phone number : +33 (0)3.83.59.83.06
Fax number : +33 (0)3.83.59.83.78
E-mail: m.dhallewin@nancy.fnclcc.fr

ABSTRACT

Background. Collagen matrices as substitution for connective tissue are known to promote wound healing. Photodynamic therapy has been anecdotally associated with improved wound healing and reduced scarring. The present study investigates the impact of collagen based scaffolding material, embedded with a liposomal formulation of meta-tetra (hydroxyphenyl) chlorin (mTHPC, Foslip®) and photodynamic therapy on wound healing in mice.

Methods. After incision in the neck region, two different types of collagen material, previously incubated with Foslip® at different concentrations, were implanted followed by illumination at 652 nm (10 J/cm², 100 mW/cm²). Mice were imaged daily up to two weeks, whereafter excision was performed and pathological analysis.

Results. Scab detachment was observed at day seven for controls whereas it occurred as early as three days for PDT at the lowest concentrations. In the latter conditions, final matrix remodelling could be observed as evidenced by elastin neosynthesis.

Conclusions. Topical application of low dose Foslip® in a collagen matrix followed by illumination considerably accelerates wound healing.

KEY WORDS

Wound healing, Photodynamic Therapy, Collagen, Foslip®

INTRODUCTION

Wound healing is a complex process of response to injury, in order to restore skin integrity. It involves the timed and balanced activity of inflammatory, vascular, connective tissue and epithelial cells. Different approaches have been advocated in order to haste this process and avoid excessive scar formation. Collagen based scaffolding materials respond to these criteria and therefore are widely used. Xenogenic collagen is a biocompatible, non-toxic substrate for cellular attachment, growth and differentiation. Also, the use of low-level light therapy (LLLT) has been advocated, however it is highly contradictory in humans as well as in rodent models [1].

Photodynamic therapy (PDT) is a process where light interacts with a photosensitizing molecule, in the presence of oxygen, in order to produce reactive oxygen species that will destroy the host cell. Whereas PDT is mainly applied in oncologic settings, it has also widely been used to target vasculature in age related macular degeneration, and is now under investigation for its microbial activity, especially in wounds or peridontitis [2]. Skin illumination to perform PDT after systemic administration of a photosensitizer is known to induce skin necrosis. However low doses (3 J/cm^2) 635 nm light appeared to hasten the process of wound healing [3]. Recent studies also reported that topical application of a photosensitizer and repeated illumination improved wound healing in terms of reepithelialisation and remodelling [4, 5].

Meta-tetra (hydroxyphenyl) chlorin (mTHPC, Foscan®) is one of the most potent second generation photosensitizers approved for the palliative treatment of head and neck cancers. Generalized skin sensitization after systemic administration has been shown to be shorter as compared to porphyrin based photosensitizers [6]. Incorporation of mTHPC in dipalmitoylphosphatidylcholine / dipalmitoylphosphatidylglycerol liposomes (Foslip®) has

been proposed in order to improve pharmacokinetics, reduce systemic side effects as well as enhance specific drug delivery [7, 8].

In the present study we investigated the impact of photodynamic treatment on the wound healing process in pre-clinical models. With this purpose, mice were implanted with collagen-based scaffolding material embedded in a liposomal formulation of mTHPC (Foslip®) and subjected to red light illumination at the injury site.

MATERIALS AND METHODS

Scaffolding material and photosensitizer

Two kinds of collagen formulations were used: Bio-Gide membrane (5 x 5 x 1 mm) (Geistlich Pharma AG, Wolhusen, Switzerland) and Kollagen Resorb sponge (5 x 5 x 5 mm) (Resorba Clinicare GmbH, Nuremberg, Germany). The origin of the collagen, collagen I and III is either porcine or equine. Foslip® was provided by Biolitec AG (Jena, Germany) and diluted with distilled water to a final concentration of 1.5 mg/ml. Sponges and membranes were immersed in Foslip® at different concentration for 30 minutes or 5 % glucose for the controls.

Mice and treatment modalities

Hairless female SKH-1 mice (Charles River, L'Arbresle, France) weighing 20-22 g (8 weeks old) were used in compliance with the French Animal Scientific Procedures Act (April 1988). Animals were kept under standard conditions and provided with food and water ad libitum. Animals were anesthetized with an intraperitoneal injection of a ketamine (Ketalar, 50 mg/ml) / Xylazine (Rompun, 2%) mixture (90/10 mg/kg body weight). A scalpel skin cut of 5 mm length was performed in the neck area and closed with a single catgut stitch after subcutaneous implantation in the loose tissue, of the collagen specimen. Thirty minutes following implantation a treated area was irradiated with 652 nm light up to 10 J/cm² at a fluence rate of 100 mW/cm² with an argon-ion-laser-pumped dye laser (Spectra-Physics, Les Ulis, France) (Table 1). All control groups of mice underwent skin injury without any further treatment (no implants); - sponge or membrane implants only (S or M), sponge or membrane with light only (S/M + light) or sponge or membrane with Foslip® (50 µg/ml) without light (S/M + Foslip®) (Table 1). The PDT groups consisted of sponges or membranes incubated in 50 µg/ml, 10 µg/ml, 5 µg/ml, 1 µg/ml or 0.5 µg/ml Foslip®.

Assessment of wound healing

6

Mice were observed daily and pictures taken until day 14. Euthanasia was performed at day 14 by anesthetic overdose and cervical dislocation and the wound area was excised, fixed in AFA fixing agent (acetic acid, formaldehyde, alcohol) for 24 hours before paraffin embedding and pathological analysis. Deparaffinized sections of 5 µm thickness of each sample were routinely stained by Hematoxylin-eosin-safran (HES) and elastic fibers were highlighted with a Weigert's elastin stain. It consisted of one hour coloration with a combination of basic fuchsin (2 g/ml) and resorcinol (4 g/ml) diluted in hot water and precipitated by 30 ml of 30% (w/v) iron trichloride before filtration. Residual powder was diluted in 90° alcohol. Then, sections were washed with 90° alcohol, 1 % (w/v) hydrochloric acid, 90°C alcohol and finally cold water. Samples were counterstained with Kernechtrot staining for 5 minutes and washed with distilled water before their dehydratation and fixation. Observations were performed with an Olympus microscope (Olympus, Rungis, France) and pictures were registered with Image analysis software.

RESULTS

Visual assessment

Scab detachment is observed at day 9 for the mice without additional manipulations beyond incision and day 7 for all other control groups (Figure 1A). All implants are detectable by subcutaneous bulging at day 14. The inflammatory response observed as oedema and redness is more pronounced for sponges than for membranes. Figure 1B displays macroscopic assessment of Foslip®-PDT treated groups. For the clarity of presentation, only typical images of groups treated with the highest, intermediate and lowest concentrations of the dye are shown. At the highest PDT-Foslip® dose, the fastest healing is observed at day 3 for the three lowest concentrations (5 µg/ml, 1 µg/ml or 0.5 µg/ml) (Table 1). Scarring is observed in all animals in the PDT group at the highest Foslip® concentration (50 µg/ml), irrespective of implant type, as well as at the lowest concentration of 0.5 µg/ml Foslip® in case of a sponge implant (Table 1).

Pathology

Dermal closure is been attained in all circumstances. Whenever a scar was seen macroscopically, this was confirmed by pathology (Table 1). PDT at the highest drug doses induces scarring for both sponges and membranes. Microscopic evidence of scarring can be observed without being macroscopically detected. This is always the case for sponges (Figure 2, A & B), except at the intermediate drug dose of 5 µg/ml (Table 1). Minimal scarring can be observed when the membranes have been embedded with Foslip® without additional illumination (Table 1). All other membrane conditions show identical features as represented in Figure 2C. The incision area can be recognized by the absence of hair follicles and flattened epidermis without folds but without any signs of excessive granulation tissue.

All implants can still be recognized, irrespective of the treatment modality. Sponges elicit a strong inflammatory reaction, exceeding the implant limits as shown in Figure 2D. Identical

features will only be observed for membranes treated with Foslip® PDT at doses of 5 µg/ml and 0.5µg/ml (Figure 2E). All other membrane conditions show normal dermis overlying the membrane (Figure 2F).

Increased collagen deposit is observed in all groups, without any differences between different treatment modalities and controls (data not shown). Elastin neosynthesis is never visualized following PDT with sponges as shown in Figure 3A, except for PDT at 1µg/ml (Table 1). Membranes with PDT at the two highest doses of 50 µg/ml and 10 µg/ml fail to induce elastin neosynthesis at day 14 (Figure 3B). We also note the presence of multiple elastin fibers in the membrane. When PDT is performed with the membranes at the three lowest concentrations, discrete elastin staining can be observed in the dermis (Figure 3C).

DISCUSSION

Wound healing is established through overlapping but very distinct steps. The first three days are characterized by clot formation and early inflammatory response. Up to day seven, scab formation is noted and pathology reveals formation of early granulation tissue and migration of the epidermal edges. Scab detachment will be observed between 8 – 12 days [9]. At this stage, epidermal differentiation is observed as well as granulation tissue and attenuation of the inflammation. The final stage of wound healing is characterized by matrix remodelling and increased elastic fiber content.

From Table 1, it appears that all modalities where collagen matrices are implanted hasten the initial phases and scab detachment occurs at or earlier than 7 days. Exogenous collagen from porcine or equine origin does not elicit generalized hypersensitivity reactions and is thus well accepted. Antibodies formed against animal collagen do not cross react with human forms and inflammatory response does not extend beyond the implant [10]. In the present study, inflammatory response never expands much further than the implantation area (Figure 2). Collagen based scaffolding material, with or without additional components such as antibiotics, growth factors or skin replacements are widely accepted and have been shown to improve healing, and although expensive, being cost effective with regard to the superior wound healing [11]. Bio Gide membranes consist of non cross-linked collagen I and III from porcine origin according to the manufacturer. Non cross-linked collagen implants have been shown to be superior to cross-linked collagen [12]. Kollagen Resorb sponges consist of "natural collagen from equine origin". Although elastin is not mentioned in the composition of the Bio-Gide membrane, elastin staining clearly demonstrates the presence of multiple elastin fibers (Figure 3).

In the present study microscopic presence of scar tissue is detected in 16/26 mice with sponges as opposed to 1/26 in the presence of a membrane (Table 1). It is thus clear that Bio Gide membranes are to be preferred over Kollagen Resorb sponges.

Matrix remodelling is the last phase of wound healing. Its main characteristic consists of elastin deposit, ensuring the tensile strength of the wound. This final stage is only completed after many months to 1 year in humans [13, 14]. The animal model that most closely mimics human skin is the pig, where elastin neosynthesis can be observed as early as 6 weeks [15]. It is well known that elastogenesis occurs much faster in rodents where it can be observed as early as one week following implant of a mixed collagen–elastin scaffold [16].

In the present paper, the only time point chosen for pathology was 2 weeks. Elastin, as shown by Weigert's staining (Figure 3), can be observed in the injured area of animals only when membranes were implanted, followed by PDT at the three lowest concentrations, which perfectly correlate with observations by Schwartz . [16]. Elastin derived peptides have been shown to have a chemotactic activity on fibroblasts and monocytes *in vitro* [17]. This was later on verified in pigs [15] where improved healing was observed. The presence of both collagen and elastin in the implants however is not sufficient to hasten the healing process since all control membranes do not significantly hasten scab detachment: seven days versus nine as opposed to three days for low dose PDT in the presence of a membrane.

From our data it appears that low dose PDT does influence healing, which can be observed through scab detachment as early as day three. PDT after systemic photosensitizer injection is known to induce skin necrosis and was reported to delay the healing process in rats before skin flap reconstruction [18]. This effect however can be minimized when mTHPC is delivered at an identical total dose but separated into two injections at both an early and late time point before illumination [19].

PDT after systemic administration of either benzoporphyrin derivative (BPD-MA) or chloraluminium sulphophtalocyanin (CASP) had no influence on wound healing as observed after pathological analysis two weeks later [20]. More recent studies have suggested a positive influence of PDT on wound healing in rats [3-5]. All three studies deal with rats and open wounds as opposed to ours where clear-cut incisions are made and sutured with positioning of a collagen based implant in mice. Jayasree et al (3) administered aminolevulinic acid (ALA) intraperitoneally or hematoporphyrin derivative orally, followed by HeNe and or NdYAG laser illumination. They noted a clearly improved macroscopic and microscopic healing after ALA based PDT, without however any effect on tensile strength at 3 weeks post injury. In another study, punch biopsy and local administration of phtalocyanines in rats followed by daily illumination at low light dose for 1 week, epithelial regeneration, collagen synthesis and matrix remodeling was more pronounced in the PDT group only [5]. Topical application of toluidine blue after punch biopsy in rats, followed by light only or PDT also improved healing as compared to controls. The difference observed between the 2 groups mainly consisted of a 100 % epidermal regeneration for PDT as opposed to 50 % in the LLLT group [4]. The beneficial effects of PDT were attributed to both the low level illumination, and the bactericidal effect of PDT. LLLT is a very controversial subject. *In vitro* and *in vivo* studies as well as human clinical trials show antagonistic results [1]. In the present study, no beneficial effect was observed when illumination was performed post collagen insertion. Though antimicrobial effect is manifest *in vitro*, most clinical studies concerning the skin fail to replicate those results [21].

In our study, PDT clearly has a positive impact on wound healing at the three lowest concentrations. Whatever the implant type, scab detachment is observed at three days only as opposed to seven for other implant groups. Also, inflammation and progressive resorption of the implant material is more pronounced in those categories.

Microscopic evidence of scarring is more frequent (16/26) when sponges are utilized as compared to membranes (1/26). Elastin neosynthesis, indicating the final stages of wound healing, is only found when PDT is applied at the three lowest concentrations and is more intense in the presence of membranes (13/13) as opposed to sponges (1/13). The latter could be attributed to the presence of exogenous elastin in the membrane complexes, which might stimulate final matrix reorganization [14, 15].

Our ongoing investigations are attempting to establish the mechanistic aspect of an improved wound healing with low dose Foslip®-PDT. One of our earlier *in vitro* studies clearly demonstrated a dose dependent macrophages activation with mTHPC-PDT [22]. At low oxidative insult, we have observed an enhanced phagocytosis and cytokines release Considering the pivotal role of macrophages-induced phagocytosis in initial stages of wound healing [9], the results of the present study could be explained by Foslip® induced photoimmunomodulation. Identification and quantification of cytokines involved may offer further hindsight to the mechanisms partaking in the healing process and will be the topic of our future research.

ACKNOWLEDGMENTS

This work was supported by Alexis Vautrin Cancer Center research funds, French Ligue Nationale Contre le Cancer. We also thank the Association Nationale Recherche et Technologie (ANRT) of France for awarding fellowship to JG. We acknowledge Biolitec AG (Jena, Germany) for providing us with Foslip®.

REFERENCES

[1] Posten W, Wrone DA, Dover JS, Arndt KA, Silapunt S, Alam M. Low-level laser therapy for wound healing: mechanism and efficacy. Dermatol Surg. 2005;31:334-40.
[2] Dai T, Huang YY, Hamblin MR. Photodynamic therapy for localized infections--state of the art. Photodiagnosis Photodyn Ther. 2009;6:170-88.
[3] Jayasree RS, Gupta AK, Rathinam K, Mohanan PV, Mohanty M. The influence of photodynamic therapy on the wound healing process in rats. J Biomater Appl. 2001;15:176-86.
[4] Garcia VG, de Lima MA, Okamoto T, Milanezi LA, Junior EC, Fernandes LA, et al. Effect of photodynamic therapy on the healing of cutaneous third-degree-burn: histological study in rats. Lasers Med Sci. 2010;25:221-8.
[5] Silva JC, Lacava ZG, Kuckelhaus S, Silva LP, Neto LF, Sauro EE, et al. Evaluation of the use of low level laser and photosensitizer drugs in healing. Lasers Surg Med. 2004;34:451-7.
[6] Hopper C. Photodynamic therapy: a clinical reality in the treatment of cancer. Lancet Oncol. 2000;1:212-9.
[7] Buchholz J, Kaser-Hotz B, Khan T, Rohrer Bley C, Melzer K, Schwendener RA, et al. Optimizing photodynamic therapy: in vivo pharmacokinetics of liposomal meta-(tetrahydroxyphenyl)chlorin in feline squamous cell carcinoma. Clin Cancer Res. 2005;11:7538-44.
[8] Lassalle HP, Dumas D, Grafe S, D'Hallewin MA, Guillemin F, Bezdetnaya L. Correlation between in vivo pharmacokinetics, intratumoral distribution and photodynamic efficiency of liposomal mTHPC. J Control Release. 2009;134:118-24.
[9] Braiman-Wiksman L, Solomonik I, Spira R, Tennenbaum T. Novel insights into wound healing sequence of events. Toxicol Pathol. 2007;35:767-79.
[10] Soo C, Rahbar G, Moy RL. The immunogenicity of bovine collagen implants. J Dermatol Surg Oncol. 1993;19:431-4.
[11] Langer A, Rogowski W. Systematic review of economic evaluations of human cell-derived wound care products for the treatment of venous leg and diabetic foot ulcers. BMC Health Serv Res. 2009;9:115.
[12] Buser D, Chen ST, Weber HP, Belser UC. Early implant placement following single-tooth extraction in the esthetic zone: biologic rationale and surgical procedures. Int J Periodontics Restorative Dent. 2008;28:441-51.
[13] Davidson JM, Giro M. Healing slack skin. J Invest Dermatol. 2006;126:2563-4.
[14] De Vries HJ, Zeegelaar JE, Middelkoop E, Gijsbers G, Van Marle J, Wildevuur CH, et al. Reduced wound contraction and scar formation in punch biopsy wounds. Native collagen dermal substitutes. A clinical study. Br J Dermatol. 1995;132:690-7.
[15] De Vries HJ, Middelkoop E, J.R M, R.P D, Wildevuur CH, Westerhof H. Dermal regeneration in native non-cross-linked collagen sponges with different extracellular matrix molecules. Wound Repair Regen. 1994;2:37-47.
[16] Schwartz D. The proliferation of elastic fibres after skin incisions in albino mice and rats: a light and electron microscopic study. J Anat. 1977;124:401-11.
[17] Antonicelli F, Bellon G, Debelle L, Hornebeck W. Elastin-elastases and inflamm-aging. Curr Top Dev Biol. 2007;79:99-155.

[18] Kubler A, Finley RK, 3rd, Born IA, Mang TS. Effect of photodynamic therapy on the healing of a rat skin flap and its implication for head and neck reconstructive surgery. Lasers Surg Med. 1996;18:397-405.
[19] Garrier J, Bressenot A, Grafe S, Marchal S, Mitra S, Foster TH, et al. Compartmental targeting for mTHPC-based photodynamic treatment in vivo: Correlation of efficiency, pharmacokinetics, and regional distribution of apoptosis. Int J Radiat Oncol Biol Phys.78:563-71.
[20] Parekh SG, Trauner KB, Zarins B, Foster TE, Anderson RR. Photodynamic modulation of wound healing with BPD-MA and CASP. Lasers Surg Med. 1999;24:375-81.
[21] Bryld LE, Jemec GB. The bacterial flora of the skin surface following routine MAL-PDT. J Dermatolog Treat. 2006;17:222-3.
[22] Coutier S, Bezdetnaya L, Marchal S, Melnikova V, Belitchenko I, Merlin JL, et al. Foscan (mTHPC) photosensitized macrophage activation: enhancement of phagocytosis, nitric oxide release and tumour necrosis factor-alpha-mediated cytolytic activity. Br J Cancer. 1999;81:37-42.

TABLES

Table 1. Macroscopic and pathological assessment of controls and Foslip®-PDT groups. Non implanted mice, membrane only (M), sponge only (S), Membranes or Sponges with light or PDT at different Foslip® concentrations.

		Treatment modality	Number of mice	Macroscopy		Pathology		
				Scab until day	Scar at day 14	Scar	Inflammation	Elastin
CONTROL GROUPS		No implant	5	9	5/5			
	MEMBRANE	No light no Foslip®	5	7				
		Light only	5	7				
		Foslip® only (50 µg/ml)	3	7		1/3		
	SPONGE	No light no Foslip	5	7		5/5	5/5	
		Light only	5	7				
		Foslip® only (50 µg/ml)	2	7			2/2	
PDT TREATED GROUPS	MEMBRANE	Foslip® 50 µg/ml	8	7	1/8	1/8		
		Foslip® 10 µg/ml	5	4				
		Foslip® 5 µg/ml	5	3			1/5	1/8
		Foslip® 1 µg/ml	4	3				4/4
		Foslip® 0,5 µg/ml	4	3			1/4	4/4
	SPONGE	Foslip® 50 µg/ml	8	7	5/8	5/8	8/8	
		Foslip® 10 µg/ml	5	4		3/5	5/5	
		Foslip® 5 µg/ml	5	3			5/5	
		Foslip® 1 µg/ml	4	3		4/4	4/4	1/4
		Foslip® 0,5 µg/ml	4	3	2/4	4/4	4/4	

LEGENDS FOR FIGURES

Figure 1. Typical macroscopic assessment of wound healing during 14 days.

A. Controls

B. Foslip®-PDT groups.

Figure 2. HES[3] staining 14 days after Foslip®-PDT treatment

Upper panel. Scarring observed with sponge implants (**A** & **B**), membrane implants (**C**). Scale bar 200 µm.

Lower panel. Typical inflammatory response (inset; scale bar 100 µm) with sponges (**D**), membranes with 5 or 0.5 µg/ml Foslip®(**E**) or absence of inflammatory response for membranes at other PDT conditions (**F**).

Figure 3. Typical Weigert's elastin staining treated with Foslip®-PDT

A. Sponge without elastin neosynthesis

B. Membrane treated at the highest Foslip® concentrations (50 and 10 µg/ml) without elastin neosynthesis and evidencing of positive elastin staining in the membrane (▼)

C. Membrane treated at the three lowest concentrations (5, 1 and 0.5 µg/ml) showing discrete dermal elastin labeling (▼)

Figure 1

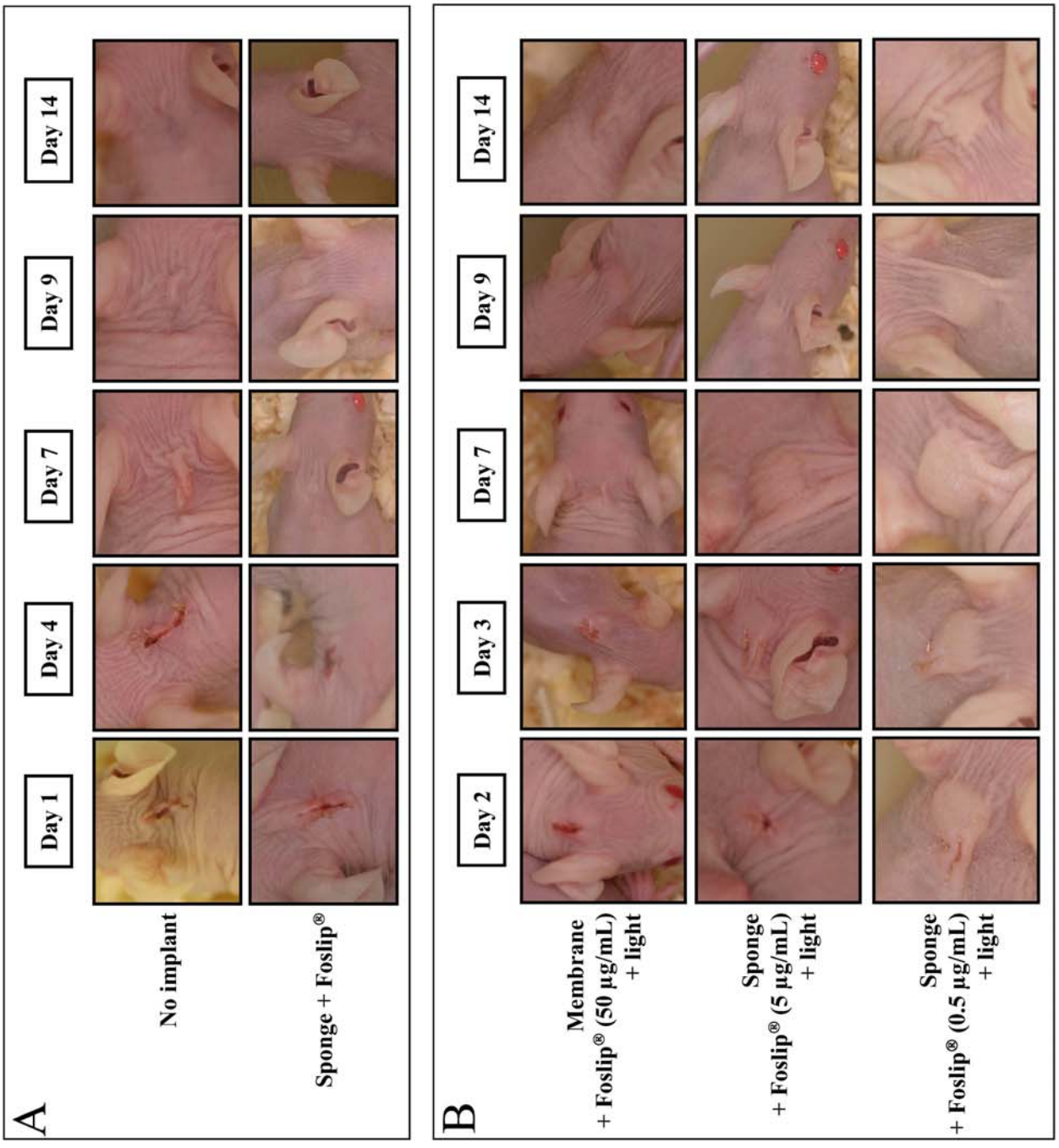
A
Day 1
Day 4
Day 7
Day 9
Day 14
No implant
Sponge + Foslip®
B
Day 2
Day 3
Day 7
Day 9
Day 14
Membrane + Foslip® (50 µg/mL) + light
Sponge + Foslip® (5 µg/mL) + light
Sponge + Foslip® (0.5 µg/mL) + light

Figure 2

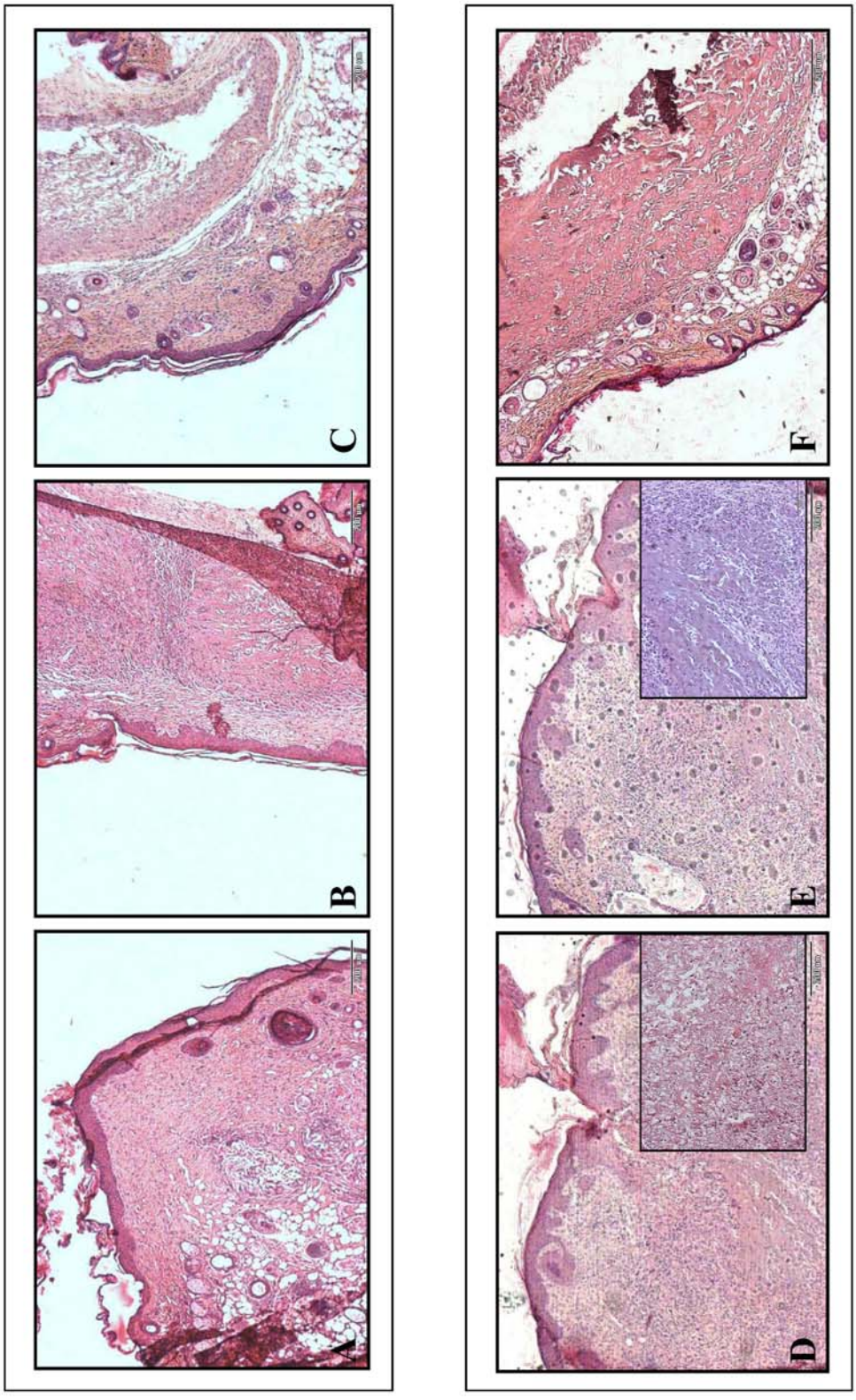

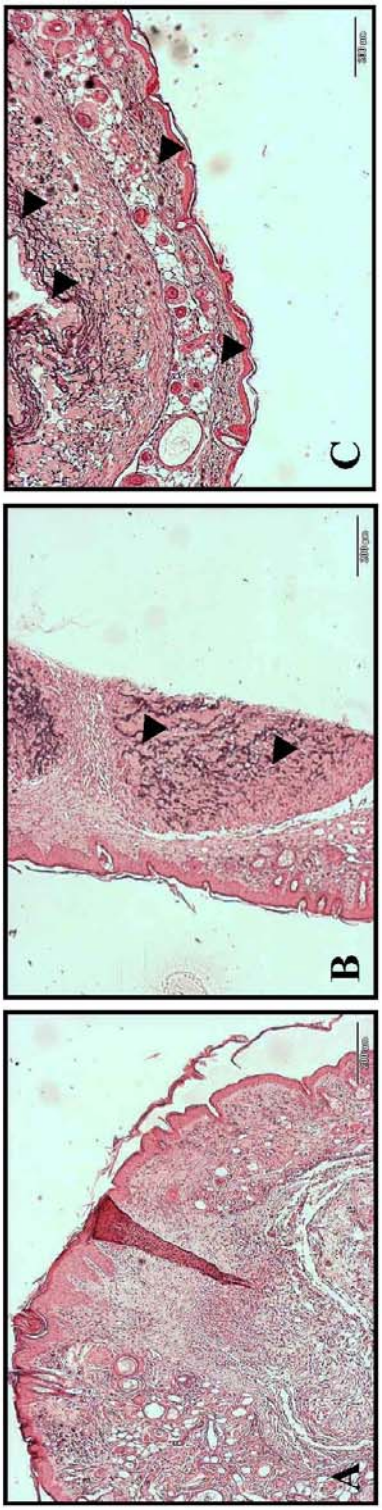

Figure 3

1.2 Assessment of apoptosis by immunohistochemistry to active caspase-3, active caspase-7, or cleaved PARP in monolayer cells and spheroid and subcutaneous xenografts of human carcinoma

Aude Bressenot, Sophie Marchal, Lina Bezdetnaya, **Julie Garrier**, François Guillemin et François Plénat

J Histochem Cytochem 2009; 57(4):289-300.

The Journal of Histochemistry & Cytochemistry

Volume 57(4): 289–300, 2009
Journal of Histochemistry & Cytochemistry
http://www.jhc.org

ARTICLE

Assessment of Apoptosis by Immunohistochemistry to Active Caspase-3, Active Caspase-7, or Cleaved PARP in Monolayer Cells and Spheroid and Subcutaneous Xenografts of Human Carcinoma

Aude Bressenot, Sophie Marchal, Lina Bezdetnaya, Julie Garrier, François Guillemin, and François Plénat

Service d'Anatomie et de Cytologie Pathologiques, Hôpital de Brabois, Centre Hospitalier Régional et Universitaire Nancy, Vandoeuvre-lès-Nancy, France (AB,FP), and Centre de Recherche en Automatique de Nancy-Centre National de la Recherche Scientifique Unité Mixte de Recherche 7039 Nancy Université, Centre Alexis Vautrin, Vandoeuvre-lès-Nancy, France (SM,LB,JG,FG)

SUMMARY Immunohistochemistry to active caspase-3, recently recommended for apoptosis detection, is inappropriate to detect apoptosis involving caspase-7. Cleavage of poly-ADP-ribose polymerase 1 (PARP-1), a major substrate of both caspases, is a valuable marker of apoptosis. Apoptosis evaluation induced in vitro either by paclitaxel or by photodynamic treatment (PDT) with Foscan in HT29 or KB monolayer cells and HT29 spheroids yielded a close percentage of labeled cells whatever the antibody used, whereas in control specimens, cleaved PARP (c-PARP) immunostaining failed to detect apoptosis as efficiently as active caspase-3 or -7 immunostaining. Studies in MDA-MB231 monolayer cells and HT29 xenografts either subjected or not subjected to Foscan-PDT resulted in a significant higher number of active caspase-3–labeled cells, although immunofluorescence analysis showed c-PARP and active caspase-3 perfectly colocalized in tumors. A restricted expression of c-PARP was obvious in the greater part of caspase-3 expressing cells from control tumor, whereas photosensitized tumors showed a higher number of cells expressing large fluorescent spots from both active caspase-3 and c-PARP. These results support the assumption that c-PARP expression was dependent on treatment-induced apoptosis. The absence of caspase-7 activation in some caspase-3–expressing cells undergoing Foscan-PDT shows the relevance of using antibodies that can discriminate caspase-dependent apoptotic pathways. (J Histochem Cytochem 57:289–300, 2009)

KEY WORDS
apoptosis
caspase-3
caspase-7
poly-ADP-ribose polymerase

THE MOLECULAR and biochemical events of apoptotic cell death have been extensively studied (reviewed in Jin and El-Deiry 2005). Many anticancer drugs induce apoptosis by molecular mechanisms mediated through mitochondrial dysfunction (Green and Kroemer 2004). Release of cytochrome c from the internal part of the mitochondrial membrane into the cytosol results in the activation of caspase cascades, in particular caspase-9, -3, -6, and -7. Because caspase-3 is the main executioner of apoptosis, IHC to the active form of caspase-3 (active casp-3) has been run to check apoptosis in paraffin sections from various tissue (Gown and Willingham 2002; Duan et al. 2003; Resendes et al. 2004; Jakob et al. 2008) and has been recommended in clinical trials as a biomarker of photodynamic treatment (PDT) activity in vivo (Miller et al. 2007). However, it is important to note that apoptosis may also occur through an activation of other executioner caspases such as caspase-7 that could be activated through a mechanism independent of the mitochondrial pathway (Davidson et al. 2005; Pyrko et al. 2007). Moreover, caspase-7 could partially substitute caspase-3 in caspase-3–deficient cells (Mooney et al. 2002; Lakhani et al. 2006). Many protein targets of active caspases are biologically important apoptotic indicators of morphological and biochemical changes associated with apoptosis (Degterev et al. 2003). One of the essential substrates cleaved by both caspase-3 and -7 is poly-ADP-ribose polymerase (PARP), an abundant DNA-binding enzyme that detects and signals DNA strand breaks (Decker and Muller 2002).

Correspondence to: F. Plénat, Service d'Anatomie et de Cytologie Pathologiques, CHU de Brabois, Allée du Morvan, 54511 Vandoeuvre-lès-Nancy, France. E-mail: f.plénat@chu-nancy.fr

Received for publication June 11, 2008; accepted November 6, 2008 [DOI: 10.1369/jhc.2008.952044].

0022-1554/08/$3.30

The presence of cleaved PARP-1 is one of the most used diagnostic tools for the detection of apoptosis in many cell types. The cleavage of PARP-1 into two fragments of 89 and 24 kDa has been considered indicative of functional caspase activation (Koh et al. 2005). However, in sections from ethanol-fixed tissues, specific antibody to cleaved PARP-1 (c-PARP) was unsuccessfully tested (Holubec et al. 2005).

In this study, we assessed apoptosis by using polyclonal antibodies to active caspase-3, active caspase-7, and c-PARP to give a precise insight into the relevance of each marker for the IHC detection of apoptosis. Moreover, the accuracy of antibodies to active caspase-7 and c-PARP to detect apoptosis in histopathology has never been reported in formaldehyde-fixed tissues. Apoptosis was induced in vitro by paclitaxel (McGrogan et al. 2008) or PDT with Foscan (Marchal et al. 2005) in monolayer HT29, KB, and MDA-MB231 carcinoma cell lines or spheroids growing HT29 cells. For the in vivo experiments, we used xenografted HT29 tumors in nude mice that were subjected to Foscan-PDT.

Materials and Methods

Monolayer Cell Cultures

HT29 is a human colon adenocarcinoma cell line, MDA-MB231 is a human mammary adenocarcinoma cell line, and KB is a human cell line related to HeLa cells. These cells were obtained from the American Type Culture Collection (Rockville, MD) and were grown in RPMI-1640 medium (Invitrogen; Cergy-Pontoise, France) without phenol red and glutamine, supplemented with 10% heat-inactivated FCS (PAN Biotech; Aidenbach, Germany), 1% penicillin (10,000 UI/ml)-streptomycin (10,000 μg/ml), and 1% 200 mM glutamine (Invitrogen). Cells were kept at 37C in a 95% air/5% CO_2 humidified atmosphere. They were subcultured every 7 days using 2.5% trypsin with 1 mM EDTA (Invitrogen).

Spheroid Cell Culture

Multicell spheroids of the HT29 cell line were initiated as previously described (Marchal et al. 2005). Briefly, 5×10^4 HT29 cells were seeded into 75-cm^2 flasks previously coated with 1% L-agarose. After 3 days, aggregates were transferred to 250-ml spinner flasks (Integra Biosciences; Chur, Switzerland) containing 150 ml culture medium. The flasks were placed on magnetic plates (Integra Biosciences) at 75 rpm in 5% CO_2 and 37C humidified atmosphere for 15 days. Spheroids reaching ~500 μm in diameter were used in experiments.

Xenografted Tumors

Studies were performed using female athymic Swiss *Foxn1^{nu}/Foxn1^{nu}* mice (Harlan; Gannat, France). All animal experiments were carried out in compliance with the French Animal Scientific Procedures Act (April 1988). Mice were housed in plastic cages under standard conditions (25C, 50% relative humidity, 12-hr light/dark cycle) and provided with food and water ad libitum. Procedure to induce HT29 tumors in nude mice was performed as previously described (Coutier et al. 2002). Briefly, 0.1 ml of 8×10^7 HT29 cells/ml in 5% glucose solution was inoculated subcutaneously into the right hind foot. The mice were treated 15 days later when the tumors reached 5 mm in diameter. Three control tumors and seven treated tumors were sampled.

For each treatment (paclitaxel and photodynamic), three experiments were performed on cell lines and cell spheroids. Induction of apoptosis in cell lines, spheroids, and tumor transplants was carried out according to the following procedure.

Paclitaxel Treatment of Monolayers and Spheroids

Monolayer Cells. For each cell line, 3×10^4 cells/ml were seeded into 75-cm^2 flasks. Forty-eight hours after seeding, paclitaxel (Taxol; Sigma-Aldrich, Saint-Quentin Fallavier, France), dissolved in 95% ethanol (100 μM), was added to the culture medium at a final concentration of 0.1 μM. Treatment was carried out for 48 hr. Control cells were treated with 95% ethanol alone (dilution, 1:1000 v/v).

HT29 Spheroids. Approximately 80 spheroids were collected and seeded in 2 ml supplemented medium containing 0.1 μM paclitaxel for 48 hr. Control spheroids were incubated with supplemented medium containing only ethanol (dilution, 1:1000 v/v).

Photodynamic Treatment

Drug Preparation and Administration. Foscan [meta-tetra(hydroxyphenyl)chlorine] was kindly supplied by Biolitec (Jena, Germany). Foscan stock solution was prepared in methanol. Further dilutions of Foscan were performed in RPMI-1640 supplemented with FCS. Injection in animals was performed with a solution of Foscan diluted in a mixture of ethanol, polyethylene glycol, and water (2:3:5) as recommended by the manufacturer. Mice were injected in the tail vein with 0.3 mg/kg body weight at 24 hr before light exposure.

Monolayer Cells. Four days before treatment, 3×10^4 cells/ml of each cell line were seeded in 60-mm-diameter Petri dishes. Logarithmically growing cells were incubated with 1 μg/ml (1.45 μM) Foscan solution in RPMI supplemented with 2% FCS for 24 hr. After two washes, RPMI supplemented with 10% FCS was added, and cells were irradiated with a 650-nm laser diode at a fluence of 0.03 J/cm^2 delivered at a fluence rate of 1.92 mW/cm^2. Control cells were incubated with Foscan and were not subjected to irra-

diation (drug, no light). Twenty-four hours after PDT, cells were collected by trypsinization, washed, and fixed in 4% formaldehyde (pH 7.4).

HT29 Spheroids. HT29 spheroids were treated according to the method previously published (Marchal et al. 2005). Briefly, after a 24-hr incubation with 4.5 μM Foscan RPMI supplemented with 10% FCS, spheroids were irradiated with a 650-nm laser diode at 5 J/cm^2 delivered at a fluence rate of 10 mW/cm^2. Control spheroids were exposed to Foscan without illumination (drug, no light).

HT29 Xenografted Tumors. Twenty-four hours after Foscan IV injection, tumors were irradiated with a 650-nm diode laser at a fluence of 10 J/cm^2 delivered at a fluence rate of 30 mW/cm^2. Control tumors were subjected to Foscan injection without irradiation (drug, no light). Twenty-four hours after PDT, the mice were sacrificed by anesthetic overdose, and the grafts were surgically removed and sectioned in 3-mm-thick slices before being processed.

Sample Collections and Fixation

Twenty-four hours after treatments, monolayer culture cells, spheroids, and tumor samples were fixed in 4% (m/v) formaldehyde (pH 7.4) for 16 hr. Tumors and pellets of monolayer culture cells and spheroids were routinely processed and embedded in paraffin. Paraffin blocks were used to generate 5-μm-thick hematoxylin and eosin–stained sections. Additional slices of transplants were also snap-frozen in isopentane precooled in liquid nitrogen. For each sample of monolayer cells, ultrastructural control was performed.

Transmission Electron Microscope

Cells were fixed overnight at 4C in 3% glutaraldehyde in 0.1 M sodium cacodylate buffer (pH 7.4) and transferred to 0.1 M phosphate buffer (pH 7.2). The cells were postfixed in 1% osmium tetroxide in S-collidine, dehydrated in graded ethanols, transferred to propylene oxide, and embedded in Epon 812. Semithin sections were stained with 1% methylene blue. The sample was further sectioned into ultrathin slices (75 nm), contrasted with uranyl acetate and lead citrate and observed on a transmission electron microscope (CM10; Philips, Eindhoven, The Netherlands).

c-PARP and Active Caspase-3 and-7 Immunolabeling

IHC detection of apoptosis-related proteins was carried out on 5-μm-thick deparaffinized sections. Before IHC, sections were subjected to heat-induced epitope retrieval by incubation in a 0.01 M sodium citrate solution (pH 6) at 120C for 10 min, followed by a 2-hr cool-down. Primary antibodies were diluted in the following buffer: 0.1 M PBS, 0.3% (m/v) BSA, 0.1% (m/v) sodium azide, 0.06% (m/v) n-ethylmaleimide, and 20% (v/v) glycerol (PAB). Active caspase-3 was detected with a species-unspecific rabbit polyclonal antibody (1:1000 diluted; BD Biosciences, Le Pont-de-Claix, France) that specifically recognize the large fragment (17 kDa) of the active protein but not full-length caspase-3. The large fragment of active caspase-7 (20 kDa) was targeted by a species-unspecific rabbit polyclonal antibody (1:50 diluted) provided by Cell Signaling (Danvers, MA). For c-PARP IHC, sections were incubated in a solution of a rabbit polyclonal antibody (1/25 diluted; Cell Signaling, Danvers, MA). This species-specific antibody detects endogenous levels of the large fragment (89 kDa) of human PARP-1 resulting from cleavage at aspartic acid 214 but does not recognize full-length PARP-1 or other PARP isoforms. All antibodies applied in this study were previously used in Western blot analysis with satisfying results (Marchal et al. 2005,2007). Primary antibodies were applied for 16 hr at 4C. The sections were washed in two changes of PBST (0.1 M phosphate buffer, pH 7.4, 0.1% (v/v) Tween 20) over 10 min and incubated with biotinylated goat anti-rabbit antibody (Dakocytomation; Trappes, France) diluted 1:200 for 1 hr at room temperature. After two PBST washes (for 10 min each), endogenous peroxidase activity was blocked by a 10-min incubation in a 6% hydrogen peroxide solution in distilled water. The slides were washed two times in PBST (for 5 min each time) and incubated in streptavidin-peroxidase (Dakocytomation) diluted 1:150 in PBST for 1 hr at room temperature. After two PBST washes of 5 min, bound peroxidase was identified using the Novared TR system (Abcys; Paris, France). Nuclear counterstaining was performed with 1/2-diluted Harris hematoxylin. Each assay was controlled negatively by processing sections in the absence of primary antibody. Good immunostaining data (i.e., low background staining and good precision) were obtained with three antibodies. False-positive cells were only observed in tissue sections of tumor transplants where endogenous biotin was detected by the streptavidin–biotin system of visualization. However, it was easy to distinguish between positive, negative, and false-positive cells. Tumor cells were never artifactually stained, and false-positive staining was limited to mastocytes in mouse connective tissue around the tumors and in sebaceous glands when present.

Determination of Apoptotic Indices

The number of apoptotic cells present in a section expressed as a fraction of the total number of cells, the so-called apoptotic index, measures an apoptotic state. For the purpose of this study, an activated caspase-3 labeling apoptotic index, an activated caspase-7 labeling apoptotic index, and a c-PARP labeling apoptotic index were calculated. The number of labeled

The Journal of Histochemistry & Cytochemistry

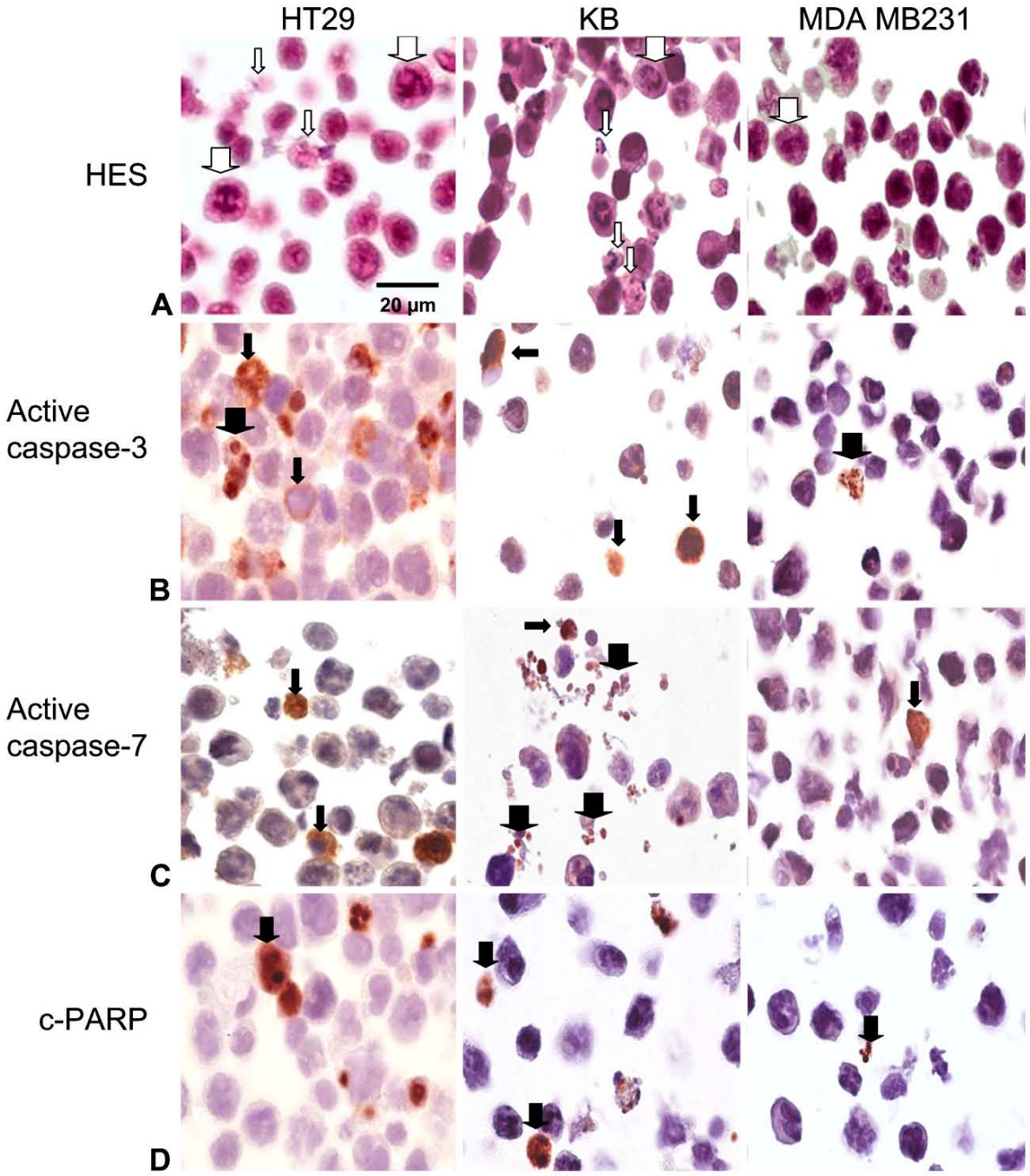

Figure 1 Apoptosis and apoptosis-related protein detection in HT29, KB, and MDA-MB231 monolayer cells subjected to 0.1 µM paclitaxel for 48 hr. (**A**) Paraffin sections were stained with standard coloration hematoxylin-eosin-safran. Note specific morphological features of apoptosis in HT29 and KB monolayers cells (thin white arrows). Numerous mitotic cells were observed in the three cell lines (thick white arrows). (**B**) Active caspase-3 labeling. Note signal cytoplasmic location (thin black arrows) and focally nuclear signal translocation (thick black arrows). (**C**) Active caspase-7 labeling. Cytoplasm location (thin black arrows) and apoptotic bodies (thick black arrows) were observed. (**D**) Cleaved poly-ADP-ribose polymerase (c-PARP) labeling. Nuclear location was noticed (thick black arrows). Harris' hematoxylin counterstain.

cells in immunostained sections were counted relative to 2000 cells in the case of cell pellets. In sections of spheroids, at least three spheroids each composed of >300 non-necrotic cells were considered for each treatment condition. Because the antibody to c-PARP was human specific and did not visualize mouse stromal apoptotic cells, whereas the antisera to active caspase-3 and active caspase-7 stained apoptotic cells in both the stroma and the tumor cell compartment, the apoptotic indices in transplants were calculated as the number of apoptotic cells per total number of epithelial tumor cells. These indices were established by counting at least 2000 cells in fields distant from necrotic areas.

Colocalization Studies

Simultaneous visualization of active caspase-3 and either active caspase- 7 or c-PARP in the same section was carried out in 5-µm-thick frozen sections of two xenografted tumors (one control and one treated). This was achieved by the sequential use of two indirect fluorescence methods whose specificity was previously checked. Active caspase-3 was stained by the first sequence and either active caspase-7 or c-PARP by the second one. Briefly, frozen sections were first fixed with 30% v/v polyethylene glycol in 95C ethanol for 10 min. They were then dried at room temperature for 15 min, washed in absolute ethanol, and rehydrated in PBST for 5 min. They were incubated in a solution of the anti-active caspase-3 rabbit antiserum (1/1000 dilution in PAB for 3 hr at room temperature). The sections were washed twice with PBST for 10 min and incubated with 1:200 biotinylated goat anti-rabbit antibody (Dakocytomation) for 1 hr at room temperature. After two PBST washes (for 10 min each), the sections were incubated in a 1:8000 Streptavidin-FluoProbe SR 101 (Interchim; Montluçon, France) in the dark at room temperature. After two PBST washes (for 5 min each), the sections were mounted in a fluorescent-free aqueous mountant glycerol/PBS (9/1, v/v). Image acquisition was immediately carried out with a fluorescent microscope (Axiophot II; Zeiss, Jena, Germany) equipped with a motorized XY stage and a cooled AxioCam HRc CCD camera (Zeiss) controlled by the Axiovision 4.4 digital image processing software. The Mark and Find module of this software was used to record the various positions photographed on the slides. Thereafter, the coverslips were removed, and the sections were soaked in 0.1 N HCl for 20 min to eliminate the tissue-bound antibodies. After two PBST washes (for 5 min each), the second immunostaining sequence was carried out following the steps used in the first sequence. The antisera to active caspase-7 and c-PARP were respectively applied at a 1:50 and 1:25 dilution, and in the third step, Streptavidin Fluo Probe Alexa 488 (Interchim; Montluçon, France), diluted 1:4000, was used in place of Streptavidin-FluoProbe SR 101. The Mark and Find module was used to relocate the fields previously recorded, which were again photographed at the same magnification. The images of the same fields recorded under the two fluorescent modalities were merged using Axiovision software. Several controls were performed. First, the absence of cross-reactivity caused by residual antibodies of the first step was checked by omitting the second primary antibody of the double immunostaining method. Second, the absence of the deleterious effect of HCl on the second antibody signal was verified.

Statistical Analysis

Mann-Whitney's *U*-test was used to determine the statistical significance, with a limit set to $p<0.05$ using Staview 5.0 software.

Results

Apoptosis and Apoptosis-related Protein Assessment in Monolayer Cell Pellets

Morphological and IHC aspect of apoptosis was studied in three monolayer cell lines after their pretreat-

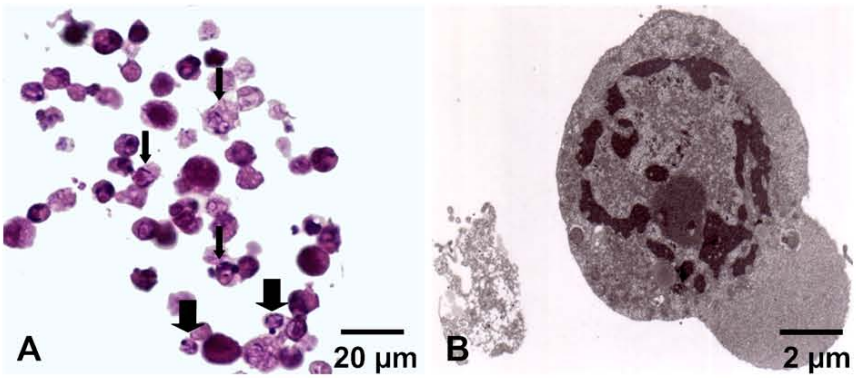

Figure 2 Apoptosis in MDA-MB231 monolayer cells subjected to Foscan-photodynamic treatment (PDT). **(A)** Paraffin sections were stained with standard coloration HES. Note specific morphological features of apoptosis such as condensed eosinophilic cytoplasm and clumped marginated chromatin (thin arrows) or apoptotic bodies (thick arrows). **(B)** Transmission electron microscopy. Ultrastructural study showed an MDA-MB231 cell with a nuclear marginated chromatin and an increase in the cytosol density typical of apoptosis.

The Journal of Histochemistry & Cytochemistry

ment with paclitaxel, an apoptosis inducer in many cell lines. Apoptosis was first recorded by morphological study on hematoxylin-eosin-safran-stained tissue sections (Figure 1A). Specific morphological changes indicative of apoptosis were identified in HT29 and KB cells but not in MDA cells (thin arrows). All cell lines, however, showed numerous cells with mitotic nuclei as a consequence of paclitaxel cytostatic treatment (thick arrows). The antibodies specific for active caspases-3 and -7 (Figures 1B and 1C) selectively stained the cytoplasm of cells (thin arrows), whose nuclear morphology was consistent with apoptosis, along with the cytoplasm of morphologically healthy-looking cells, thus suggesting that these antibodies recognized activated protein at the early stage of apoptosis. Active caspase-3, opposite to caspase-7, was also occasionally detected in nuclei (thick arrows), thus featuring a translocation of the protein to the nucleus (Figure 1B). In apoptotic cells, whose nuclei were still not fragmented, c-PARP staining was limited to nuclear chromatin (Figure 1D, thick arrows) and was distributed rather uniformly and diffusely over the whole nuclear area. Apoptotic bodies were clearly stained by all three markers.

After Foscan-PDT, a similar aspect in stained cells detected either by active caspase-3, active caspase-7, or c-PARP antibodies was obtained in HT29 and KB compared with paclitaxel treatment (data not shown). In MDA-MB231cells, typical apoptotic features including specific chromatin distribution and cytoplasm densification were observed both in HES (Figure 2A) and ultrastructural examinations (Figure 2B). The chromatin was predominantly arranged as a circumferential layer of heterochromatin, whereas the central chromatin had a dispersed granula rand speckled appearance. An increase in electron density was observed in the cytosol (Figure 2B).

Similar ultrastructural modifications were observed in other cells treated by PDT along with HT 29 and KB cells after paclitaxel treatment (data not shown).

The apoptotic indices (AIs) obtained from all three markers in HT29, KB, and MDA-MB231 cell lines are shown in Figure 3. Overall, <4% of the cells were detected by the three markers in controls. We noticed that the number of cells labeled with the antibody to c-PARP gave statistically significant lower results compared with other markers. Irrespective of cell lines, mean AIs in control were 0.47 ± 0.2% for c-PARP, 1.28 ± 1.03% for active caspase-3 ($p = 0.02$), and 1.19 ± 0.71% for active caspase-7 ($p = 0.008$). Similarly, paclitaxel-treated MDA-MB231 cells showed significantly less c-PARP–labeled cells (0.68 ± 0.30%) than active caspase-3 (1.72 ± 0.28%)– or active caspase-7 (1.79 ± 0.46%)–labeled cells ($p<0.05$). In paclitaxel-treated HT29 and KB cells, c-PARP labeling (22.7 ± 15.0% and 15.4 ± 5.4%, respectively) and active caspase-7 labeling (23.8 ± 19.8 and 14.3 ± 3.5%,

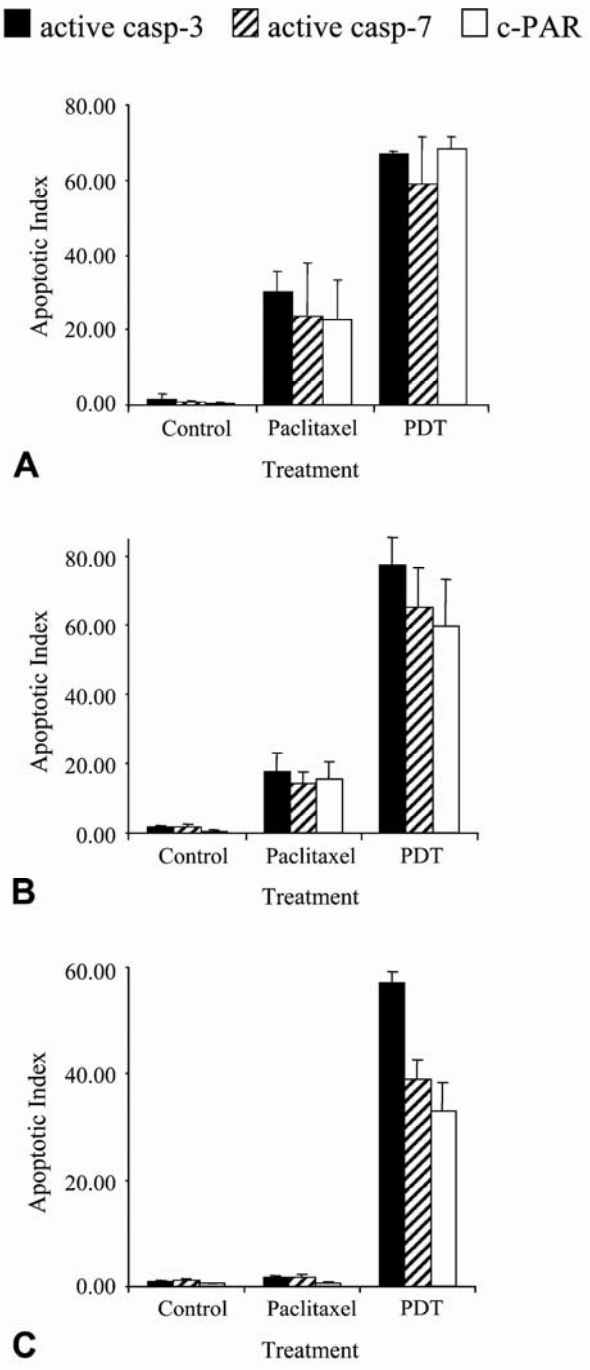

Figure 3 Apoptotic index from active caspase-3, active caspase-7, or c-PARP staining applied on control or treated HT29 (**A**), KB (**B**), and MDA-MB231 (**C**) cells. Cells were treated either by paclitaxel or Foscan-PDT. Results are expressed as mean apoptotic index (AI) ± SD of three experiments determined from at least 2000 tumor cells in each section. *Significantly different values ($p<0.05$).

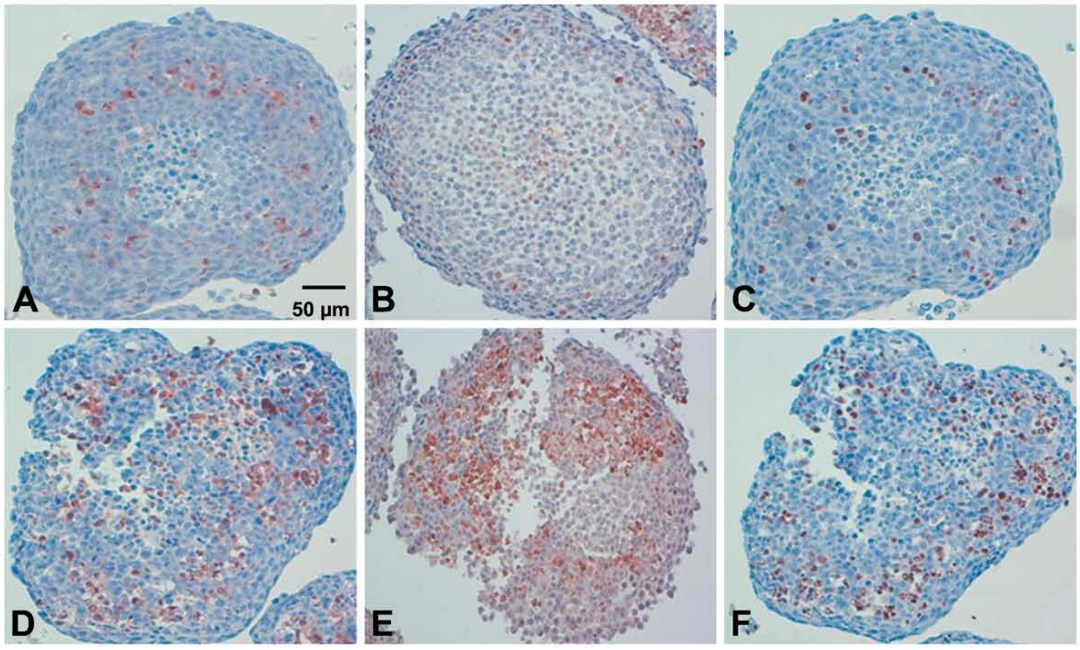

Figure 4 IHC on paraffin sections of HT29 spheroids to active caspase-3 (**A,D**), active caspase-7 (**B,E**), or c-PARP (**C,F**) applied without treatment (**A–C**) or subjected to Foscan-PDT (**D–F**). Note the distribution of apoptotic cells at the periphery of necrotic area. Loss of cell cohesion was noticeable in spheroids subjected to Foscan-PDT (**D–F**). Harris' hematoxylin counterstain.

respectively) gave close AIs, whereas active caspase-3 labeling yielded slightly but not significantly greater AIs (30.2 ± 7.6% and 17.8 ± 5.2%, respectively). In Foscan-photosensitized cells, IHC analysis to active caspase-3, caspase-7, or c-PARP did not result in a statistically significant difference in HT29 (67.1 ± 0.8%, 58.8 ± 18.2%, and 68.2 ± 4.7%, respectively) or KB cells (77.3 ± 8.2%, 65.0 ± 11.5%, and 59.6 ± 13.7%, respectively). In MDA-MB231 cells, active caspase-3 clearly provided greater AI (57.0 ± 2.1%) than either active caspase-7 (38.9 ± 3.8%) or c-PARP (32.9 ± 5.5%) labeling ($p<0.05$).

Apoptosis-related Protein Assessment in Spheroids

IHC to active caspase-3, active caspase-7, and c-PARP was applied to 29 spheroids subjected to different treatment protocols. Figure 4 shows the distribution of cells detected by the antibodies to active caspase-3, active caspase-7, and c-PARP in control spheroids (Figures 4A, 4B, and 4C, respectively) and in spheroids subjected to Foscan-PDT (Figures 4D, 4E, and 4F, respectively). Control spheroids showed a few labeled cells around the necrotic core as clearly shown in the spheroids immunostained with either antiactive caspase-3 (Figure 4A) or anti-c-PARP antibody (Figure 4C). In Foscan-photosensitized spheroids (Figures 4D–4F), the number of labeled cells increased in the area between the outer rim and the necrotic core. In addition, we noted a loss of cell cohesion. Distribution pattern of staining was the same irrespective of the technique used. AIs determined from non-necrotic cells of untreated or treated either by paclitaxel or Foscan-PDT spheroids are presented in Table 1. In control spheroids, from 9.1% to 17.3% labeled cells were counted according to the method applied, with the lowest value for c-PARP (9.1 ± 2.3%). The highest and identical scores were obtained with active caspase-3 (17.4 ± 3.0%) and active caspase-7 (17.0 ± 4.4%) labeling and were found sig-

Table 1 Quantification of apoptotic cells by IHC to c-PARP and active caspase-3 and -7 in paraffin-embedded section of control[a] and paclitaxel[b] or Foscan-photosensitized[c] HT29 spheroids

	Apoptotic index[d]		
Markers	Control cells	Paclitaxel	Foscan-PDT
Active caspase-3	17.4 + 3.0	34.7 + 1.9	38.4 + 0.4
Active caspase-7	17.0 + 4.4	32.3 + 7.1	40.3 + 3.8
c-PARP	9.1 + 2.3[e]	32.4 + 2.2	41.3 + 0.7

[a]Control tumors were obtained from both untreated HT29 and non-irradiated cell spheroids.
[b]HT29 spheroids were incubated with 0.1 µM paclitaxel for 48 hr.
[c]HT29 spheroids were subjected to 4.5 µM Foscan for 24 hr before irradiation (10 mW/cm^2, 5 J/cm^2).
[d]Mean + SD of at least three experiments.
[e]Significantly different ($p<0.05$).
c-PARP, cleaved poly-ADP-ribose polymerase; PDT, photodynamic treatment.

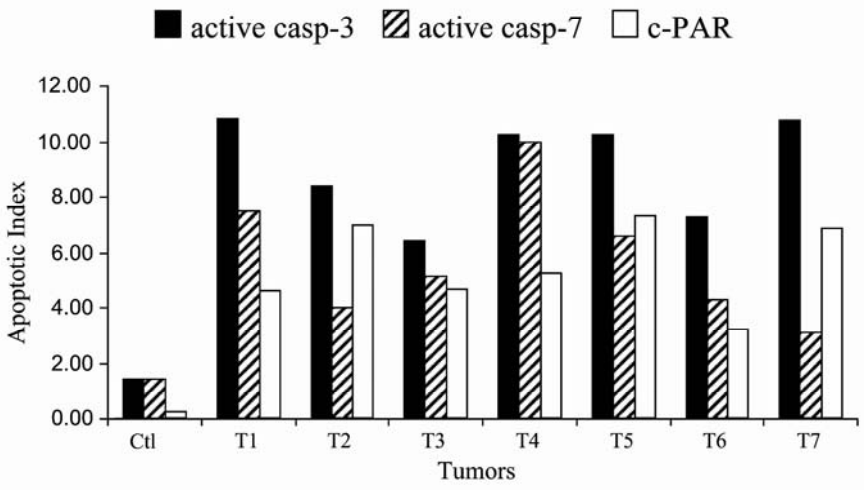

Figure 5 Apoptotic index from active caspase-3, active caspase-7, or c-PARP staining applied on HT29 subcutaneous xenografts subjected to Foscan (0.3 mg/kg, IV) photosensitization (10 J/cm^2, 30 mW/cm^2, 24 hr after injection). Note the variability between tumors. AIs were determined from at least 2000 tumor cells in each section.

nificantly different from c-PARP value ($p<0.05$). In paclitaxel-treated spheroids IHC toward active caspase-3, active caspase-7, and c-PARP resulted in equivalent AIs (34.7 ± 1.9%, 32.3 ± 7.1%, and 32.4 ± 2.2%, respectively). A similar observation was found in Foscan-photosensitized spheroids (38.4 ± 0.4%, 40.3 ± 3.8%, and 41.3 ± 0.7%, respectively).

Apoptosis-related Protein Assessment in HT29 Subcutaneous Xenografts

The density of apoptotic cells was assessed in three control tumors and in seven xenografts 24 hr after Foscan-PDT (Figure 5). Variability in the level of apoptosis was patent. Overall, the extent of apoptosis detected with c-PARP in control tumors was significantly lower (0.2 ± 0.2%) than active caspase-3 (1.4 ± 1.2%) or active caspase-7 (1.4 ± 0.7%) immunostaining ($p<0.05$). In Foscan-photosensitized tumors, active caspase-3 labeling prevailed in all cases. This observation was confirmed by the comparison of AIs averaged for each marker (Table 2). Maximal staining (8.3 ± 2.9%) was obtained for active caspase-3 and was found significantly different ($p<0.02$) from active caspase-7 (4.9 ± 1.5%) and c-PARP (5.0 ± 2.0%).

Overlaid images taken from immunofluorescence experiments performed on a tissue section subjected successively to active caspase-3 and c-PARP in control (Figure 6A) or in Foscan-photosensitized tumors (Figure 6B) provided additional information. In all labeled cells, c-PARP (shown in green) colocalized with active caspase-3 (shown in red), thus providing yellow spots. In some cases, tiny yellow spots were enclosed in red signals suggesting limited expression of c-PARP. This feature was predominantly observed in control tumors (Figure 6A). A careful examination of immunostained tissue sections (Figures 6C and 6D) confirmed this observation. Many apoptotic cells from control tumors showed nuclei containing a limited part of labeled antigenic sites (Figure 6C), whereas photosensitized tumors showed a higher number of cells with a large expression of c-PARP (Figure 6D). These cells were noticed without apoptotic-related nuclear morphological change, suggesting that apoptosis in these cells was at an early stage.

Another observation from immunofluorescence analysis was the poor correlation between active caspase-3 (red) and active caspase-7 (green) in Foscan-photosensitized tumors (Figure 7). Expression of active caspase-7 was not detectable in all active caspase-3–expressing cells. As a result, some labeled cells exhibited only a red signal. Conversely, all cells detected by the antibody to active caspase-7 expressed active caspase-3 antigen, thus showing yellow spots.

Discussion

Two major apoptotic pathways, namely the extrinsic (through membrane death receptor) and intrinsic (through mitochondria), are governed by caspases, a

Table 2 Quantification of apoptotic cells by IHC to c-PARP and active caspase-3 and -7 in paraffin-embedded section of control[a] and Foscan-photosensitized[b] HT29 xenografted tumors

	Apoptotic index[c]	
Markers	Control tumors	Foscan-PDT
Active caspase-3	1.4 ± 1.2	8.3 ± 2.9[d]
Active caspase-7	1.4 ± 0.7	4.9 ± 1.5
c-PARP	0.2 ± 0.2[d]	5.0 ± 2.0

[a]Control tumors were obtained from both untreated HT29 and non-irradiated tumors.
[b]Nude mice were injected with 0.3 mg/kg Foscan 24 hr before tumor irradiation (30 mW/cm^2, 10 J/cm^2).
[c]Mean ± SD of at least three experiments.
[d]Significantly different ($p<0.05$).
c-PARP, cleaved poly-ADP-ribose polymerase; PDT, photodynamic treatment.

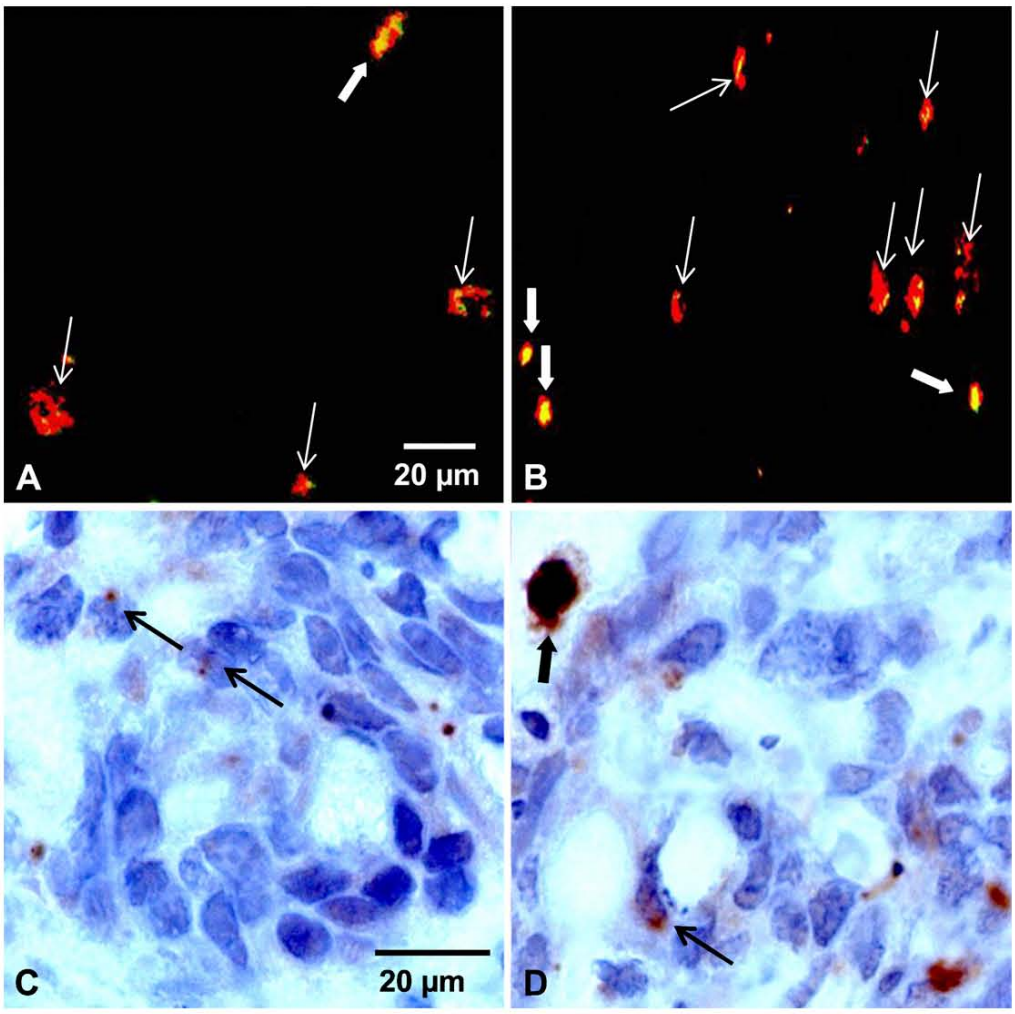

Figure 6 Merging of immunofluorescence images obtained from control tumors (**A**) or Foscan (0.3 mg/kg, IV)-photosensitized (10 J/cm^2, 30 mW/cm^2) HT29 subcutaneous xenografts (**B**) frozen 24 hr after treatment. Frozen sections were first subjected to active caspase-3 (red fluorescence) and then to c-PARP (green fluorescence). Colocalization between both markers showed large yellow spots (thick white arrows) or tiny yellow spots (thin white arrows) caused by c-PARP expression. c-PARP IHC on paraffin sections of control tumors (**C**) and photosensitized tumors (**D**). Thin black arrows indicate limited expression of c-PARP, whereas the thick black arrow indicates a large expression of c-PARP in nuclei of apoptotic cells.

family of proteases that cleave substrates at Asp-Xxx sequence. Based on their function, caspases have been divided into initiators or executioners of apoptosis. The executioner class includes caspase-3, caspase-6, which is processed by caspase-3 (Slee et al. 2001), and caspase-7. The precise role of caspase-7 during apoptosis remains elusive (Slee et al. 2001; Lakhani et al. 2006), whereas caspase-3 is generally considered to be the primary executioner of apoptosis. Therefore, the development of antibodies targeting either the active form of caspase-3 or cleaved substrates resulting from its activation warrants investigation (Holubec et al. 2005; Jakob et al. 2008).

In this study, we proposed to extend the investigation to caspase-7 processing and PARP-1 cleavage. Caspases-3 and -7 have some overlapping but also some distinct roles in apoptosis. It has been shown that caspase-3 controls DNA fragmentation and morphological changes of apoptosis (Slee et al. 2001; Lakhani et al. 2006). Caspase-7 plays a little role in these processes but could be important in the loss of cellular viability (Lakhani et al. 2006). In this context, PARP, which is generally recognized as a substrate of both caspases-3 and -7 with a strong affinity for the latter (Germain et al. 1999), could be a very useful marker of apoptosis. We performed an IHC study of apoptosis

The Journal of Histochemistry & Cytochemistry

The Journal of Histochemistry & Cytochemistry

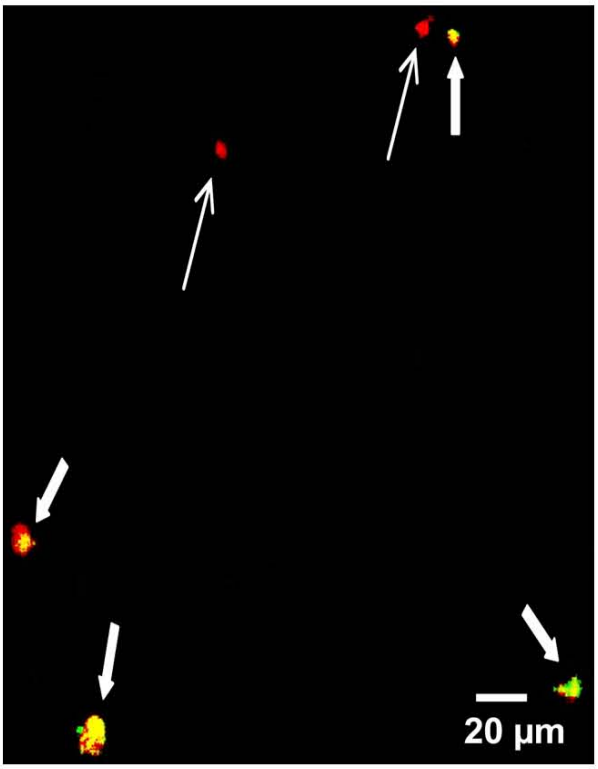

Figure 7 Merging of immunofluorescence images obtained from Foscan (0.3 mg/kg, IV)-photosensitized (10 J/cm^2, 30 mW/cm^2) HT29 subcutaneous xenografts frozen 24 hr after treatment. Frozen sections were first subjected to active caspase-3 (red fluorescence) and then to active caspase-7 (green fluorescence). Colocalization between both markers showed yellow spots (thick arrows). Red spots (thin arrows) indicate active caspase-3 expression only.

at three different levels of preclinical models, monolayer cells from three cell lines (HT29, KB, and MDA-MB231), HT29 cell spheroids that mimic avascular microtumors, and HT29 tumors xenografted in nude mice. Apoptotic cells at the late stage of the process showed morphological criteria (chromatin condensation with a marked accumulation of densely stained chromatin at the edge of the nucleus and cell fragmentation with formation of apoptotic bodies) that enabled their identification by standard hematoxylin and eosin staining. However, in paclitaxel-treated cells, abnormal mitotic figures resembling those of apoptosis could be confusing (Figure 1A). Active caspase-3 immunostaining was confirmed as a highly sensitive method that could clearly show the different steps in the location of caspase-3 activation from cytoplasmic to nuclear translocation of the protein (Figure 1B). This latter feature was not observed with active caspase-7 (Figure 1C), which does not translocate into the nucleus after induction of apoptosis (Kamada et al. 2005), thus supporting the difference between the two caspases in their respective role in the nuclear morphological changes during apoptosis. c-PARP labeling in the whole area of apoptotic nuclei (Figure 1C) was anticipated because PARP-1 is a DNA-binding enzyme that signals DNA strand breaks. Moreover, we applied an antibody to the large 85-kDa fragment of c-PARP, which has been shown to be translocated from the nucleolus to the nucleoplasm during apoptosis, whereas the short 29-kDa fragment is retained in nucleoli (Alvarez-Gonzalez et al. 1999). Compared with active caspase-3 or -7 labeling, the use of the antibody to c-PARP resulted in a poor staining of cells undergoing physiological apoptosis in control samples or in apoptosis-resistant MDA-MB231 cells treated with paclitaxel (Figure 3; Tables 1 and 2). Further analysis performed by merging the immunofluorescence images indicated a high level of colocalization between active caspase-3 and c-PARP in HT29 tumors (Figures 6A and 6B). A similar observation has been earlier reported in medulloblastomas (Puig et al. 2001). However, immunofluorescence from c-PARP labeling was restricted to tiny spots (Figure 7A), indicating a limited expression of the protein that could explain the difficulty to detect the cleaved form of PARP by enzymatic IHC. After treatment in vitro of HT29 or KB cells either by paclitaxel or by Foscan-PDT, the pattern of c-PARP labeling was close to those of active caspases-3 and -7 (Figures 3A, 3B, and 4). Likewise, in Foscan-photosensitized MDA-MB231, IHC to c-PARP and active caspase-7 resulted in a non-significantly different AI values (Figure 3C). These results suggest that cell damage either increased the number of antigenic sites and/or modified the extend of expression of c-PARP large fragments over the nucleus. In fact, both events could be related to the overactivation of full-length PARP-1 shortly before or simultaneously to the cleavage of PARP by caspases (Germain et al. 1999; Simbulan-Rosenthal et al. 1999; D'Amours et al. 2001). It has been recently reported that the nucleolus serves as a storage supplying PARP-1 in response to heavy DNA damage (Mortusewicz et al. 2007). Thus, the translocation of 85-kDa PARP fragments from the nucleolus to the nucleoplasm could occurs along with covalently bound poly(ADP-ribose) generated by the poly(ADP-ribosyl)ation catalyzed by the massive recruitment of PARP-1 from nucleoli to damage sites (Alvarez-Gonzalez et al. 1999). Taken together, these observations could imply a close relationship between the activity of PARP poly(ADP-ribosyl)ation, the amount of antigenic sites and the distribution of cleaved fragments over the nucleus after treatment. In this context, the percentage of c-PARP–labeled cells (5.0 ± 2.0%; Table 2) in Foscan-photosensitized HT29 tumors could represent an accurate evaluation of photoinduced apoptosis, whereas apoptotic assessment through caspases-3 or -7 activation includes both basic physiological and treatment-induced apoptosis.

Both treatments, paclitaxel and Foscan-PDT, trigger apoptosis in cells by the activation of caspases-3 and -7 (Goncalves et al. 2000; Kottke et al. 2002; Marchal et al. 2005). Caspase-7 has been recently presumed to play a major role in the induction of apoptosis under severe oxidative stress of the endoplasmic reticulum (Reddy et al. 2003; Rao et al. 2004). This molecular pathway has been strongly suggested after Foscan-PDT in the mammary adenocarcinoma MCF-7 cell line that lacks caspase-3 (Marchal et al. 2007). IHC to active caspase-3 and active caspase-7 applied on HT29 and KB monolayer cells and HT29 spheroids treated by either paclitaxel or Foscan-PDT showed a close percentage of cells expressing caspase-3 or caspase-7 activation (Figures 3A and 3B; Table 1). Thus, equal involvement of both caspases in the apoptotic pathway may be presumed. On the other hand, in Foscan-photosensitized MDA-MB231 cells (Figure 3C) or HT29 tumors (Table 2), active caspase-3 labeling was predominant. Colocalization obtained from merged immunofluorescence images indicated that active caspase-7 was not expressed in all caspase-3–expressing cells (Figure 7), suggesting that Foscan-PDT–induced apoptosis was mainly processed through the activation of caspase-3 in HT29 tumors. Likewise, MDA-MB231 monolayer cells could be more susceptible to caspase-3 activation after Foscan-PDT than HT29 and KB cell lines.

In conclusion, the use of c-PARP as a marker of physiological apoptosis is doubtful, whereas it could be a useful indicator of treatment-induced apoptosis probably by DNA damage. The biological significance in the different pattern of expression of active caspase-3 and -7 in Foscan-photosensitized tumors needs further study. As a general rule, the use of different antibodies to differentiate caspase-dependent apoptotic pathways in vivo is relevant.

Acknowledgments

We thank Biolitec AG for providing the Foscan.

Literature Cited

Alvarez-Gonzalez R, Spring H, Muller M, Burkle A (1999) Selective loss of poly(ADP-ribose) and the 85-kDa fragment of poly(ADP-ribose) polymerase in nucleoli during alkylation-induced apoptosis of HeLa cells. J Biol Chem 274:32122–32126

Coutier S, Bezdetnaya LN, Foster TH, Parache RM, Guillemin F (2002) Effect of irradiation fluence rate on the efficacy of photodynamic therapy and tumor oxygenation in meta-tetra (hydroxyphenyl) chlorin (mTHPC)-sensitized HT29 xenografts in nude mice. Radiat Res 158:339–345

D'Amours D, Sallmann FR, Dixit VM, Poirier GG (2001) Gain-of-function of poly(ADP-ribose) polymerase-1 upon cleavage by apoptotic proteases: implications for apoptosis. J Cell Sci 114: 3771–3778

Davidson DJ, Haskell C, Majest S, Kherzai A, Egan DA, Walter KA, Schneider A, et al. (2005) Kringle 5 of human plasminogen induces apoptosis of endothelial and tumor cells through surface-expressed glucose-regulated protein 78. Cancer Res 65: 4663–4672

Decker P, Muller S (2002) Modulating poly (ADP-ribose) polymerase activity: potential for the prevention and therapy of pathogenic situations involving DNA damage and oxidative stress. Curr Pharm Biotechnol 3:275–283

Degterev A, Boyce M, Yuan J (2003) A decade of caspases. Oncogene 22:8543–8567

Duan WR, Garner DS, Williams SD, Funckes-Shippy CL, Spath IS, Blomme EA (2003) Comparison of immunohistochemistry for activated caspase-3 and cleaved cytokeratin 18 with the TUNEL method for quantification of apoptosis in histological sections of PC-3 subcutaneous xenografts. J Pathol 199:221–228

Germain M, Affar EB, D'Amours D, Dixit VM, Salvesen GS, Poirier GG (1999) Cleavage of automodified poly(ADP-ribose) polymerase during apoptosis. Evidence for involvement of caspase-7. J Biol Chem 274:28379–28384

Goncalves A, Braguer D, Carles G, Andre N, Prevot C, Briand C (2000) Caspase-8 activation independent of CD95/CD95-L interaction during paclitaxel-induced apoptosis in human colon cancer cells (HT29–D4). Biochem Pharmacol 60:1579–1584

Gown AM, Willingham MC (2002) Improved detection of apoptotic cells in archival paraffin sections: immunohistochemistry using antibodies to cleaved caspase 3. J Histochem Cytochem 50: 449–454

Green DR, Kroemer G (2004) The pathophysiology of mitochondrial cell death. Science 305:626–629

Holubec H, Payne CM, Bernstein H, Dvorakova K, Bernstein C, Waltmire CN, Warneke JA, et al. (2005) Assessment of apoptosis by immunohistochemical markers compared to cellular morphology in ex vivo-stressed colonic mucosa. J Histochem Cytochem 53:229–235

Jakob S, Corazza N, Diamantis E, Kappeler A, Brunner T (2008) Detection of apoptosis in vivo using antibodies against caspase-induced neo-epitopes. Methods 44:255–261

Jin Z, El-Deiry WS (2005) Overview of cell death signaling pathways. Cancer Biol Ther 4:139–163

Kamada S, Kikkawa U, Tsujimoto Y, Hunter T (2005) Nuclear translocation of caspase-3 is dependent on its proteolytic activation and recognition of a substrate-like protein(s). J Biol Chem 280: 857–860

Koh DW, Dawson TM, Dawson VL (2005) Mediation of cell death by poly(ADP-ribose) polymerase-1. Pharmacol Res 52:5–14

Kottke TJ, Blajeski AL, Meng XW, Svingen PA, Ruchaud S, Mesner PW Jr, Boerner SA, et al. (2002) Lack of correlation between caspase activation and caspase activity assays in paclitaxel-treated MCF-7 breast cancer cells. J Biol Chem 277:804–815

Lakhani SA, Masud A, Kuida K, Porter GA Jr, Booth CJ, Mehal WZ, Inayat I, et al. (2006) Caspases 3 and 7: key mediators of mitochondrial events of apoptosis. Science 311:847–851

Marchal S, Fadloun A, Maugain E, D'Hallewin MA, Guillemin F, Bezdetnaya L (2005) Necrotic and apoptotic features of cell death in response to Foscan photosensitization of HT29 monolayer and multicell spheroids. Biochem Pharmacol 69:1167–1176

Marchal S, Francois A, Dumas D, Guillemin F, Bezdetnaya L (2007) Relationship between subcellular localisation of Foscan and caspase activation in photosensitised MCF-7 cells. Br J Cancer 96:944–951

McGrogan BT, Gilmartin B, Carney DN, McCann A (2008) Taxanes, microtubules and chemoresistant breast cancer. Biochim Biophys Acta 1785:96–132

Miller JD, Baron ED, Scull H, Hsia A, Berlin JC, McCormick T, Colussi V, et al. (2007) Photodynamic therapy with the phthalocyanine photosensitizer Pc 4: the case experience with preclinical mechanistic and early clinical-translational studies. Toxicol Appl Pharmacol 224:290–299

Mooney LM, Al-Sakkaf KA, Brown BL, Dobson PR (2002) Apoptotic mechanisms in T47D and MCF-7 human breast cancer cells. Br J Cancer 87:909–917

Mortusewicz O, Ame JC, Schreiber V, Leonhardt H (2007) Feedback-regulated poly(ADP-ribosyl)ation by PARP-1 is required for rapid

response to DNA damage in living cells. Nucleic Acids Res 35: 7665–7675

Puig B, Tortosa A, Ferrer I (2001) Cleaved caspase-3, caspase-7 and poly (ADP-ribose) polymerase are complementarily but differentially expressed in human medulloblastomas. Neurosci Lett 306:85–88

Pyrko P, Schonthal AH, Hofman FM, Chen TC, Lee AS (2007) The unfolded protein response regulator GRP78/BiP as a novel target for increasing chemosensitivity in malignant gliomas. Cancer Res 67:9809–9816

Rao RV, Ellerby HM, Bredesen DE (2004) Coupling endoplasmic reticulum stress to the cell death program. Cell Death Differ 11: 372–380

Reddy RK, Mao C, Baumeister P, Austin RC, Kaufman RJ, Lee AS (2003) Endoplasmic reticulum chaperone protein GRP78 protects cells from apoptosis induced by topoisomerase inhibitors: role of ATP binding site in suppression of caspase-7 activation. J Biol Chem 278:20915–20924

Resendes AR, Majo N, Segales J, Espadamala J, Mateu E, Chianini F, Nofrarias M, et al. (2004) Apoptosis in normal lymphoid organs from healthy normal, conventional pigs at different ages detected by TUNEL and cleaved caspase-3 immunohistochemistry in paraffin-embedded tissues. Vet Immunol Immunopathol 99: 203–213

Simbulan-Rosenthal CM, Rosenthal DS, Iyer S, Boulares H, Smulson ME (1999) Involvement of PARP and poly(ADP-ribosyl)ation in the early stages of apoptosis and DNA replication. Mol Cell Biochem 193:137–148

Slee EA, Adrain C, Martin SJ (2001) Executioner caspase-3, -6, and -7 perform distinct, non-redundant roles during the demolition phase of apoptosis. J Biol Chem 276:7320–7326

The Journal of Histochemistry & Cytochemistry

1.3 Animal models for photodiagnosis and photodynamic therapy

Marie-Ange D'Hallewin, **Julie Garrier**, Marion Helle, Lina Bezdetnaya et François Guillemin

Photothéranostique, Israël Journal of Chemistry, (soumise sur invitation).

ANIMAL MODELS FOR PHOTODIAGNOSIS AND PHOTODYNAMIC THERAPY

MA. D'Hallewin, J. Garrier, M. Helle, L. Bezdetnaya, F. Guillemin

Centre de Recherche en Automatique de Nancy (CRAN-UMR 7039), Nancy-University, CNRS, Centre Alexis Vautrin, Vandœuvre-lès-Nancy, France.

ABSTRACT

A prerequisite for starting a clinical trial is evidence of a positive impact of the technique or drug used in animals. The choice of the animal models is thus very important and should mimic as closely as possible the human situation. A variety of animal models has been validated for pharmaceutical trials. The situation in phototheranostics however is not fully clear. This is due to the very complex interplay of various elements such as vascularisation, oxygenation, drug availability and biodistributrion, light absorption and scattering etc. The present paper will give general information on aspects of animal models that have to be considered in phototheranostics as well as highlight some typical animal models that are useful for the investigation of light tissue interactions.

INTRODUCTION

Photo-theranostics imply the diagnosis and subsequent treatment of a disease, with the help of a single molecule that acts both as a fluorophore for diagnostic purposes and a photosensitizer for eradication of the lesion. Animal models to test those molecules and /or devices for optical diagnosis and/or light delivery should thus mimic as closely as possible the human situation. Originally, drug screening was performed on animals with peritoneal tumors induced by intraperitoneal injection of leukaemia cells [1]. Since 1976 a broad panel of various other tumor cell lines, including solid human tumors representative of the major types of cancer are being tested in rodents, following subcutaneous, intraperitoneal or intravenous administration [2]. Actually, most drugs are developed towards specific molecular targets. Likewise, animal models are developed in order to express those targets through genetical engineering.

PDT being a radiation therapy, animal models require different selection criteria and commonly used models are inappropriate. The unique interaction between photosensitizer incorporated in cells, light and molecular oxygen necessitates a model that is comparable to the human situation in terms of vascularisation and blood flow, scattering and absorption coefficient of the tissue as well as its depth. Different questions arise when considering an appropriate animal model such as which cell line, immucompetent animal or not, implantation site for example. The choice of the model will depend on the scientific question to be answered.

Spontaneous tumors are extremely rare but tumors can be generated by administration of carcinogens. This is an extremely time consuming procedure, with a rather low reproducibility rate, which also can induce exposure risks to the persons handling the animals. This method is however recommended for testing of optical diagnostic techniques since all steps in carcinogenesis can be evaluated. Optical techniques have thus been assessed for UV or chemically induced skin diseases [3-4] as well as oral cancer using the hamster check pouch model [5]. The latter will be discussed in more details below.

One of the first reports studying subcutaneous tumors dates from 1953 [6]. Hewitt injected subcutaneously ascitis forming sarcoma cells. He found that adult mice were more resistant to tumor growth but that this could be overcome by enhancing the number of inoculated cells. This technique is very ease and reproducible without need for anaesthesia of the animal and allows for visual assessment of tumor growth as well as response. However, tumor take rates as well as response to drugs can vary largely according to the site of

implantation [7-10]. Tumor host environment is thus very important and also affects PDT efficacy. Indeed, Chan *et al.* showed that certain phtalocyanine derivatives that were the most active in vitro failed to have any tumor reductive effect on subcutaneous tumors [11]. In another experiments Gibson et al. demonstrated that human mesothelioma cells and rat mammary carcinoma had an inversed sensitivity to PDT, at an equal photosensitizer uptake, when investigated in vitro or in subcutaneous implants [12]. This can probably be attributed to the differences in vascularisation according to the host environment. Indeed, Chen *et al*. showed that orthotopic prostate tumors were had a higher vessel density, with more permeative vessels and less hypoxic as opposed to subcutaneous tumor nodules [13]. Accordingly, photosensitizer concentration was higher in prostatic locations at short intervals post administration whereas at longer intervals, PDT efficacy was the highest due to the better oxygenation [13]. Orthotopic models are also essential when dealing with optical diagnoses with regard to optical characteristics of the tissue. Optical characteristics of human an canine tissue are fairly identical, which is probably also true for rodents [14]. Differences will reside in the density of hair follicles, pigmentation thickness of different tissue layers, amount of subcutaneous fat for example. Drawbacks for orthotopic implantation are amongst others, the fact that they frequently necessitate some surgical skills, anaesthesia and potential postoperative mortality.

Another important aspect is the choice of cell line. Most pharmacological studies are performed in nude animals presenting tumors from human origin. With regard to the impact of immune reactions in PDT, syngeneic strains in immunocompetent animals are probably to be preferred [15]. Tumors can either be induced by injection of cells, or implantation of solid tumor lumps. Cells produce higher tumor take rates whereas biopsies have a more invasive and metastatic potential and frequently include central necrotic areas [16-18]. When comparing large studies, it appears that using primary tumors more closely reflects clinical response as compared to injection of cell lines [19-20]. Tumor take rates can be enhanced when first growing them subcutaneously and/or some passages in monolayer cultures [9]. In order to grow epithelial tumors, the environment must first be prepared by a chemical action in order to accept tumor implantation and subsequent tumor growth [9, 21].

The most commonly studied animals or rats and mice. The choice however will depend on the study object, for instance when biodistribution of photosensitizers in rodents cannot be directly correlated to humans. Indeed, it was shown that mTHPC remains constant in human plasma for at least 12 hours, whereas mice plasma has lost almost all mTHPC 6 hours after i.v. delivery of Foscan® [22]. Biodistribution in Syrian hamsters is comparable to

humans, albeit with a reduced fluorescence [23]. When wound healing is to be considered, pig skin is a better choice than rodents. Indeed, matrix remodelling and elastin neosynthesis, the final stages in wound healing, are finalized after several months in humans, starting after 6 weeks in pigs but can be observed as early as 1 week in mice [24-26]. The study of adverse events that occur in clinical practice also will influence the choice of animal type. When considering oesophageal strictures, PDT should not be performed in rodents since the light dose required to induce submucosal damage will already have provoked lethal pulmonary changes and only pigs will develop oesophageal fibrosis at high fluences [27].

The choice of animal model, with regard to the very complex interactions observed in photo-diagnostics and photodynamic therapy, is thus essential and can dramatically influence obtained results. The primary consideration when choosing the correct model is the ultimate aim of the study and the scientific question with a perfect background of all parameters involved in light tissue interactions. In this paper we wanted to highlight some animal models, including non-cancerous models, which can be of interest in photo-therasnostics.

OSTEOARTHRITIS

Rheumatoid arthritis (RA) is a systemic chronic inflammatory disease characterized by symmetrical polyarticular synovitis and ensuing cartilage erosion resulting in bone destruction in the final stages. As today, treatment is mostly palliative consisting in analgesics and anti-inflammatory drugs. Surgical synovectomy is an open arthroscopic approach while radiation synovectomy consists in intra-articular application of radioactive agents with associated potential radiation hazards. The presence of severe bone destruction will require replacement surgery. Recently, renewed interest has arisen concerning potential benefits of photodynamic treatment of inflamed synovial tissue [28-29]. Different sensitizers have shown a pronounced accumulation in this tissue type [29-32].

Determining the right animal model to evaluate PDT effect will depend on the aims of the study. Intra-articular light delivery necessitates larger animals such as hares or rabbits whereas transdermal illumination can be performed in rats or mice. Synovitis can be induced in a single joint by intra-articular inoculation of pro-inflammatory drugs, whereas systemic administration of RA promoting factors will initialize polyarticular arthritis. The latter offers the advantage that multiple irradiation settings can be tested on a single rodent. Various drugs can be used for joint injection such as collagenese [33], destructive murine fibroblast comparable to synovial fibroblasts present in RA [28], methylated bovine serum or ovalbumine

following systemic immunisation [29-30]. Polyarthritis can be obtained by a single intradermal or subcutaneous administration of either collagen II or pristine in rats [34]. Different joints will be affected according to the inductor agents and 80 to 100 % of the rats will develop RA.

The rats are anaesthetized by isoflurane inhalation and extension of the hind paw reveals a whitish appearance of the patellar tendon. Intra-articular injection is performed through the latter. Irrespective of the inductor, symptoms are most acute after 1 week and thereafter progressively decrease. Polyarthritis symptoms are maximal at 2 to 3 weeks and remain stable for at least 2 weeks. The development of the disease can be visually assessed with the apparition of swelling and redness. Joint swelling can be measured with a calliper and a redness system scoring also can be used to evaluate arthritis grade. More generalized oedema is evaluated by measuring the displaced volume after insertion of the paw into a tube containing a water solution, the opposite paw taken as a control. Blood analysis will show appearance of rheumatoid factors such as specific antibodies to cyclic citrullinated proteins, acute phase serum amyloid or the presence of nitric oxide. Histological assessment evaluates hyperplasia of cells, hypertrophy of the synovial layer and the density of inflammatory infiltrate

BLADDER CANCER

Although the incidence of bladder cancer is relatively low, the prevalence is rather high due to the very high recurrence rates of non-muscle invasive cancer [35]. Furthermore the presence of carcinoma in situ (CIS) that cannot be detected by conventional methods has been shown to be an important risk factor for disease progression because specific survival is heavily affected by the presence of CIS [36]. Early detection of such lesions is thus mandatory to reduce mortality rates. Fluorescence guided cystoscopy has been shown to increase detection rate, as well as decrease progression and recurrence in humans [37]. Nevertheless, the high number of false positive fluorescence as well as the fast photobleaching observed remain troublesome. Hence the need for the development other more specific fluorophores is highly timely.

Spontaneous bladders tumors are rare in rodents but can be induced by addition of various agents in drinking water or food. Although these models are useful when studying chemoprevention, the process of tumor induction takes more than 8 months. Heterotopic implants cannot be used for the evaluation of intravesical treatments or diagnostic techniques

based on optical characterization, with regard to the differences in absorption and diffusion properties of the bladder wall as compared to skin and muscle. An ideal orthotopic model should be easy to perform with a high reproducibility. Animals must be immunocompetent and tumors must be of urothelial origin and staging should be controlled. When endoscopic procedures have to be applied, female rats are to be preferred over male animals and mice with regard to diameter and anatomy of the urethra.

Tumors are induced by intravesical administration of urinary bladder cancer cells, from human or rodent origin, generated spontaneously or through chemo-induction [38-39]. The cell lines used have been selected to ensure rapid *in vitro* growth, efficient tumor growth when implanted subcutaneously and stable characteristics, potential metastatic behaviour and expression of specific molecular markers [38, 40]. However, those cell lines are composed of a unique cell type, which does not necessarily reflect pathological conditions observed in humans. This may in turn affect therapeutic outcome but interferes less with diagnostic approaches.

Tumor cell adhesion and subsequent growth necessitate damage to the epithelial layers. Removal of the protective glycosaminoglycan layer can be obtained by intravesical instillation of trypsin or poly-L-lysene, which ensures about 80% tumor take rates [41]. Removal of umbrella and intermediate cells with remaining basal cells does not prevent adhesion and results in 100 % tumor take rates [21]. Contact time with the damaging agent is crucial, since excessive damage will provoke important inflammatory reactions or even bladder perforation with ensuing animal death. [21, 42]. Mechanical damage such as electrocautery or mechanical abrasion of the dome requires more technical skills with a high risk or perforation [43-44]. Furthermore, tumors are frequently more invasive, or at least covered by normal urothelium, which will alter both therapeutic and diagnostic results [21, 45]. The amount of instilled cells must be sufficient and a minimum of 10^4 to 10^5 cells is to be administered for good tumor take rates [41, 46]. Lengthening the contact time with cells also promotes tumor growth. One hour seems to be an appropriate time period. Prolonging this will cause an increasing urinary volume with either leakage, thus loss of cells, or reflux and apparition of upper urinary tract lesions [47-48].

Tumor stages have to be controlled when assessing therapeutic effect. This is difficult to achieve in models with multifocal lesions following acid induction and instillation with syngeneic bladder cancer cells [49]. After localized desepithelialization, a single tumor will develop at the injury site with a predictable evolution in stage [21. Carcinoma in situ present at

day 3 will become invasive after one week in all rats. Instillation of human bladder cancer cells (BIU 87) in immunodefficient mice develops slower with superficial lesions at day 7 and progressive invasion at 2 weeks [50] . The number of cells passages will also influence tumor stage with increasing amount of invasive lesions after increasing in vitro and/or in vivo passages [21, 51-52].

Rats are anaesthetized with an intraparietal injection of sodium pentobarbital, 45 mg/kg, which ensures a deep anaesthesia for 3 hours. They are placed in a supine position and catheterized with a guide wire. A 14 G canula, previously lubricated, is then introduced over the guide wire. The shape of the catheter top must be slightly conical to dilate the urethra without provoking any damage. The bladder is then emptied by gentle abdominal pressure. The de-epithelializing agent is then instilled for an appropriate time before emptying the bladder and several rinses with PBS. Maximal bladder content is about 0.5 ml and the bladder volume can be assessed abdominal palpation. Cells are then instilled and the catheter is clamped for 1 hour before removal. Tumors can be detected as early as three days post induction with random growth of tumors at different stages as shown in figure 1, ten days after instillation of tumor cells.

HAMSTER CHEEK POUCH MODEL

Oral cancer is the sixth most common cancer worldwide with an annual estimated incidence of 275.000 [53]. Main established risk factors are smoking, tobacco or betel nut chewing, alcohol and radiation. Despite huge efforts to improve therapeutic outcome, survival rates have not improved over the last decade with a 5-year survival rate inferior to 60%. This is mainly due to local recurrences, metastases and second primary cancers in the upper aero-digestive tract [54]. Survival is closely associated to tumor stage as for example cancer of the tongue with survival rates up to 80% at early stages dropping to 10% for late stage disease. Early diagnosis is thus mandatory in order to reduce morbidity and mortality rates of oral cancer. Nevertheless, despite increased public education, the proportion of patients presenting with advanced disease has not changed over the last forty years [55]. Detections is a real challenge since a 1 mm^3 nodule, which is barely detectable with the naked eye, already contains 10^6 cells [56]. Different optical techniques have been developed over the last decades in order to enhance sensitivity and specificity of cancer diagnosis. Before being validated for clinical use, these techniques have to be extensively tested in animals. It is thus very important that they mimic as closely as possible human carcinogenesis.

The Syrian golden hamster cheek pouch model is presently the animal model that most accurately represents the cellular and molecular changes that occur with the initiation and progression in human oral cancer [57]. Salley originally described this model in 1954, with the aim to produce an orthotopic epithelial cancer [58]. The cheek pouch can be inverted, with a very thin overlying skin and is thus easy to observe with transillumination while the animal is immobilized in a special device [59] (Johansen). Carcinogenesis is induced by the application of hydrocarbons dissolved in acetone or benzene. A paintbrush is dripped in the solution and applied to the pouch. The best results were obtained with 9,10-dimethyl-1,2-benzanhtracene (DMBA) in an acetone solution. One can observe different modifications going from hyperplasia over benign papilloma, dysplasia, carcinoma in situ to invasive carcinoma. In order to standardize the procedure, Morris further investigated the impact of the age of the animal, concentration of the drug and duration of the application [60]. Younger animals are more susceptive to tumor induction than older ones and 5 weeks seems to be an ideal age. High concentrations are too toxic whereas very low concentrations fail to produce tumor growth, with 0.5 % a good tumor inducer. Three weekly applications were more efficient than two. Morris also developed a new application technique, since the drip brush initially mentioned showed signs of leakage from the carcinogen in the mouth and on the paws, with secondary tumor induction and higher toxicity to the animals. By first wiping the brush to the container, the amount of leakage is minimalized and induction is restricted to the pouch. This model is conventionally used for prevention, diagnosis, and treatment studies. Since this model is very labour intensive, thrice-weekly DMBA application for approximately 16 weeks, and exposes the investigator to carcinogens during this time period, a variant of this model has been described based on sustained release of DMBA [61]. Cotton sutures are impregnated with DMBA and fixed in the submucosa of the deepest portion of the pouch. Release of DMBA is 95 % completed at 15 months and tumor take rates are 90 % at 20 weeks as opposed to 100% with the “traditional” method. This technique requires inhalation anaesthesia and some surgical skills. The handling of the animal during carcinogenesis period however is reduced by a factor 10. Since those surgical sutures are not commercialized, this model has only been described by Vancouver research groups, with devoted chemists to produce the specific surgical thread [61-62].

DMBA induced epithelial oral cancer reflects many aspects of human cancer development such as gene expression, immune derived cytokines, epidermal growth factor and the development of neovascularisation [63]. However, the pouch mucosa is much thinner than the rest of the oral mucosa, as well as human mucosa, and has a single submucosal

connective tissue [64]. This will influence light distribution, which in turn might hamper correlation of optical diagnostic findings between hamsters and humans. The hamster cheek pouch model remains however the gold standard for optical diagnosis of cancer at various stages in carcinogenesis. Steady state or time resolved spectroscopy, autofluorescence, or exogenous fluorescence, life-time imaging or optical coherence tomography are amongst the many techniques that have been studied [62, 65-69].

AGE RELATED MACULAR DEGENERATION

Age related macular degeneration (AMD) is the main cause of blindness in the elderly. The first clinical markers are the accumulation of lipofucsin in the retinal pigment epithelium, and deposits of lipids, so-called drusen, between the retinal pigment epithelium and the basement membrane and within Bruch's membrane. Oxidation of those lipids damages the lysosomal membranes and leakage of hydrolytic enzymes will results in cell damage to the retina and so called "dry" AMD [70]. No medical or surgical treatment is available for this condition, however vitamin supplements with high doses of antioxidants have been suggested, or immune system regulators to suppress oxydative stress and immune activation pathways . This form can be induced in rats by exposition to blue or white light in rodents [71-72]. In a further stage, disruption of Bruch's membrane will result in inflammation, that will provoke choroidal neovascularization (CNV) or so-called "wet" AMD [73]. Neovessels formation will induce leakage of blood and proteins below the macula, with ensueing inflammatory reaction and ultimately irreversible fibrosis. There are thus three major systems involved with the formation and progression of CNV: inflammation, proteolysis, and angiogenesis.

Three categories of animal models can be discerned; laser induced, surgically induced and genetically engineered. All models have their advantages and disadvantages and should be chosen in function of the study object. Small animal models (mice and rat) are indicated for *ex vivo* studies, whereas for *in vivo* observations and longitudinal studies, larger animals such as rabbits, pigs or monkeys are more suitable. In general, disruption of Bruch's membrane is essential for CNV development. This can be achieved by laser photocoagulation. The original model was developed in monkeys and later in rats [74-75]. Many different laser types and illumination settings have been proposed using argon, krypton or diode lasers, emitting in the red, green or blue spectral regions [76]. Spot sizes vary from 50 to 500µ, laser output from 10 to 400 mW, during 0.05 to 0.1 seconds. Onset of vascular leakage occurs within 1 to 3 weeks following injury. Other surgical techniques can be

proposed, mostly based on injection of VEGF or VEGF inducing substances for specific research areas mostly related to molecular pathways in CNV genesis and progression [76].

CHICK CHORIOALLANTOIC MEMBRANE

The chick chorioallantoic membrane (CAM) assay is a commonly used method for studying angiogenic activities or drug delivery *in vivo* [77-78]. It is a vascular membrane found in eggs of birds and reptiles. The first tumor transplantation to the CAM was described a century ago but CAM tumor models remain sparse and poorly characterized as compared to murine models [79-80].

The first day of incubation is considered the first day of embryonic development, (embryo development day or EDD) [78]. Three extra-embryonic membranes are protecting and nourishing the embryo during his development: the yolk sac membrane, the amnion and the CAM. The latter is a transparent and highly vascularized membrane formed during EDD 4 to 5 by the fusion of the mesodermal layers of both the allantois and the chorion. This results in a highly vascularized mesodermal structure in which arteries, veins and an intricate capillary plexus will proliferate until EDD 11 [81]. It is connected to the embryonic circulation by the allantoic arteries and veins, which are associated with lymphatic vessels [82]. The CAM acts as a respiratory organ until hatching, for the storage of excretions, electrolytes transport (sodium and chloride) from the allantoic sac and mobilization of calcium from the shell to start bone mineralization [83]. Several features of the CAM change during embryonic development such as the composition of the extracellular matrix, the degree of differentiation of both endothelial cells and vessels, the characteristics of the inter-endothelial junctions as well as the location of the vessels within the CAM [82]. It is thus crucial to use embryos at the same EDD. The CAM assay is characterized by several major advantages such as the ease of access, the extensive vascularization, the relatively simple experimental approach and the natural immunodeficient environment, thus enabling the use of human antibodies. It is a perfect model for photonics approaches since it is a very thin (< 100µ) and transparent membrane.

The CAM has been used as a host to study tumor cell intravasation and dissemination and formation of spontaneous metastasis [84]. After superficial inoculation, cells will penetrate the vasculature and develop metastatic locations in the embryo. The choice of the cell type however is important since cell lines derived from tumors with a low metastatic potential

exhibit the same behavior in the CAM and no not show any signs of invasive growth [85]. Moreover, cells have to grow very fast since there remains only 5 to 9 days between tumor inoculation and hatching. Experimental metastasis is achieved much faster by direct injection of tumor cells in the allantoic vein. Nevertheless, one has to choose cell lines with invasive characteristics, identical to the ones that allow tumor growth in the membrane [85].

Before opening, fertilized chicken eggs are washed with sterile water and transferred to a hatching incubator at 37.4°C and 80% of humidity equipped with an automatic rotator. At EDD 3, under laminar flow, 6-7 ml of albumin are removed with a sterile syringe connected to a 20-gauge needle through a hole drilled at the narrow apex. A round window is cut into the shell allowing embryo detachment from the eggshell. Embryo development is controlled and dead eggs or eggs with malformations are excluded. The window is then sealed with tape and static incubation is continued and controlled every 2 days until EDD10. On EDD10, a 1 cm inner diameter Teflon ring is placed on the CAM surface. Secondly, CAM ectodermic epithelium is superficially abraded with a scalpel in the center of the ring and 40 µl of an exponentially growing cells suspension is deposited. Cell concentration is different for each cell line and for some of them it appears necessary to add growth factors such as VEGF. A vascularized tumor is obtained at EDD14-15 and eggs need to be sacrificed at EDD17 before hatching. Figure 2 shows a typical image of a CAM implanted with EMT6 cells at different EDD's.

LYMPHATIC METASTASES

Breast cancer is the most frequently diagnosed cancer in women, and the second leading cause of death [86] (Morimoto 2009). Lymph node invasion is one of the first signs of tumor progression, due to the special features of lymphatic vessels, which allow for an easy traffic of interstitial fluids and immune cells for example [87]. Correct lymph node status evaluation is thus essential in order to offer patients the most appropriate treatment option. Current clinical techniques to localize first lymph node station or so-called sentinel lymph node, imply the use of radio labeled drugs. Their selectivity and specificity also depends on the degree of invasion of the node [88]. Innovative diagnostic techniques should thus be tested on breast cancer models with a spontaneous development of lymphatic metastases.

Subcutaneous implantation of human breast cancer cell lines in immunodificient rodents often fails to induce tumor progression, since mouse microenvironment differs and orthotopic implants are more appropriate [89]. Orthotopic implantation of cancer cells will

lead to the formation of primary tumors and subsequent invasion of lymphatic and/or blood vessels and growth of secondary tumors [90]. Syngeneic mouse models have been developed by rounds of transplantation / metastasis formation and selection [91]. Numerous strains show either the absence of local tumor growth, absence of metastases or dissemination, which is preferentially hematogenous or lymphatic.

As an example, 10^6 4T1 cells are injected in the first mammary fat pad of mice. After approximately 3 weeks tumors have reach the maximal ethical volume of 1000mm^3. Lymph node invasion is detected in 30 to 60% of the animals according to the technique used. Gold standard in cancer diagnosis remains of course pathology but detection of single cells in a lymph node remains problematical, resulting in a low degree of tumor detection of 30%. Reverse transcription polymerase chain reaction (RT-PCR) aims at the detection of cytokeratin 19, which is expressed by the tumor cells but not the native tissue, which enhances tumor detection by 20% [92]. Figure 3 shows a mice bearing an orthotopic breast cancer (not visible on this image) after subcutaneous administration of NIR quantum dots that migrate from the injection site to the first sentinel lymph node.

ORGAN METASTASES

One of the easiest organ metastasis models is the peritoneal carcinomatosis model. The original report for this model by Goldie et al. dates from 1951 [93]. They found that tumor cells inoculated in the peritoneal cavity were able to grow in the peritoneal fluid, with the same pattern as *in vitro*, and a growth rate proportional to the number of inoculated cells. Injection of peritoneal fluid of inoculated mice in other mice led to the development of peritoneal lesions, identical to the ones observed after injection of mashed tumor bearing organs or subcutaneous induced tumors [94]. This model is now widely used in oncologic research with either syngeneic cell strains in rats, or human cell lines in nude rodents [95-96]. Tumors are multifocal, non-encapsulated with a minimal amount of necrosis. According to the cell line used, usually 1 to 2 x 10^6 cells are injected intraperitoneally and peritoneal growth is observed after 1 to 3 weeks following inoculation. These tumors further invade adjacent organs, which can lead to retroperitoneal, supradiaphragmatic and abdominal wall locations [97]. This model is also capable of inducing distant metastases and has extensively been described compared to subcutaneous tumors in nude mice [97]. Tumor spread is both lymphatic, with massive invasion of mediastinal lymph nodes, and hematogenous with lung metastases.

Liver metastases are a common feature associated with colorectal cancer. The optical properties of this extremely highly vascularized organ necessitate an orthotopic model for theranostics approaches. When a solitary lesion is to be obtained, a subcapsular or intraparenchymal administration after laparotomy, of either a cell suspension or tumor fragments is reproducible with acceptable complication rates [98-99]. Creating metastases that are more closely related to the clinical context necessitates vascular migration of cells. Orthotopic implantation of cells can induce spontaneous metastases but the model has a low reproducibility [100]. Direct intrasplenic or intraportal injection have the highest reproducibility but necessitate certain surgical skills to reduce peri- operative mortality [101-102]. The choice of cell line seems to be very important since tumor growth will be more observed with aggressive cell types.

Bone metastases can be an interesting topic for optical diagnosis. Orthotopic syngeneic growing tumors in rodents seldom metastasize to the bone. Some selected combinations have been shown to produce skeletal localizations from breast or prostate origin [103-104]. Reports on human cell lines in immunodificient animals are more frequent and have been used in imaging studies [105-107].

CONCLUSION

Many animal models have been developed for drug screening including genetically modified animals, in order to be as closely as possible comparable to humans. When considering opto-theranostics, those models are inappropriate. Diagnostic applications first of all require identical optical characteristic of tissues between humans an animals. Orthotopic models are thus mandatory, taken into account the differences in tissue thickness for rodents. Ideally, tumors should be induced so that all changes observed during carcinogenesis in humans can be reproduced. A draw back for this animal model is the time needed to obtain tumor growth as well as a relative lack of reproducibility.

Rough screening of PDT effect can be performed in the simplest animal model that consists in the subcutaneous injection of tumor cells. When more specific questions are to be addressed, other models including the CAM model, must be critically assessed with regard to the parameters that are to be investigated.

REFERENCES

[1] P. Harrison. Perspective on the history of tumor models. In; Teicher BA editor. Tumor models in cancer research 2002, pp 3-19.
[2] J.M. Venditti, R.A Wesley, J. Plowman . *Adv Pharmacol Chemother*. 1984,*20*, 1-20.
[3] K.G. Phillips, R. Samatham, N. Choudhury, J.C. Gladish, P. Thuillier, S.L. Jacques..*J Biomed Opt.* 2010, *15*, 041514.
[4] M. Amouroux, G. Díaz-Ayil, W.C. Blondel, G. Bourg-Heckly, A. Leroux, F. Guillemin.*J Biomed Opt*. 2009,*14*,014011.
[5] J.A. Jo, B.E. Applegate, J. Park, S. Shrestha, P. Pande, I.B. Gimenez-Conti, J.L. Brandon. *IEEE Trans Biomed Eng.* 2010,*57*,2596-9..
[6] H.B. Hewitt . *Br J Cancer*. 1953,*7*,367-83
[7] R. Stephenson, C.P. Dinney, K. Gohji, N.G. Ordonez, J.J. Killion, I.J. Fidler. *Invest Urol* 1981, *19*, 20-3.
[8] B.A. Teicher. *Mol Cancer Ther*. 2006,*5,* 2435-43
[9] Y. Kang, M. Omura, A. Suzuki, T. Oka, Y. Nakagami, C. Cheng, Y. Nagashima, T. Inoue. *Cancer Sci*. 2006,*97*,996-1001.
[10] M.G. Donelli, R. Rosso, S. Garattini..*Int J Cancer*. 1967,*2*,421-4.
[11] W.S. Chan, C.M. West, J.V. Moore, I.R. Hart. *Br J Cancer*. 1991,*64*,827-32.
[12] S.L. Gibson, T.H. Foster, R.H. Feins, R.F. Raubertas , M.A. Fallon, R. Hilf *Br J Cancer*. 1994,*69*,473-81.
[13] B. Chen, B.W. Pogue, X. Zhou, J.A. O'Hara, N. Solban, E. Demidenko, P.J. Hoopes, T. Hasan. *Clin Cancer Res*. 2005,*11*,720-7.
[14] R. Splinter, W.F. Cheong, M.J. van Gemert, A.J. Welch. *Lasers Surg Med*. 1989,*9*,37-41.
[15] P. Mroz, A. Szokalska, M.X. Wu, M.R. Hamblin. *PLoS One*. 2010,5,e15194.
[16] B.C. Giovanella, S.O. Yim, J.S. Stehlin, L.J. Jr.Williams. *J Natl Cancer Inst*. 1972,*48*,1531-3.
[17] X. Wang, Z. An, J. Geller, R.M. Hoffman. *Prostate*. 1999,*39*,182-6.
[18] M. Pocard, H. Tsukui, R.J. Salmon, B. Dutrillaux, M.F. Poupon. *In Vivo*. 1996,*10*,463-9.
[19] J.I. Johnson, S. Decker, D. Zaharevitz, L.V. Rubinstein, J.M. Venditti, S. Schepartz, S. Kalyandrug, M. Christian, S. Arbuck, M. Hollingshead, E.A. Sausville. *Br J Cancer*. 2001,*84*,1424-31.
[20] C.C Scholz, D.P. Berger, B.R. Winterhalter, H. Henss, H.H. Fiebig. *Eur J Cancer*. 1990,*26*,901-5.
[21] S. El Khatib, S. Berrahmoune, A. Leroux, L. Bezdetnaya, F. Guillemin F, M.A. D'Hallewin. *Cancer Biol Ther* 2006, *5*, 1327-31
[22] M. Triesscheijn, M. Ruevekamp, R. Out, T.J. Van Berkel, J. Schellens, P. Baas, F.A. Stewart. *Cancer Chemother Pharmacol*. 2007,*60*,113-22.
[23] T. Glanzmann, M. Forrer, S.A. Blant, A. Woodtli, P. Grosjean, D. Braichotte, H. van den Bergh, P. Monnier, G. Wagnières. *J Photochem Photobiol B*. 2000,*57*,22-32.
[24] H.J. De Vries, J.E. Zeegelaar, E. Middelkoop, G. Gijsbers, J. Van Marle, C.H. Wildevuur, W. Westerhof. *Br J Dermatol* 1995, *132*, 690-697.
[25] H.J. De Vries, E. Middelkoop, J.R. Mekkes, R.P. Dutrieux, C.H. Wildevuur, H. Westerhof. *Wound Repair Regen* 1994, *2*, 37-47.
[26] D. Schwartz. *J Anat* 1977, *124*, 401-411.
[27] Y. Perry, M.W. Epperly, H.C. Fernando, E. Klein, S. Finkelstein, J.S. Greenberger, J.D. Luketich. *J Surg Res*. 2005,*123*,67-74.

[28] B. Funke , A. Jungel , S. Schastak , K. Wiedemeyer, F. Emmrich, U. Sack, *Lasers Surg Med*. 2006, *38*, 866-74.
[29] A. Hansch, O. Frey, M. Gajda, G. Susanna, J. Boettcher, R. Bräuer, W.A. Kaiser, *Lasers Surg Med.* 2008, *40*, 265-72.
[30] K. Trauner, R. Gandour-Edwards, M. Bamberg, N.S. Nishioka, T. Flotte, S. Autry, T. Hasan, *Lasers Surg Med*. 1998, *22*, 147-56.
[31] A.D. Beischer, P. Bhathal, R. de Steiger, D. Penn, S. Stylli, *ANZ J Surg*. 2002 , *72*, 517-22.
[32] D. Gabriel, N. Busso, ZA. So, H. van den Bergh, R. Gurny, N. Lange, *J Control Release*. 2009, *138*, 225-34.
[33] T. Kikuchi, T. Sakuta, T. Yamaguchi, *Osteoarthritis Cartilage*. 1998, *6*, 177-86.
[34] W. Hou, L. Meng, L. Tian, W. Zhu, C. Jiang, S. Lu, *Clin Exp Rheumatol*. 2010, *28*, 532-8.
[35] C. Murta-Nascimento, B.J. Schmitz-Dräger, M.P. Zeegers, G. Steineck, M. Kogevinas, F.X. Real, N. Malats, *World J Urol*. 2007, *25*, 285-95.
[36] I. Fukui, M. Yokokawa, H. Sekine, T. Yamada, K. Hosoda, D. Ishiwata, K. Oka, T. Sarada, T. Tohma, T. Yamada, *Cancer.* 1987, *59*, 164–73.
[37] Y. Shen, H.B. Grossman, A. Stenzl, M. Burger, Y. Fradet, L.A. Mynderse, M.S. Soloway, J.A. Witjes, M. Kriegmair, A. Karl. *J Urol*. 2010, *184*, 1907-13.
[38] S.M. Cohen, J.P. Jacobs, M. Arai, S. Fukushima, G.H. Friedell, *Invest Urol.* 1981, *19*, 136-41.
[39] R. Oyasu , *Food Chem Toxicol*. 1995, *33*, 747-55.
[40] C.J. Herman, P.D. Vegt ,F.M. Debruyne, G.P.Vooijs, F.C. Ramaekers, *Am J Pathol*. 1985, *120*, 419-26.
[41] E.S. Chan, A.R. Patel, A.K. Smith, J.B. Klein, A.A. Thomas, W.D. Heston, W.A. Larchian, *J Urol.* 2009, *182*, 2926-31.
[42] D.R. Siemens, J.C. Austin, W.A. See, J. Tartaglia, T.L. Ratliff, *J Urol*. 2001, *165*, 667-71.
[43]P. Sindhwani, J.A. Hampton, M.M. Baig, R. Keck, S.H. Selman, *J Urol.* 2001, *166*, 1498-501.
[44] P.E. Werthman, K.E. Drazan, J.T. Rosenthal, R. Khalili, A. Shaked, *J Urol*. 1996, *155*, 753-6.
[45] J.F. Bisson, R.M. Parache, P. Droulle, D. Notter, C. Vigneron, F. Guillemin, *Int J Cancer*. 2002, *102*, 280-5.
[46] S. Berrahmoune, L. Bezdetnaya, A. Leroux, F. Guillemin, M.A. D'Hallewin, *J Urol*. 2009, *181*, 1381-6.
[47] B.A. Hadaschik, P.C. Black, J.C. Sea, A.R. Metwalli, L. Fazli, C.P. Dinney, M.E. Gleave, A.I. So, *BJU Int*. 2007, *100*, 1377-84.
[48] T. Watanabe, N. Shinohara, A. Sazawa, T. Harabayashi, Y. Ogiso, T. Koyanagi, M. Takiguchi, A. Hashimoto, N. Kuzumaki, M. Yamashita, M. Tanaka, H.B. Grossman,W.F. Benedict, *Cancer Gene Ther*. 2000, *7*, 1575-80.
[49] Z. Xiao, T.J. McCallum, K.M. Brown, G.G. Miller, S.B. Halls, I. Parney, R.B. Moore, *Br J Cancer*. 1999, *81*, 638-46.
[50] L. Chong, Y. Ruping, B. Jiancheng, Y. Guohong, F. Yougang, W. Jiansong, G. Xiang, H. Jie, X. Shusheng, *Cancer Biol Ther*. 2006, *5*, 394-8.
[51] H.C. Arentsen, K. Hendricksen, E. Oosterwijk, J.A. Witjes, *World J Urol*. 2009, *27*, 313-7.
[52] K. Hendricksen, J. Molkenboer-Kuenen, E. Oosterwijk, C.A. Hulsbergen-van de Kaa, J.A. Witjes, *BJU Int*. 2008, *101*, 889-93.
[53] J. Ferley, P. Pisani, D.M. Parkin, IARC Cancer Base Lyon IARC Press 2004

[54] G.L. Day, W.J. Blot, *Cancer*. 1992, *70*, 14-9.
[55] S.E. Scott, E.A. Grunfeld, M. McGurk, *Community Dent Oral Epidemiol*. 2006, *34*, 337-43.
[56] S.Q. Lam, J. Hung, B. Palcic, *Trends Photochem Photobiol* 1991, *3*, 309-22.
[57] E. Vairaktaris, S. Spyridonidou, V. Papakosta, A. Vylliotis, A. Lazaris, D. Perrea, C. Yapijakis, E. Patsouris, *Oral Oncol*. 2008, *44*, 315-24..
[58] J.J. Salley, *J Dent Res* 1954, *33*, 253-62
[59] E. Johansen, *J Dent Res* 1952, *3*, 361-5.
[60] A.L. Morris, . *J Dent Res* 1961, *40*, 3-15.
[61] B. Heller, A.M. Kluftinger, N.L. Davis, N.F. Quenville, *Am J Surg*. 1996, *172*, 678-80.
[62] I. Pathak, N.L. Davis, Y.N. Hsiang, N.F. Quenville, B. Palcic B, *Am J Surg*. 1995,*170*, 423-6.
[63] S. Nagini, P.V. Letchoumy, T.A. Ramachandran, *Oral Oncol*. 2009, 45, 31-7.
[64] F. Walker, J. Carter, G.P. Crawford, H. Laird, A.M. Lessells, J.E. Pollet, *Br J Exp Pathol*. 1970, *51*, 379-84..
[65] D.G. Farwell, J.D. Meier, J. Park, Y. Sun, H. Coffman, B. Poirier, J. Phipps, S. Tinling, D.J. Enepekides, L. Marcu, *Arch Otolaryngol Head Neck Surg*. 2010, *136*, 126-33.
[66] Farwell, L. Marcu, *Opt Lett*. 2009, *34*, 2081-3.
[67] Y. Sun, J. Phipps, D.S. Elson, H. Stoy, S. Tinling, J. Meier, B. Poirier, F.S. Chuang, D.G.
[68] R.N. Graf, F.E. Robles, X. Chen, A. Wax, *J Biomed Opt*. 2009, *14*, 064030.-8
[69] M.C. Skala, K.M. Riching, A. Gendron-Fitzpatrick, J. Eickhoff, K.W. Eliceiri, J.G. White, N. Ramanujam, *Proc Natl Acad Sci* 2007, *104*, 19494-9.
[70] U.T. Brunk, A. Terman, *Free Radic Biol Med*. 2002, *33*, 611-9..
[71] A.R. Wielgus, R.J. Collier, E. Martin, F.B. Lih, K.B. Tomer, C.F. Chignell, J.E. Roberts, *Photochem Photobiol Sci*. 2010, *9*, 1505-12.
[72] T. Maeda, A. Maeda, M. Matosky, K. Okano, S. Roos, J. Tang, K. Palczewski, *Invest Ophthalmol Vis Sci.* 2009, *50*, 4917-25.
[73] M. Nozaki, B.J. Raisler, E. Sakurai, J.V. Sarma, S.R. Barnum, J.D. Lambris, Y. Chen, K. Zhang, B.K. Ambati, J.Z. Baffi, J. Ambati, *Proc Natl Acad Sci U S A*. 2006, *103*, 2328-33.
[74] S.J. Ryan, *Trans. Am Ophtaml Soc* 1979, *127*, 707-45.
[75] E.T. Dobi, C.A. Puliafito, M. Destro, *Arch Ophthalmol*. 1989, *107*, 264-9.
[76] H.E. Grossniklaus, S.J. Kang, L. Berglin, *Prog Retin Eye Res*. 2010, *29*, 500-19.
[77] M. Hagedorn, M. Balke, A. Schmidt, W. Bloch, H. Kurz, S. Javerzat, B. Rousseau, J. Wilting, A. Bikfalvi, *Dev Dyn* 2004, *230*, 23-33.
[78] A. Vargas, M. Zeisser-Labouebe, N. Lange, R. Gurny, F. Delie, *Adv Drug Deliv Rev* 2007, *59*, 1162-1176.
[79] J.B. Murphy, P. Rous, *J Exp Med* 1912, *15*, 119-132.
[80] E.I. Deryugina, J.P. Quigley, *Histochem Cell Biol* 2008, *130*, 1119-1130.
[81] D.O. DeFouw, V.J. Rizzo, R. Steinfeld, R.N. Feinberg, *Microvasc Res* 1989, *38*, 136-147.
[82] D. Ribatti, B. Nico, A. Vacca, L. Roncali, P.H. Burri, V. Djonov, *Anat Rec* 2001, *264*, 317-324.
[83] K. Kunzi-Rapp, P. Kaskel, R. Steiner, R.U. Peter, G. Krahn, *Pigment Cell Res* 2001, *14*, 9-13.
[84] E.I. Deryugina, E.M. Conn, A. Wortmann, J.J. Partridge, T.A. Kupriyanova, V.C. Ardi, J.D. Hooper, J.P. Quigley, *Mol Cancer Res*. 2009, *7*, 1197-211.
[85] M.C. Subauste, T.A. Kupriyanova, E.M. Conn, V.C. Ardi, J.P. Quigley, E.I. Deryugina. *Clin Exp Metastasis*. 2009,26,1033-47.

[86] T. Morimoto, T. Nagao, K. Okazaki, M. Kira, Y. Nakagawa, A. Tangoku, *Breast Cancer*. 2009, *16*, 2-9.
[87] J.P. Sleeman, W. Thiele, *Int J Cancer*. 2009, *125*, 2747-56
[88] T. Heuser, T. Rink, E. Weller, H. Fitz, H.H. Zippel, R. Kreienberg, T. Kühn, *Breast Cancer Res Treat.* 2001, *67*, 125-32.
[89] X. Fu, P. Le, R.M. Hoffman, *Anticancer Res.* 1993, *13*, 9001-4
[90] G.H. Heppner, F.R. Miller, P.M. Shekhar, *Breast Cancer Res*. 2000, *2*, 331-4.
[91] C.J. Aslakson, F.R. Miller, *Cancer Res*. 1992, *52*, 1399-405.
[92] G. Cserni, I. Amendoeira, N. Apostolikas, J.P. Bellocq, S. Bianchi, G. Bussolati, W. Boecker, B. Borisch, C.E. Connolly, T. Decker, P. Dervan, M. Drijkoningen, I.O. Ellis, C.W. Elston, V. Eusebi, D. Faverly, P. Heikkila, R. Holland, H. Kerner, J. Kulka, J. Jacquemier, M. Lacerda, J. Martinez-Penuela, C. De Miguel, J.L. Peterse, F. Rank, P. Regitnig, A. Reiner, A. Sapino, B. Sigal-Zafrani, A.M. Tanous, S. Thorstenson, E. Zozaya, C.A. *Eur J Cancer*. 2003, *39*, 1654-67.
[93] H. Goldie, M.D. Felix, *Cancer Res*. 1951, *11*, 73-80.
[94] H. Goldie,B.R. Jeffries, A.M Jones, M. Walker, *Cancer Res*. 1953, *13*, 566-72
[95] P. Collinet, F. Sabban, M. Cosson, M.O. Farine, R. Villet, D. Vinatier, S. Mordon, *Photochem Photobiol.* 2007, *83*, 647-51.
[96] N.J. Harlaar, J.W. Hesselink, J.S. de Jong, G.M. van Dam, *Eur Surg Res.* 2010, *45*, 308-13.
[97] A.P. Kyriazis, L. DiPersio, G. Michael, A.J. Pesce, J.D. Stinett, *Cancer Res* 1978, *38*; 3186-90.
[98] D. Lechaux, A. Gervais, L. Dazord, P.A. Eliat, F. Franconi, L. Lemaire, N. Rioux-Leclercq, V. Catros-Quemener, *Anticancer Res*. 2002, *22*, 151-8.
[99] F. Marchal, N. Tran, S. Marchal, A. Leroux, L. Bolotine, F. Guillemin, J.P. Villemot, *Oncol Rep* 2005, *14*, 1203-7.
[100] A. Thalheimer, C. Otto, M. Bueter, B. Illert, S. Gattenlohner, M. Gasser, M. Fein, C.T. Germer, A.M. Waaga-Gasser AM. *Eur Surg Res*. 2009,*42*,195-200.
[101] R. Lafreniere, S.A. Rosenberg, *J Natl Cancer Inst*. 1986, *76*, 309-22.
[102] G. Gambarota, A. Veltien, H. van Laarhoven, M. Philippens, A. Jonker, O.R. Mook,W.M. Frederiks, A. Heerschap, *MAGMA*. 2004, *17*, 281-7.
[103] M. Lelekakis, J.M. Moseley, T.J. Martin, D. Hards, E. Williams, P. Ho, D. Lowen, J. Javni, F.R. Miller, A. Slavin, R.L. Anderson, *Clin Exp Metastasis*. 1999, *17*, 163-70.
[104] M. Koutsilieris, *In Vivo*. 1992, *6*, 199-203.
[105] A. Wetterwald, G. van der Pluijm, I. Que, B. Sijmons, J. Buijs, M. Karperien, C.W. Löwik, E. Gautschi, G.N. Thalmann, M.G. Cecchini, *Am J Pathol*. 2002, *160*, 1143-53.
[106] M. Edinger, T.J. Sweeney, A.A. Tucker, A.B. Olomu, R.S. Negrin, C.H. Contag, *Neoplasia.* 1999, *1*, 303-10.
[107] M. Yang, E. Baranov, A.R. Moossa, S. Penman, R.M. Hoffman, *Proc Natl Acad Sci U S A*. 2000, *97*, 12278-82.

FIGURES

Figure 1

A Macroscopic view of a rat bladder, 10 days post intravesical administration of syngeneic AY27 cells showing multiple tumors at different stages.
B Set up for bladder PDT with trifurcated canula with a; guide wire, b; laser fiber, c;syringe for bladder filling

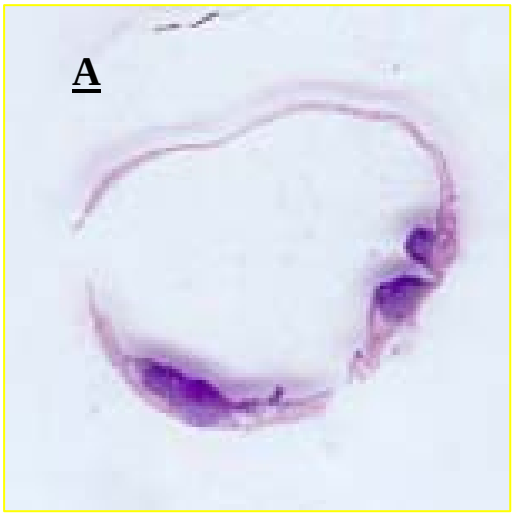

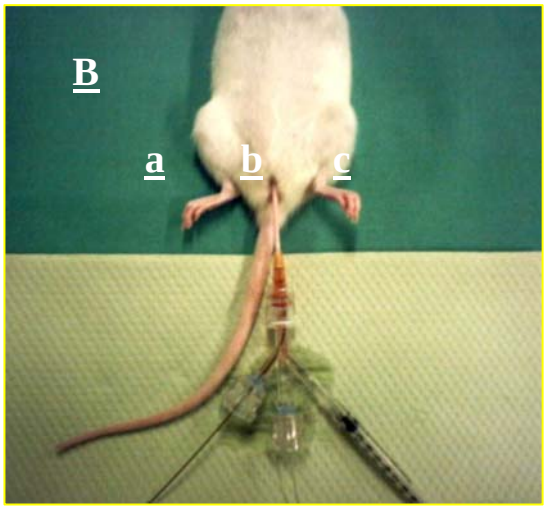

Figure 2

EDD 17 after a fixation with 4% paraformaldehyde.
High panel: Photographies of EMT6 tumours on CAM at low (A) and high (B) magnifications.
Lower panel: Hematoxylin-Eosin-Safran staining of EMT6 tumours at magnification 10x (C) or 40x (D, E, F).

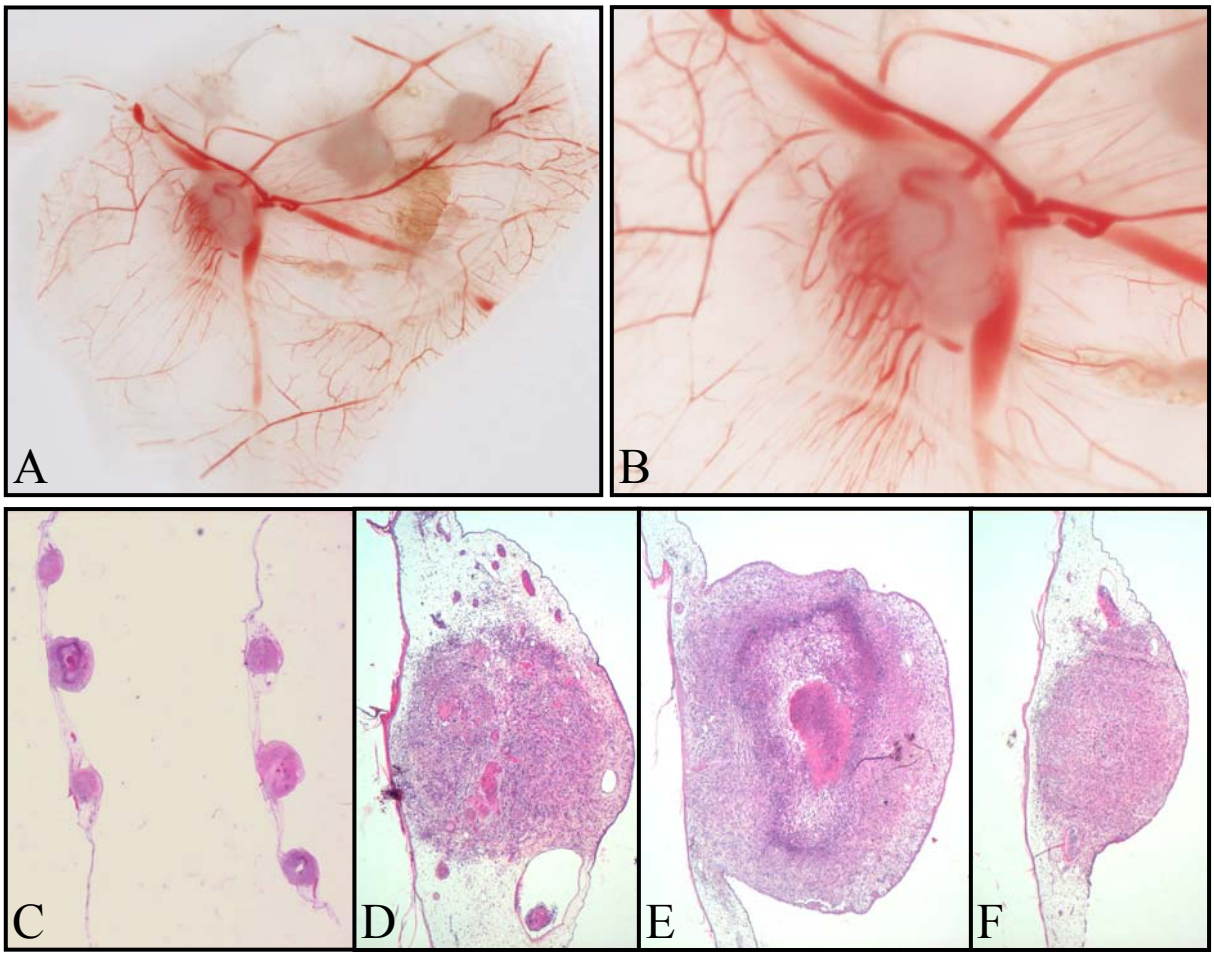

Figure 3

***In vivo* fluorescence imaging of the right flank of mice axillar lymph node 5 min after s.c. injection of 20 pmol of Quantum Dots.**
The imaging system used is a Fluobeam® (Fluoptics, Grenoble, France) with an excitation wavelength of 690 nm and a CCD camera with a 750-nm longpass emission filter, exposure time 10 ms.

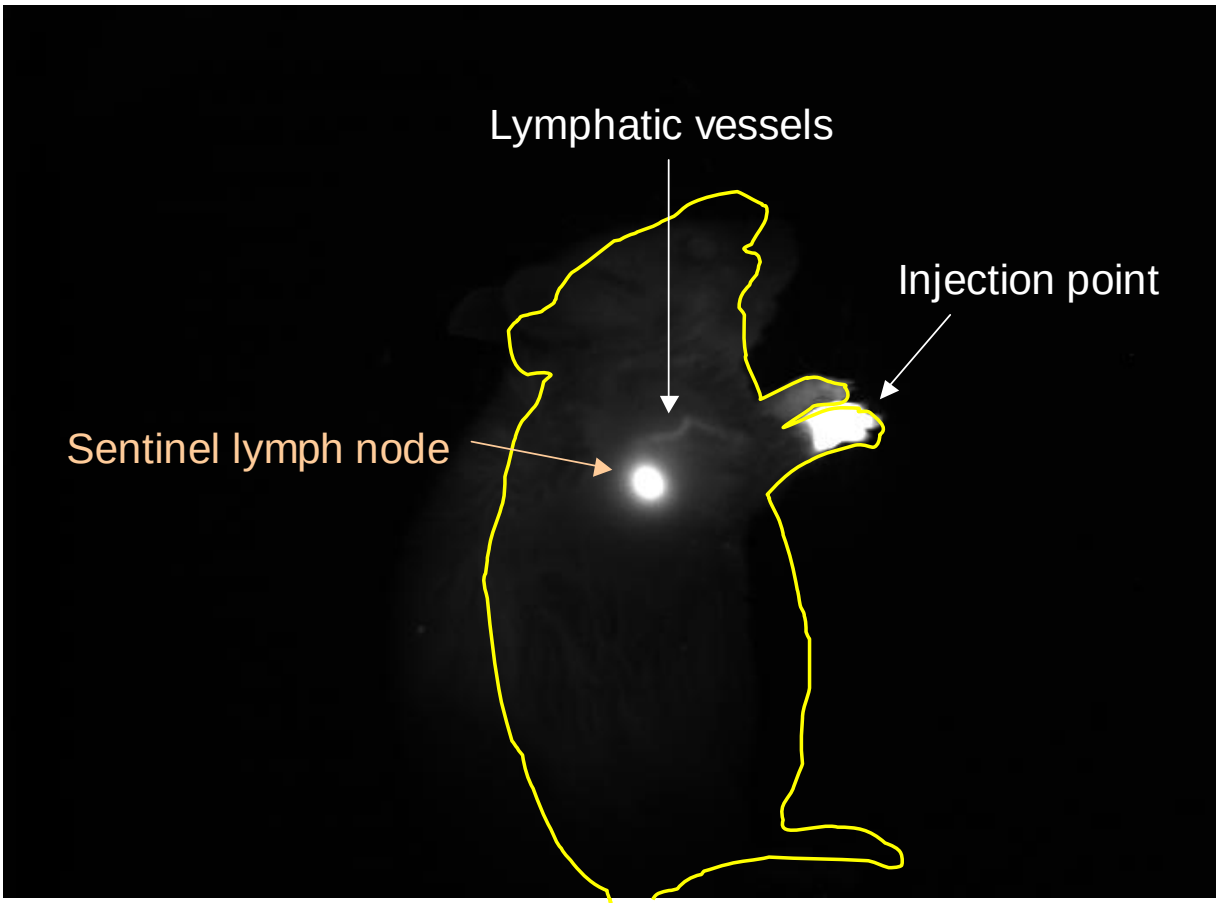

2. COMMUNICATIONS

2.1 Communications orales

5ème Forum du Cancéropôle du Grand Est.
2-3 novembre 2011, Strasbourg, France.
« Effet tumoricide photoinduit par le ciblage cellulaire et vasculaire de tumeurs ».
J. Garrier, A. Bressenot, S. Gräfe, S. Marchal, S. Mitra, TH. Foster, F. Guillemin, L. Bezdetnaya.
Prix du Jeune Chercheur récompensant la meilleure communication orale.

14ème Congrès de la Société Européenne de Photobiologie (ESP).
1er-6 septembre 2011, Genève, Suisse.
« Vascular damage photoinduced by liposomal formulations of mTHPC: influence of drug release ».
J. Garrier, V.Reshetov , C. Ruch, V.Zorin, F. Guillemin, L. Bezdetnaya.

Section spéciale: programme du 13ème Congrès Mondial IPA - International Photodynamic Association en association avec EPPM & HNODS.
« mTHPC-based biodegradable nanoparticles for cancer treatment ».
L. Bezdetnaya, H.P. Lassalle, **J. Garrier**, M.A. D'Hallewin, S. Marchal, F. Guillemin.
Photodiagnostic and Photodynamic therapy, 2011;8(2):73-230.

Participation à la réalisation d'un documentaire télévisé (France 3 région) portant sur les nanotechnologies, diffusé en février 2011 (Emission « C'est à savoir »)

6ème Journée Claude Huriet de la Recherche Biomédicale.
17 décembre 2010, Nancy, France.
« Effet tumoricide photoinduit par le ciblage cellulaire et vasculaire de tumeurs».
J. Garrier, A. Bressenot, S. Gräfe, S. Marchal, S. Mitra, TH. Foster, F. Guillemin, L. Bezdetnaya.
Prix Bernard Fortier pour la meilleure communication orale en recherche expérimentale.

3ème Congrès des Sociétés Franco-italienne de Photobiologie (SFPb)
25-26 Octobre 2010, Paris, France.
« Spatio-temporal redistribution of mTHPC from lipid nanovesicles in chick chorioallantoic membrane model ».
J. Garrier, V. Reshetov, D. Dumas, V. Zorin, A. François, MA. D'Hallewin, F. Guillemin, L. Bezdetnaya.

13ème Congrès de la Société Européenne de Photobiologie (ESP).
5-10 septembre 2009, Wroclaw, Pologne.
« Compartmental targeting for Foscan® based photodynamic treatment *in vivo*: correlation between efficiency, pharmacokinetics and regional distribution of apoptosis ».
J. Garrier, A. Bressenot , S. Gräfe, S. Marchal, F. Plénat, F. Guillemin, L. Bezdetnaya.

1er Congrès GDR 3049 PHOTOMED Médicaments Photoactivables-Photochimiothérapie.
29 mai 2008, Centre Alexis Vautrin, Nancy, France.
« Le dommage sélectif apoptotique des vaisseaux et du parenchyme de la tumeur après PDT induit par la m-THPC ». **J. Garrier**

12ème Congrès de l'European Society for Photobiology (ESP).
1er au 6 septembre 2007, Bath, Royaume-Uni.
« Intracellular and intratissular distribution of Foscan® modulates apoptosis induced by photodynamic therapy ».
S. Marchal, A. François, **J. Garrier**, A. Bressenot, F. Guillemin, L. Bezdetnaya.

2.2 Communications par affichage

3ème Congrès des Sociétés Franco-italienne de Photobiologie (SFPb).
25-26 Octobre 2010, Paris, France.
« Spatio-temporal redistribution of mTHPC from lipid nanovesicles in chick chorioallantoic membrane model».
J. Garrier, V. Reshetov, D. Dumas, V. Zorin, A. François, MA. D'Hallewin, F. Guillemin, L. Bezdetnaya.

Doctoriales de Lorraine.
16-21 mai 2010, Ventron, France.
« Ciblage et destruction de tumeurs par la thérapie photodynamique ». **J. Garrier**.

5ème Colloque International en « Thérapie cellulaire, Bioingénierie et Médecine Régénératrice ».
10,11 et 12 septembre 2008, Faculté de Médecine de Nancy, France.
« Relation entre la distribution intratumorale du Foscan®, l'apoptose photoinduite et l'efficacité du traitement dans un modèle de tumeur d'adénocarcinome colique humain (HT29) xénogreffé chez la souris nude ».
J. Garrier, S. Marchal, A. Bressenot, F. Plénat, F. Guillemin. L. Bolotine.

IIIème Journée Claude Huriet de la recherche médicale.
23 novembre 2007, Faculté de Médecine-CHU de Nancy, Nancy France.
« Relation entre la distribution intratumorale du Foscan®, l'apoptose photoinduite et l'efficacité du traitement dans un modèle de tumeur d'adénocarcinome colique humain (HT29) xénogreffé chez la souris nude ».
J. Garrier, S. Marchal, A. Bressenot, F. Plénat, F. Guillemin. L. Bolotine.

1er Forum du Cancéropôle du Grand Est.
19 octobre, Palais des congrès, Vittel France.
« Relation entre la distribution intratumorale du Foscan®, l'apoptose photoinduite et l'efficacité du traitement dans un modèle de tumeur d'adénocarcinome colique humain (HT29) xénogreffé chez la souris nude ».
J. Garrier, S. Marchal, A. Bressenot, F. Plénat, F. Guillemin. L. Bolotine.

International Conference on Vascular targeted therapies in oncology
4 au 6 octobre 2007, Mandelieu France.
« Vascular and cellular targeting induced by Foscan®-based photodynamic therapy of cancer ».
L. Bezdetnaya, **J. Garrier**, S. Marchal, MA. D'Hallewin, F. Guillemin.

Ciblage passif de tumeurs photoinduit par la mTHPC

La thérapie photodynamique (PDT) est une modalité de traitement des petites tumeurs accessibles à la lumière. Elle repose sur l'action combinée d'un photosensibilisateur qui, en présence d'oxygène et sous l'effet d'une irradiation lumineuse, induit la synthèse d'espèces réactives de l'oxygène cytotoxiques. L'effet tumoricide de la PDT se traduit par des dommages directs sur les cellules ainsi que des dommages indirects de la néovascularisation tumorale et une activation du système immunitaire.

Dans cette étude, nous avons démontré dans une première partie l'intérêt de se baser sur la distribution intratumorale de la mTHPC et non pas sur les études de biodistribution pour l'optimisation des conditions de traitement par PDT et en particulier de l'intervalle drogue-lumière (IDL). Un co-ciblage des vaisseaux et du parenchyme tumoral via un fractionnement de l'administration de la mTHPC a permis d'obtenir un taux de guérisons de 100%. Cette efficacité a été corrélée à la potentialisation de la mort des cellules par apoptose et valorisée par son association à des dommages secondaires cutanés restreints. La stratégie de fractionnement de l'administration s'avère donc être très prometteuse dans un contexte clinique.

Dans la seconde partie de cette étude, nous avons établi la redistribution de la mTHPC *in vivo* dans le modèle de la membrane chorioallantoïdienne de poulet (CAM) à partir de formulations liposomales (Foslip®, Fospeg®) et son impact sur les dommages vasculaires photoinduits par la PDT.

Mots Clés : Thérapie photodynamique, ciblage passif, mTHPC, dommages vasculaires et cellulaires, intervalle drogue-lumière, liposomes, membrane chorioallantoïdienne

---

Photoinduced passive targeting with mTHPC

Photodynamic therapy (PDT) is a therapeutic strategy for the treatment of small localized tumors accessible to the visible light irradiation. It is based on the combined action of photosensitizer (PS), light and molecular oxygen. Tumoricidal effect of PDT is triggered by direct damage of malignant cells and indirect vascular damage followed by an activation of the immune system.

The present study investigates the relationship between photoinduced apoptosis in each compartment of interest (vascular versus neoplastic) and mTHPC-PDT treatment efficiency in function of the intratumoral distribution of mTHPC. The latter was defined by the drug-light intervals. In the first part, we demonstrated the importance of the intratumoral distribution of mTHPC to optimize photodynamic parameters. The fractionation of the PS administration permitted to obtain a tumor cure rate of 100% correlated to a massive apoptosis of pathological tissues. Moreover, this treatment strategy induced only limited skin damages and few inflammation which could be an advantage in clinical context.

In the second part, we evidenced the mTHPC redistribution from liposomal formulations (Foslip®, Fospeg®) *in vivo* in the chick chorioallantoic membrane model (CAM) and its influence on photoinduced vascular damage.

Key Words : Photodynamic therapy, passive targeting, mTHPC, vascular and cellular damage, drug light interval, liposomes, chorioallantoic membrane